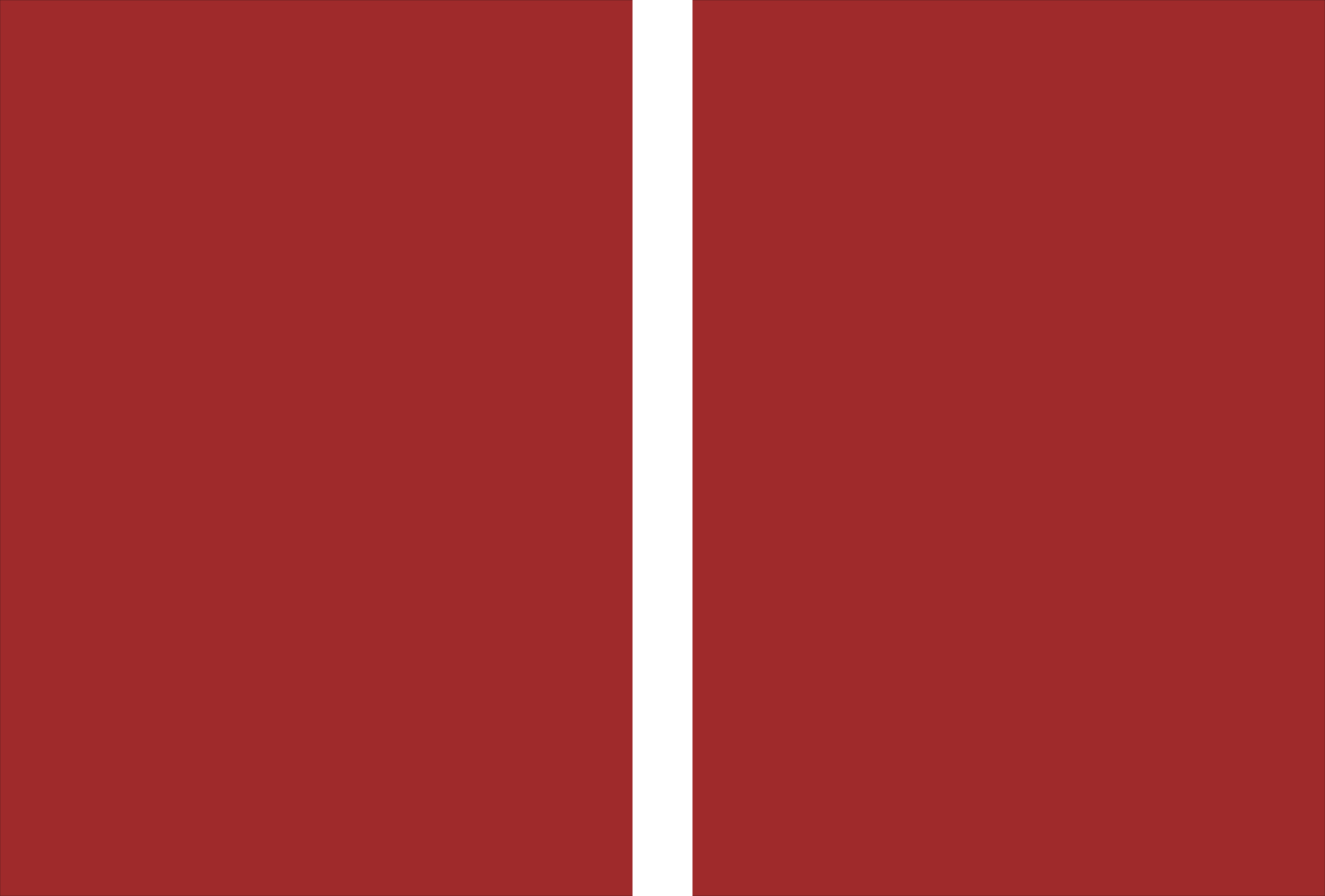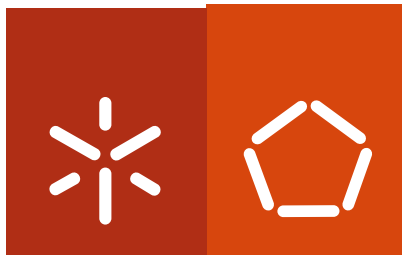Universidade do Minho
Escola de Engenharia

Gisela Andreia Monteiro da Luz

Bioactive Glass Nanoparticles combined with natural-based polymers for biomedical applications

Outubro de 2012

Universidade do Minho

Escola de Engenharia

Gisela Andreia Monteiro da Luz

Bioactive Glass Nanoparticles combined with natural-based polymers for biomedical applications

Programa Doutoral em Engenharia Biomédica

Trabalho efetuado sob a orientação do
Professor João F. Mano

Outubro de 2012

Autor   Gisela Andreia Monteiro da Luz

E-mail   gisela.luz@dep.uminho.pt

Telefone   +351 253 510900

BI: 12438138

Título da tese   Bioactive Glass Nanoparticles combined with natural based polymers for biomedical applications

Orientador   Doutor João Filipe Collardele da Luz Mano

Ano de conclusão 2012

Doutoramento em Engenharia Biomédica

Gisela Luz

Gisela Andreia Monteiro da Luz

"When you are a Bear of Very Little Brain, and you Think of Things, you find sometimes that a Thing which seemed very Thingish inside you is quite different when it gets out into the open and has other people looking at it."

A.A. Milne, *Winnie-the-Pooh*

Acknowledgments

I would like to thank my supervisor Prof. João Mano, for pushing me further every day. All his ideas, full of passion for Science, kept me in a dynamic rhythm self-fuelled by motivating results. When I look back, I recognize that I could not have done this without him.

I have always believed more in examples than in words. Prof. Aranzázu del Campo is a great example of what I believe a scientist should be. Her accuracy and dedication in science were quite inspiring. I would like to thank her for the opportunity of working in her lab.

I would also like to thank Prof. Rui Reis. By following his dream he created great opportunities for me and my colleagues.

In the 3B´s I met wonderful friends: Maria Susano, Ana Luísa Pereira, Isa Monteiro, Ana Rita Duarte and Simone Silva. I love you girls. I cannot thank you enough for the relieving laughs, for listening to me, for the wonderful cakes, for the valuable friendship! Thank you so much for respecting my personality and allowing me to live in my own bubble.

I want also to thank Sofia Caridade and Anabela Alves, although maybe they do not realize the difference they made in my life, when at some point they supported me.

I have definitely to thank Edith Ariza and Elsa Ribeiro, for the long, but not boring hours spent with SEM analysis. In front of both SEM equipments I experienced the most frustrating and happy moments of all this experience. They had always nice words to me, and their knowledge was a great input in my work. It was a pleasure to work with them.

Tiago, Inês and Filipa… always there over the years when I need a friend! And when thanking my friends, I cannot forget my special friend Cecília. She came from a magic world and gave me so much support during this PhD!

My father is the most enthusiastic fan of my work. I was amazed by how he would keep track of all my publications without even having a scientific background. When you have someone in your life that believes you can win a Nobel Prize, you just cannot avoid but working harder. The same for my aunt Helena that feels so genuinely proud of me, for each little achievement since I was in high school. Thank you for believing in me more than I can possibly do.

I surely have to thank my sister and my brother in law for making my life so much easier during this PhD, when they brought my Alfacinha to Braga. Also for the uncountable times that they went to pick me when I arrived from Braga and for all the support.

I am truly blessed, and deeply thankful for the family that I have. I recognize that all that I am able to achieve comes from the guidance and full support that I receive from them.

I am so lucky that I even found a second family in Braga. Thank you so much Luzia, Carla and D. Helena for all your kindness. Because of you, I never felt vulnerable in this city. I will never forget the uncountable things that you did for me, especially for letting me feel that I could always count on you for absolutely anything!

Finally, I would like to sincerely thank both my mother and my boyfriend Daniel. They were the ones that cooked for me while I was writing another paper. They were the ones to whom I would call just to explode, cry, or laugh. They were the ones that made me feel safe when my life was a big mess. I am positively sure that I would not have kept my sanity during these four years without their patience, kindness and advice. Thank you so much.

Bioactive Glass Nanoparticles combined with natural based polymers for biomedical applications

Abstract

Bone tissue engineering has assisted in the last decades to an evolution in which merely replacement implants gave room to more complex regenerative approaches. Several challenges still remain. Although biocompatibility and biodegradability mechanism are now reasonably known and controlled, they still need to precisely match the physiological rhythm of bone renewal, while maintaining the adequate structural properties to support the host tissue growth. These mechanisms are first regulated at the nanoscale through the cellular interactions with the materials. Therefore, there is an urge to begin the control of materials surface interaction with the environment at the nanoscale and to go up to the micro and macro levels that are comprised in the natural bone structure.

The main goal of this thesis was to give a step further in producing *in vitro* materials able to mimic the structural and chemical environment necessary to bone growth. Therefore, micro and nanofabrication techniques were used to recapitulate the complex environment of mineralized tissues. As bone is based in a mineral/organic natural composite, bioactive glass and chitosan were chosen as materials to be combined in order to mimic bone structure. Bioactive glass was engineered at the nanoscale, to better follow Nature´s path.

In a first stage of the work, the production of bioactive glass nanoparticles was studied and optimized. The influence of changing experimental parameters such as temperature and pH were evaluated, as well as the composition of the BG-NPs. All of the considered factors showed to be important when setting important characteristics of the BG-NPs as size, morphology and bioactivity. A ternary and a binary system were compared. The different characteristics showed by both systems indicate that in the future, it will be easy to adapt the BG-NPs to the environment requirements, namely degradation rate and subsequently ionic release to assure efficiently hydroxyapatite layer deposition necessary for bone growth while maintaining safe cytotoxicity levels.

Following of the BG-NPs evolution in the sol-gel system since the early stages of production showed that hollow BG-NPs are easily obtained through Ostwald-ripening. This template free route presents a great potential for drug-delivery systems.

Moreover, the procedure may be simply adapted to produce dense nanospheres with controllable sizes, only through the addition of different PEG size chains.

Chitosan, a natural origin polymer, was then combined with the developed bioactive glass nanoparticles to obtain nanocomposites. Two strategies were followed. BG-NPs were dispersed in a chitosan solution and then transformed in membranes through a traditional solvent casting procedure. Bioactive polymeric nanocomposites were easily obtained by using different BG-NPs (from a ternary system based on SiO_2-CaO-P_2O_5 and a quaternary system based on SiO_2-CaO-P_2O_5-MgO). Both the bioactivity potential and the osteoblastic response *in vitro* were evaluated.

A microcontact printing technique was employed to print BG-NPs on the surface of the chitosan membranes. Mineralized patterns were obtained and cells showed a tendency to attach accordingly to the created pattern.

Finally, moving up to the 3D level, a novel bottom-up approach was addressed aiming to summarize bone´s natural multihierarchical structure. In this work, it was proved in a very simple procedure, how a drop of aqueous suspension of BG-NPs left to dry on a superhydrophobic surface leads to the self-assembly of the BG-NPs, creating a bioactive glass based aggregate comprising the nano, micro and macro levels. Besides having a hierarchical organization, that is known to give mineralized materials their great mechanical properties, these systems also allow for the inclusion of drugs as was proved by dispersing dyeing additives in the macrospheres. Their bioactive character may also be adapted to the host tissue requirements by changing the water evaporation ratio only by adjusting the environment temperature.

The topics explored in this this thesis contributed for a deeper understanding of the BG-NPs production. Moreover, the described research work is based on simple techniques highly competitive against other existing technologies for bone´s structure mimicking.

Nanopartículas de vidro bioactivo combinadas com polímeros de origem natural para aplicações biomédicas

Resumo

Nas últimas décadas, a Engenharia de Tecidos ósseos, assistiu a uma extraodinária evolução. O desenvolvimento de implantes com funções de mero suporte deu lugar a complexas estratégias de regeneração do osso. Apesar dos significativos avanços obtidos nesta área, subsistem ainda importantes desafios. Actualmente os mecanismos na base dos conceitos de biocompatibilidade e degradabilidade são já conhecidos e razoavelmente controlados. Persiste no entanto a necessidade de adequar estes conceitos, de um modo efectivo, aos ritmos fisiológicos da renovação óssea. Estes mecanismos começam por ser regulados à nanoescala através de interacções celulares com a superfície dos materiais e estendem-se para aos níveis micro e macrométrico.

O principal objectivo desta tese prendeu-se com a necessidade de produzir *in vitro*, materiais capazes de mimetizar estrutural e quimicamente o complexo ambiente necessário ao crescimento de tecido ósseo saudável. Neste sentido, técnicas de fabricação à escala nano e micro foram utilizadas com intenção de reproduzir a estrutura dos tecidos naturalmente mineralizados.

Sendo o osso um compósito natural baseado numa fase mineral e orgânica, os materiais escolhidos para reproduzir esta combinação foram o vidro bioactivo e o quitosano. No caso do vidro bioactivo, este foi trabalhado à nanoescala, para melhor reproduzir as estratégias encontradas na Natureza.

Numa primeira fase da investigação, a produção de nanopartículas de vidro bioactivo foi estudada e optimizada. A influência de algumas condições experimentais, nomeadamente a temperatura e o pH, foi avaliada, tal como a composição química das nanopartículas. Todos os pontos considerados mostraram ser relevantes para definir características importantes como o tamanho das nanopartículas, a morfologia e a bioactividade. Dois sistemas diferentes de vidro bioactivo ternário e binário foram comparados. As diferentes caracterís-

ticas mostradas por ambos os sistemas, demonstram que no Futuro, as propriedades das nanopartículas podem ser facilmente adaptadas aos requisitos do local de implantação.

O acompanhamento da evolução das nanopartículas de vidro bioactivo no sistema sol-gel, desde os seus primeiros momentos de formação, mostra que é possível obter nano-partículas ocas através do fenómeno de amadurecimento de Ostwald. Este procedimento não envolve a necessidade de recorrer a um molde para criar estruturas ocas e oferece um grande potencial para sistemas de libertação de fármacos. O procedimento foi ainda adap-tado de modo a que nanoesferas densas, com tamanhos controláveis, fossem obtidas uni-camente devido à adição de cadeias PEG com diferentes tamanhos.

O quitosano, um polímero de origem natural, foi combinado com as nanopartículas desenvolvidas de modo a obter nanocompósitos de material orgânico e inorgânico. Para este propósito, duas estratégias diferentes foram seguidas. Numa primeira abordagem, as nanopartículas de vidro bioactivo foram dispersas numa solução de quitosano e posterior-mente processadas em membranas por evaporação do solvente. Como resultado, obtive-ram-se nanocompósitos bioactivos de base polimérica usando diferentes nanopartículas de vidro bioactivo (sistema ternário SiO_2-CaO-P_2O_5 e sistema quaternário SiO_2-CaO-P_2O_5-MgO). Tanto o potencial bioactivo quanto a resposta osteoblástica foram avaliados *in vitro*. Numa segunda abordagem, a técnica de impressão por microcontacto foi utilizada para criar padrões mineralizáveis de nanopartículas de vidro bioactivo na superfície de membranas de quitosano. As células cultivadas sobre estes substratos alinharam-se de acordo com o padrão previamente formado.

Finalmente, ao nível 3D, uma nova estratégia foi seguida tendo em vista a obtenção de estruturas multihierárquicas semelhantes às encontradas no osso. A deposição de gotas de suspensão aquosa de nanopartículas de vidro bioactivo em superfícies superhidrofóbicas permitiu, por associação espontânea induzida por evaporação, a obtenção de agregados esféricos de nanopartículas, exibindo níveis de organização à escala nano, micro e macro-métrica.

Os tópicos explorados nesta tese contribuem para uma melhor compreensão da produção de nanopartículas de vidro bioactivo. O trabalho de investigação aqui descrito baseou-se em técnicas simples e altamente competitivas em oposição a outras técnicas já existentes com vista à mimetização da estrutura óssea.

Table of Contents

List of Abbreviations and Acronyms

A ALP - Alkaline phosphatase

B BG - Bioactive glass

BG-NPs - Bioactive glass nanoparticles

BMPs - Bone morphogenetic proteins

BTE - Bone Tissue Engineering

C Calcein-AM - Calcein acetoxymethyl esther

Ca/P - Calcium/Phosphorus ratio

D DMEM - Dulbecco's modified Eagle medium

2D - two dimensional

3D - three dimensional

dsDNA - double-stranded DNA

E ECM - Extracellular matrix

EDX - Energy dispersive X-ray spectroscopy

EISA - Evaporation Induced self-assembly

F FBS - fetal bovine serum

FTIR - Fourier transform infrared spectroscopy

G GAGs - Glycosaminoglycans

H HAp – Hydroxiapatite

M mCP or µCP – Microcontact printing

MTS - 3-(4,5-dimethylthiazol-2-yl)-5(3-carboxymethoxyphenyl)-2(4-sulfofenyl)-2H-tetrazolium

P PBS - phosphate buffered saline

PDLLA - poly-(D, L-lactic) acid

PDMS - (Poly)dimethylsiloxane

PEG - Poly(ethylene) glycol

PFDTS - perfluorodecyltriethoxysilane

% w/v - percentage of weight/volume

% v/v - percentage of volume/volume

R RT - Room temperature

S SAMs - Self-assembled monolayers

SBF - Simulated body fluid

SEM - Scanning electron microscopy

T TCPS - Tissue culture polystyrene

TEM - Transmission electron microscopy

U UV – Ultraviolet

X XRD - X-ray diffraction

Z Z or ζ-potential - Zeta potential

List of Figures

Chapter III

Chapter IV

Chapter IV - Appendix

Chapter V

Chapter VI

Chapter VII

Chapter VIII

List of Tables

Chapter III

Chapter IV

List of Publications

A - Publications resulting from the work performed during this PhD

International refereed journals

1. **Luz, Gisela M.**; Mano, João F., Biomimetic design of materials and biomaterials inspired by the structure of nacre, Philosophical transactions of the royal society A - Mathematical Physical and Engineering Science, 2009, 367, 1893, pp: 1587-1605 DOI: 10.1098/rsta.2009.0007.

2. **Luz, Gisela M.**; Mano, João F., Mineralized structures in nature: Examples and inspirations for the design of new composite materials and biomaterials, Composites Science and Technology, 2010, 70 (13), pp: 1777-1788, DOI: 10.1016/j.compscitech.2010.05.013.

3. **Luz, Gisela M.**; Leite, Alvaro J.; Neto, Ana I.; Song, Wenlong; Mano, João F., Wettable arrays onto superhydrophobic surfaces for bioactivity testing of inorganic nanoparticles, Materials Letters, 2011, 65 (2), pp: 296-299, DOI: 10.1016/j.matlet.2010.09.056.

4. **Luz, Gisela M.**; Mano, João F., Preparation and characterization of bioactive glass nanoparticles prepared by sol-gel for biomedical applications, Nanotechnology, 2011, 22 (49), nr: 494014, DOI: 10.1088/0957-4484/22/49/494014.

5. **Luz, Gisela M.**; Boesel, Luciano; del Campo, Aranzázu; Mano, João F., Micropatterning of Bioactive Glass Nanoparticles on Chitosan Membranes for Spatial Controlled Biomineralization, Langmuir, 2012, 28 (17), pp: 6970-6977, DOI: 10.1021/la300667g.

6. **Luz, Gisela M.**; Mano, João F., Nanotectonics approach to produce hierarchically organized bioactive glass nanoparticles-based macrospheres, Nanoscale, 2012, 4 (20), pp: 6293-6297, **DOI:** 10.1039/C2NR31895D.

7. **Luz, Gisela M.**; Mano, João F., Chitosan/bioactive glass nanoparticles composites for biomedical applications, Biomedical Materials, 2012, 7, nr: 054104, **DOI:**10.1088/1748-6041/7/5/054104.

8. **Luz, Gisela M.**; Mano, João F., Nanoengineering of bioactive glass: From hollow to dense nanospheres, submitted.

Book chapters

1. **Luz, Gisela M.**; Mano, João F., Nacre inspired biomaterials, In Biomimetic approaches in the development of biomaterials, Ed. Mano, João F., Wiley-VCH, 2012.

2. **Luz, Gisela M.**; Mano, João F., Nanoscale design in biomineralization towards the development of new biomaterials for bone tissue engineering, In Tissue Engineering using ceramics and polymers: 2nd Edition, Ed. Boccaccini, Aldo R., Woodhead Publishing, 2013.

Communications in international conferences

Oral Presentations

1. **Luz, Gisela M.**; Boesel, Luciano; del Campo, Aranzázu; Mano, João F., Micropatterning of Bioactive Glass Nanoparticles on Chitosan Membranes for Spatial Controlled Biomineralization, Montpellier, France, September 2011.

1. **Luz, Gisela M.**; Mano, João F., Biocomposites and biomimetic nano-structured coatings combining bioactive glass-ceramic nanoparticles and chitosan for biomedical applications, V International Materials Symposium, Materiais 2009, Lisboa, Portugal, April 2009.

2. **Luz, Gisela M.**; Mano, João F., New biomimetic nano-structured coatings combining bioactive glass-ceramic nanoparticles and chitosan for bone tissue engineering, TERMIS World Congress, Seoul, South Korea, September 2009.

3. **Luz, Gisela M.**; Mano, João F., Biocomposites and biomimetic nano-structured coatings combining bioactive glass-ceramic nanoparticles and chitosan for biomedical applications, Frontiers in Polymer Science, Mainz, Germany, June 2009.

4. **Luz, Gisela M.**; Mano, João F., New biomimetic nano-structured coatings combining bioactive glass-ceramic nanoparticles and chitosan for bone tissue engineering, TERMIS-EU, Galway, Ireland, June 2010.

5. **Luz, Gisela M.**; Boesel, Luciano; del Campo, Aranzázu; Mano, João F., Micropatterning of bioactive glass nanoparticles on chitosan membranes for spatial controlled biomineralization, XXXVIII Congress of the European Society for Artificial Organs (ESAO 2011) and IV Biennial Congress of the International Federation on Artificial Organs (IFAO 2011), Porto, Portugal, October 2011.

B. Publications resulting from collaborative work within and outside the 3B's

International refereed journals

1. Hong, Zhongkui; **Luz, Gisela M.**; Hampel, Paul J.; Jin, Minshan; Liu, Aixue; Chen, Xuesi, Mano, João F., Mono-dispersed bioactive glass nanospheres: Preparation and effects on biomechanics of mammalian cells, Journal of Biomedical Materials Research Part A, 2010, 95A (3), pp: 747-754, **DOI:** 10.1002/jbm.a.32898.

2. Bernardo, Vasco; **Luz, Gisela M.**; Alves, Natália M.; Mano, João F., Cell Behavior In New Poly (L-Lactic Acid) Films With Crystallinity Gradients, Materials Letters, 87, 2012, pp: 105-108.

3. Mota, Joana; Yu, Na; Caridade, Sofia G.; **Luz, Gisela M.**; Gomes, Manuela E.; Reis, Rui L.; Jansen, John A.; Walboomers, Frank X.; Mano, João F., Chitosan/Bioactive Glass Nanoparticles Composite Membranes for Periodontal Regeneration, Acta Biomaterialia, 2012, 8 (11), November 2012, pp: 4173‑4180.

4. Caridade, Sofia G.; Merino, Esther G.; Martins, Gabriela V., **Luz, Gisela M.**; Membranes of poly(d,l-lactic acid)/Bioglass® with asymmetric bioactivity for biomedical applications, Journal of Bioactive and Compatible Polymers, 2012, 27 (5), pp: 429-440.

Communications in international conferences

Oral Presentations

1. Caridade, Sofia G.; Merino, Esther G.; **Luz Gisela M.**, Alves, Natália M. and Mano, João F., New chitosan/Bioglass® composite membranes for guided tissue regeneration, Society for Biomaterials, Seattle, United States of America, April 2010.

Structure of the Thesis

The present thesis is divided into 4 parts containing 8 chapters. Both Parts 1 and 3 are based on articles already published or submitted to international peer reviewed journals. Part 1 also contains a book chapter. The respective original publication is identified in the beginning of each chapter.

Part 1 is an introductory overview of bone tissue engineering (BTE) strategies inspired in Nature and mainly focused on nanoscale approaches.

Part 2, corresponding to Chapter III, summarizes the techniques and materials used to produce the developed materials. Characterization techniques are also presented as a complement of the information given in each of the experimental chapters.

Part 3 comprises 5 experimental chapters based on published or submitted articles. Chapter IV and V present fundamental research aiming to fully understand the behavior and control of BG-NPs. Several experimental conditions were tested and their influence on the BG-NPs size, morphology and bioactive character was evaluated. Regarding Chapter IV, an appendix was added, introducing a complementary work that describes an expedite alternative to characterize biomaterials for BTE.

Chapter VI presents a 2D application of the BG-NPs. Chitosan based nanocomposites were developed containing BG-NPs. Bioactivity *in vitro* was accessed. Also the effect of doping the particles is evaluated in terms of the biological response when cells interacted with the nanocomposites.

Chapter VII consists of an adapted approach to produce bioactive chitosan based membranes in which the bioactive micropatterns were spatially controlled.

In Chapter VIII a 3D strategy to produce hierarchically organized bioactive structures having the BG-NPs as subunits is presented.

Part 4 summarizes the goals achieved in this work. General conclusions are drawn and future remarks are set.

PART 1 - Introduction

Chapter I

Nanoscale design in biomineralization towards the development of new biomaterials for bone tissue engineering

Chapter II

Mineralized structures in nature: Examples and inspirations for the design of new composite materials and biomaterials

Chapter I

Nanoscale design in biomineralization towards the development of new biomaterials for bone tissue engineering *

Abstract

New advances in BTE demand the development of materials that not only replace bone, but are also able to regenerate the damaged tissue based on external or even internal stimulus.

Researchers are being inspired on bone's extraordinary hierarchical architecture and also in the natural mineralization process, to develop new devices and materials.

In this chapter, recent advances of nanoscale design in biomineralization towards the development of new biomaterials for BTE are presented. The importance of designing the materials at the nanoscale is highlighted and justified by the necessary interaction with the biological environment occurring at the nanoscale.

1. Introduction

The possibility of applying Nanotechnology approaches in biomaterials science is giving rise to new trends in the orthopedic domain. Specifically, the advent of sensitive techniques and a better understanding of important scientific phenomena, together with the motivation of meeting clinicians' claims, are making BTE a challenge with increasingly interest for regenerative approaches instead of merely replacement solutions. Several scientific fields are being merged in order to fulfill the demanding complexity of such task.

Being able to design nanostructured materials is of crucial significance, since cell interactions with biomaterials will occur at the nano-level. The challenge of bottom-up approaches able to mimic nature´s outstanding mineralized structures is facilitated by the actual nanotechnology tools.

Advances in nanotechnology also allow the development of novel nanodevices that not only have better cytocompatibility and bioactive properties but can also behave as unique drug delivery platforms. Moreover, these current approaches allow for the production of hierarchical architectures with organized multilevel structures, a key feature of natural materials.

Despite the bright future foreshadowed by nanotechnology in BTE, important limitations still need to be overcome regarding the actual methodologies. Cytotoxicity of nanomaterials requires careful assessment. Additionally, technical difficulties, as assuring proper vascularization of scaffolds also need to be addressed.

In the following subsections, important concepts regarding the matter of this chapter will be defined. In part 2, several concrete examples of new approaches in BTE are presented as well as the rational behind them. The aim of this chapter is not to provide in-depth insights into the different nanoscale designs inspired in the biomineralization process but to give an overview of possibilities and limitations when nanodevices are applied in BTE.

1.1. The Biomineralization process

Biomineralization is a natural process by which living forms influence the precipitation of mineral materials. By finding ways of mineralizing, living organisms not only developed an outstanding evolutionary advantage, but they also achieved mobility. [1] The resulting highly organized structures fulfill a variety of important functions heading protection and mechanical purposes. [1, 2] Some examples are skeleton in mammals, exoskeleton in insects, and shells in mollusks. [3] Usually, biomineralization is an extracellular process were inorganic based materials are formed on the outer wall of the cell, within the cell wall, or in the immediate surrounding tissue areas. However, intracellular Biomineralization is also possible, and in this case, mineral formation will occur within the cell, as it is reported for some algae, for instances. [4]

Biomineralization is a matrix mediated process. An organic template directs the inorganic phase nucleation and growth in a well-ordered manner. The whole process is strictly controlled by chemical, physical, morphological and structural mechanisms. [3]

Biominerals comprise calcium carbonates, like calcite, aragonite and vaterite; Silica, like opals; Bioapatites with the general formula $Ca_{10-x+\eta}X_y(PO_4)_{6-x}(CO_3)_x(OH)_{2-x+}$ accounting for the possible inclusion of ions (x), the substitution of CO_3^{2-} for PO_4^{3-}, and the presence of calcium vacancies; and Iron Oxides and Hydroxides as magnetite. [1, 5]

The intimate association of inorganic and organic phases is a hallmark of biomineralization resulting in organic/inorganic hybrid materials with complex shape, hierarchical organization and superior materials properties as high resistance and lightness. [3, 6]

Another exciting characteristic of these natural composites is their ability to respond to external stimuli at the cellular level being than able to remodel and self-repair. This characteristic is dependent on several organic molecules. For instances in bone, osteocalcin, the most abundant noncollagenous protein [7], will coordinate calcium ions in a spatial orientation that is complementary to calcium ions in a hydroxyapatite crystal lattice. This protein also plays an important role in cell signaling for the recruitment of osteoclasts and osteoblasts for bone resorption and deposition, respectively. [8]

It is of critical importance to unravel the process of biomineralization in order to understand how both bone and tooth are formed, and therefore to produce biomaterials able

to mimic bone structure in the nanoscale details. [9, 10] Moreover, this knowledge would be also useful in other areas regarding pathological mineralization, for example in cardiovascular disease. [11]

Finally, biomineralization illustrates how nature can design complex, hierarchical, and structurally/morphologically controllable materials to be used in BTE based solely in weak components such as brittle minerals, soft proteins and water. [2, 12] Moreover, these materials are produced at mild temperature and pressure conditions, with relatively low energy consumption, making these systems a fascinating natural source of inspiration for scientists and engineers. [2]

1.2.   Bone structure and properties

Bone is a dynamic, highly vascularized tissue that is formed from a composite of 60% mineral (mostly nanoscale hydroxyapatite crystals), 30% organics (including collagen, glyco-proteins, proteoglycans, and sialoproteins) and 10% of water. [13, 14] Its complex cellular architecture continues to remodel throughout the lifetime of an individual, giving bone an innate ability to regenerate injuries below a critical size, helped by local or recruited stem cells. [15, 16] However, some injuries are beyond the limit that the body can self repair, namely cases of severe fractures, bone tumor resections, age-related restrictions, scarring and inflammation processes. In these cases a human approach is required in order to assure proper healing. [15, 16] However, mimicking bone´s natural structure and mechanical profile is still a challenge in BTE.

High toughness and flaw tolerance are generally associated with natural biomineralized composites. They are believed to be intimately related to an advantageous hierarchical arrangement of structural motifs at the nanoscale. Bone tissue also presents this hierarchical architecture and it is organized in seven different levels. [17] This structure is summarized in figure I.1.

Beginning at the nanoscale, at the order of 1 nm, one will find the aminoacids that form the collagen molecules. The collagen molecule or tropocollagen is approximately 300 nm long and 1.5 nm in diameter and has a 3D polypeptide stranded structure - See figure I.1 VIIa. The collagen molecules will associate in collagen fibrils with a diameter of 200

nm. [18, 19] Together with smaller quantities of various proteoglycans and glycoproteins these components represent the organic part of the bone. [20] The organic/inorganic association characteristic of this tissue is due to the presence of hydroxyapatite crystals aligned along the type I collagen fibrils c-axis. The dimensions of the crystal will be 50 x 25 nm of length and width and with 2-3 nm thickness, presenting plate-shape morphology. The mineralized collagen fibrils will be arranged in lamellae (3-7 µm thick) [14] of fibrils arrays each one having a different pattern according to the fibrils orientation. The concentric association of these fibrils arrays results in a final collagen fiber with a diameter of 2 µm [18]. The rotation of the crystals sub layers, together with the rotation of the collagen fibril bundles around their axis, enhance the isotropic properties of bone found at the macroscopic scale, giving it its strength. [2, 21] The lamellae are formed by the secondary osteons, interstitial lamellae and the inner and outer circumferential lamellae.

The mineral amount present in the bone tissue is also very important in determining its mechanical properties and function. [22] This parameter will be defined by bone´s cells activity. Osteoclasts will release an enzyme that destroys the bone tissue, forming tunnels along the longitudinal axis of bone. Then, osteoblasts will rebuild the secondary osteons cylindrical tubes, by secreting circular rings of lammelae that surround the vascular or Haversian canal in the center of the osteon or Haversian system with a diameter of 200 µm and 10-20 mm long. [14, 18] - See figure I.1. III. When osteoblasts are trapped in the newly synthetized organic osteoid that will soon mineralize, they become osteocytes. Nutrient supply will be facilitated to osteocytes through a microcirculating system called canaliculi - See Figure I.1. IIb. [14, 17, 23]

The last and macroscopic level of the hierarchical architecture corresponds to the group of closely packed osteons that compose the cortical bone. [17, 23] Figure I.1. summarizes the seven levels of bone hierarchy.
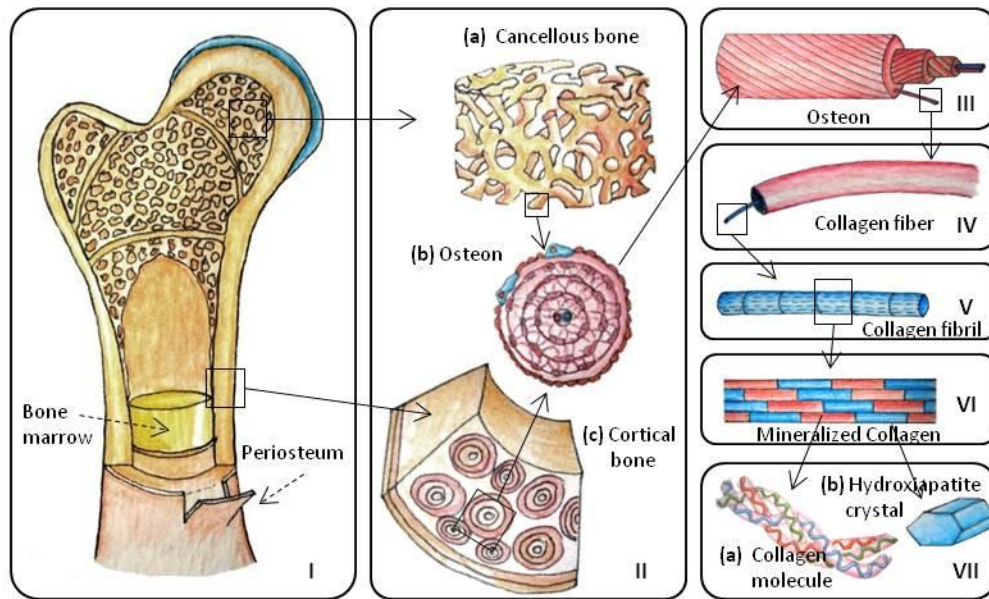
Fig. I. 1. Schematics of the seven levels of the bone hierarchy.

I - Bone; **II a** - Cancellous bone; **II b** - Osteon cross section; **II c** - Cortical bone showing the densely packed osteons; **III** - Osteon with surrounding lamellae and Haversian canal; **IV** - Collagen fiber; **V** - Collagen fibril; **VI** - Mineralized fibrils; **VII a** - Collagen molecule showing the triple helice; **VII b** - Plate-like apatite crystal.

Mechanical support attributed to the skeletal system is essentially provided by cortical bone that, from a biomechanical perspective, behaves like semi brittle, viscoelastic, and orientation dependent material. [14, 18] It is the already described lamellar morphology of cortical bone that is responsible for the hinder of crack propagation and increase of toughness. [23]

Cancellous bone - See Figure I.1. II a - is a lighter, less dense form of osseous tissue consisting of trabecular plates and bars that are found in the highly vascular inner parts of bone where hematopoiesis and ion exchange occur. [18] Regarding cancellous or trabecular bone, the stiffness and strength values will depend on if it is a weight or non-weight-bearing regions varying greatly depending on location in the body. Stiffness of cancellous has modulus values in the range of 1-9.7 GPa. Weight-bearing trabecular systems can sustain superior-inferior compression levels of as much as 310 MPa and those from non-weight-bearing regions typically fail at stresses from 120 MPa to 150 MPa. [24]

Cortical bone presents tensile strength of 3.1-180 GPa and modulus of 3.9-71 GPa. These values are two to three orders of magnitude greater than that of cancellous bone.

[18, 25] The compressive strength (130-180 MPa) and modulus (4.9-34 GPa) of cortical bone are also greater than those of cancellous bone. [26]

1.3.   Bone Tissue Engineering

The term Tissue Engineering is defined by Langer and Vacanti, as *''an interdisciplinary field of research that applies the principles of engineering and the life sciences towards the development of biological substitutes that restore, maintain, or improve tissue function''*. [27]

Recently, tissue engineering has gained increasing support as a method to treat debilitating musculoskeletal disorders affecting bone, ligament, and cartilage such as osteoarthritis and osteoporosis over traditional methods, due to its interdisciplinary approach that focus on tissue regeneration rather than on its replacement. [15, 28] Figure I.2. summarizes bone replacement and regeneration strategies.
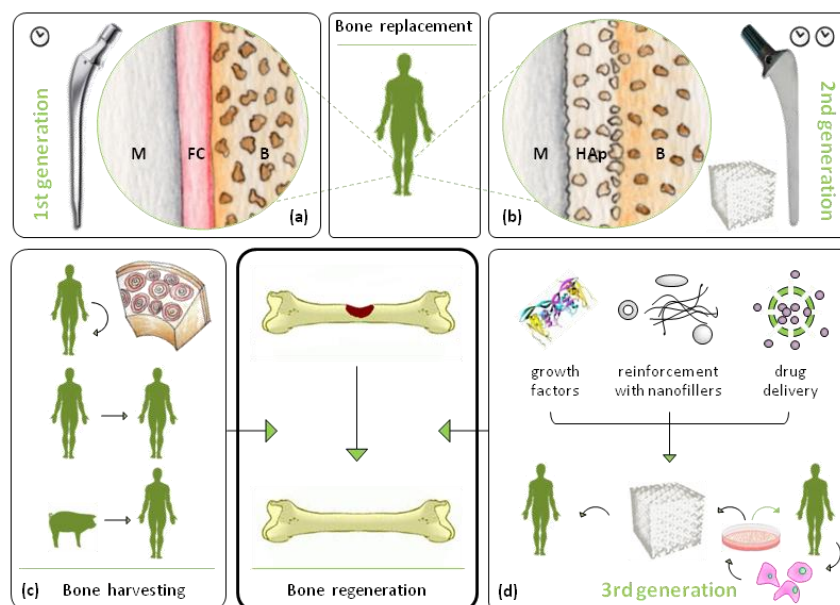
Fig. I. 2. Evolution of bone replacement and regeneration strategies.

> **(a)** First generation implants: M - Metal, FC - Fibrous capsule, B - Bone; **(b)** Second generation implants: M - Metal, HAp - Hydroxiapatite, B - Bone; **(c)** Bone harvesting; **(d)** Third generation BTE strategies.

The so called first generation biomaterials (from the 1960s to early 1980s) were represented by prostheses, aiming only to match bone physical properties while causing a minimal toxic reaction - See figure I.2. (a). They were based on nearly inert materials. This type of materials stimulates the host tissue to produce a nonadherent fibrous capsule around them with the purpose of isolating the foreign object. With time, this natural protection mechanism may cause the deterioration of the implant. These types of materials do not regenerate bone, since they do not present specific bioactivity. They are used merely as bone replacement devices. Metals, ceramics, and polymers may be included in the nearly inert materials group. [29]

Bioactive materials arrived on the 1980s and initiated the second generation of biomaterials. Their significance in bone tissue regeneration is related to the strong chemical bond between the host tissue and the material will avoid the development of a fibrous capsule that will compromise the fixation of the implant and the success of the intervention overtime. [30] See figure I.2. (b).

Regarding the BTE field, the concept of bioactivity is directly related to the ability of a material to bond chemically to the bone, through the formation of an apatitic layer *in vivo*, or to the ability of inducing the precipitation of hydroxyapatite when immersed in simulated body fluid (SBF) *in vitro*. [31-33] The degradation behavior of bioactive materials must be synchronized with the cellular events leading to new bone growth. [34]

Bioactive materials are classified according to the time taken for more than 50% of the interface to bond to bone ($t_{0.5bb}$). The Bioactivity index (I_B) is calculated using the formula (1): [33]

$$I_B = 100/t_{0.5bb} \ (1)$$

An I_B value greater than 8 (class A), means that the material will bond to both soft and hard tissue. Materials with an I_B value less than 8 (class B), but greater than 0, will bond only to hard tissue. This leads to the distinction of two different classes: Class A comprises bioactive glasses which exhibit rapid and strong bonding to bone by means of a series of chemical reactions at the bone tissue interface. They are defined as being osteoproductive, and osteoconductive. [35] Moreover, bioactive glasses are also able to bond to soft connective tissue. On the other hand, Class B relates to materials which bond slowly only to bone,

like synthetic hydroxyapatite. They are classified as bioactive ceramics, and only present osteoconductive properties. [35]

When a bioactive material bonds to soft tissue, whether *in vitro* or *in vivo,* collagen fibers (which are comprised in all soft tissues) become embedded and bonded within the growing apatitic layer on the bioactive materials' surface. [33][36]

Bioactive materials may be used as coating for prostheses or as scaffolds and fillers - see figure I.2. (b). 3D, porous, degradable, polymeric scaffolds provide mechanical support while allowing the ingrowth of new bone as the scaffold degrades. The pore size of scaffolds needs to be greater than 30 μm to allow bone ingrowth. [25]

A more recent approach would be the extraction of cells from a patient and later transplantation after proper cell culture, or culturing of the cells in a 3D scaffold for implantation in a defect. [37, 38] See figure I.3. (d). With strategies combining both biological systems and engineered substrates, biomaterials are now on their third generation. The actual goal is to elicit specific cellular responses at the level of molecular biology. Such a shift from a materials and mechanics approach to biological based tissue repair requires careful understanding of the application of molecular biology to bone regeneration. [39]

Bone repair typically involves the use of autografts, allografts, xenografts, and synthetic materials. [28, 40] These alternatives are depicted in figure I.2. (c). Autologous bone grafting is normally the first choice for bone replacement. However the use of autologous bone is limited by its short supply and pain resulting from the harvest process. [41] On the other hand, obtaining tissue from another biological source implies a certain risk of rejection and disease transfer. Tissue engineering may be a suitable solution to the actual limitations. [28, 42]

There are still some important limitations in BTE that need to be overcome, namely cell necrosis occurring within the inner core of a mineralized scaffold [37] or the inadequacy of its structural properties to the functionality of the tissue. The solutions may lay in a BTE nanoscale approach regarding the development of new techniques and materials or combinations of both, in order to obtain the organized structure that gives bone its successful mechanical properties and cellular interactions. The design principles employed to develop hierarchical approaches aiming to mimic natural materials formation processes, can be extrapolated to the whole class of biomedical materials, including polymers, metals, ceramics or hybrid combinations. [43]

A BTE biomaterial-based device ideally would present a certain set of characteristics related to each one at the macro, micro and nanolevels. Beginning at the macrolevel, biocompatibility, biodegradability and mechanical properties are the essential criteria to be fulfilled. At the micro level the key features for assuring the biodevice success are determined by tissue architecture, surface chemistry, surface stiffness, cell migration, nutrient delivery and vascularization ability. Ultimately, at the nanolevel, bioactive factors, cell adhesion, mineralization and gene expression will play a valuable role on defining the device fate. [44]

Biomaterials are classified according to their response when implanted in the body. Therefore, they are named: bioactive, nearly inert materials and resorbable. While the former concepts were already described above, resorbability is defined as the ability of a material to support the bone growth during the healing process, and later gradually degrade in metabolizable residues, being therefore a very desirable feature on a biomaterial. [29] Both polymers and ceramics may have adjustable bioresorbability.

Bioceramics are special compositions of ceramic materials in the form of powders, coatings, or bulk devices. They are suitable to repair, augment or replace diseased or damaged bony tissue. [35] Other materials, as metals and polymers are also used in bone repair applications. However they are not naturally bioactive, meaning that they will strongly bond to bone *in vivo* or will not develop an apatitic layer when immersed in SBF. [45, 46] Metals, as stainless steel (316L), cobalt-based alloys, titanium, and titanium-based alloys are mostly used for bone replacement due to their remarkable mechanical properties. [29, 47]

Both synthetic and natural occurring biodegradable polymers are used for BTE applications. [48]

The most common synthetic polymers found in bone regeneration applications are aliphatic polyesters, namely poly (glycolic acid) (PGA), the stereoisomers forms of poly (lactic acid) (PLA) [49-52] and their copolymer poly (lactic-*co*-glycolide) (PLGA) and also the poly(ε-caprolactone) (PCL). [53, 54] It is also possible to find applications based on polyesters such as poly(hydroxybutyrate) [55, 56], poly(propylene fumarate)-diacrylate [57-59] and polyurethane [60]. The degradation of these materials occurs by hydrolytic route through de-esterification being the resulting products removed by natural excretion pathways. [61]

Natural-origin polymers are normally based in polysaccharides such as starch, chitin or chitosan, or proteins, like silk fibroin and collagen. [53, 54, 62] Also hyaluronan, gelatin and alginate have been proposed as natural biopolymers for BTE. [38, 63]

Chitosan has been widely studied in the biomedical field since its polysaccharide backbone is structurally similar to glycosaminoglycans, the major component of the extra-cellular matrix (ECM) of bone and cartilage. [38] Several chitosan scaffolds were already developed for bone tissue engineering applications. However, both mechanical and biological properties still need improvements. [38]

Collagen is another example of a natural polymer with potential use as a material device in BTE. It represents 89 % of the organic matrix and 32 % of the volumetric composition of bone. Because it has ductile properties and excellent biocompatible properties, it is a good solution in tissue engineering and repair, since its usage can help to increase the characteristic poor fracture toughness of ceramics. Furthermore, collagen has the advantage of being able to self-assemble with hydroxyapatite in a bone-like structure. [63]

Despite the challenge that relies in creating nanodevices and materials that are able to regenerate bone, some special points must be considered. As in every other biomaterial, the influence of the topography on the host tissue response is one of the most important concerns during the design and manufacture of a biomaterial.[64-66] Moreover, a biomaterial aiming to be applied for bone regeneration must be based on the following important features: Biocompatibility with bone cells; Bioactivity/Promotion of hydroxyapatite mineralization and osseointegration; Suitable mechanical properties/Support of the formation of natural bone; Biodegradability. They need also to provide adequate mechanical support regarding the function of the bone and respecting the overall hierarchy, and interactions between the natural stiff inorganic (mineral apatite) crystals and the soft organic (collagen) layers. [18, 21, 67, 68]

Biomimetic mineralization relays on the use of organic molecules to prepare inorganic crystals with ordered structures seldom found in natural minerals. [69] Some examples of minerals synthesized via biomimetic mineralization are: $CaCO_3$, [70] $BaSO_4$, $BaCO_3$, [71] and hydroxyapatite. Organic additives are used as templates. They are vital in biomimetic mineralization as they determine the morphologies and properties of mineral crystals. [69]

In the next section several nanodevices developed for BTE applications, and somehow inspired by the mineralization process will be presented, as well as the rational behind their development.

2. Nanoscale-design

2.1. Materials and techniques

Whether a bone defect is going to be repaired with an orthopedic implant or with a tissue engineered construct, its success will always be determined by the biomaterial choice. This happens because, as was already mentioned, the most important requirement on BTE is assuring an immediate interaction between the biomaterial and the host tissue. [72] Traditional materials such as ceramics, metals and polymers, already used in BTE, are being now reinvented at the nanoscale and adapted to meet specific targets and functionalities, such as delivery systems of drugs and proteins or matrices for bone cells regulation. [73]

Commonly, the concept "nanomaterial" refers to materials with a nano-sized topography or composed of nano-sized basic units comprising dimensions in the scale range of 1 to 100 nm. These will include nanostructured materials, nanocrystals, nanocoatings, nanoparticles and nanofibers all of them based respectively on basic components, grain sizes, individual layers, particles and fibers within the range of 1-100 nm. [72]

Surface properties such as roughness, charge, chemistry and wettability are crucial for healthy functionality of the general cellular system and will influence protein adsorption. [72, 74] Since nanoscale protein interactions are essential to control cell functions such as proliferation, migration, and ECM production, it is advantageous to optimize these interactions by tailoring the biomaterial´s surface. [72, 75]

Current techniques for producing hierarchical structures for mineralization at the macroscale include electrospinning, [76] directional freezing, [77-79] and biotemplating, [80]. However, the majority of these techniques fail to orientate the nucleation of hydroxyapatite.

New approaches and methodologies aiming to mimic bone are now arising. In the production of BTE nanostructures, several techniques are used. Vapor-liquid-solid method, [81] thermal evaporation, [82] controlled precipitation, [83] sol-gel route, microemulsions, [84] template and biomimetic synthesis, [85] flame spray, [86] gas aggregation, [87] dip coating and spin coating [88]. In the special case of strategies to produce micro/nanomaterials with multilevel structures, one can find self-assembly, [89] template synthesis, [90] Ostwald ripening or Kirkendall effect, [91] and evaporation induced self-assembly (EISA) [92]. Other strategies may be used to extend the efficiency of the engineered structures. For instances, layer-by-layer can be used to include functional components, such as BMPs, into the developed nanodevices. [93, 94] Furthermore, recreation of the cellular microenvironment through the production of ECM by cells seeded on the implanted constructs is also possible. [18, 95]

Sol-gel processing has an inherent flexibility that makes it a proper technique for producing nanostructures typically in the order of a few nanometers in size. Besides the possibility of setting the desired stoichiometric chemical composition, the obtained compounds will have compositional homogeneity at a molecular level and a sol stability conferred by electrostatic stabilization. [88, 96] Above all, sol-gel processing offers many advantages for the processing of materials such as organic-inorganic hybrids, nanocomposites, and coatings on complex patterned surfaces, making this process very popular for BTE applications. [88]

The multitude of properties resulting from the conjugation of the above mentioned techniques, result in complex structures that broadens their potential applications and successfully address the demanding BTE requirements.

2.2. Nanoparticles

Due to their size and easy dispersability, nanoparticles can be applied in a multitude of already existing biomedical devices and strategies, enhancing mechanical properties and increasing or attributing the bioactive character of the material, or even both. Nanoparticles may also work as an independent nanodevice, in applications such as nanocarriers. Moreo-

ver, the wide variety of core materials available, coupled with tunable surface properties, make nanoparticles an excellent platform for a broad range of biomedical applications. [97]

Bioactive nanoparticles are often based on ceramics, due to the common ability of these materials to induce hydroxyapatite precipitation. Several preparation methods are commonly followed to synthetize inorganic nanoparticles, namely controlled precipitation, sol-gel technique, microemulsions, template synthesis and biomimetic synthesis. [85] Physical methods as flame spray [86] and gas aggregation source are also used [87].

It is extremely important that the chosen method allows for composition, shape, size, and aggregation control in order to assure that the developed particles meet the application requirements. [98] Commonly, solution based synthesis are chosen to synthetize nanoparticles, since a more accurate control of the stoichiometry is achieved. [85]

Inorganic nanoparticles have been used in combination with polymeric matrixes to develop new biomaterials, that provide a microenvironment that more closely mimics natural bone tissue physiology, namely nanofiber composites, layer-by-layer coatings, scaffolds, injectable materials and imprinting towards the creating of patterned bioactive surfaces. [10, 59] The resulting nanodevices are valuable alternatives to the original approach of using ceramic blocks to fill bone defects. Moreover, the development of polymer/inorganic hybrids has been recognized as a strategy to improve the mechanical behavior of ceramic-based materials. Compared with microsized bioactive ceramic particles, nanosized particles have a larger surface area and can form a tighter interface with polymer matrix in composites, resulting thus in better mechanical properties. Moreover, the high specific surface area of nanoceramics allows not only for a faster release of ions but also a higher protein adsorption and thus bioactivity will also be increased. [99, 100]

Silica is an abundant biocontaminant with high biocompatibility, commonly designed in nanoparticles. For instances, monodispersed, spherical silica nanoparticles may be synthesized at room temperature (RT) by the hydrolysis of tetramethyl orthosilicate (TMOS) in alcohol media under catalysis by ammonia. [101] Xu *et al* prepared polyethylene glycol (PEG)-coated silica nanoparticles with sizes ranging from about 50-350 nm in diameter using this methodology. These nanoparticles, being able to encapsulate certain reagents in their matrixes, were found suitable for biomedical applications, namely *in vivo* diagnosis, analysis, and measurements. [101]

Silica nanoparticles were reported as having inhibitory effects on osteoclasts and stimulatory effects on osteoblasts, *in vitro*. [102] The mechanism of bioactivity is a consequence of an intrinsic capacity to antagonize activation of NF-κB, a signal transduction pathway required for osteoclastic bone resorption but inhibitory to osteoblastic bone formation. Therefore, it was possible to demonstrate that silica nanoparticles promote a significant enhancement of bone mineral density in mice *in vivo*, providing evidences for the potential application of silica nanoparticles as a pharmacological agent to enhance bone mineral density and protect against bone fracture. [102]

One popular example of a material successfully synthetized in the form of nanoparticles, also having a silica base, is bioactive glass. Nanoscale bioactive glasses have been gaining attention due to their superior osteoconductivity and cytocompatibility when compared to micro bioactive glass materials. [62, 86] Bioactive glasses are the gold standard material for bone regeneration. It consists of a silicate network incorporating sodium, calcium and phosphorus in different relative proportions. [62] It is known that the therapeutic effect of bioactive glasses arises from the influence of soluble calcium and silicate species on the genetic expression of osteoprogenitor cells. [103] Bioactive glass can promote the proliferation and activity of fibroblasts and accelerate the process of vascularization, facilitating the healing of skin wounds. [104] Due to their high surface area, bioactive glass nanoparticles (BG-NPs) have enhanced dissolution. This could cause an undesirable increase in Ca^{2+} ions in culture medium, since the increased intracellular Ca^{2+} ions level may induce apoptosis of the cells. However, this drawback was not reported so far indicating that the BG-NPs are biocompatible. [105-107] Preparation methods of nanosized bioactive glasses are similar to the ones used for the general inorganic nanoparticles.

The first work mentioning the preparation of BG-NPs was from Xia and Chang [108] in 2007. They developed a quick alkali-mediated sol-gel method to obtain 20-40 nm sized particles, being the size in this range controlled through addition of ammonia solution. The obtained particles are depicted in figure I.3. The gelation time was around 2 min, and decreased with the increase of the concentration of the ammonia solution. Calcination of gel powders was done at 600 °C, being the final powder an amorphous glass. [108]
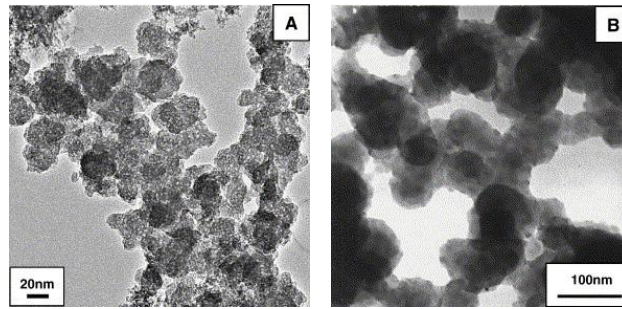
Fig. I. 3. TEM images of calcinated BG-NPs.

(A): Nanoparticles prepared using 1 M ammonia solution; (B) Nanoparticles prepared using 2 M ammonia solution. Reproduced with permission from [108].

In the meanwhile Vollenweider *et al* [109] developed also BG-NPs but this time the 20 to 50 nm diameter particles were obtained by flame spray synthesis. The authors then treated demineralized human dentin with the obtained nanoparticles and compared the remineralization potential of the nanosized particles with a micrometer-sized, commercial reference material (PerioGlas). The substantially higher remineralization rate induced by nanometer-sized vs. micrometric bioactive glass particles confirmed the importance of particle size in clinical bioglass applications. [109]

Misra *et al* [55] performed a study were they also compared the influence of using bioactive glass micro particles versus nanoparticles in a composite based on poly(3hydroxybutyrate) (P(3HB)). The micro particles were melt-derived while the nanoparticles were flame spray synthesized. Changes on structural, thermal, and mechanical properties of P(3HB)/bioactive glass composites were investigated and the results confirmed that the addition of nanosized bioactive glass particles had a more significant beneficial effect on the mechanical and structural properties of a composite system in comparison with microparticles, as well as enhancing protein adsorption, two desirable effects for the application of the composites in tissue engineering. [55]

In order to develop BG-NPs with improved dispersibility, Hong *et al* [110] added an innovation to the sol-gel synthesis of bioactive-glass nanoparticles. SiO_2-CaO-P_2O_5 ternary BG-NPs with 30-100 nm in diameter were obtained via the combination of sol-gel and coprecipitation methods. The precursors were hydrolyzed in acidic condition and subsequently condensed and precipitated in an alkaline solution. The great advantage of this method is that the agglomeration of nanoparticles via the linkage of H_2O molecules during

the drying process is inhibited by lyophilization of the gel particles. After calcination, a well dispersed bioactive glass nanoparticle can be obtained without grinding and sieving, lowering thereby production costs. [110]

Nanoparticles are often used as nanofillers. However, their shape may influence the final mechanical properties of the materials. For instances, it was reported that needle-like or short-fiber inorganic particles can improve the mechanical performance of polymer-inorganic composites much more effectively than spherical fillers. [111, 112] Therefore, Hong *et al* [113] developed rice-shaped particle with the composition SiO_2 - CaO - P_2O_5 ≈ 6:74:20 (mol). The size distribution of the rice-shaped nanoparticles was quite narrow with most of the particles having around 70 nm in diameter and 215 nm in length. [113] An *in vitro* investigation with MG-63 osteoblast-like cells revealed a high cytocompatibility of such BG-NPs compared with the microsized ones. [86]

Nanofillers shape is not the only property that needs to be addressed. Several studies are being conducted in order to better understand the influence of characteristics as composition, preparation conditions and size of BG-NPs.

Luz *et al* [107] compared the bioactive behavior of BG-NPs from the binary (SiO_2-CaO) and ternary (SiO_2-CaO-P_2O_5) systems. They concluded that the best bioactivity results are not only related to the composition but also with the preparation conditions. BG-NPs from the ternary system have more bioactive character than BG-NPs from the binary one. Moreover, the sol-gel pH also influences the final bioactivity of the particles. Higher preparation pHs bioactivity in particles, as well as the heat treatment. This happens due to the increasing amorphousness of the samples when submitted to these conditions. On the other hand, a higher crystallinity may lower the dissolution rate to ineffective values. [107] Nevertheless, binary bioactive glasses with the composition SiO_2-CaO are still bioactive and possess desirable biological properties. Bioactive glasses offer the possibility of easily adapting their composition to meet specific needs. Some works showed that doping bioactive glasses with different ions can add value to these materials. [114] For instance, magnesium, one of the main substitutes for calcium in biological apatite, [115] when included in the bioactive glasses formulation, can enhance osteoblastic adhesion. [116, 117] Other elements were also already used to dope bioactive glass, namely Sr, which is known to enhance osteoblastic differentiation [118] and Ag_2O which confers bacteriostatic and bactericidal properties to bioactive glass [119]. Also the processes leading to the formation of different

nanoparticles need to be fully understood in order to control their morphology and both chemistry and physical behavior. The impact of the nano-size of these inorganic structures is also being studied.

Hong *et al* studied the effect of bioactive glass on the biomechanical properties of various mammalian cells. By recurring to atomic force microscopy (AFM) for measuring the biomechanical properties of mammalian cells, they concluded that binary BG-NPs can significantly decrease the plasma membrane stiffness of bone marrow stem cells. However, when the study was conducted with bovine aortic endothelial cells, the stiffness was increased and the elongation of the cells was stimulated forming endothelial networks. These results indicate that the vascularization process may be facilitated due to the implantation of BG-NPs. [105]

Research regarding the optimization of BG-NPs is still being done in order to overcome some limitations mostly related to morphology control and aggregation issues. For instances, BG-NPs (Si:P:Ca = 29:13:58 weight ratio) of about 40 nm diameter were prepared via the sol-gel method an then low-molecular-weight PLLA was successfully grafted onto the surface of BG-NPs nanoparticles via the coupling of diisocyanate. The aim was to improve the phase compatibility between the polymer and the inorganic phase. [51]

El-Kady *et al* [50] used a modified alkali-mediated sol-gel route to obtain BG-NPs. The modified sol-gel method resulted in a reduction of the gelation time to about a minute rather than days as in the traditional sol-gel process. Furthermore, fast gelation prevented the aggregation and growth of colloidal particles to sizes larger than 100 nm. The proposed method is thus capable of delivering nanoparticles of sizes less than 100 nm with minimum agglomeration. [50]

The polyvalence of nanoparticles in BTE was already mentioned. They can be used in multitude of applications, and due to their reactivity resulting from the nanoscale dimensions, simple approaches may have great results.

Recently, Luz *et al* [92], inspired on colloidal crystals, used BG-NPs as building blocks for the construction of hierarchical organized structures by self-assembly. In a very simple strategy, drops of BG-NPs aqueous suspensions were left to evaporate on biomimetic superhydrophobic surfaces. The crystallization degree of the structures was controlled by the evaporation rates taking place at RT or at 4°C. Spherical aggregates were obtained with a hierarchical ordered morphology from nano- to micro- and macroscale. The crystallization

degree of the structures influenced the Ca/P ratio of the apatitic film formed at their surface, after 7 days of immersion in SBF. This allows the regulation of bioactive properties and the ability to release potential additives that could be also incorporated in such particles with a high efficiency. The impact of such technology is high, allowing the production of microspheres with biomedical applications using a highly competitive method against other existing technologies until now. [92]

Metals processed at the nanoscale may also be useful in biomedical applications. [97] For instances, silver is known to have an antibacterial action, representing thereby a good solution to the infections on the surface of implants, one of the main problems in reaching a suitable level of osseointegration. [121] Hydroxyapatite/silver nanocomposites have already been designed to accomplish this aim. [121] The combination of the bioactivity of the ceramic matrix with the biocide activity of the silver nanoparticles gives these nanocomposites an interesting range of applications in BTE. [121]

Finally, still regarding nanoparticles for BTE, a new class of biomaterials with additional functionalities targeting the bone must be mentioned.

Magnetic properties are being included in bone related biomaterials in order to enhance the therapeutic potential of novel nanodevices. The combination of magnetic properties with biocompatible composition is considered to open the door to new biofunctional nanomaterials with broaden action on repairing bone injuries while healing it. Magnetic nanoparticles, normally iron oxide nanoparticles, are used for *in vivo* biomedical applications in areas related to therapeutic (hyperthermia and drug-targeting) and diagnostic applications (nuclear magnetic resonance imaging). [122-124] A remarkable advantage of this type of systems comprising magnetic nanomaterials is the possibility to use external magnetic fields to guide the drug carriers to precisely target areas of the body with minimal or non-invasive methods. [125] Regarding cancer treatment, hyperthermia consists of heating tumors up to temperatures between 43 and 47°C. Within this interval, the malignant cells are selectively destroyed whereas the healthy ones only undergo small and/or reversible damage. [126] The use of biomaterials as implantable thermoseeds is a very interesting methodology to focus the heat into the target region without overheating the surrounding healthy tissues. [126]

Specifically for bone repair and related cancer therapy, the materials and carriers should be biocompatible with bone, such as the cases of hydroxyapatite and bioactive glass-

es. Ruiz-Hernandez *et al* [126] were the first to run hyperthermia heating experiments as well as preliminary biocompatibility assays for bioactive glass implantable thermoseeds. They concluded that the presence of sol-gel glass modifies the magnetic properties, improving the heating power. The ability to reach hyperthermic temperature range together with the bioactive behavior makes bioactive glass a very promising candidate for bone cancer treatment. [126]

Either based on ceramic, polymeric or metallic compositions, nanoparticles play an increasingly important role in nanomedicine and in BTE in particular. Efforts are already being made in order to move a step further regarding the optimization of these polyvalent nanodevices.

Nanoparticles surfaces are now being engineered in a mimicking strategy aiming to overcome the body´s physiological barriers. Nanoparticles used for multimodal diagnostics and for target-specific drug/gene delivery applications are covered with biomolecules that mimic the ones present on the cell membrane, such as proteins, peptides, and carbohydrates. These strategies assure that upon injection in the blood stream or following oral administration, the nanoparticles will reach the intended target. [127]

Clinically, the use of nanoparticles *in vivo* is mainly related to bioimaging and therapy. In order for BTE nanodevices to be successfully implanted *in vivo*, aspects such as bioconjugation and nanotoxicity need to be explored. [128]. Nanoparticles can offer a multitude of functionalities due to the possibility of controlling their dimensions, morphology and composition. Hence, they are good candidates for a promising avenue in BTE research.

2.3. Nanofibers and Nanotubes

Nanofibers are often used in the preparation of scaffolds for BTE. The rationale for using nanofibers is related to the theory that cells attach and organize well around fibers with diameters smaller than the diameter of the cells. [28] In fact, it has been reported that cells might migrate through fibrous matrices by pushing the fibers aside. [72] Therefore, materials offering low resistance to the amoeboid movement of the cells, such as nanoscale fibers are more suitable for promoting cell migration. [129] Moreover, nanofibers can mimic the physical structure of the major constructive elements in the native ECM. [130, 131]

Nanofibers are normally produced by electrospinning. Briefly, a high voltage is applied to the polymer solution to draw out nanofibers that are then collected on a ground plate in the form of a mesh. Nanofibers can be cross-linked in order to adjust solubility or mechanical properties. They can also be modified in order to increase their biocompatibility or bioactivity. Nanofibers may be also produced by self-assembly. Collagen fibrils of bone itself are formed by self-assembly of the collagen triple helices and the hydroxyapatite crystals. The hydroxyapatite crystals grow within these fibrils in such a way that their c axes are oriented along the long axes of the fibrils. [132]

There are several examples in the literature of the application of self-assembly phenomena to the production of nanofibers resembling the ones existing in ECM.

Fischer *et al* [133] chose collagen and hyaluronic acid as polymers for constructing a nanofiber mesh based scaffold because they are the main components of the ECM and have been utilized in electrospinning. The collagen/hyaluronic acid meshes were cross-linked to render them insoluble and conjugated with gold nanoparticles to promote biocompatibility. The results showed that the produced scaffolds were successful in promoting cellular attachment, being thereby a suitable choice for a tissue engineered solution to promote cell growth. [133]

Hartgerink *et al.* [134] described a self-assembly based method for producing a nanostructured fibrous scaffold resembling the ECM. The work was based on the self-assembly of a peptide-amphiphile via a pH-controlled and reversible mechanism. The design of this peptide-amphiphile allows the nanofibers to be reversibly cross-linked to enhance or decrease their structural integrity. After cross-linking, they are capable of nucleating hydroxyapatite in an alignment similar to that observed at the lowest level of hierarchical organization of bone in that the crystallographic *c* axis of hydroxyapatite is oriented along the long axis of the organic fibers. [134] Figure I.4. shows the evidences of mineralization of the fibers.
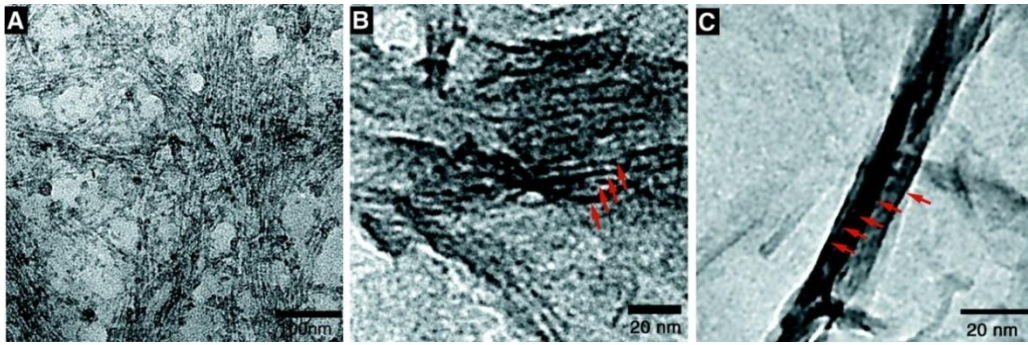
Fig. I. 4. TEM micrographs of the cross-linked peptide-amphiphile fibers.

(**a**) Incubated for 10 min in $CaCl_2$ and Na_2HPO_4 solution. (**b**) After 20 min, forming hydroxyapatite crystals (red arrows) are observed in parallel arrays on some of the peptide-amphiphile fibers. (**c**) After 30 min, mature hydroxyapatite crystals (red arrows) completely cover the peptide-amphiphile fibers. Reproduced with permission from [134].

Also, injectable scaffolds with controllable release are possible. Hosseinkhani *et al* [135] produced a 3D scaffold by mixing a peptide-amphiphile aqueous solution with BMP-2 suspension. A 3D network of nanofibers was formed with an extremely high aspect ratio and high surface areas. *In vivo* release profile of BMP-2 from 3D network of nanofibers was investigated. It was demonstrated that the subcutaneous injection of an aqueous solution of peptide-amphiphile together with BMP-2 in rats, resulted in the formation of a transparent 3D hydrogel at the injected site and induced significant homogeneous ectopic bone formation around that area in marked contrast to BMP-2 injection alone or peptide-amphiphile injection alone. This kind of strategy represents a promising procedure to improve tissue regeneration. [135]

Electrospinning is also an effective way of producing controllable nanofibers for BTE. [136] By adjusting both concentration and feeding rate, it is possible to influence bioactivity. [137] This technique may be applied not only to pure polymeric solutions, but also to produce inorganic based nanofibers. [137]

Chen *et al* [137] used electrospinning method to prepare bioactive TiO_2 fibers films. An acetic acid/ethanol/tetrabutyltitanate/polyvinylpyrrolidone solvent system was used as precursor for the electrospinning. The TiO_2 fiber structures (including its fiber diameter, morphology, and phase composition) could be controlled by changing feeding rate, precur-

sor concentration and sintering temperature, proving that the electrospinning method is an effective way to prepare bioactive TiO_2 fiber films. [137]

Nanotubes may also be prepared by electrospinning using a polymeric sacrificial template that will be later sacrificed by a heat-treatment after proper cover of the desired material. Mi-Kyung *et al* [138] used a nanofiber mesh of a polymer (polycaprolactone) as a template that was mineralized within solutions via a biomimetic process. A subsequent heat-treatment (over 500 °C) completely eliminated the inner polymer, resulting in preserving the surface mineral phase in the form of nanotubes with diameters of hundreds of nanometers with nonwoven mesh, replicating the initial nanofiber template. [138]

Also, polycaprolactone nanowires were synthesized through template synthesis. The *in vitro* tests showed enhanced biological response. [90]

Researchers are now exploring nanofibers in a multitude of forms that can be used in bone related applications. For instances, magnetic properties were attributed to hydroxyapatite nanotubes by embedding magnetic nanoparticles within the inorganic tubes. [73] The magnetic hydroxyapatite nanotubes were produced using a template made of magnetite nanoparticles/ polycaprolactone and later they underwent surface mineralization and thermal treatment.

Also, Zhao *et al*, [139] used single-walled carbon nanotubes as a scaffold for the growth of artificial bone material. The tubes were chemically functionalized with phosphonates and poly(aminobenzene sulfonic acid). The negatively charged functional groups on the nanotubes attracted the calcium cations and lead to self-assembly of hydroxyapatite and well-aligned plate-shaped hydroxyapatite crystals with 3nm thickness were obtained after 14 days of mineralization. [139]

As already mentioned, at the smallest length scale of bone, collagen triple helices spontaneously form nanoscale bundles, which act as a template for the crystallization of hydroxyapatite nanocrystals. Researchers are making an effort to produce nanofibers able to mimic bone structure while maintaining the ability of inducing crystal nucleation and growth of hydroxyapatite. Although this strategy represents a good approach to follow, and despite the good results already obtained, there are still good opportunities for optimization.

2.4.   Nanopatterns

At the nanolevel, every aspect of the biointerface of the biomaterial surface will have a considerable effect on the desired cellular response. Therefore, it would be of great value if researchers could control the chemical and physical characteristics at the material´s surface. Nanopatterns have been created in order to control cell interactions with surface by means of an imposed pattern with controlled geometry and periodicity. Specific cellular responses may then be targeted. [43]

Despite its significance, just a few works regarding mineralized patterns have been produced till the date.

Ozawa and Yao [140] were the first to create mineralizable patterns at the microscale. They presented two different methods for the formation of an apatite micropattern by a combination of a biomimetic process and transcription of a resist pattern. These two kinds of strategies for forming apatite micropatterns are applicable for the development of various smart biomaterials, such as cellular biosensing devices, by combining the bioaffinity of apatite with properties of other functional materials at the microscale. However, one can go even further and produce micropatterns based on bioactive nanoparticles.

Tan *et al* [43] inspired by natural mineralization process created a material with a complex structural form in which a nanometer scale mineral phase is organized in a controlled fashion on a micrometer scale template that is preset by a controllable microfabrication process. The micrometer scale structures were created using photolithography and reactive ion etching techniques. Acidic moieties were generated on the surface through silanization and succinylation. Later, a layer of nanostructured calcium phosphate was formed on the patterned surface in supersaturated calcium phosphate solution. The developed materials were biocompatible with bone cells, inducing a range of desirable cellular responses. [43]

Shi *et al* [41] produced smart surfaces capable of controlling and triggering the occurrence of biomineralization in biodegradable substrates. The bioactive substrates were prepared from poly(L-lactic acid) and reinforced with Bioglass®. A hollowed polycarbonate mask was used to expose only certain regions of the substrate surface to plasma treatment, allowing for the insertion of poly(N-isopropylacrylamide) (PNIPAAm) into specifically desig-

nated areas creating therefore a mineralizable pattern. It is found that such treatment, together with temperature, could trigger the formation of apatite on the biodegradable substrate upon immersion in SBF above the PNIPAAm lower critical solution temperature. On the other hand, no apatite is formed at RT. A control experiment on a material that is not subjected to surface treatment does not show any evidence of mineral deposition at the two analyzed temperatures. By patterning the surface, it was possible to merge the temperature switching and spatial control of biomimetic apatite formation. This concept could also extend to the biomimetic production of other minerals, where it would be triggered by another kind of stimulus (e.g., pH or ionic strength) in substrates with more complex geometries. [12]

Luz *et al* [141] showed how bioactive nanoparticles may be easily patterned on a surface by micro contact printing. This technique allowed the creation of a mineralizable pattern on a chitosan membrane using a poly(dimethylsiloxane) (PDMS) stamp inked in a BG-NPs pad. [141] This membrane was then immersed in SBF and an apatitic pattern was created. Cells were also cultured on these membranes and results showed that L929 cells replicated the initial inorganic pattern preferring the environment created by the BG-NPs ionic release rather than migrating to chitosan. Depending on the nanoparticles chemistry and on the pattern created, cellular response can be directed and studied at the nanoscale. In addition to the opportunity to study cell behavior when exposed to mineralizable nanoparticles, this work opens new possibilities of potential applications, not only in BTE, but also in guided tissue regeneration for skin and osteochondral areas and also in angiogenesis. [141]

It is already known that nanometer features tightly control osteoblast behavior. [142] Therefore, it would be also desirable that non mineralizable substrates could be also successfully patterned at the nanoscale for BTE applications.

Lamers *et al* [142] evaluated the role of different nanometer features, like (an)isotropy, pattern depth, width and spacing on (initial) cellular behavior by using a very high throughput biochip. They observed that isotropic nanosquares do not induce morphological changes on osteoblasts, but they specifically enhance motility up to a maximum at a pattern spacing of 400 nm. These results are summarized on figure I.5.
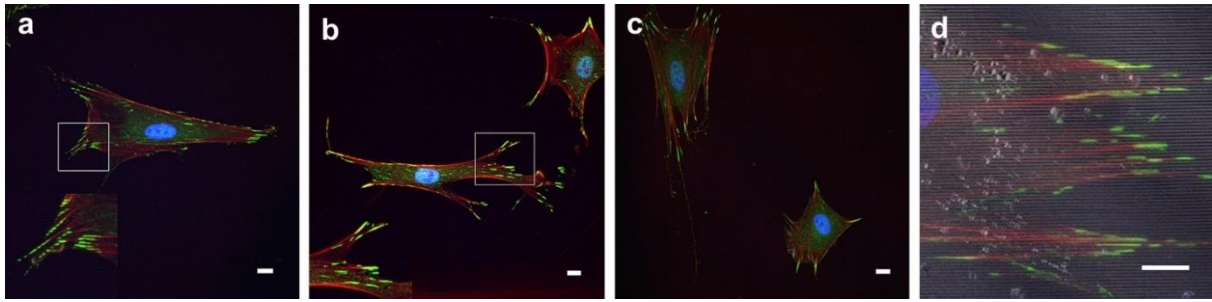
Fig. I. 5. Immunofluorescence micrograph of osteoblast-like cells cultured on nanogrooved substrates. Focal adhesions (α-vinculin, green) on a groove width of **(a)** 500 nm (153 nm depth) were mostly aligned with the groove direction, whereas alignment of focal adhesions to a groove width of **(b)** 150 nm (120 nm depth) had diminished and was random on a groove width of **(c)** 50 nm (17 nm depth). **(d)** An overlay of a fluorescent micrograph with a light micrograph. α-Vinculin staining on a width of 300 nm (158 nm depth) shows that focal adhesions mainly reside on top of the ridges. Green, vinculin; red, F-actin; blue, nuclei. Bars: 10 μm. Reproduced with permission from [142].

Puckett *et al* [143, 144] were also able to control the osteoblastic alignment on nanopatterned titanium. They showed that the orientation of the nanosurface coating of metal implants is also an important parameter when trying to enhance the osteoblastic adhesion. Osteoblast functions where studied on nanopatterned titanium substrates created by electron beam evaporation as a means to control the direction of bone growth. These patterns appear to better promote bone cell functions more similar to long bones of the body. As a result of mimicking the structure and properties of bone, initial formation of anisotropic bone upon implantation could occur. [144]

Other works show that the grafting of titanium bone implants with nanoparticles containing Arg-Gly-Asp-Cys peptide (RGDC) improves the adhesion behavior of cells seeded on these materials. [145]

Li *et al* [146] developed a novel method that allows the easy deposition of a wide variety of predetermined topographical geometries of nanoparticles of a bioactive material on both metallic and non-metallic surfaces. Using different mesh sizes and geometries of a gold template, hydroxyapatite nanoparticles suspended in ethanol have been electrohydrodynamically sprayed on titanium and glass substrates under carefully designed electric field conditions. Thus, different topographies, e.g. hexagonal, line and square, from

hydroxyapatite nanoparticles were created on these substrates. The thickness of the topography could be controlled by varying the spraying time. [146]

By precisely controlling material structures on both micrometer and nanometer length scale by using patterning techniques, researchers have proved that it is possible to create new materials with direct application in BTE. Moreover, the developed techniques can be extrapolated to all the classes of biomedical materials, namely polymers, metals, ceramics or hybrid combinations.

The obtained knowledge can aid the further development of smart surfaces that control cell behavior and account for improved osseointegration around orthopedic and dental implants. [142]

2.5. Drug delivery systems

Bacterial infection commonly occurs after orthopedic surgeries. The administration of antibiotics by oral or intravenous via presents several drawbacks, such as systemic toxicity and limited bioavailability. Targeted drug delivery systems for local delivery at the site of the implantation offer great advantage in the orthopedic field. [147]

Nanostructures, in particular nanoparticles may act as suitable and promising drug delivery systems due to their ability of enhancing endocytosis of drugs by targeting cells and also by facilitating capillary penetration. [97, 148]

The efficacy of drug delivery systems based on nanostructures may address some issues related to the properties of currently used drugs, namely solubility, *in vivo* stability, pharmacokinetics, and biodistribution. [97] Nevertheless, drug delivery systems are experiencing great progresses in the past few years. Researchers are developing ways to use internal stimuli to control drug release instead of external ones in order to avoid cell damage. [149-153] For instances, these kind of systems allow the release of drugs when exposed to the acidic pHs of cancer cells lysosomes, integrating targeted drug delivery with internal stimulus induced self-release.

Although drug delivery has been a polymer-dominated field, the blossoming of nanotechnology means that ceramic materials are now showing much promise for numerous drug delivery applications. [148]

Ceramic nanodevices present some useful characteristics not shared by their polymer-based homologous. First, they usually have longer biodegradation times and are slowly degradable, meaning that it is easier to control drug release kinetics and also to retain drugs for longer times after administration. Also, the small swelling ratios of ceramics prevent the release of a high amount of drugs as is commonly seen in polymeric hydrogels, such as poly(2-hydroxyethyl methacrylate) drug-delivery systems. [148] Since ceramics are normally bioactive, they can be of an extraordinary value when approaching drug delivery especially targeted for bone.

Merging drug delivery science with BTE may bring outstanding results for this field. Mineralization at the nanoscale can be used as an ingenious way to control both particles structure by reinforcement and the drug release by controlling the dissolution. Some examples found in the literature indicate that drug delivery is being associated with mineralization and bone regeneration.

Min *et al* [154] developed micelles with a core-shell-corona structure that in the aqueous phase provided the three distinct functional domains: an hydrated poly(ethylene glycol) outer corona for prolonged circulation, the anionic poly(L-aspartic acid) middle shell for calcium phosphate mineralization, and the hydrophobic poly(L-phenylalanine) inner core for doxorubicin loading. The doxorubicin release from the doxorubicin-loaded mineralized micelles at physiological pH was efficiently inhibited, whereas at an endosomal pH (pH 4.5), doxorubicin release was facilitated due to the rapid dissolution of the calcium phosphate mineral layers in the middle shell domains. The calcium phosphate mineralization on assembled nanoparticles may serve as a useful guide for enhancing the antitumor therapeutic efficacy of various polymer micelles and nanoaggregates. [154]

Another *in-situ* biomineralization approach leads to the production of poly(*N*-isopropylacrylamide) and calcium phosphates hybrid nanocomposites. [155] Biomimetic self-assembly enabled the interaction between PAA and Ca^{2+} leading to the formation of a homogeneous and robust nanocomposite. Smart drug release was possible since the nanocomposites were pH- and thermal-responsive. The introduction of calcium phosphates nanocrystallines decreases the permeation of the encapsulated drug effectively. [155]

In another work, [156] titanium was anodized to possess nanotubular surface structures suitable for drug delivery. The nanotubes were 200 nm deep and had 80 nm of inner diameter. These surfaces were able to promote bone cell functions (such as adhesion and

differentiation) *in vitro* and *in vivo* compared with unanodized titanium. In order to test local drug delivery, anodized titanium with nanotubular structures were loaded with penicillin-based antibiotics using a co-precipitation method in which drug molecules were mixed in SBF to collectively precipitate with calcium phosphate crystals. Results showed for the first time that such co-precipitated coatings on anodized nanotubular titanium could release drug molecules for up to three weeks whereas previous studies have demonstrated only a 150 min release of antibiotics through simple physical adsorption. These findings represent a promising surface treatment for titanium that could be used for local drug delivery for improving orthopedic applications. [156]

Also, TiO_2 nanotubes filled with gentamicin were able to reduce bacterial adhesion on their surface while still being able to enhance osteoblast differentiation. [147] The results related to this experiment are presented on figure I.6.
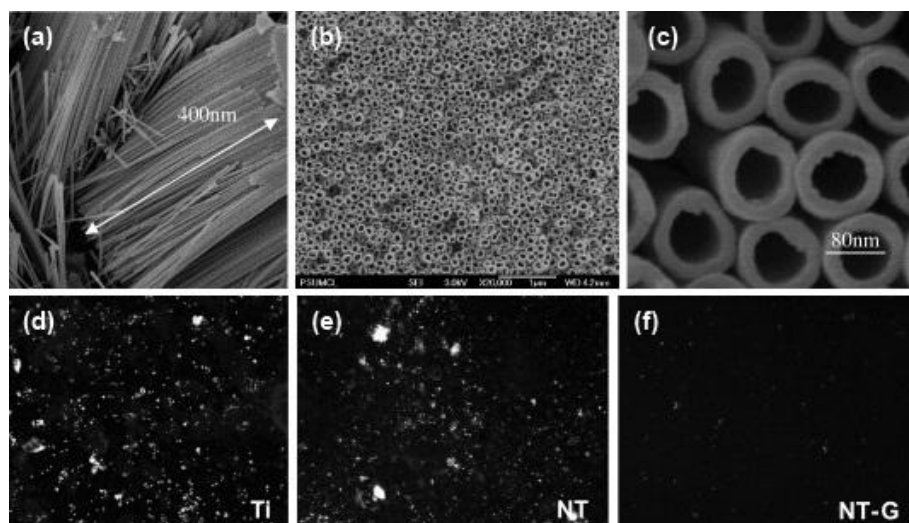
Fig. I. 6. SEM images of titania nanotubular surfaces and fluorescence images of bacterias cultured on titanium surfaces.

(a) cross-sectional view of mechanically fractured sample showing that the length of the tubes is approximately 400 nm; **(b)** Top view of nanotubular surface; **(c)** High magnification top view of nanotubular surface showing the tube diameter of approximately 80 nm. Figures **(d)**, **(e)** and **(f)** show fluorescence microscope images of bacteria stained with Syto 9 after 1 h of culture on titanium **(d)**, nanotubes **(e)** and nanotubes filled with gentamicin **(f)**. Reproduced with permission from [147].

A plethora of nanodevices may be used for drug delivery systems in BTE, namely nanoparticles, nanofibers, nanoscaffolds, liposomes, dendrimers and nanogels.

For instances, a nanogel of cholesterol-bearing pullulan in combination with prostaglandin E_2 showed efficacy in inducing new bone formation. [157]

Nanodevices have become excellent platforms to design targeted drug delivery systems for biomedical applications in general. For BTE in particular when bioactive materials like ceramics are chosen, several advantages may be numbered, such as their ability to modulate drug release kinetics, incorporate multifunctional molecules and target specific focus sites. Furthermore, the potential and development of hybrid or composite ceramic-polymer drug delivery systems that incorporate the benefits from other types of materials should not be neglected. [148]

Although some challenges remain, mostly regarding toxicity issues, [158] it is important to continue the effort of understanding the metabolism and elimination routes from the body of drug delivery nanoplatforms in order to guarantee promising avenues to diagnose, understand and treat numerous bone diseases through drug delivery while regenerating the tissue.

2.6.   Nanocomposites

Natural mineralized composites, such as bone, tooth and shells, result from the mixture of two or more phases, where at least one of them is in the nanometer size range. They exhibit ordered, complex, hierarchical microstructures that current man-made composite materials cannot achieve. [2, 159]

Experiments show that the improved strength and toughness of natural biocomposites is caused by a structural and functional organization at different length scales, including a nanometer scale. [160, 161] These characteristics should be taken into account when fabricating bioinspired advanced materials. [79]

It was already shown that ceramics at the nanoscale stimulate the interactions between materials and cells. [105] Inorganic biomaterials present high brittleness. It is therefore difficult to obtain porous scaffolds based solely on pure inorganic materials (such as bioceramics or bioglasses). However, the combination of inorganic nanoparticles or

nanofibers with polymeric systems enables the reinforcement of nanocomposites improving their mechanical properties. Hence, these systems possess the potential to be used in a series of orthopedic applications, including BTE and regeneration. [62] Biopolymers are biodegradable and also contain structural groups similar to natural extracellular components, being thus suitable for implantation in living bodies. [38]

Besides the biodegradability and biocompatibility, nanocomposites for BTE also require an appropriate porous structure and also the ability to induce hydroxyapatite precipitation in SBF solution in order to obtain tissue regeneration from both a chemical and a biological activity. [60]

The choice of the technique used in the production process of the BTE device will be important to direct the final characteristics of the nanocomposites. Techniques such as thermally induced phase-separation method, [49] sol-gel, solvent casting, electrospinning or combinations of more than one technique, such as solid-liquid phase separation method combined with solvent extraction [50] are normally used to produce BTE nanocomposites.

Through freeze-drying, adequate microporosity is assured for cellular migration. [105, 162, 163] Cross-linking can be also used to combine different materials and improve their mechanical properties. For instances, Wang *et al* [164] synthesized a sol-gel derived bioactive nanocomposite containing BG-NPs and phosphatidylserine through cross-linking of collagen and hyaluronic acid by using 1-ethyl-3-(3-dimethylaminopropyl) carbodiimide and N-hydroxysuccinimide. [164]

Self-assembly technique is a very suitable technique for BTE, since bone itself is based on self-assembly of hierarchical structures in collagen matrix, and involves the spontaneous nucleation of Ca/P ions and the oriented array of formed hydroxyapatite crystals on collagen template. [63]

Collagen allows the most successful mimicking approaches. It has been shown to align hydroxyapatite *in vitro* on the nanoscale [165] and has been recently mineralized with macroscopic domains of oriented hydroxyapatite by utilizing its liquid-crystalline behavior. [166]

Recently, Wang *et al* [63] produced a hydroxyapatite/collagen biomimetic nanocomposite prepared through self-assembly. Hydroxyapatite nanocrystals formed as preferentially oriented needles with 50 - 100 nm in length on the collagen fibers matrix. The obtained nanocomposite is analogous in both composition and nanostructured architecture

to native bone. Longer aging time promotes the growth and purification of nano-hydroxyapatite on collagen based on a chemical bonding. [63]

In such a biomimetic physiological environment, calcium phosphates mineralize and nucleate directly on the collagen molecules templates through self-assembly. Hydroxyapatite crystals are oriented in the c-axis direction parallel to the long axis of the collagen fibril via electrostatic interactions between the lateral COO^- in the triple helix structure of collagen and Ca^{2+} in the surface of hydroxyapatite. [63]

Inorganic materials used to reinforce nanocomposites are normally: hydroxyapatite, β-tricalcium phosphate, calcium phosphate and montmorillonite. [38] These materials will also give a bioactive character to the nanocomposites.

A popular nanofiller is BG-NPs. To avoid the possible aggregation of nanoparticles in polymeric matrix due to incompatibility, and negative consequences for the mechanical properties, surface modification of the particles can be done. For instances, low-molecular-weight PLLA was grafted onto the surface of the sol-gel-derived BG-NPs by diisocyanate and the ring-opening polymerization of the L-lactide. [52] By grafting organic molecules on BG-NPs, their dispersion is improved on the polymeric matrix and thereby the mechanical properties did not decrease. [52]

In general, the inclusion of ceramic nanoparticles in a polymeric matrix has positive consequences, namely: alteration of the water uptake and consequently the degradation rate and increasing of the biocompatibility, bioactivity and cytocompatibility. Furthermore, the induction of a nanostructured topography on the surface of the composites improves protein adsorption in comparison to the unfilled polymer and the composites containing micron-sized bioactive glass particles. [55]

Besides 3D porous scaffolds structures, nanocomposites membranes have been also applied in the field of bone tissue regeneration. Specifically, in guided tissue/bone regeneration, membranes are used as barriers to prevent the faster growing soft tissue cells from entering the defect space and to regenerate periodontal ligament, cementum, and bone. Membranes are important for guided tissue regeneration since they can improve healing of surrounding tissues. By directing soft tissue growth, infection will be prevented and repair will be facilitated. [18]

Chitosan/BG-NP composite membranes were developed to be used as barrier membranes to soft tissues with possible applications in periodontal regeneration. [167] It is pos-

sible to target the nanocomposites properties by adjusting the formulations of the inorganic part. Luz *et al* [117] showed this by preparing chitosan nanocomposite membranes using two distinct BG-NPs systems, namely $SiO_2:CaO:P_2O_5(mol.\%)=55:40:5$ and $SiO_2:CaO:P_2O_5:MgO(mol.\%)=64:26:5:5$. [117] The chitosan/Magnesium based nanoparticles composite presented moderate bioactive character. Also, their higher hydrophilicity was found to stimulate a better osteoblastic response towards cellular differentiation and mineralization.

Finally, nanofibers dispersed on a biodegradable polymeric matrix have been also used to reinforce BTE composites. [168]

Regarding the multitude of works that develop nanocomposites for BTE, some conclusions can be drawn. In general, the addition of nanoparticles has a significant stiffening effect on the composite modulus. Surface modification is also useful to establish a deeper bonding between inorganic and organic material, which will also improve the nanocomposite mechanical properties. [51, 52, 55, 169] Interconnected pores [56] with pore sizes in the range 150-500 μm [162] have been obtained. In BTE applications, interconnected pores with interconnection sizes above 300 μm are reported to be necessary to avoid hypoxic conditions and favor osteogenesis. [170]

Nanocomposites represent a viable solution in BTE strategies. By varying parameters such as the polymer cross-link or the size and composition of the nanofillers, it is possible to adapt the composite chemical and physical characteristics to a specific clinical need.

2.7. Nanogels and Injectable Systems

Nanomedicine devices and techniques allow the improvement of minimally invasive procedures that can bring great benefit for the orthopaedic field. Injectable matrixes may also deliver encapsulated cells and bioactive agents.

Particularly targeting the orthopaedic reconstructive and regenerative medicine, Chitosan-β-glycerophosphate salt formulations were mixed with BG-NPs in order to conceive injectable thermo-responsive hydrogels with rheological properties and gelation points adequate for intracorporal injection. *In vitro* bioactivity tests, using incubation protocols in SBF,

allowed the observation of bone-like apatite formation in the hydrogel formulations containing bioactive nanoparticles. [171]

Besides the inclusion of nanoparticles in organic/inorganic nanocomposites, nanoparticles can also work as fillers in a variety of moldable and injectable systems, as bone cements. Calcium phosphate cements possess the advantage of self-hardening to form hydroxyapatite in the bone cavity, avoiding thereby the problem of sintered hydroxyapatite implants that require a perfect match between implant shape and bone defect. [28, 172] Although calcium phosphate based cements present very high osteoconductivity, their brittleness and low strength limit their use to only non-stress bearing locations. [173] Nanoscaled fillers inclusion on these systems may help to improve the composites strength until they match the ones of cortical bone.

Since bone cements under stress can develop cracks, some modifications may be performed in order to precisely tune the mechanical properties of the bone cements. For instances, Xu *et al* [174] fused silica particles with silicon carbide whiskers to roughen the whisker surfaces for enhanced retention in the resin matrix. [173] The strength of the nanocomposites was three times higher than the strength achieved in previous studies for conventional bioactive composites containing hydroxyapatite particles in this type of resins. The mechanical properties of the final composite nearly matched those of cortical bone and trabecular bone. [173]

Stevens *et al* [41] injected calcium-cross-linked alginate gels or modified hyaluronic acid gels into an artificial space between the tibia and the periosteum in rabbit. This stimulated bone and cartilage formation from resident progenitor cells in the inner layer of the periosteum. Injectable systems show that complex tissues can be generated from relatively simple materials by using the body as a bioreactor. [41]

BTE approaches using injectable systems have been developed as a good scaffolding solution for irregularly shaped bone defects or with difficult access. Besides, the advantage of being minimally invasive injectable systems also offers the possibility of being combined with living cells or therapeutic drugs. Hence, they represent a very complete tissue engineering solution.

The development of targeted gels is also important for tissue regeneration because matrix elasticity is sufficient to induce lineage-specific differentiation of progenitor cells. [175] For instances, Discher *et al* [175, 176] showed that the differentiation of human

mesenchymal stem cells is dependent on the 2D matrix elasticity of collagen-coated poly-acrylamide substrates on which they were cultured. The cells grown on moderately firm substrates, with E of 10 kPa, similar to that of muscle, exhibited upregulated myogenic markers, whereas the others proceeded down an osteogenic pathway when cultured on a stiffer substrate (E of 35 kPa, similar to that of crosslinked collagen of osteoids).

Owing to their tissue-like elasticity, PEG-based hydrogels are highly desirable as 3D scaffolds for tissue regeneration. Also, their high permeability can mimic the native ECM. However, their applications are limited by their poor mechanical properties and bioinert nature, which restrict cell adhesion and spreading. To overcome these limitations, a novel hierarchical nanocomposite hydrogel composed of PEG diacrylate and hydroxyl mesoporous silica nanoparticles was developed via *in situ* free-radical polymerization. Structural and physicochemical characterization shows that hydroxyl mesoporous silica nanoparticles act as both reinforcing agents and adhesion sites in the hydrogel system, which significantly enhances mechanical properties and cellular affinity. Due to the anchoring effect of the hydroxyl mesoporous silica nanoparticles, the hybrid hydrogels possessed greatly enhanced mechanical properties as compared to the pure PEG hydrogels. Furthermore, the introduction of hydroxyl mesoporous silica nanoparticles into hydrogel systems may be beneficial for osteogenesis, making these nanocomposite hydrogel a promise scaffold for BTE. [177]

By recurring to injectable systems cells, drugs and molecular signals can be delivered to irregularly shaped bone defects in a minimally invasive manner. These injectable materials can also work as a scaffold especially in locations that are not easily accessible.

2.8. Surfaces functionalization and templating

Many studies claim that the processes of biomineralization initiation and control are based on collagen templates and on the recognition of Ca^{2+} by a variety of noncollagenous biomolecules, [178] such as acidic proteins rich in aspartate, glutamate and its derivative γ-carboxyglutamate, phosphorylated residues such as phosphoserine, [179] and also acidic glycosaminoglycans (GAGs) and other polysaccharides, which are significant bone constituents. [180, 181] Soluble macromolecules interact with the matrix to control mineral deposition, crystal habit, and orientation within a structural framework that acts a template for

nucleation and growth of hydroxyapatite. [182, 183] While biopolymers provide a base for the initial organization of mineral ions into a crystallographic layer, biomolecules are also presumed to play an inhibitory role in mineralization by binding to specific crystal surfaces, thus preventing further growth of that surface. [181, 184] In face of this knowledge, controlled organization of well-defined, bioinspired architectures based on organic-inorganic hybrid materials is of great interest for applications in tissue regeneration. [182]

In an effort to mimic the composition of mineralized tissue in artificial systems, several organic templates have been investigated for their ability to nucleate biological minerals on the nanoscale, including self-assembled monolayers, [11] biopolymers, phospholipids [185] and poly(amino acids). [181] Most of these systems fail to mimic the hierarchical structure of bone, since they are not able to induce the nanoscale crystallographic alignment of hydroxyapatite.

Medical devices able to induce osseointegration regardless of the implantation site, or both bone quantity or quality need to exhibit the right functional groups for apatite nucleation on their surfaces. [10] Some functional groups have been shown to induce bone-like apatite formation, namely Ti-OH, Zr-OH, Nb-OH, Ta-OH, -COOH, Si-OH and PO_4H_2. [10] These groups have in common a negatively charged character, given by the neutral isoelectric points at pH values much lower than 7. They will attract Ca^{2+}, PO_4^{3-} and CO_3^{2-} from the environment forming an amorphous layer that will later crystalize in hydroxyl carbonate apatite with oriented apatite crystals. [11, 186]

Since the ECM, which is responsible for templating hydroxyapatite in mineralized tissues, contains 1D, fiber-like nanostructures, nanodevices mimicking these structures are gathering researcher's attention. For instances, peptide amphiphiles containing a hydrophobic alkyl tail covalently attached to a peptide sequence were recently used to study biomimetic mineralization. [182] In this study the authors showed that the ability to nucleate oriented hydroxyapatite using a fibrous supramolecular template depends strongly on the details of its nanoscale architecture. Mineral oriented relative to the principal axis of the fibers, as it occurs in mammalian bone, were only nucleated on calcium binding nanostructures with curved, cylindrical architectures, and not on chemically similar ones with flat surfaces. When cylindrical nanostructures were part of a hierarchically aligned monodomain gel containing bundles of nanofibers, the ability to nucleate oriented crystals over multiple length scales was maintained. The templates described in this study may also be interesting

to investigate the role of alignment in cell signaling and preparation of therapeutic constructs to promote *in vivo* regeneration of mineralized tissues. [182]

Besides the peptide-based self-assembly approach for designing templates for biomineralization, cylindrical assemblies of filamentous bacteriophage bearing acidic coat proteins have already demonstrated oriented hydroxyapatite mineralization. [187, 188]

Surfaces can also be functionalized targeting the control of cell behavior, and indirectly the cellular mineralization process. Rezania and Healy [189] functionalized solid materials surfaces with peptide sequences incorporating both cell- and heparin-adhesive motifs. They were able to enhance the degree of cell surface interactions and hence, influence the long-term formation of mineralized ECM *in vitro*. [189]

In order to design new BTE devices regarding biomineralization at the nanoscale, it is important to understand the main mechanisms responsible for apatite induction. Surface functionalization may be a very useful tool to attribute bioactivity to materials not able to induce apatitic deposition for themselves. Moreover, mimicking nature´s organic templates towards the biomineralization process initiation may be the key to obtain hierarchical organized nanostructures similar to the ones that can be found in bone.

3. Final remarks

BTE field is evolving and presents a plethora of innovative features aiming to meet the challenging demands of clinicians. Materials for bone replacement are no longer required to be inert. Nowadays the challenge of BTE is the design of a matrix that mimics the natural properties of bone while providing a temporary scaffold for tissue regeneration, still maintaining the resorbable, bioactive and biocompatible characteristics. A new class of smart materials is being created not only to replace bone, but also to regenerate the damaged tissue based on external or even internal stimulus.

Bone has been an inspirational source for tissue engineering, since it presents an extraordinary hierarchical architecture with notable biological and mechanical properties. It is known that its structure is based on aligned collagen bundles embedded with nanometer-sized inorganic hydroxyapatite crystals, however, the relationship between morphology of

the organic matrix and orientation of mineral is poorly understood. Unraveling the underlying mineralization process and how that knowledge can lead to the development of new devices and materials sharing the same remarkable mechanical properties of this natural nanocomposite is the main goal of BTE.

The central goal of this chapter was to bring forward some of the recent advances of nanoscale design in biomineralization towards the development of new biomaterials for BTE in the field of Nanomedicine applied to the bone. In section 1, some important concepts related to the issues being discussed were presented, as well as a brief review of the physiological and anatomical characteristics of bone tissue. Section 2 described the latest nanotechnology trends applied to the physical and chemical mimicking of bone environment using synthetic materials.

Hybrid organic-inorganic structures mimicking the composition of mineralized tissue for functional bone scaffolds were analyzed. The combination of biodegradable polymers (synthetic and natural) with nanoscale bioactive ceramics or fibers is emerging as a powerful approach toward third generation bioactive materials comprising injectable osteoconductive biomaterials, thin coatings and films or self-assembling osteoconductive nanobiomaterials. The impressive possibilities are closely linked to the broad range of properties they offer.

The nanostructures were recognized as being a key point for the successful achievement of bone regeneration. These devices must possess the ability of sensing biological demands and also to adapt to the mutability of the biological environment. In order to mimic the complex hierarchical structure of bone new methodologies are arising or being adapted to meet nanoscale design challenges. Modern materials and devices are being created, based on a dynamic interaction with the biological environment starting at the nanoscale allowing bone tissue regeneration to be targeted at the cellular signals level. These materials need to be able to communicate with cells and direct them to adhere, proliferate migrate or differentiate.

A number of open issues still need to be addressed. Some parameters of modern BTE devices lack optimization. Namely, degradation rate and mechanical properties are required to match with new bone formation and also bone vascularization needs to be improved in order to avoid necrosis of the host tissue surrounding the implant. This is an important point limiting the upscale of bioartificial devices. On the other hand, long-term

health effects of nanomaterials are still not fully understood. The development of scalable and reproducible manufacturing methods is also important. In the future, polyvalent devices comprising abilities as support, therapeutics and bioactivity will be implanted in bone tissues able to respond perfectly to the demanding *in vivo* environment. These materials will be able to release drugs to specific organs. Efficient combination of growth factors with the materials will also improve their efficacy in regenerating healthy bone. However, this increasingly complexity of nanodevices may compromise their financial viability regarding translation to clinical due to the level of chemical and physical complexity required for these materials to be able to influence cell behavior.

Acknowledgements

References

[1] Skinner HCW, Jahren AH. . Biomineralization. In: Turekian KK, Holland HD, editor. Treatise on Geochemistry: Elsevier; 2003. p. 1-69.

[2] Luz GM, Mano JF. Mineralized structures in nature: Examples and inspirations for the design of new composite materials and biomaterials. Composites Science and Technology 2010; 70:1777-88.

[3] Tampieri A, Sprio S, Sandri M, Valentini F. Mimicking natural bio-mineralization processes: A new tool for osteochondral scaffold development. Trends in Biotechnology 2011; 29:526-35.

[4] Borowitzka MA. Morphological and cytological aspects of algal calcification. International Review of Cytology-a Survey of Cell Biology 1982; 74:127-62.

[5] Skinner HCW. Minerals and Human Health. In: Vaughan DJ, Wogelius RA, editor. Environmental Mineralogy. Budapest, Hungary: Eotvos University Press; 2000. p. 383-412.

[6] Mann S. Biomineralization and biomimetic materials chemistry. Journal of Materials Chemistry 1995; 5:935-46.

[7] Hauschka PV, Lian JB, Cole DEC, Gundberg CM. Osteocalcin and matrix Gla protein: Vitamin K-dependent proteins in bone. Physiological Reviews 1989; 69:990-1047.

[8] Hoang QQ, Sicheri F, Howard AJ, Yang DSC. Bone recognition mechanism of porcine osteocalcin from crystal structure. Nature 2003; 425:977-80.

[9] Palmer LC, Newcomb CJ, Kaltz SR, Spoerke ED, Stupp SI. Biomimetic Systems for Hydroxyapatite Mineralization Inspired By Bone and Enamel. Chemical Reviews 2008; 108:4754-83.

[10] Alves NM, Leonor IB, Azevedo HS, Reis RL, Mano JF. Designing biomaterials based on biomineralization of bone. Journal of Materials Chemistry 2010; 20:2911-21.

[11] Dey A, Bomans PHH, Mueller FA, Will J, Frederik PM, de With G, et al. The role of prenucleation clusters in surface-induced calcium phosphate crystallization. Nature Materials 2010; 9:1010-4.

[12] Shi J, Alves NM, Mano JF. Thermally responsive biomineralization on biodegradable substrates. Advanced Functional Materials 2007; 17:3312-8.

[13] Salgado AJ, Coutinho OP, Reis RL. Bone tissue engineering: State of the art and future trends. Macromolecular Bioscience 2004; 4:743-65.

[14] Athanasiou KA, Zhu CF, Lanctot DR, Agrawal CM, Wang X. Fundamentals of biomechanics in tissue engineering of bone. Tissue Engineering 2000; 6:361-81.

[15] Place ES, Evans ND, Stevens MM. Complexity in biomaterials for tissue engineering. Nature Materials 2009; 8:457-70.

[16] Einhorn TA. Enhancement of fracture-healing. Journal of Bone and Joint Surgery-American Volume 1995; 77A:940-56.

[17] Weiner S, Wagner HD. The material bone: Structure mechanical function relations. Annual Review of Materials Science 1998; 28:271-98.

[18] Eliza L. S. Fong BMW, F. Kurtis Kasper, and Antonios G. Mikos. Building Bridges: Leveraging Interdisciplinary Collaborations in the Development of Biomaterials to Meet Clinical Needs. Advanced Materials 2012; 24(36):4995-5013.

[19] Vanderrest M, Garrone R. Collagen family of proteins. Faseb Journal 1991; 5:2814-23.

[20] Mescher A. Junqueira's Basic Histology: Text and Atlas. New York Mcgraw-Hill 2009.

[21] Ritchie RO. The conflicts between strength and toughness. Nature Materials 2011; 10:817-22.

[22] Currey JD. The design of mineralised hard tissues for their mechanical functions. Journal of Experimental Biology 1999; 202:3285-94.

[23] Ott I, Kienzler R, Schroeder R. Aging in the cortical bone: a constitutive law and its application. Archive of Applied Mechanics 2010; 80:527-41.

[24] Brown TD, Ferguson AB. Mechanical property distributions in the cancellous bone of the human proximal femur. Acta Orthopaedica Scandinavica 1980; 51:429-37.

[25] Yang SF, Leong KF, Du ZH, Chua CK. The design of scaffolds for use in tissue engineering. Part 1. Traditional factors. Tissue Engineering 2001; 7:679-89.

[26] Goldstein SA. The mechanical-properties of trabecular bone - Dependence on anatomic location and function. Journal of Biomechanics 1987; 20:1055-61.

[27] Langer R, Vacanti JP. Tissue engineering. Science 1993; 260:920-6.

[28] Laurencin CT, Ambrosio AMA, Borden MD, Cooper JA. Tissue engineering: Orthopedic applications. Annual Review of Biomedical Engineering 1999; 1:19-46.

[29] Barone DTJ, Raquez JM, Dubois P. Bone-guided regeneration: from inert biomaterials to bioactive polymer (nano) composites. Polymers for Advanced Technologies 2011; 22:463-75.

[30] Hench LL. Biomaterials: a forecast for the future. Biomaterials 1998; 19:1419-23.

[31] Kokubo T, Ito S, Huang ZT, Hayashi T, Sakka S, Kitsugi T, et al. Ca, P-rich layer formed on high-strenght bioactive glass-ceramics A-W. Journal of Biomedical Materials Research 1990; 24:331-43.

[32] Kokubo T, Takadama H. How useful is SBF in predicting in vivo bone bioactivity? Biomaterials 2006; 27:2907-15.

[33] Hench LL. Bioactive ceramics. In: Ducheyne PaL, J., editor. Bioceramics: Materials Characteristics versus In vivo behavior. New YorK: Annals of New York Academy of Sciences; 1988. p. 54-71.

[34] Rezwan K, Chen QZ, Blaker JJ, Boccaccini AR. Biodegradable and bioactive porous polymer/inorganic composite scaffolds for bone tissue engineering. Biomaterials 2006; 27:3413-31.

[35] Hench LL, Wheeler DL, Greenspan DC. Molecular control of bioactivity in sol-gel glasses. Journal of Sol-Gel Science and Technology 1998; 13:245-50.

[36] Dubok VA. Bioceramics - Yesterday, today, tomorrow. Powder Metallurgy and Metal Ceramics 2000; 39:381-94.

[37] Cartmell SH, Porter BD, Garcia AJ, Guldberg RE. Effects of medium perfusion rate on cell-seeded three-dimensional bone constructs in vitro. Tissue Engineering 2003; 9:1197-203.

[38] Peter M, Binulal NS, Nair SV, Selvamurugan N, Tamura H, Jayakumar R. Novel biodegradable chitosan-gelatin/nano-bioactive glass ceramic composite scaffolds for alveolar bone tissue engineering. Chemical Engineering Journal 2010; 158:353-61.

[39] Polak JM, Hench LL, Kemp P. Future Strategies For Tissue And Organ Replacement In: College I, editor.: Imperial College Press; 2002.

[40] Kneser U, Schaefer DJ, Polykandriotis E, Horch RE. Tissue engineering of bone: the reconstructive surgeon's point of view. Journal of Cellular and Molecular Medicine 2006; 10:7-19.

[41] Stevens MM, Marini RP, Schaefer D, Aronson J, Langer R, Shastri VP. In vivo engineering of organs: The bone bioreactor. Proceedings of the National Academy of Sciences of the United States of America 2005; 102:11450-5.

[42] Venugopal JR, Low S, Choon AT, Kumar AB, Ramakrishna S. Nanobioengineered electrospun composite nanofibers and osteoblasts for bone regeneration. Artificial Organs 2008; 32:388-97.

[43] Tan J, Saltzman WM. Biomaterials with hierarchically defined micro- and nanoscale structure. Biomaterials 2004; 25:3593-601.

[44] Santo VE, Gomes ME, Mano JF, Reis RL. From nano- to macro-scale: nanotechnology approaches for spatially controlled delivery of bioactive factors for bone and cartilage engineering. Nanomedicine 2012; 7:1045-66.

[45] Hench LL. Bioceramics - From concept to clinic Journal of the American Ceramic Society 1991; 74:1487-510.

[46] Kokubo T, Ito S, Sakka S, Yamamuro T. Formation of a high-strength bioactive glass ceramic in the system MgO-CaO-SIO2-P2O5. Journal of Materials Science 1986; 21:536-40.

[47] Kohn DH. Metals in medical applications. Current Opinion in Solid State & Materials Science 1998; 3:309-16.

[48] Nair LS, Laurencin CT. Biodegradable polymers as biomaterials. Progress in Polymer Science 2007; 32:762-98.

[49] Hong ZK, Reis RL, Mano JF. Preparation and in vitro characterization of scaffolds of poly(L-lactic acid) containing bioactive glass ceramic nanoparticles. Acta Biomaterialia 2008; 4:1297-306.

[50] El-Kady AM, Ali AF, Farag MM. Development, characterization, and in vitro bioactivity studies of sol-gel bioactive glass/poly(L-lactide) nanocomposite scaffolds. Materials Science & Engineering C-Materials for Biological Applications 2010; 30:120-31.

[51] Liu A, Hong Z, Zhuang X, Chen X, Cui Y, Liu Y, et al. Surface modification of bioactive glass nanoparticles and the mechanical and biological properties of poly(L-lactide) composites. Acta Biomaterialia 2008; 4:1005-15.

[52] Liu Ai-xue, Wei Jun-chao, Chen Xue-si, Jing Xia-bin, Cui Yang, Liu Yi. Novel composites of poly(L-lactide) and surface modified bioactive SiO2-CaO-P2O5 gel nanoparticles: Mechanical and biological properties. Chinese Journal of Polymer Science 2009; 27:415-26.

[53] Mano JF, Sousa RA, Boesel LF, Neves NM, Reis RL. Bloinert, biodegradable and injectable polymeric matrix composites for hard tissue replacement: state of the art and recent developments. Composites Science and Technology 2004; 64:789-817.

[54] Seal BL, Otero TC, Panitch A. Polymeric biomaterials for tissue and organ regeneration. Materials Science & Engineering R-Reports 2001; 34:147-230.

[55] Misra SK, Mohn D, Brunner TJ, Stark WJ, Philip SE, Roy I, et al. Comparison of nanoscale and microscale bioactive glass on the properties of P(3HB)/Bioglass (R) composites. Biomaterials 2008; 29:1750-61.

[56] Zheng H, Wang Y, Yang C, Chen X, Zhao N. Investigation on the porous biomaterial for bone reconstruction with addition of bio-mimetic Nano-Sized inorganic particles. In: Pan WGJH, editor. High-Performance Ceramics Iv, Pts 1-32007. p. 1534-7.

[57] Horch RA, Shahid N, Mistry AS, Timmer MD, Mikos AG, Barron AR. Nanoreinforcernent of poly(propylene fumarate)-based networks with surface modified alumoxane nanoparticles for bone tissue engineering. Biomacromolecules 2004; 5:1990-8.

[58] Shi XF, Hudson JL, Spicer PP, Tour JM, Krishnamoorti R, Mikos AG. Rheological behaviour and mechanical characterization of injectable poly(propylene fumarate)/single-walled carbon nanotube composites for bone tissue engineering. Nanotechnology 2005; 16:S531-S8.

[59] Kim K, Dean D, Lu A, Mikos AG, Fisher JP. Early osteogenic signal expression of rat bone marrow stromal cells is influenced by both hydroxyapatite nanoparticle content and initial cell seeding density in biodegradable nanocomposite scaffolds. Acta Biomaterialia 2011; 7:1249-64.

[60] Rocha de Oliveira AA, de Carvalho SM, Leite MF, Orefice RL, Pereira MM. Development of biodegradable polyurethane and bioactive glass nanoparticles scaffolds for bone tissue engineering applications. Journal of Biomedical Materials Research Part B-Applied Biomaterials 2012; 100B:1387-96.

[61] Vert M, Li SM, Spenlehauer G, Guerin P. Bioresorbability and biocompatibility of aliphatic polyesters. Journal of Materials Science-Materials in Medicine 1992; 3:432-46.

[62] Boccaccini AR, Erol M, Stark WJ, Mohn D, Hong ZK, Mano JF. Polymer/bioactive glass nanocomposites for biomedical applications: A review. Composites Science and Technology 2010; 70:1764-76.

[63] Wang Z, Yan Y, Wan T. Fabrication and characterization of hydroxyapatite/collagen bone-like nanocomposite through a self-assembly method. Science and Engineering of Composite Materials 2012; 19:177-82.

[64] Ito Y. Surface micropatterning to regulate cell functions. Biomaterials 1999; 20:2333-42.

[65] Singhvi R, Stephanopoulos G, Wang DIC. Effects of substratum morphology on cell physiology - Review. Biotechnology and Bioengineering 1994; 43:764-71.

[66] Curtis A, Wilkinson C. Topographical control of cells. Biomaterials 1997; 18:1573-83.

[67] Gupta HS, Seto J, Wagermaier W, Zaslansky P, Boesecke P, Fratzl P. Cooperative deformation of mineral and collagen in bone at the nanoscale. Proceedings of the National Academy of Sciences of the United States of America 2006; 103:17741-6.

[68] Fratzl P, Gupta HS, Paschalis EP, Roschger P. Structure and mechanical quality of the collagen-mineral nano-composite in bone. Journal of Materials Chemistry 2004; 14:2115-23.

[69] Sun Z-W, An Q-F, Zhao Q, Shangguan Y-G, Zheng Q. Study of Polyelectrolyte Complex Nanoparticles as Novel Templates for Biomimetic Mineralization. Crystal Growth & Design 2012; 12:2382-8.

[70] Sommerdijk NAJM, de With G. Biomimetic CaCO3 Mineralization using Designer Molecules and Interfaces. Chemical Reviews 2008; 108:4499-550.

[71] Zhu J-H, Yu S-H, Xu A-W, Coelfen H. The biomimetic mineralization of double-stranded and cylindrical helical BaCO3 nanofibres. Chemical Communications 2009:1106-8.

[72] Christenson EM, Anseth KS, van den Beucken LJJP, Chan CK, Ercan B, Jansen JA, et al. Nanobiomaterial applications in orthopedics. Journal of Orthopaedic Research 2007; 25:11-22.

[73] Singh RK, El-Fiqi AM, Patel KD, Kim H-W. A novel preparation of magnetic hydroxyapatite nanotubes. Materials Letters 2012; 75:130-3.

[74] Wilson CJ, Clegg RE, Leavesley DI, Pearcy MJ. Mediation of biomaterial-cell interactions by adsorbed proteins: A review. Tissue Engineering 2005; 11:1-18.

[75] Benoit DSW, Anseth KS. The effect on osteoblast function of colocalized RGD and PHSRN epitopes on PEG surfaces. Biomaterials 2005; 26:5209-20.

[76] Zhang Y, Venugopal JR, El-Turki A, Ramakrishna S, Su B, Lim CT. Electrospun biomimetic nanocomposite nanofibers of hydroxyapatite/chitosan for bone tissue engineering. Biomaterials 2008; 29:4314-22.

[77] Zhang HF, Hussain I, Brust M, Butler MF, Rannard SP, Cooper AI. Aligned two- and three-dimensional structures by directional freezing of polymers and nanoparticles. Nature Materials 2005; 4:787-93.

[78] Wegst UGK, Schecter M, Donius AE, Hunger PM. Biomaterials by freeze casting. Philosophical Transactions of the Royal Society a-Mathematical Physical and Engineering Sciences 2010; 368:2099-121.

[79] Deville S, Saiz E, Nalla RK, Tomsia AP. Freezing as a path to build complex composites. Science 2006; 311:515-8.

[80] Sotiropoulou S, Sierra-Sastre Y, Mark SS, Batt CA. Biotemplated nanostructured materials. Chemistry of Materials 2008; 20:821-34.

[81] Westwater J, Gosain DP, Usui S. Control of the size and position of silicon nanowires grown via the vapor-liquid-solid technique. Japanese Journal of Applied Physics Part 1-Regular Papers Short Notes & Review Papers 1997; 36:6204-9.

[82] Pan ZW, Dai ZR, Wang ZL. Nanobelts of semiconducting oxides. Science 2001; 291:1947-9.

[83] Hong Z, Reis RL, Mano JF. Preparation and in vitro characterization of novel bioactive glass ceramic nanoparticles. Journal of Biomedical Materials Research Part A 2009; 88A:304-13.

[84] Sang L, Huang J, Luo D, Chen Z, Li X. Bone-like nanocomposites based on self-assembled protein-based matrices with Ca2+ capturing capability. Journal of Materials Science-Materials in Medicine 2010; 21:2561-8.

[85] Cushing BL, Kolesnichenko VL, O'Connor CJ. Recent advances in the liquid-phase syntheses of inorganic nanoparticles. Chemical Reviews 2004; 104:3893-946.

[86] Mackovic M, Hoppe A, Detsch R, Mohn D, Stark WJ, Spiecker E, et al. Bioactive glass (type 45S5) nanoparticles: in vitro reactivity on nanoscale and biocompatibility. Journal of Nanoparticle Research 2012; 14.

[87] L. Martínez MD, E. Román, M. Ruano, D. Llamosa P., and Y. Huttel. Generation of Nanoparticles with Adjustable Size and Controlled Stoichiometry: Recent Advances. Langmuir 2012.

[88] Limmer SJ, Seraji S, Wu Y, Chou TP, Nguyen C, Cao GZ. Template-based growth of various oxide nanorods by sol-gel electrophoresis. Advanced Functional Materials 2002; 12:59-64.

[89] Murugan R, Ramakrishna S. Development of nanocomposites for bone grafting. Composites Science and Technology 2005; 65:2385-406.

[90] Porter JR, Henson A, Popat KC. Biodegradable poly(epsilon-caprolactone) nanowires for bone tissue engineering applications. Biomaterials 2009; 30:780-8.

[91] Zhao Y, Jiang L. Hollow Micro/Nanomaterials with Multilevel Interior Structures. Advanced Materials 2009; 21:3621-38.

[92] Luz GM, Mano, J. F. Nanotectonics approach to produce hierarchically organized bioactive glass nanoparticles-based macrospheres Nanoscale 2012; 4 (20):6293-7.

[93] Gribova V, Auzely-Velty R, Picart C. Polyelectrolyte Multilayer Assemblies on Materials Surfaces: From Cell Adhesion to Tissue Engineering. Chemistry of Materials 2012; 24:854-69.

[94] Hammond PT. Building biomedical materials layer-by-layer. Materials Today 2012; 15:196-206.

[95] Thibault RA, Mikos AG, Kasper FK. Protein and Mineral Composition of Osteogenic Extracellular Matrix Constructs Generated with a Flow Perfusion Bioreactor. Biomacromolecules 2011; 12:4204-12.

[96] Brinker CJ, Scherer GW. Sol-Gel-Glass. 1. Gelation and gel structure. Journal of Non-Crystalline Solids 1985; 70:301-22.

[97] De M, Ghosh PS, Rotello VM. Applications of Nanoparticles in Biology. Advanced Materials 2008; 20:4225-41.

[98] Munoz-Espinoza R, Weiss CK, Landfester K. Inorganic nanoparticles prepared in miniemulsion. Current Opinion in Colloid & Interface Science 2012; 17:212-24.

[99] Han BQ, Lavernia EJ, Mohamed FA. Mechanical properties of nanostructured materials. Reviews on Advanced Materials Science 2005; 9:1-16.

[100] Suryanarayana C. Nanocrystalline Materials. International Materials Reviews 1995; 40:41-64.

[101] Xu H, Yan F, Monson EE, Kopelman R. Room-temperature preparation and characterization of poly (ethylene glycol)-coated silica nanoparticles for biomedical applications. Journal of Biomedical Materials Research Part A 2003; 66A:870-9.

[102] George R. Beck S-WH, Corinne E. Camalier, Masayoshi Yamaguchi, Yan Li, Jin-Kyu Lee, M. Neale Weitzmann. Bioactive silica-based nanoparticles stimulate bone-forming osteoblasts, suppress bone-resorbing osteoclasts, and enhance bone mineral density in vivo. Nanomedicine: Nanotechnology, Biology and Medicine 2012; 8:793-803.

[103] Lin Q, Lan X, Li Y, Ni Y, Lu C, Chen Y, et al. Preparation and characterization of novel alkali-activated nano silica cements for biomedical application. Journal of Biomedical Materials Research Part B-Applied Biomaterials 2010; 95B:347-56.

[104] Cai L, Cong M, Juanjuan Z, Yuli L, Xiaofeng C. Healing Effect of Bioactive Glass Ointment on Full-thickness skin Wounds. Biomedical Materials 2012; 7.

[105] Webster TJ, Ergun C, Doremus RH, Siegel RW, Bizios R. Enhanced functions of osteoblasts on nanophase ceramics. Biomaterials 2000; 21:1803-10.

[106] Hong Z, Luz GM, Hampel PJ, Jin M, Liu A, Chen X, et al. Mono-dispersed bioactive glass nanospheres: Preparation and effects on biomechanics of mammalian cells. Journal of Biomedical Materials Research Part A 2010; 95A:747-54.

[107] Luz GM, Mano, J. F. Preparation and characterization of bioactive glass nanoparticles prepared by sol-gel for biomedical application. Nanotechnology 2011; 22:494014.

[108] Xia W, Chang J. Preparation and characterization of nano-bioactive-glasses (NBG) by a quick alkali-mediated sol-gel method. Materials Letters 2007; 61:3251-3.

[109] Vollenweider M, Brunner TJ, Knecht S, Grass RN, Zehnder M, Imfeld T, et al. Remineralization of human dentin using ultrafine bioactive glass particles. Acta Biomaterialia 2007; 3:936-43.

[110] Hong Z, Liu A, Chen L, Chen X, Jing X. Preparation of bioactive glass ceramic nanoparticles by combination of sol-gel and coprecipitation method. Journal of Non-Crystalline Solids 2009; 355:368-72.

[111] Unal H, Mimaroglu A, Alkan M. Mechanical properties and morphology of nylon-6 hybrid composites. Polymer International 2004; 53:56-60.

[112] Du S, Tian Y, Liu J, Liu H, Chen Y. Large-scale preparation of needle-like zinc oxide with high electrical conductivity. Materials Letters 2006; 60:3133-6.

[113] Hong Z, Merino EG, Reis RL, Mano JF. Novel Rice-shaped Bioactive Ceramic Nanoparticles. Advanced Engineering Materials 2009; 11:B25-B9.

[114] Gentleman E, Fredholm YC, Jell G, Lotfibakhshaiesh N, O'Donnell MD, Hill RG, et al. The effects of strontium-substituted bioactive glasses on osteoblasts and osteoclasts in vitro. Biomaterials 2010; 31:3949-56.

[115] Gutowska I, Machoy Z, Machalinski B. The role of bivalent metals in hydroxyapatite structures as revealed by molecular modeling with the HyperChem software. Journal of Biomedical Materials Research Part A2005; 75A:788-93.

[116] Webster TJ, Ergun C, Doremus RH, Bizios R. Hydroxylapatite with substituted magnesium, zinc, cadmium, and yttrium. II. Mechanisms of osteoblast adhesion. Journal of Biomedical Materials Research 2002; 59:312-7.

[117] Luz GM, Mano JF. Chitosan/bioactive glass nanoparticles composites for biomedical applications. Biomedical Materials 2012:7:054104.

[118] Isaac J, Nohra J, Lao J, Jallot E, Nedelec J-M, Berdal A, et al. Effects of strontium-doped bioactive glass on the differentiation of cultured osteogenic cells. European Cells & Materials 2011; 21:130-43.

[119] Bellantone M, Williams HD, Hench LL. Broad-spectrum bactericidal activity of Ag2O-doped bioactive glass. Antimicrobial Agents and Chemotherapy 2002; 46:1940-5.

[120] Danhier F, Ansorena E, Silva JM, Coco R, Le Breton A, Preat V. PLGA-based nanoparticles: An overview of biomedical applications. Journal of Controlled Release 2012; 161:505-22.

[121] Miranda M, Fernandez A, Lopez-Esteban S, Malpartida F, Moya JS, Torrecillas R. Ceramic/metal biocidal nanocomposites for bone-related applications. Journal of Materials Science-Materials in Medicine 2012; 23:1655-62.

[122] Tartaj P, Morales MD, Veintemillas-Verdaguer S, Gonzalez-Carreno T, Serna CJ. The preparation of magnetic nanoparticles for applications in biomedicine. Journal of Physics D-Applied Physics 2003; 36:R182-R97.

[123] Corot C, Robert P, Idee J-M, Port M. Recent advances in iron oxide nanocrystal technology for medical imaging. Advanced Drug Delivery Reviews 2006; 58:1471-504.

[124] Ferrari M. Cancer nanotechnology: Opportunities and challenges. Nature Reviews Cancer 2005; 5:161-71.

[125] Medeiros SF, Santos AM, Fessi H, Elaissari A. Stimuli-responsive magnetic particles for biomedical applications. International Journal of Pharmaceutics 2011; 403:139-61.

[126] Ruiz-Hernandez E, Serrano MC, Arcos D, Vallet-Regi M. Glass-glass ceramic thermoseeds for hyperthermic treatment of bone tumors. Journal of Biomedical Materials Research Part A 2006; 79A:533-43.

[127] Gong Y-k, Winnik FM. Strategies in biomimetic surface engineering of nanoparticles for biomedical applications. Nanoscale 2012; 4:360-8.

[128] Bear J, Charron G, Teresa Fernandez-Argueelles M, Massadeh S, McNaughter P, Nann T. In Vivo Applications of Inorganic Nanoparticles. In: BoossBavnbek BKBLJPFRE, editor. BetaSys: Systems Biology of Regulated Exocytosis in Pancreatic Beta-Cells2011. p. 185-220.

[129] Rodriguez-Lorenzo LM, Saldana L, Benito-Garzon L, Garcia-Carrodeguas R, de Aza S, Vilaboa N, et al. Feasibility of ceramic-polymer composite cryogels as scaffolds for bone tissue engineering. Journal of Tissue Engineering and Regenerative Medicine 2012; 6:421-33.

[130] Zhang YZ, Su B, Venugopal J, Ramakrishna S, Lim CT. Biomimetic and bioactive nanofibrous scaffolds from electrospun composite nanofibers. International Journal of Nanomedicine 2007; 2:623-38.

[131] Kadler KE, Holmes DF, Trotter JA, Chapman JA. Collagen fibril formation. Biochemical Journal 1996; 316:1-11.

[132] Traub W, Arad T, Weiner S. 3-Dimensional ordered distribution of crystals in turkey tendon collagen-fibers. Proceedings of the National Academy of Sciences of the United States of America 1989; 86:9822-6.

[133] Fischer RL, McCoy MG, Grant SA. Electrospinning collagen and hyaluronic acid nanofiber meshes. Journal of Materials Science-Materials in Medicine 2012; 23:1645-54.

[134] Hartgerink JD, Beniash E, Stupp SI. Self-assembly and mineralization of peptide-amphiphile nanofibers. Science 2001; 294:1684-8.

[135] Hosseinkhani H, Hosseinkhani M, Khademhosseini A, Kobayashi H. Bone regeneration through controlled release of bone morphogenetic protein-2 from 3-D tissue engineered nano-scaffold. Journal of Controlled Release 2007; 117:380-6.

[136] Prabhakaran MP, Ghasemi-Mobarakeh L, Ramakrishna S. Electrospun Composite Nanofibers for Tissue Regeneration. Journal of nanoscience and nanotechnology 2011; 11:3039-57.

[137] S. J. Chen HYY, B. C. Yang. Bioactive TiO_2 fiber films prepared by electrospinning method. Journal of Biomedical Materials Research Part A 2012.

[138] Mi-Kyung K, Jung-Ju K, Ueon Sang S, Hae-Won K. Production of a biomimetic apatite nanotube mesh via biotemplating a polymer nanofiber mesh. Materials Letters 2010; 64; 2655‒2658.

[139] Zhao B, Hu H, Mandal SK, Haddon RC. A bone mimic based on the self-assembly of hydroxyapatite on chemically functionalized single-walled carbon nanotubes. Chemistry of Materials 2005; 17:3235-41.

[140] Ozawa N, Yao T. Micropattern formation of apatite by combination of a biomimetic process and transcription of resist pattern. Journal of Biomedical Materials Research 2002; 62:579-86.

[141] Luz GM, Boesel L, del Campo A, Mano JF. Micropatterning of Bioactive Glass Nanoparticles on Chitosan Membranes for Spatial Controlled Biomineralization. Langmuir 2012; 28:6970-7.

[142] Lamers E, van Horssen R, te Riet J, van Delft FCMJM, Luttge R, Walboomers XF, et al. The influence of Nano scale topographical cues on initial osteoblast morphology and migration. European Cells & Materials 2010; 20:329-43.

[143] Puckett S, Webster T. Control of osteoblast alignment on nano patterned titanium. Nanomedicine-Nanotechnology Biology and Medicine 2007; 3:348.

[144] Puckett SD, Lu J, Webster TJ. COLL 449-Ti nanopatterns for directing bone growth. Abstracts of Papers of the American Chemical Society 2007; 234.

[145] Minh Ngoc N, Lebarbe T, Zouani OF, Pichavant L, Durrieu M-C, Heroguez V. Impact of RGD Nanopatterns Grafted onto Titanium on Osteoblastic Cell Adhesion. Biomacromolecules 2012; 13:896-904.

[146] Li X, Huang J, Edirisinghe MJ. Novel patterning of nano-bioceramics: template-assisted electrohydrodynamic atomization spraying. Journal of the Royal Society Interface 2008; 5:253-7.

[147] Popat KC, Eltgroth M, LaTempa TJ, Grimes CA, Desai TA. Decreased Staphylococcus epidermis adhesion and increased osteoblast functionality on antibiotic-loaded titania nanotubes. Biomaterials 2007; 28:4880-8.

[148] Yang L, Sheldon BW, Webster TJ. Nanophase Ceramics for Improved Drug Delivery: Current Opportunities and Challenges. American Ceramic Society Bulletin 2010; 89:24-31.

[149] Park C, Lee K, Kim C. Photoresponsive Cyclodextrin-Covered Nanocontainers and Their Sol-Gel Transition Induced by Molecular Recognition. Angewandte Chemie-International Edition 2009; 48:1275-8.

[150] Mal NK, Fujiwara M, Tanaka Y. Photocontrolled reversible release of guest molecules from coumarin-modified mesoporous silica. Nature 2003; 421:350-3.

[151] Lu J, Choi E, Tamanoi F, Zink JI. Light-activated nanoimpeller-controlled drug release in cancer cells. Small 2008; 4:421-6.

[152] Nguyen TD, Liu Y, Saha S, Leung KCF, Stoddart JF, Zink JI. Design and optimization of molecular nanovalves based on redox-switchable bistable rotaxanes. Journal of the American Chemical Society 2007; 129:626-34.

[153] Hernandez R, Tseng HR, Wong JW, Stoddart JF, Zink JI. An operational supramolecular nanovalve. Journal of the American Chemical Society 2004; 126:3370-1.

[154] Min KH, Lee HJ, Kim K, Kwon IC, Jeong SY, Lee SC. The tumor accumulation and therapeutic efficacy of doxorubicin carried in calcium phosphate-reinforced polymer nanoparticles. Biomaterials 2012; 33:5788-97.

[155] Shi J, Qi W, Li G, Cao S. Biomimetic self-assembly of calcium phosphate templated by PNIPAAm nanogels for sustained smart drug delivery. Materials Science & Engineering C-Materials for Biological Applications 2012; 32:1299-306.

[156] Yao C, Webster TJ. Prolonged Antibiotic Delivery From Anodized Nanotubular Titanium Using a Co-precipitation Drug Loading Method. Journal of Biomedical Materials Research Part B-Applied Biomaterials 2009; 91B:587-95.

[157] Kato N, Hasegawa U, Morimoto N, Saita Y, Nakashima K, Ezura Y, et al. Nanogel-based delivery system enhances PGE(2) effects on bone formation. Journal of Cellular Biochemistry 2007; 101:1063-70.

[158] Motskin M, Wright DM, Muller K, Kyle N, Gard TG, Porter AE, et al. Hydroxyapatite nano and microparticles: Correlation of particle properties with cytotoxicity and biostability. Biomaterials 2009; 30:3307-17.

[159] Ji B, Gao H. Mechanical Principles of Biological Nanocomposites. In: Clarke DRRMZF, editor. Annual Review of Materials Research, Vol 402010. p. 77-100.

[160] Mayer G. Rigid biological systems as models for synthetic composites. Science 2005; 310:1144-7.

[161] Saeed Younis YK, Leonid Bloch, and Emil Zolotoyabko. Inhomogeneity of Nacre Lamellae on the Nanometer Length Scale. Crystal growth and design 2012; 12 (9): 4574-4579.

[162] Peter M, Binulal NS, Soumya S, Nair SV, Furuike T, Tamura H, et al. Nanocomposite scaffolds of bioactive glass ceramic nanoparticles disseminated chitosan matrix for tissue engineering applications. Carbohydrate Polymers 2010; 79:284-9.

[163] Peter M, Kumar PTS, Binulal NS, Nair SV, Tamura H, Jayakumar R. Development of novel alpha-chitin/nanobioactive glass ceramic composite scaffolds for tissue engineering applications. Carbohydrate Polymers 2009; 78:926-31.

[164] Wang YJ, Yang CR, Chen XF, Zhao NR. Development and characterization of novel biomimetic composite scaffolds based on bioglass-collagen-hyaluronic acid-phosphatidylserine for tissue engineering applications. Macromolecular Materials and Engineering 2006; 291:254-62.

[165] Deshpande AS, Beniash E. Bioinspired synthesis of mineralized collagen fibrils. Crystal Growth & Design 2008; 8:3084-90.

[166] Nassif N, Gobeaux F, Seto J, Belamie E, Davidson P, Panine P, et al. Self-Assembled Collagen-Apatite Matrix with Bone-like Hierarchy. Chemistry of Materials 2010; 22:3307-9.

[167] Mota J YN, Caridade SG, Luz G, Gomes ME, Reis RL, Jansen JA, Walboomers XF, Mano JF. Chitosan/bioactive glass nanoparticle composite membranes for periodontal re-generation. Acta Biomaterialia 2012; 8(11):4173-80.

[168] Chen L, Yu Q, Wang Y, Li H. BisGMA/TEGDMA dental composite containing high as-pect-ratio hydroxyapatite nanofibers. Dental Materials 2011; 27:1187-95.

[169] Khaled SM, Sui R, Charpentier PA, Rizkalla AS. Synthesis of TiO2-PMMA nanocomposite: Using methacrylic acid as a coupling agent. Langmuir 2007; 23:3988-95.

[170] Karageorgiou V, Kaplan D. Porosity of 3D biornaterial scaffolds and osteogenesis. Bio-materials 2005; 26:5474-91.

[171] Couto DS, Hong ZK, Mano JF. Development of bioactive and biodegradable chitosan-based injectable systems containing bioactive glass nanoparticles. Acta Biomaterialia 2009; 5:115-23.

[172] Miyamoto Y, Ishikawa K, Fukao H, Sawada M, Nagayama M, Kon M, et al. In-vivo set-ting behavior of fast-setting calcium-phosphate cement. Biomaterials 1995; 16:855-60.

[173] Xu HHK, Smith DT, Simon CG. Strong and bioactive composites containing nano-silica-fused whiskers for bone repair. Biomaterials 2004; 25:4615-26.

[174] Sitharaman B, Shi X, Tran LA, Spicer PP, Rusakova I, Wilson LJ, et al. Injectable in situ cross-linkable nanocomposites of biodegradable polymers and carbon nanostructures for bone tissue engineering. Journal of Biomaterials Science-Polymer Edition 2007; 18:655-71.

[175] Engler AJ, Sen S, Sweeney HL, Discher DE. Matrix elasticity directs stem cell lineage specification. Cell 2006; 126:677-89.

[176] Engler AJ, Griffin MA, Sen S, Bonnetnann CG, Sweeney HL, Discher DE. Myotubes dif-ferentiate optimally on substrates with tissue-like stiffness: pathological implications for soft or stiff microenvironments. Journal of Cell Biology 2004; 166:877-87.

[177] Shengbing Y, Jing W, Honglue T., Fanyan Z., Changsheng L. Soft Matter 2012; 8; 8981-8989.

[178] Bradt JH, Mertig M, Teresiak A, Pompe W. Biomimetic mineralization of collagen by combined fibril assembly and calcium phosphate formation. Chemistry of Materials 1999; 11:2694-701.

[179] Wu Y, Ackerman JL, Strawich ES, Rey C, Kim HM, Glimcher MJ. Phosphate ions in bone: Identification of a calcium-organic phosphate complex by P-31 solid-state NMR spectroscopy at early stages of mineralization. Calcified Tissue International 2003; 72:610-26.

[180] Grzesik WJ, Robey PG, Bone matrix RGD glycoproteins: Immunolocalization and interaction with human primary osteoblastic bone cells in vitro. Journal of Bone and Mineral Research 1994; 9: 487-496.

[181] Bradley JV, Bridgland LN, Colyer DE, Duer MJ, Friscic T, Gallagher JR, et al. NMR of Biopolymer-Apatite Composites: Developing a Model of the Molecular Structure of the Mineral-Matrix Interface in Calcium Phosphate Biomaterials. Chemistry of Materials 2010; 22:6109-16.

[182] Newcomb CJ, Bitton R, Velichko YS, Snead ML, Stupp SI. The Role of Nanoscale Architecture in Supramolecular Templating of Biomimetic Hydroxyapatite Mineralization. Small 2012; 8:2195-202.

[183] Olszta MJ, Cheng X, Jee SS, Kumar R, Kim Y-Y, Kaufman MJ, et al. Bone structure and formation: A new perspective. Materials Science & Engineering R-Reports 2007; 58:77-116.

[184] Shaw WJ, Ferris K. Structure, Orientation, and Dynamics of the C-Terminal Hexapeptide of LRAP Determined Using Solid-State NMR. Journal of Physical Chemistry B 2008; 112:16975-81.

[185] Collier JH, Messersmith PB. Phospholipid strategies in biomineralization and biomaterials research. Annual Review of Materials Research 2001; 31:237-63.

[186] Hench LL, Thompson I. Twenty-first century challenges for biomaterials. Journal of the Royal Society Interface 2010; 7:S379-S91.

[187] Wang F, Cao B, Mao C. Bacteriophage Bundles with Prealigned Ca2+ Initiate the Oriented Nucleation and Growth of Hydroxylapatite. Chemistry of Materials 2010; 22:3630-6.

[188] He T, Abbineni G, Cao B, Mao C. Nanofibrous Bio-inorganic Hybrid Structures Formed Through Self-Assembly and Oriented Mineralization of Genetically Engineered Phage Nanofibers. Small 2010; 6:2230-5.

[189] Rezania A, Healy KE. Biomimetic peptide surfaces that regulate adhesion, spreading, cytoskeletal organization, and mineralization of the matrix deposited by osteoblast-like cells. Biotechnology Progress 1999; 15:19-32.

Chapter II

Mineralized structures in nature: Examples and inspirations for the design of new composites *

Abstract

Through the natural evolutionary process, organisms have been improving amazing mineralized materials for a series of functions using a relatively few constituent elements. Biomineralization has been widely studied in the last years. It is important to understand how minerals are produced by organisms and also their structure and the corresponding relationship with the properties and function. Moreover, one can look at minerals as a tool that could be used to develop high performance materials, through design inspiration and to find novel processing routes functioning at mild conditions of temperature, pressure and solvent type. As important as the molecular constituents are structural factors, which include the existence of different levels of organization and controlled orientation. Moreover, the way how the hierarchical levels are linked and the interfacial features play also a major role in the final behavior of the biogenic composite. The main aim of this work is to review the latest contributions that have been reported on composite materials produced in nature, and to relate their structures at different length scales to their main functions and properties. There is also an interest in developing new biomimetic procedures that could induce the production of calcium phosphate coatings, similar to bone apatite in substrates for biomedical applications, namely in orthopedic implants and scaffolds for tissue engineering and regenerative medicine; this topic will be also addressed. Finally, the latest proposed approaches to develop novel synthetic materials and coatings inspired from natural-based nanocomposites are also reviewed.

1. Introduction

Nature, through the evolutionary process, has been able to design and produce highly sophisticated materials, used for a variety of functions, including for structural purposes [1] and [2]. The physical properties of biological systems, such as the mechanical performance, are typically far better than that of the equivalent synthetic materials, with similar compositions and processed with present technologies. Moreover, these materials are produced at mild temperature and pressure conditions, with relatively low energy consumption. Finally, such systems are made with significant weak components such as brittle minerals, soft proteins and water. Therefore, nature has been a fascinating source of inspiration for scientists and engineers. Biomimetics is an emerging field of science that includes the study of how nature designs, processes and assembles/disassembles molecular building blocks to fabricate high performance hard polymer-based composites (e.g., mollusk shells, bone, tooth) and/or soft materials (e.g., skin, cartilage, tendons), and then applies these designs and processes to engineer new molecules and materials with unique properties. [3-5]

Biologically inspired design or adaptation or derivation from nature is referred to as 'biomimetics'. It means mimicking biology or nature. The field of biomimetics is highly interdisciplinary. It involves the understanding of biological functions, structures and principles of various objects found in nature by biologists, physicists, chemists and material scientists, and the design and fabrication of various materials and devices of commercial interest by engineers, material scientists, chemists and others. [6]

Mineralized biological materials are a subgroup of this immense world that has fascinating many researchers due to their unique structure and performance. Despite the large variety of existing biocomposites, only about 60 minerals are used by organisms, approximately half of them containing calcium. [7-8]. It has been recognized that some constituents, such as calcium carbonate or silica, exist recurrently in very different mineralized organizations and processed by completely diverse living organisms. As important as the molecular constituents are structural factors, which include the existence of different levels of organization and controlled orientation. Moreover, the way how the hierarchical levels are connected also plays a major role in the final behavior of the biogenic composite. The main

aim of this work is to review the latest contributions that have been reported on natural mineralized materials, and to relate their structures at different length scales (molecular, nanometric, micrometric and macroscopic levels) to their main functions and properties. An emphasis will be done on discussing topics that include how the different hierarchical levels are organized and what would be the contribution of both the organic fraction and water that existing within such structures. A series of examples of mineralized structures will be presented, including the fracture surface of shells, bone and teeth. The study of the structure–function relationships in bone has been particularly investigated, together with studies in the area of calcium phosphates, as hydroxyapatite constitutes the inorganic component in this tissue. In this context, much work has been done in the development of new procedures that could induce the production of calcium phosphate coatings in substrates for biomedical applications, namely in orthopedic implants and tissue engineering scaffolds; this topic will be also reviewed. Finally, the latest proposed approaches to develop novel synthetic materials and coatings inspired from natural-based composites are also reviewed. The difficulties associated with such biomimetic routes will be pointed out, related to the complex architecture found in the biogenic composites and with interfacial arguments. In fact, many aspects of biomineralization are far from being clearly understood and suggestions on how such fundamental knowledge could be transposed to useful synthetic strategies for developing completely new materials offers a series of stimulating research opportunities for researchers.

2. Structure of mineralized biocomposites and properties relationships

2.1. General considerations

It has been recognized that biological composites exhibit a series of organized structures on discrete scale levels, ranging from the molecular to the macroscopic. [9, 10] The components at each level are interrelated with each other such that the performance for the required functions can be optimized. The different levels are assembled through a bottom-up approach using nanofabrication methodologies, mediated by cellular signals. It is

interesting to notice that the hard mineral component in natural composites exhibit nanometric sizes, at least in one direction, displays an anisotropic geometry and is immersed in a soft organic matrix. For example (see more details later), enamel is composed by 15–20 nm thick and 1000 nm long crystals, with low soft protein matrix content; dentin and bone contains plate-like crystals (2–4 nm thick) and double the quantity of protein matrix; nacre is made of plate-like crystals (200–500 nm thick) and contains a very small amount of soft matrix. In a pure fracture-mechanics perspective Gao and co-workers showed that nanometer scale plays a key role in allowing these biological systems to achieve their superior mechanical properties. [11, 12] Below a critical size on the nanometer length scale, the mineral crystals fail no longer by propagation of pre-existing cracks, but by uniform rupture near their limiting strength. This increase of robustness is also achieved through the hierarchical organization, as studied by modeling self-similar composite structures mimicking the nanostructure of bone. Such mechanistic analysis also allowed the understanding the importance of the anisotropic structure of the mineral crystals that can explain how nature can produce stiff composites with low mineral content (e.g., bone): it was shown that the large aspect ratio of mineral crystals in bone can fully for the softness of the matrix. [12]

Another important aspect in the common structure of many mineralized biological materials, namely the ones that were produced to fulfill a multipurpose function (e.g., mollusk shells, skeleton of sea urchins, lamellar bone and biogenic silica) is that they seem to be designed to reduce the extent of mechanical anisotropy. [13] Here, the idea of multipurpose material is related to material produced by a variety of different organisms of the same taxon, and used in anatomically different environment. Therefore, they should function under many different situations and should respond mechanically more or less equally from all different directions. In these systems one may observe highly anisotropic structures at some hierarchical level (for example, the mineralized fibrils within the layers of lamellar bone), but it seems that the design strategy throughout the entire levels of structure is to enhance, as much as possible, the isotropic character of the material. [13]

An interesting example of structural hierarchy was reported for a silica-based mineralized skeleton of a sponge, providing a unique example of how glass, a classic brittle material, can be used as a structural element in the biological world. [14] The assembly towards the glassy cage of this organism involves at least seven hierarchical levels, all contributing to

mechanical performance. Silica nanospheres are arranged into concentric layers, held together by organic layers, to yield lamellar fibers. Those are organized in bundles to produce flexural rigid composite microscopic beams. The beams are arranged in a rectangular lattice that, together with other structural motifs, provides adequate mechanical features of the glass skeletal system at the macroscopic scale. Some more examples of mineralized biocomposites will be given, where the relationship between structure and performance or function will be highlighted. As the main applications of nature inspired synthetic materials that were intended to be focused are in the biomedical field, a special attention will be given to human mineralized tissues (bone and teeth). Shells will be also discussed as calcium carbonate-rich nanocomposites as they also exhibit particular structural features and properties that can also be interesting in the orthopedic field.

2.2. Bone

Bone refers to a family of materials that all have the mineralized collagen fibril as their basic building block. [15] The general structure of bone is summarized in Fig. II.1.A. Plate-shaped crystals, with 50×25 nm of length and width and with 2–3 nm thickness, of carbonated hydroxyapatite, with crystals aligned along their c-axis, are embedded in a type-I collagen framework. The fibrils consist of triple-helix collagen chains with 1.5 nm diameter and 300 nm length. Their ends are separated by holes of ca. 35 nm and the neighboring molecules are vertically offset by 68 nm. The apatite crystals are nucleated at specific regions on or within the collagen fibrils. They grow in the hole zones that exists between neighboring collagen molecules. For the particular case of lamellar bone the fibrils are then arranged in parallel arrays, with crystals aligned (sub-layers). The consecutive sub-layers rotate through the lamellar plane by an average of 30°, forming a so-called plywood-like structure. As each lamella is composed of five sub-layers, the total rotation is 150°, thus forming an asymmetric structure. Moreover, the collagen fibril bundles rotate around their axis within the five sub-layers. Both facts enhance the isotropic properties of bone found at the macroscopic scale, as previously reported. Moreover, this type of architecture hinders crack propagation and increases toughness. Fig. II.1.B displays a typical lamellar morphology found in cortical bone, showing a cryogenic fracture surface of a bovine femur. The layered

texture reveals the complex and periodic structure of the lamellar bone, being in agreement of the plywood-like structure. The lamellae that form cortical bone have three forms of appearance: the secondary osteons, interstitial lamellae and the inner and outer circumferential lamellae. The secondary osteons are cylindrical tubes, which are permanently re-built by the remodeling process. The remodeling is regulated by the mineral metabolism and the appearance of microcracks caused by fatigue. Osteoblasts destroy the bone tissue, forming a tunnel along the longitudinal axis of bone. The tunnel is then filled up by circular rings of lamellae surrounding the vascular canal, both of them forming together the so called haversian system or osteon, a cylindrical motif, formed by concentric layers of lamellae and are usually oriented in the longitudinal direction of bone. [16] The micrograph in Fig. II.1.B also reveals the existence of an Haversian canal, found in the in central region of the osteon. For further details read. [15]
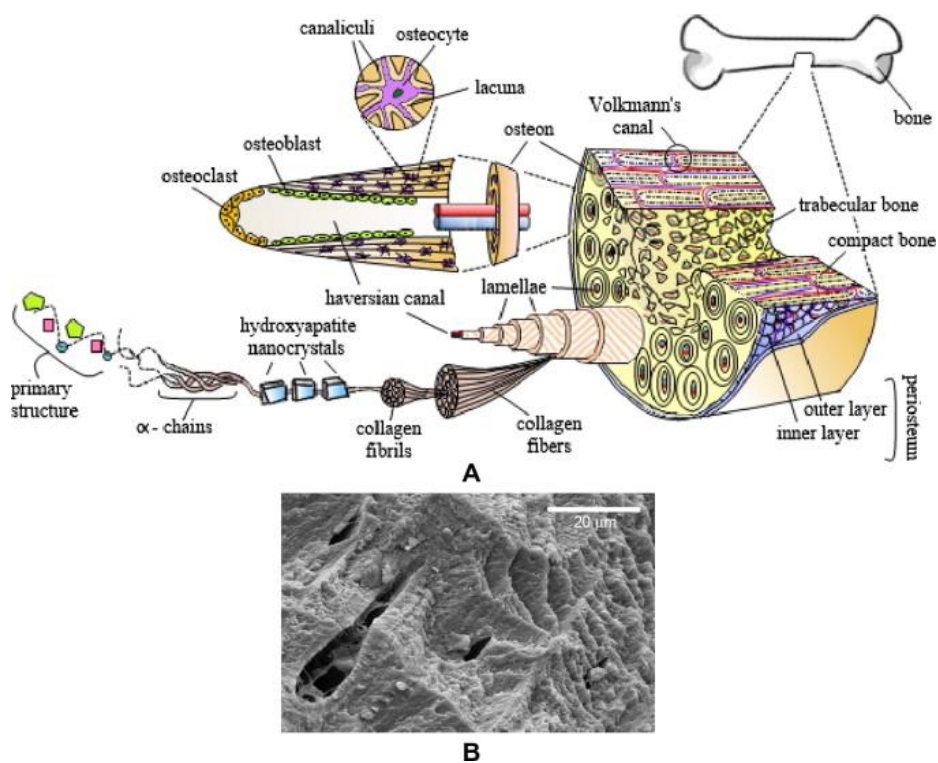
Fig. II. 1. Bone structure and morphology.

> **(a)** The general structure of bone, showing its hierarchical organization; **(b)** fracture surface of a bovine cortical bone revealing a lamellar morphology.

Comparing different types of bone, it can be concluded that the main determinant of mechanical properties is the amount of mineral in the tissue. [17] A clear trend between stiffness and mineral content is found when various types of bone are compared. The stiffness and strength values in the cancellous bone, varies depending on the weight or non-weight-bearing regions. Stiffness has modulus values in the range of 1–9.7 GPa. Weight-bearing trabecular systems can sustain superior–inferior compression levels of as much as 310 MPa and those from non-weight-bearing regions typically fail at stresses of from 120 MPa to 150 MPa. [18] The near-linear relationship found in this trend shows that the failure of bone in bending is determined by the strain to which it is subjected. [17] Concomitantly, the increase in the Young's modulus is associated with a decrease in the strain at failure. Despite the importance of the mineral content, the organic matrix plays a major role in the mechanical performance of bone, contributing for its plastic deformation, and the overall hierarchical microstructure is essential for its toughness. [19] Experiments on bone fracture showed that crack propagation is prevented by various complex ways, discussed by Nalla *et al* [20] In that study it was possible to experimentally demonstrate that local criterion for fracture in human cortical bone is consistent with a strain-based criterion, rather than being stress-controlled. More correlations between mechanical properties and structure found not only in bone but in a vast number of natural materials were excellently reviewed by Meyers *et al* [21]

2.3. Teeth

Mammalian tooth is a structural and functional gradient composite consisting of a hard, inert, component, the enamel, supported by the less mineralized, more resilient, and vital hard connective tissue, dentin, which is formed from and supported by the dental pulp - See Fig. II.2.A. Tooth is an engineering tool performing daily functions of mastication: teeth are subjected to stresses of about 20 MPa, 3000 times a day but their fracture is rare. It is hypothesized that this is partly due to the hardness and stiffness of enamel and partly to the toughness and relative compliance of dentin. [2]
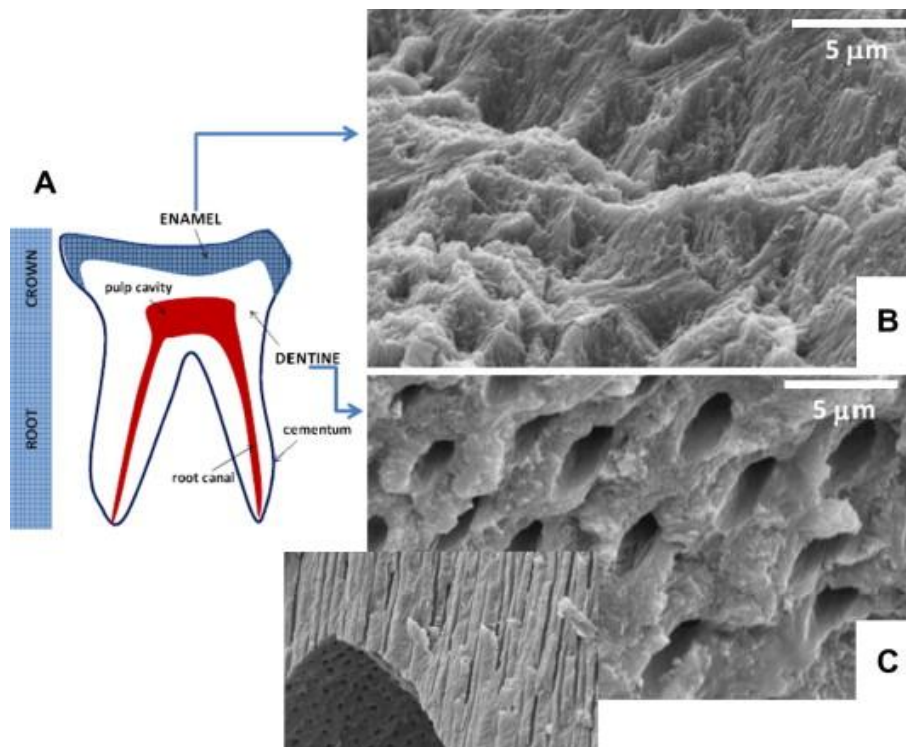
Fig. II. 2 Mineralized structure of tooth.

(a) Schematic drawing showing the enamel and dentin regions; (b) SEM micrograph of enamel and (c) SEM micrograph of dentin, showing the tubular morphology, surrounded by dense peritubular dentin – the longitudinal cut along the tubules is seen in the inset image.

Enamel is the most highly mineralized tissue found in the vertebrate body and also the hardest, being constituted by approximately 97% mineral (w/w), 1% organic material and 2% water. The basic structure is the nanosized fibril-like carbonate apatite crystals, much larger than the apatite crystals found in bone: in newborn mammals, they can be at least 100 µm long and 50 nm diameter [2]. The crystals are bound together, forming rods, or prisms, which are in turn arranged in a decussating, plywood-like structure. [17] Fig. 2B shows a SEM picture of a fracture surface of enamel of a 6 years old infant tooth. The topography reveals the formation of unique structures consisting of aligned prisms or rods with ~5 µm diameter, which run approximately perpendicular from the dentin–enamel junction towards the tooth surface. Each rod consists of tightly packed carbonated hydroxyapatite crystals, with very high aspect ratio. More details in the microstructure, detected, for example using atomic force microscopy can be found elsewhere. [22] In that work it was found, for nano-indentation experiments, that the stiffness is different in the two main direction of

the rods orientation. However, Fig. II. 2.B shows that, at a micron-level, different fiber orientations exist that could allow the enhancement of the isotropic behavior of the material, as discussed previously for other mineralized tissues.

Dentin has a similar composition to that of bone, its crystals being much thinner than those in enamel (ca. 2 × 50 × 25 nm) [2]. The tissue comprises a network formed by randomly intertwined mineralized collagen fibrils. Dentin is permeated by tubules, as shown in Fig. 2C that radiate from the pulp cavity towards the dentin-enamel junction. The mechanical performance in the region of such junction was analyzed by Imbeni *et al* in order to understand the mechanism that provides a crack-arrest barrier for flaw formed in the brittle enamel [23]: it was suggested that the interface never debonds but rather the crack penetrates and stop after a short travel through dentin.

2.4. Mollusk shells and nacre

Shells mainly consist of calcium carbonate (calcite or aragonite) forming multilayered microstructures, and a small amount of organic component (1–5 wt.%), mainly located within the inter-crystalline boundaries. Despite this composition, and owing to the special composite microstructure, mollusk shells present an enhancement in toughness by three orders of magnitude with respect to non-biogenic calcium carbonate. [24, 25] In fact, the arrangement of the crystals forces the deflection of a crack to a direction with an unfavorable stress state and prolongs the crack propagation, enhancing the energy absorption in the direction of crack travel. [26] However, as it will be seen later, other mechanisms should be taken into account to explain the amazing mechanical features of mollusk shells.

In some organisms the two calcium carbonate polymorphs may be found, but separated in different layers. [7, 27] A typical example is the shell of mussel (*Mytilus* sp.), where two layers can be found: an inner nacreous layer, a 'brick-and-mortar' of plate-like aragonite crystals (Fig. 3A), and an outer prismatic layer, with a honeycomb-like network structure of a polygonal prism formed by large crystals of calcite (Fig. II.3.B). During the growth of shells, the prismatic layer is first deposited and the nacre is added as the shell thickness increases with time. [8] These animal's shells have both calcite (90%) and aragonite (10%). The prismatic layer is based on long calcite crystals (rhombohedral) that are produced in a space

between a closely packed sheet of epithelial cells and a highly insoluble protein layer called the periostracum (covering the external surface of the shell). The nacreous layer is based on aragonite crystals (orthorhombic) deposited after the calcite layer so the mineralization is confined to the space between the cell layer and the growth front of the mineralization structure. [8] The crystallographic texture of aragonite is characterized by a nearly perfect *c*-axis alignment normal to the plane of the tiles. As in the prismatic layer, nucleation of aragonite tiles involves the induction of a single crystal in each nucleation site, with the particularity that in this case the orientation of the crystal is controlled in all three-dimensions relative to the structure of the organic matrix substrate. [7] Nucleation of the aragonite crystals takes place at a specific site on the surface which is known to have unique calcium-binding properties and to be rich in sulphur, presumably in the form of sulphate. [7]
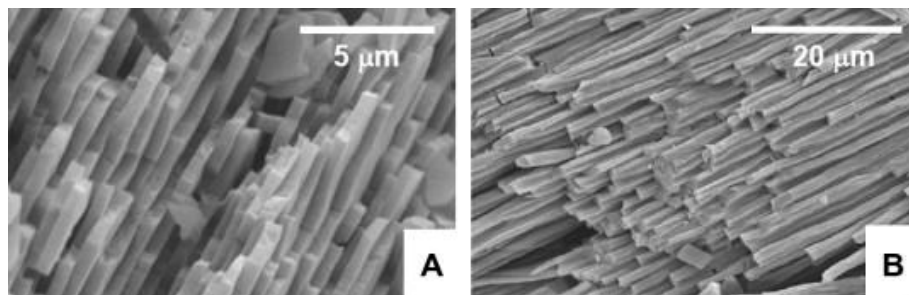
Fig. II. 3. SEM micrograph showing the fracture surface of the nacre **(a)** and prismatic **(b)** structure of mussel shell.

The nacreous layer is a laminate, with a thickness of about 0.5 µm, consisting of aragonite polygonal tablets between thin sheets of organic matrix. This matrix is formed by a protein-polysaccharide and limits the thickness of the crystals and is structurally important in the mechanical design of the shell. [7, 8] It reduces the number of voids in the wall, inhibiting crack propagation by dissipating energy related to an expanding defect along the organic layers rather than through the inorganic crystals. The organization and composition of the organic matrix in nacreous system was very well described by Addadi and Weiner [7], and reviewed later by the same group [28]. The mineral component is formed within an organic matrix composed of by β-chitin, silk-like proteins, and acidic glycoproteins rich in aspartic acid. It was hypothesized that the beta-chitin would be organized in aligned fibrils in the interlamellar sheets of the organic matrix, whereas the silk would be placed within the

sheets. [28] Nacre is stiff (E = 60-80 GPa) while maintaining a relatively high toughness (J_{IC} = 1.5 kJ/m^2, this is about 1000 times the toughness of aragonite). [29] Other mechanisms have been also proposed to explain the remarkable mechanical performance of nacre. A strength anisotropy perpendicular to the layers of 5 MPa vs. 540 MPa [21, 25, 30] and a relatively small difference in tensile and compressive strength of 170 MPa vs. 230 MPa [31], justifies the high toughness, possibly attributed to the existence of intertile mineral bridges in combination to the organic "glue". Fig. II. 4. summarizes the strength of nacre with respect to various loading directions.
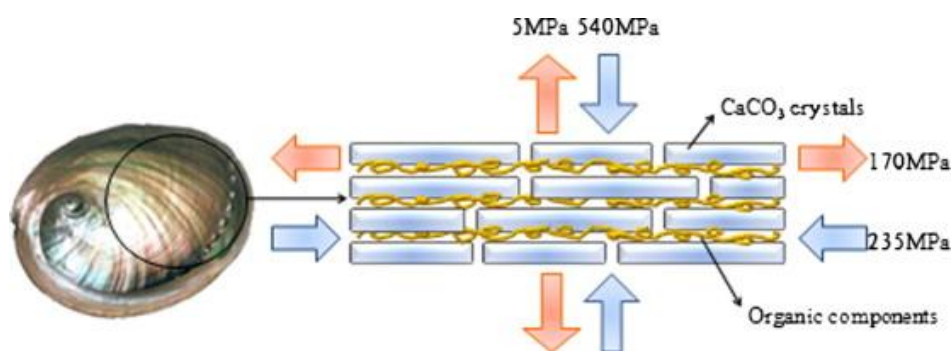
Fig. II. 4. Compressive and ultimate tensile strengths of nacre under different loading direction.

Wang *et al* examined the inelastic deformation of nacre, and conclude that this would involve interlamellae shearing [32]; moreover, these authors reported the existence of nano-asperities onto the aragonite tablets, which could provide resistance to interfacial sliding. Based on atomic force microscopy (AFM) and scanning ion conductance, Schaffer *et al* [33] suggested that mineral bridges could exist between the successive aragonite tablets, which were confirmed by Song *et al*, using TEM. [34] This particular nanostructure significantly influences the mechanical performance of the organic matrix layers of nacre, helping to arrest crack propagation. [35] Moreover, it was found that the individual aragonite platelets in nacre consist of the assembly of cobble-like polygonal nanosized grains (with sizes of about 32 nm) providing a ductile nature to such microstructures. [33] Such deformability of the aragonite platelets is relevant for the nacre's fracture toughness. A more recent work reports *in situ* AFM observations of the nanogranular texture of the aragonite platelets during mechanical deformation. [36] Under this process nanograin rotation and deformation occur, facilitated by the existence of the biopolymer spacing between the nanograins, which

will contribute to energy dissipation in nacre. The water present at the nanograin interfaces also contributes for the viscoelastic features in nacre. In fact, it was found that water has a significant positive effect on the macroscopic mechanical properties of mollusk shells. [37, 38]

Other morphologies, different from the prismatic and nacreous ones can be found in seashells. Fig. II.5. A shows the typical crystalline arrangement in an oyster shell, where it is clear a non-uniform arrangement of the elongated crystals. One can find then an additional upper level in the hierarchical organization of the shell in a cross-lamellar like organization, which will have a role in crack deflection during the fracture process. Similar microstructures were analyzed in another seashell. [39, 40] The cross-lamellar structure is a three-dimensional array of closely packed aragonite crystals, which are packed together tightly with their long axes and straight sides all aligned to form a sheet or lamella tens of microns wide and thick. [41] As previously mentioned in Section 2.1, this kind of morphology will enhance the isotropy of the macroscopic material.

Cross-lamellar morphologies can also be detected in gastropods. The shells of a conch (*Muricopsis* sp.) and of a terrestrial snail (*Helix* sp.) observed in the present work exhibit principally a cross-lamellar structure – see Fig. II. 5. B and C, respectively.
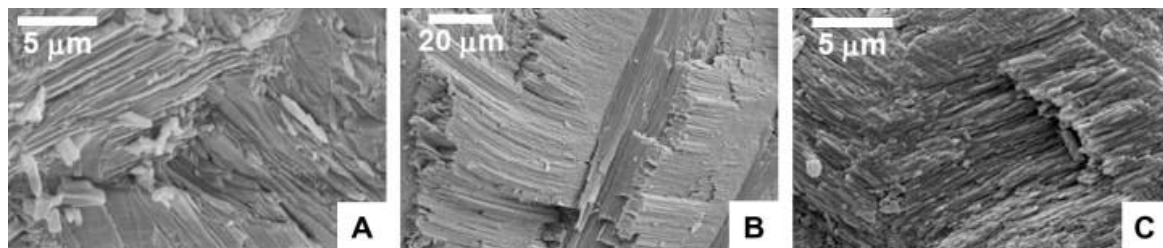
Fig. II. 5. Fracture surface of the cross-lamellar structure of different shells.
(a) Oyster shell; **(b)** Conch shell (*Muricopsis* sp.); **(c)** and a snail shell (*Helix* sp.).

The micro-architecture of nacre (mother of pearl) has been classically illustrated as a 'brick-and-mortar' arrangement. It is clear now that hierarchical organization and other structural features play an important role in the amazing mechanical properties of this natural nanocomposite. The more important structural characteristics and mechanical properties of nacre are exposed as a base that has inspired scientists and engineers to develop biomi-

metic strategies that could be useful in areas such as materials science, biomaterials development and nanotechnology. [42]

3. The importance of the interface in biogenic composites

Although presenting a hierarchical organization, any biocomposite is a complete structural system in itself, composed by different levels that are held together by specific interactions between the components. Therefore, the final mechanical and functional performance will be highly influence by the surface-to-surface interactions, including the interactions between the organic and inorganic components. Whatever the nature of the bonding between levels, adequate adhesion is required for system structural integrity. For example, it was suggested that one of the mechanisms associated with the good toughness of bone is that cracks propagation is prevented by unbroken collagen fibrils that bridges the crack. [20] In another study the total deformation of bone was studied together with the local deformation of the fibrils and mineral particles, by combining *in situ* tensile testing with high brilliance synchrotron X-ray diffraction and scattering. [43] The results were consistent with a hierarchical and coupled deformation mechanism starting from the nanoscale, where the organic matrix is relevant in the amount of strain transferred to the mineral platelets. This is a clear indication of the importance of the organic component, and its good liaison with the apatitic phase, on the mechanical performance of a mineralized tissue. The importance of the nano microstructure of the inorganic component in nacre for its mechanical properties has been referred to in Section 2.4. The particular interactions existing between the organic and aragonitic components also play an important role in the toughness of nacre. The inorganic insoluble layer between the nacre tablets can be seen as an adhesive that holds the tablets together. Smith *et al* used AFM to perform force-extension experiments in single-molecules of the organic material that was exposed on a freshly cleaved nacre surface. [44] The curves obtained did not exhibited a smooth and continuous shape as usually found in soft materials; instead, the individual fibers elongate in a stepwise manner, producing a series of saw tooth jumps, as folded domains or loops are pulled open. Such "sacrificial" (either intra- or interchain) bonds existing within the structure of the organic

molecules are believed to be in the origin of such peculiar behavior found on the nano-mechanical features of such macromolecules and will provide high energy of break.

The same kind of sacrificial bond and hidden length mechanism contributes to the mechanical properties of the bone composite. [45] In this case it was suggested that bone consists of mineralized collagen fibrils that are glued together by a non-fibrillar organic matrix. AFM measurements were also performed to get nano-mechanics information, where two pieces of bone are put in contact in solution, one on the AFM cantilever and one as a sample; the pieces were pressed together and pulled apart during which the forces were measured. It was seen that when the glue between the two pieces is stretched, energy is dissipated through rupturing of sacrificial bonds and the stretching of hidden length. This mechanism will contribute to the toughness of bone by increasing the amount of energy necessary for a crack to propagate. It was also suggested that specific interactions between the collagen-rich organic matrix and the ceramic nanoparticles could be on the origin of the minimum in the loss factor observed at 37 °C when on perform viscoelastic measurements as a function of temperature. [4] Such finding could be assigned to the fact that the molecular motions associated to damping may damage the bone structure. The minimization of damping at meaningfully temperatures and frequencies may then reduce this harmful process.

4. Biomimetic calcium phosphate coatings in the biomedical area

One of the most important applications that can arise from the study of biomineralization is in the treatment of medical pathologies or injuries in calcified tissues. In orthopedic applications the surface properties of implants play a fundamental role for the fixation to the bone tissue, in order to assure their long term function. However, artificial materials implanted into bone defects are usually encapsulated by a fibrous tissue, isolating it to the surrounding bone and thus compromising their use in bone repair. This tendency has been overcome by using or coating the implant with bioactive ceramics or glasses that spontaneously integrate with bone *in vivo.* [41] Among these materials, Bioglass®, BG, in the $Na_2O–CaO–SiO_2–P_2O_5$ system, was found to exhibit excellent bone bonding capability and

has been used clinically since 1985. [46] Upon implantation, bioactive ceramics and glasses produce a layer of apatite at the interface with bone, consisting of nanocrystals of carbonate-ion-containing apatite that has a defective structure and low crystallinity (see [41] and references cited therein). Much work has been developed to enhance the bioactivity of materials. They may involve procedures such as the introduction of bioactive particles of ceramics or glasses into the polymer (bioactive composites) or over its surface, or by chemically modifying the surface of the polymeric material, with groups that enhance the nucleation and growth of apatite. The so-called biomimetic preparation of calcium phosphate coatings on implant materials has emerged as a new concept and several methodologies have been proposed, especially implemented in polymeric-based systems, as it can be carried out at low temperatures. [47, 48]

An essential question is to assess the bioactive performance of materials *in vitro*. It was proposed that the formation of bone-like apatite *in vivo* could be reproduced in a simulated body fluid (SBF) with ion concentrations nearly equal to those of human blood plasma. Therefore, *in vivo* bone bioactivity of a material can be predicted from the apatite formation on its surface upon immersion in SBF. [49, 50, 51]

An example is given in Fig. II.6. where one can see the formation of a calcium phosphate layer in constructs for bone tissue engineering applications. Such kind of biodegradable porous structures can be seeded with the patient's own cells and differentiated into osteoblasts; when enough tissue is formed *in vitro* within the material, the hybrid construct is implanted in the bone defect in order to promote the formation of new bone. In a particular study PLLA/Bioglass® were prepared by compression molding followed by salt leaching. This allows for the production of porous structures with smooth surfaces (see Fig. II.6.A-left). Upon immersion in SBF an apatite layer is formed exhibiting a typical cauliflower morphology, which is composed by nano-sized carbonated hydroxyapatite crystals, i.e. very similar to the ceramic component found in bones (Fig. II.6.A-right). The combination of salt and another polymeric water soluble porogen, such as poly(ethylene oxide), PEO, permits the formation of pores with a textured surface due to the fingerprint left by PEO spherulites that are leached out during the scaffold processing [52] – see Fig. II.6.B-left. It was found that when Bioglass® is present in such textured scaffolds the ceramic formed upon immersion in SBF has a completely different nature that could lead to a different biological performance of the implant – see Fig. II.6.B-right [53]. This result demonstrates the relevance of surface

topography in the morphology of the calcium phosphate coating that is developed during immersion in SBF.
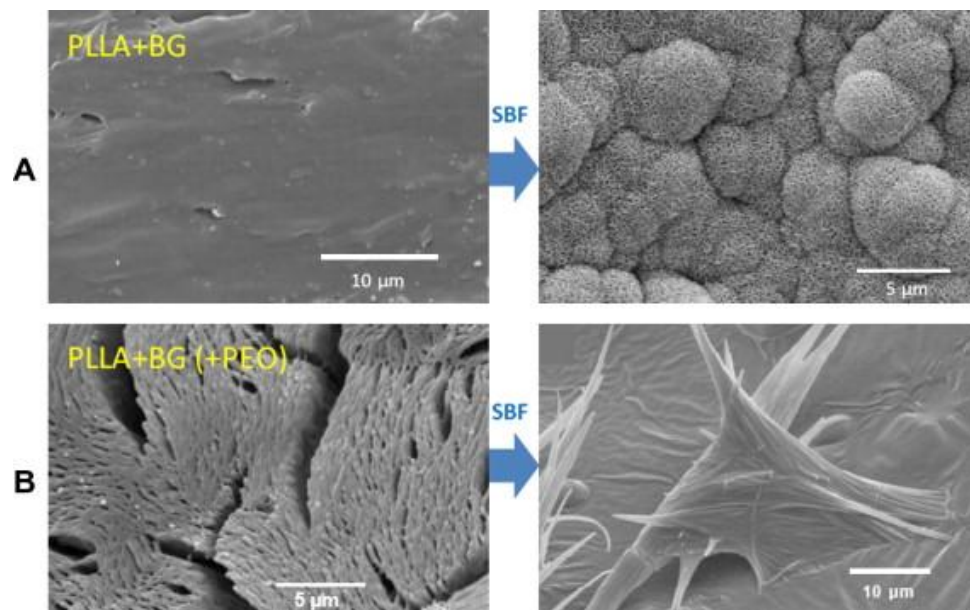
Fig. II. 6 . SEM images of the PLLA/Bioglass® scaffold.

    (a) (left) Smooth surface of the scaffold and (right) after one day of immersion in SBF, where the typical cauliflower-like morphology of the apatite layer is observed. **(b)** (left) Rough patterned surface of the porous scaffold where also PEO was used as a porogen and (right) after 1 day of immersion in SBF, where a completely different calcium phosphate coating was formed. Data based on results from [53].

Calcium phosphate coatings can also be used as reservoirs for the release of relevant therapeutic agents. An interesting concept is the inclusion of cytokines or morphogenetic factors, such as BMP-2, into biomimetic calcium phosphate coatings [54], which enhance the performance of the scaffold.

There is a strong interest in developing "smart" materials for a range of biomedical applications, which are able to respond to the trigger of different external variables, such as temperature, pH or ionic strength. [55] Such devices can be used in controlled drug delivery, cell culture substrates or sensors/actuators. In this context it would be interesting if one could trigger the onset of mineralization onto the surface of a biomaterial when immersed in SBF upon some change of an external variable, such as temperature, pH, light or salt con-centration. For example, "smart" surfaces were produced in poly(l-lactic acid)/Bioglass®

composites where a temperature-responsive polymer was grafted onto the surface: the precipitation of bone-like apatite occurred at physiological temperature, but was prevented at RT. [56] Such concept was extended to pH-responsive systems, where chitosan was grafted onto such composites [57]: in this case calcification occurred just at physiological pH and was prevented in acidic media, where the surface is more hydrophilic. Calcified responsive particles were also prepared where the release profile of a previously encapsulated drug could be dependent on both temperature and pH. [58]

Mimicking biomineralization under microgravity was performed by Sinha *et al.* [59] The authors carried out on-board during the flight of first recoverable space capsule (SRE-1) launched by Indian Space Research Organization, a polymer matrix mediated synthesis of hydroxyapatite nanoparticles under microgravity. In contrast, of a defect free large crystal formation under microgravity in solution crystallization, the present study revealed an order of magnitude reduction in the dimensions of hydroxyapatite nanoparticles synthesized by a biomimetic process with respect to its 1 g counterpart.

5. Biomimetic nacre-inspired nano/micro laminated materials and biomaterials

Biomimetic strategies should not attempt to copy directly the structures or functions of biological composites but rather gather key concepts from these systems that can be somewhat adapted within a synthetic concept. Therefore, as commented by Green *et al*, biomimetic composites should be habitually less complex than their biological counterparts and, to date, hierarchical architectures as observed in biological composites, remain outside the current technologies. [60] Advances in polymer technology have permitted to produce hierarchical structures in plastic pieces, using, for example, semi-crystalline or liquid–crystalline polymers. [61]

Much effort has been made to mimic the general structure and properties of natural composites, especially the synthetic production of nacre-like materials. Here are presented the latest advances on the synthetic design and production of nacre-inspired materials, in particular to be used in biomedical applications. The basic structural motif in nacre is the assembly of oriented plate-like aragonite crystals with a 'brick' ($CaCO_3$ crystals) and 'mortar'

(macromolecular component) organization. Many works recognized that such structure would be associated with the excellent mechanical properties of nacre, and biomimetic strategies have been proposed to produce new layered nanocomposites. [42]

A simple example of nacre mimicking was the production of laminated a Si_3N_4/BN composite, using a roll compaction technique, imitating the layered microstructure found in nacre [62]. The fracture surface of this material exhibits clear crack deflection and the fracture toughness was 28 MPa m$^{1/2}$ and works of fracture more than 4000 J/m^2. It would be much more interesting to fabricate nanolaminate structures at mild conditions, i.e. aqueous solutions and environmental temperatures and pressures. Moreover, it would be also important to have a good control of the organic/inorganic interface. Manne and Aksay reviewed some methodologies of producing nanolaminates [63], based on the use of inorganic particles. Four categories are addressed and discussed, namely Langmuir–Blodgett deposition, covalent self-assembly, alternating sequential adsorption and intercalation of organics into layered inorganic structures. Another approach proposed by Sellinger *et al* was based on a self-assembly process. [64] The process starts with a solution of silicates, coupling agents, surfactant, organic monomers and initiators in a water/ethanol mixture; during dip-coating micellar structures are formed and assemble into interfacially organized liquid–crystalline mesophases, thereby simultaneously organizing both the inorganic and organic precursors into the desired laminated structure. Organic polymerization, combined with continuous inorganic polymerization, lock-in the nanocomposite morphology through covalent bonds within the organic–inorganic interface. Note that most of the approaches presented do not enable the production of thick nanocomposites with pre-defined complex geometries. Thick hybrid films, based on nanocomposites containing clay with layered structure were produced by Bonderer *et al*, exhibiting excellent stiffness and strength. [65] Nanostructured organic–inorganic films were produced by Tang *et al*, also based on the layer-by-layer method, in which layers with more than 5 µm could be obtained. [66] The multi-layered films were produce by sequential immersion of a glass slide in solutions of a polycation and anionic montmorillonite clay. The tensile strength of the prepared multi-layers approached that of nacre, whereas their ultimate Young modulus was similar to that of lamellar bone. In another work the layer-by-layer technique was combined with chemical bath deposition to prepare TiO_2/organic polymer multilayered films with a nacre-like architecture. [67] Osteoconductive glass–ceramic nanoparticles were produced by a sol–gel

methodology and showed to be bioactive when combined with polymers. [68, 69] Layer-by-layer nanostructured hybrid coatings were also obtained by the sequential deposition of a substrate in a suspension of such bioactive glass–ceramic nanoparticles (exhibiting a negatively charged surface) and a solution of a positively charged polymer (chitosan) [70] – see Fig. II.7. Such biodegradable coatings were found to promote the deposition of apatite upon immersion in SBF (Fig. II.7) and are believed to have potential to be used in a series of orthopedic applications.
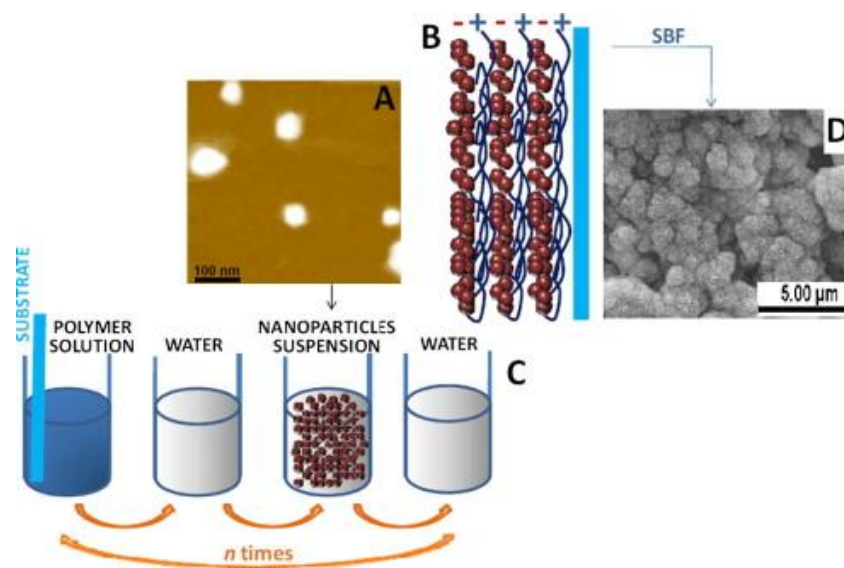
Fig. II. 7. Layer-by-layer with BG-NPs and Chitosan.

Bioactive nanoparticles (AFM image in **a**) were used to produce multilayered coatings **(b)** by alternate dipping a substrate in a chitosan solution, water and nanoparticles suspension **(c)**. Upon immersion in SBF an apatite layer could be detected onto the surface **(d)**. Data based on results from [70].

During the formation of sea ice the solutes present in sea water are expelled from the forming ice and entrapped within channels between the ice crystals; such principle was applied by Deville *et al* to ceramic particles dispersed in water to build nacre-like architectures. [71] First, layered materials are prepared through a freeze-casting method; the porous scaffolds are then filled with a second phase, e.g., an organic component, in order to produce a dense composite. Such simple methods should allow the production of layered composites with complex shapes and very interesting mechanical properties.

We refereed before to the fact that the formation of nacre involves the use of organic macromolecules as templates for the nucleation of the minerals and the control of the final material's shape. It was shown that a nacre-mimetic architecture could be synthetically reproduced through an appropriate combination of inorganic crystals and organic polymers [72, 73]. The specific interactions existing between the two components during crystallization of K_2SO_4 in the presence of poly(acrylic acid) generate the nanoscopic architecture (20 nm diameter blocks), and the switching between the modes of growth explains the formation of the macroscopic structure (microscopic nacre-like layered structure). [72] Similar experiments were carried out with $CaCO_3$ and poly(acrylic acid), where it was seen that, as in real biominerals, the synthetic mineral was generated from bridged nanocrystals with incorporated organic polymer. [73] Such bottom-up approaches may be useful to the design and synthesis of biomaterials for hard tissues, such as scaffolds for bone replacement or regeneration. [74]

Other bottom-up approaches are based on self-assembling. Also inspired by this natural material, Launey et al demonstrated that the concept of hierarchical design can be applied to conventional compounds such as alumina and poly(methyl methacrylate) (PMMA) by using ice-templated structures. With a flexible approach (that can be extended to other materials) they produced bulk hybrid materials with exceptional toughness that can be nearly 300 times higher (in energy terms) than either of their constituents. Like in nacre, the best synthetic materials reflect the natural concept of a hard ceramic phase providing for material strength, separated by a softer ''lubricant'' phase to relieve stresses in order to enhance toughness. The result is a high toughness ceramic, with strength of 200 MPa and a fracture toughness that is ≈300 times (in J-terms) larger than the main constituent, Al_2O_3, and exceeds values of 30 MPa m$^{1/2}$ ($J_c ≈ 8000$ J m^{-2}). Future work is being directed towards the formation of hybrid materials with much higher inorganic contents, the manipulation of the properties of the soft lubricating phase and extending this concept to other material combinations. In particular, the authors are attempting to process ceramic scaffolds infiltrated with higher melting point metals with the objective of developing strong and tough ceramic-based materials that can operate at elevated temperatures. [75] Lin et al reported a simple electrodeposition technology that enabled the creation of an inorganic–organic nanocomposites assembling gibbsite ($Al(OH)_3$) nanoplatelets/polyvinyl alcohol in a single step. The oriented layered nanostructures mimic the ordered brick-and-mortar nanostruc-

ture found in the nacreous layer of mollusk shells. The electrodeposited inorganic/organic nanocomposite films are obtained by applying direct-current electric field that enables the preferential alignment of gibbsite nanoplatelets and the co-deposition of non-ionic-type polymer between the inorganic nanosheets. The resulting self-standing nanocomposite films are optically transparent and flexible, even though the weight fraction of the brittle inorganic phase is higher than 80%. [76]

Tseng *et al*, fabricated a nacre like ZnO structure with three levels of hierarchy by a biomimetic method under mild conditions where the biopolymer gelatin was used as structure directing agent. The gelatine contains many polar amino acids, as surface protecting agent for the polar surfaces of ZnO. They found that the ZnO–gelatin microcrystal with well-defined hexagonal twin plate shape is built by the stacking of nanoplates. The irregularly edged nanoplates can adjust themselves to each other throughout the microcrystal, resulting in a roughly hexagonal edge. Similar to nacreous architecture, the nanoplate of ZnO was constructed from the oriented attachment of ZnO nanoparticles. The synthesis of the hierarchical ZnO structure in this paper could lead to new approaches to control the crystal size, orientation, and spatial patterning. [77]

Ekiz *et al* [78] used a novel technique called Hot-press Assisted Slip Casting (HASC) to produce artificial nacre-like laminar composites. This method combines hot-pressing and slip-casting to improve alignment and volume fraction of the reinforcement, allowing the production of Bulk nano-laminar composites. Alumina flakes were used as filler in an epoxy matrix. Flexural tests on Chevron notched specimens revealed a high work-of-fracture in the case of the fabricated composites reaching to 254 J/m^2. Main fracture mechanism is debonding of flakes from the matrix. With its high volume fraction (60%) of reinforcement phase and high degree of flake alignment, a nacre-like microstructure was achieved with a relatively efficient, cost effective and simple hybrid conventional method. The authors believe that with suitable raw materials HASC can be a very promising means to fabricate bulk biomimetic high work of fracture nano-laminar composites that can be used in numerous applications, increasing volume fraction of the filler and decreasing porosity that can lead to maximized mechanical performance.

Cai and Tang [79] suggested a new model of ''bricks and mortar'' based on the biological aggregation of apatite nanoparticles. An inorganic phase, amorphous calcium phosphate, acts as ''mortar'' to cement the crystallized ''bricks'' of nano-hydroxyapatite. Mean-

while, biological molecules control the nano-construction. By using hydroxyapatite nanospheres as the building blocks, highly ordered enamel like and bone-like apatite are hierarchically constructed in the presence of glycine (Gly) and glutamate (Glu), respectively.

6. Tissue engineering of mineralized structures

The overall goal of tissue engineering is to create functional tissue grafts that can regenerate or replace defective or worn out tissues and organs. [80] Tissue engineering strategies combines cells, biodegradable scaffolds, and bioactive molecules to recapitulate natural processes of tissue regeneration and development. The scaffold is basically an artificially substrate that will support cell proliferation and differentiation while maintaining its stability. Along the development of new tissue, the scaffold must degrade. These processed materials are viable under *in vitro* and *in vivo* conditions, allowing the integration of the scaffold with the living tissues. [81] Material choices are guided by the need to restore cell signaling and to match the mechanical behavior of the tissue being engineered. [82] An ideal scaffold needs to accomplish certain requirements to be able to stimulate the body's repair mechanisms. These include having a pore network large and open enough for cells and blood vessels to penetrate and the ability to bond to bone. [83] In the orthopedic area, the ideal scaffold should promote early mineralization and support new bone formation while at the same time allowing for replacement by new bone. Osteoconductive scaffolds may be readily prepared by including bioactive ceramic or glasses within the polymeric matrix. [84]

When studying biomineralization processes, calcium phosphates are of special importance because they are the most important inorganic constituents of biological hard tissues in vertebrates. They consist of the same ions as the mineral in natural bones. [85] Biologically formed calcium phosphates are often nanocrystals that are precipitated under mild conditions. They are disposed in complicated hierarchical structures, always based in small blocks of nanometer size scale. Mimicking the formation of natural calcium phosphate hard tissues contributes significantly to the biological function of engineered materials. Many advances have been made in biomaterials with the rapid growth of nanotechnology, allow-

ing the possibility of applying nano-calcium phosphates three-dimensional scaffolds in the repair of hard and soft skeletal tissues. [81, 86, 87].

Cai and Tang [79] present an interesting reflection over nano-calcium phosphates, showing that the capability of synthesizing and processing nano-calcium phosphates with controlled structures and topographies, in an attempt to simulate the basic nano-units of natural materials, provides the possibility of designing novel proactive bioceramics necessary for enhanced repair efficacy. Specifically, nano-hydroxyapatite can be seen as an ideal biomaterial able to mimic the building units of biological tissues such as bone, dentin, and enamel being of an extreme importance in hard tissue engineering due to its good biocompatibility and bone/enamel integration. The various primary positive results, regarding the biocompatibility and biomimicity of novel nanostructured bioceramics to natural bone, merit further confirmation (as a deep study of how these materials interact with cells) and also express a concern with the biological security of using nano particles, due to the danger of reaching the circulatory system by penetration into blood vessels. As bone biogenesis is thought to occur by templated mineralization of hard apatite crystals by an elastic protein scaffold, Song *et al* [75] attempted to recapitulate this process with synthetic biomimetic hydrogels (cross-linked polymethacrylamide and polymethacrylate polymers) functionalized to mimic the mineral nucleating proteins of bone. Strong adhesion between the organic and inorganic materials was achieved for hydrogels functionalized with either carboxylate or hydroxyl ligands. They investigated the integration of biomimetic mineral-nucleating ligands with calcium phosphates using a mineralization approach described elsewhere [88], discovering that the morphology and crystallinity of the mineral, as well as the binding strength at the polymer–mineral interface, were governed by the structure and density of the templating ligands. These results provide a framework for generating synthetic composites with defined organic/inorganic interfaces similar to natural bone.

The current challenge in bone tissue engineering is to fabricate a bioartificial bone graft mimicking the extracellular matrix (ECM) with effective bone mineralization, resulting in the regeneration of fractured or diseased bones. [89] In order to evaluate the potential of using nanostructured substrates for bone tissue regeneration, Prabhakaran *et al* [89] used electrospinning to prepare biocomposite polymeric nanofibers blending poly-l-lactide (PLLA), collagen and nano-hydroxyapatite. Osteoblasts grown on PLLA/collagen/hydroxyapatite nanofibrous scaffolds showed higher cell proliferation, and

increased ALP activity and mineralization, than the PLLA and PLLA/hydroxyapatite scaffolds. Hence the obtained biocomposite PLLA/collagen/hydroxyapatite nanofibers revealed to be promising structural scaffolds with suitable cell recognition sites, biocompatibility, osteoconductivity and sufficient mechanical strength for bone tissue engineering. Also based on this principle, nano-hydroxyapatite/collagen based composites, inspired from research on natural bone, have received great attention. The composites are prepared by directly mixing the nano-hydroxyapatite and collagen. Nano-hydroxyapatite is produced using modern ceramic technologies, while collagen is purified from animal tissue as fixing agent for hydroxyapatite. The weak binding between hydroxyapatite and collagen make them no cooperation effect *in vivo* for bone defects repair. The collagen degrades fast, but hydroxyapatite ceramic remains in the original form which do not attend the remodeling progress of bone. Researchers have also tried to develop mimetic methods to prepare nano-hydroxyapatite/collagen composites. One method involves the immersion in a simulated body fluid (SBF), used to improve the biocompatibility of conventional metal, alloy and polymer implants. Another method involves co-precipitation of collagen fibrils and nano-hydroxyapatite spontaneously, and is a promising route for achieving the same hierarchical structure in synthetic materials as in bone. [90] Cui *et al* [90] present a review on self-assembly of mineralized collagen composites including recent work involving biomimetic synthesis of new materials with the structure of mineralized collagen, focusing mainly on materials containing type-I collagen, with mineralization by Ca–P crystals.

A new class of biomimetic molecules that can form gels from aqueous solutions was proposed by Stupp and co-workers. [91, 92]. They introduced the concept of amphiphilic peptide, consisting of a peptide sequence covalently bonded to a very hydrophobic segment that is stable and neutral in aqueous solution. By changing the pH or the electrolyte environment (e.g., put the molecules in contact with physiological fluids) the molecules self-assemble giving rise to a complex 3D network of nanofibers and to mechanically consistent gels with very high water contents, being adequate to act as a synthetic extracellular matrix to be used in different applications in the field of regenerative medicine. By designing the peptides sequences appropriately it is possible to induce the precipitation of bone-like apatite onto such nanofibers [91], indicating that they could find applications in the orthopedic area.

Sol-gel derived bioactive glasses are also relevant on mineralized structures tissue engineering because they have a nanoporosity that can control degradation rate [87]. They can be foamed to produce scaffolds that mimic cancellous bone macrostructure. Bioactive glass foams with optimized nanoporosity are strong in compression; however, they have low toughness and pore strength when loaded in tension. Therefore an ideal scaffold would have all the properties of the glasses with enhanced toughness. This can only be achieved by creating new nanoscale composites. Resorbable polymers must interact with the silica based inorganic network at the nanoscale to maintain bioactivity and controlled resorption. A scaffold like this would regenerate diseased or damaged bone to its original healthy state. [83]

In order to understand the complex mineralization processes involved in bone-matrix mineralization, and adapt these strategies to the design of materials, Spoerke *et al* [93] developed an artificial, *in vitro* biomineralization process that utilizes a nanofiber gel as a substrate for biomimetic hydroxyapatite mineralization in three-dimensions. The system employs alkaline phosphatase (a natural enzyme secreted by osteoblasts, which liberates phosphates necessary for HA mineralization from organic phosphates) and a phosphory-lated, anionic nanofiber gel matrix to template HA nanocrystals with size, shape, and crystal-lographic orientation resembling natural bone mineral. Although the authors do not intend to mimic, functionally or structurally, any single bone protein, they believe that the assem-bly of peptide amphiphile nanofibers into a scaffolding framework could lead to biomimetic materials to promote bone regeneration, or the synthesis of hybrid materials with crystallographically defined structures. Data suggested that neither a nanofiber matrix alone, nor calcium enrichment alone will promote the ALP-mediated template mineraliza-tion observed in the PA gels, both spatial and temporal elements are necessary to achieve biomimetic mineralization in synthetic materials.

A high degree of hierarchy, gives bone its optimal bio-physical response. The current inorganic scaffold production processes do not allow the generation of a biomimetic orga-nized hierarchical structure, due to the consistent limitations in the current chemical pro-cessing technology for biomaterials. The development of hierarchically organized bone scaf-folds would surpass the current solutions in the synthetic bone substitutes matter.

Some authors [94-97] were inspired by nature. Tampieri *et al* [94] was specifically in-spired by natural wood templates, in the development of hierarchically structured bio-

materials. Wood exhibits a remarkable combination of high strength, stiffness and toughness at low density due to the unique hierarchical architecture of the cellular microstructure. Hence, the alternation of fiber bundles and channel-like porous areas makes wood an elective material to be used as a template in starting the preparation of a new bone substitute characterized by a biomimetic hierarchical structure. In their work, the authors developed a new biomimetic hydroxyapatite bone scaffold having highly organized micro- and macro-porosity, by implementing a multi-step procedure involving chemical–physical transformations of a natural wood template: pyrolysis of ligneous raw materials to produce carbon templates; vapor or liquid calcium infiltration to transform carbon into calcium carbide; oxidation process to yield calcium oxide; carbonation by hydrothermal autoclave treatments in controlled environment for further conversion to calcium carbonate and, finally, phosphatization through a hydrothermal process. This complex chemical process leads to the synthesis of biomimetic hydroxyapatite hierarchically organized scaffolds. Such synthesized structures maintain the 3D porous morphology of the starting native wood, thus allowing cell in-growth and reorganization and consequently providing the necessary space for vascularization due to the unidirectional oriented pore structures on the micrometer scale. The hierarchical architecture of the wood cellular microstructure and the hydroxyapatite constituting phase allow this new biomimetic material to be considered as an innovative charming inorganic scaffold for bone regeneration and engineering.

7. Concluding remarks

Nature offers a variety of hard materials exhibiting different hierarchical and oriented structures using a limited source of minerals and organic molecules. Such systems are produced in a bottom-up fashion under mild and aqueous solution conditions. These materials are designed to fulfill their structural and functional requirements. The lessons taken from the study of the structure–properties relationships of biocomposites and the mechanisms of biogenic composite formation can inspire the development of new concepts both for the design and the processing of man-made materials. The field of biomimetics has been developed faster in the last years, due to the recent developments of: (i) biology applied to materials science, including the use of biomaterials in tissue engineering and regenerative

medicine; (ii) nanoscience and nanotechnology and (iii) supramolecular chemistry. Such tools will enable the translation the enormous amount of work that has been accumulated from the observation of nature, namely the structure–properties/functions relationships found in natural nanocomposites, into useful devices.

Acknowledgments

References

[1] Wainwright SA, Biggs WD, Currey JD, Gosline JM. Mechanical design in organisms. Princeton: Princeton University Press; 1982.

[2] Vincent J. Structural biomaterials. Princeton: Princeton University Press; 1990.

[3] Ball P. Life's lessons in design. Nature 2001; 409(6818):413–6.

[4] Mano JF, Reis RL. Some trends on how one can learn from and mimic nature in order to design better biomaterials. Materials Science and Engineering C: Biomimetic and Supramolecular Systems 2005; 25(2):93–5.

[5] Sanchez C, Arribart H, Guille MMG. Biomimetism and bioinspiration as tools for the design of innovative materials and systems. Nature Materials 2005; 4(4):277–88.

[6] Bhushan B. Biomimetics: lessons from nature – an overview. Philosophical Transactions. Series A. Mathematical, Physical and Engineering Sciences 2009; 367(1893):1445–86.

[7] Addadi L, Weiner S. Control and design principles in biological mineralization. Angewandte Chemie - International Edition English 1992; 31(2):153–69.

[8] Mann S. Biomineralization: principles and concepts in bioinorganic materials chemistry. New York: Oxford University Press; 2001.

[9] Baer E, Hiltner A, Morgan RJ. Biological and synthetic hierarchical composites. Physics Today 1992; 45(10):60–7.

[10] Currey JD. Mater science - Hierarchies in biomineral structures. Science 2005; 309(5732):253–4.

[11] Gao HJ *et al* Materials become insensitive to flaws at nanoscale: lessons from nature. Proceedings of the National Academy of Sciences of the USA2003; 100(10):5597–600.

[12] Gao HJ. Application of fracture mechanics concepts to hierarchical biomechanics of bone and bone-like materials. International Journal of Fracture 2006; 138(1– 4):101–37.

[13] Weiner S, Addadi L, Wagner HD. Materials design in biology. Materials Science and Engineering C: Biomimetic and Supramolecular Systems 2000; 11(1):1–8.

[14] Aizenberg J et al. Skeleton of Euplectella sp.: structural hierarchy from the nanoscale to the macroscale. Science 2005; 309(5732):275–8.

[15] Weiner S, Wagner HD. The material bone: structure mechanical function relations. Annual Review of Materials Science 1998; 28:271–98.

[16] Ott I, Kienzler R, Schroder R. Aging in the cortical bone: a constitutive law and its application. Archive of Applied Mechanics 2010; 80(5):527–41.

[17] Currey JD. The design of mineralised hard tissues for their mechanical functions. Journal of Experimental Biology 1999; 202(23):3285–94.

[18] Brown TD, Ferguson AB. Mechanical property distributions in the cancellous bone of the human proximal femur. Acta Orthop Scand 1980; 51(3):429–37.

[19] Fratzl P et al. Structure and mechanical quality of the collagen–mineral nanocomposite in bone. Journal of Materials Chemistry 2004; 14(14):2115–23.

[20] Nalla RK, Kinney JH, Ritchie RO. Mechanistic fracture criteria for the failure of human cortical bone. Nature Materials 2003; 2(3):164–8.

[21] Meyers MA et al. Biological materials: structure and mechanical properties. Progress in Materials Science 2008; 53:1–206.

[22] Habelitz S et al. Mechanical properties of human dental enamel on the nanometre scale. Archives of Oral Biology 2001; 46(2):173–83.

[23] Imbeni V et al. The dentin–enamel junction and the fracture of human teeth. Nature Materials 2005; 4(3):229–32.

[24] Currey JD. Mechanical-properties of mother of pearl in tension. Proceedings of the Royal Society B: Biological Sciences 1977; 196(1125):443–63.

[25] Jackson AP, Vincent JFV, Turner RM. The mechanical design of nacre. Proceedings of the Royal Society B: Biological Sciences 1988; 234(1277):415–40.

[26] Li XD, Nardi P. Micro/nanomechanical characterization of a natural nanocomposite material – the shell of Pectinidae. Nanotechnology 2004; 15(1):211–7.

[27] Weiner S, Addadi L. Design strategies in mineralized biological materials. Journal of Materials Chemistry 1997; 7(5):689–702.

[28] Levi-Kalisman Y et al. Structure of the nacreous organic matrix of a bivalve mollusk shell examined in the hydrated state using cryo-TEM. Journal of Structural Biology 2001; 135(1):8–17.

[29] Barthelat F, Espinosa HD. An experimental investigation of deformation and fracture of nacre – mother of pearl. Experimental Mechanics 2007; 47(3):311–24.

[30] Meyers MA et al. Mechanical strength of abalone nacre: role of the soft organic layer. Journal of the Mechanical Behavior of Biomedical Materials 2008; 1(1):76–85.

[31] Menig R et al. Quasi-static and dynamic mechanical response of Haliotis rufescens (abalone) shells. Acta Materialia 2000; 48(9):2383–98.

[32] Wang RZ et al. Deformation mechanisms in nacre. Journal of Materials Research 2001; 16(9): 2485–93.

[33] Schaffer TE et al. Does abalone nacre form by heteroepitaxial nucleation or by growth through mineral bridges? Chemistry of Materials 1997; 9(8):1731–40.

[34] Song F, Zhang XH, Bai YL. Microstructure and characteristics in the organic matrix layers of nacre. Journal of Materials Research 2002; 17(7):1567–70.

[35] Song F, Soh AK, Bai YL. Structural and mechanical properties of the organic matrix layers of nacre. Biomaterials 2003; 24(20):3623–31.

[36] Li XD, Xu ZH, Wang RZ. In situ observation of nanograin rotation and deformation in nacre. Nano Letters 2006; 6(10):2301–4.

[37] Neves NM, Mano JF. Structure/mechanical behavior relationships in crossed lamellar sea shells. Materials Science and Engineering C: Biomimetic and Supramolecular Systems 2005; 25(2): 113–8.

[38] Barthelat F. Biomimetics for next generation materials. Philosophical Transactions. Series A. Mathematical, Physical and Engineering Sciences 2007; 365:2907–19.

[39] Pokroy B, Zolotoyabko E. Microstructure of natural plywood-like ceramics: a study by high-resolution electron microscopy and energy-variable X-ray diffraction. Journal of Materials Chemistry 2003; 13(4):682–8.

[40] Lin AYM, Meyers MA, Vecchio KS. Mechanical properties and structure of Strombus gigas, Tridacna gigas, and Haliotis rufescens sea shells: a comparative study. Materials Science and Engineering C: Biomimetic and Supramolecular Systems 2006; 26(8):1380–9.

[41] Kokubo T, Kim HM, Kawashita M. Novel bioactive materials with different mechanical properties. Biomaterials 2003; 24(13):2161–75.

[42] Luz GM, Mano JF. Biomimetic design of materials and biomaterials inspired by the structure of nacre. Philosophical Transactions. Series A. Mathematical, Physical and Engineering Sciences 2009; 367(1893):1587–605.

[43] Gupta HS et al. Cooperative deformation of mineral and collagen in bone at the nanoscale. Proceedings of the National Academy of Sciences of the USA 2006; 103:17741–6.

[44] Smith BL et al. Molecular mechanistic origin of the toughness of natural adhesives, fibres and composites. Nature 1999; 399(6738):761–3.

[45] Fantner GE et al. Sacrificial bonds and hidden length dissipate energy as mineralized fibrils separate during bone fracture. Nature Materials 2005; 4(8):612–6.

[46] Hench LL. The story of Bioglass. Journal of Materials Science: Materials in Medicine 2006; 17(11): 967–78.

[47] Oliveira AL, Mano JF, Reis RL. Nature-inspired calcium phosphate coatings: present status and novel advances in the science of mimicry. Current Opinion in Solid State & Materials Science 2003; 7(4–5):309–18.

[48] Alves NM et al. Designing biomaterials based on biomineralization of bone. Journal of Materials Chemistry 2010; 20(15):2911–21.

[49] Kokubo T, Takadama H. How useful is SBF in predicting in vivo bone bioactivity? Biomaterials 2006; 27(15):2907–15.

[50] Bohner M, Lemaitre J. Can bioactivity be tested in vitro with SBF solution? Biomaterials 2009; 30(12):2175–9.

[51] Muller L, Muller FA. Preparation of SBF with different HCO3-content and its influence on the composition of biomimetic apatites. Acta Biomaterialia 2006; 2(2):181–9.

[52] Ghosh S et al. The double porogen approach as a new technique for the fabrication of interconnected poly(L-lactic acid) and starch based biodegradable scaffolds. Journal of Materials Science: Materials in Medicine 2007; 18(2):185–93.

[53] Ghosh S, Reis RL, Mano JF. Bio-inspired mineral growth on porous spherulitic textured poly(L-lactic acid)/bioactive glass composite scaffolds. Advanced Engineering Materials 2008; 10(8):B18–22.

[54] Liu Y, de Groot K, Hunziker EB. BMP-2 liberated from biomimetic implant coatings induces and sustains direct ossification in an ectopic rat model. Bone 2005; 36(5):745–57.

[55] Mano JF. Stimuli-responsive polymeric systems for biomedical applications. Advanced Engineering Materials 2008; 10(6):515–27.

[56] Shi J, Alves NM, Mano JF. Thermally responsive biomineralization on biodegradable substrates. Advanced Functional Materials 2007; 17:3312–8.

[57] Dias CI, Mano JF, Alves NM. PH-responsive biomineralization onto chitosan grafted biodegradable substrates. Journal of Materials Chemistry 2008; 18(21):2493–9.

[58] Shi J et al. Biomineralized polysaccharide beads for dual-stimuli-responsive drug delivery. Macromolecular Bioscience 2008; 8(3):260–7.

[59] Sinha A et al. Mimicking biomineralization under microgravity. Materials Science and Engineering C: Biomimetic and Supramolecular Systems 2009; 29(3):779–84.

[60] Green D et al. The potential of biomimesis in bone tissue engineering: lessons from the design and synthesis of invertebrate skeletons. Bone 2002; 30(6):810–5.

[61] Baer E, Hiltner A, Keith HD. Hierarchical structure in polymeric materials. Science 1987; 235(4792):1015–22.

[62] Wang CA et al. Biomimetic structure design – a possible approach to change the brittleness of ceramics in nature. Materials Science and Engineering C: Biomimetic and Supramolecular Systems 2000; 11(1):9–12.

[63] Manne S, Aksay IA. Thin films and nanolaminates incorporating organic/ inorganic interfaces. Current Opinion in Solid State & Materials Science 1997; 2(3):358–64.

[64] Sellinger A et al. Continuous self-assembly of organic–inorganic nanocomposite coatings that mimic nacre. Nature 1998; 394(6690): 256–60.

[65] Bonderer LJ, Studart AR, Gauckler LJ. Bioinspired design and assembly of platelet reinforced polymer films. Science 2008; 319(5866):1069–73.

[66] Tang ZY et al. Nanostructured artificial nacre. Nature Materials 2003; 2(6):413-U8.

[67] Burghard Z et al. Nanomechanical properties of bioinspired organic–inorganic composite films. Advanced Materials 2007; 19(7):970–4.

[68] Hong Z, Reis RL, Mano JF. Preparation and in vitro characterization of novel bioactive glass ceramic nanoparticles. Journal of Biomedical Materials Research Part A 2009; 88A(2):304–13.

[69] Hong ZK, Reis RL, Mano JF. Preparation and in vitro characterization of scaffolds of poly(L-lactic acid) containing bioactive glass ceramic nanoparticles. Acta Biomaterialia 2008; 4(5):1297–306.

[70] Couto DS, Alves NM, Mano JF. Nanostructured multilayer coatings combining chitosan with bioactive glass nanoparticles. Journal of Nanoscience and Nanotechnology 2009; 9(3):1741–8.

[71] Deville S et al. Freezing as a path to build complex composites. Science 2006; 311(5760):515–8.

[72] Oaki K, Imai H. The hierarchical architecture of nacre and its mimetic material. Angewandte Chemie International Edition 2005; 44(40):6571–5.

[73] Oaki Y et al. Bridged nanocrystals in biominerals and their biomimetics: classical yet modern crystal growth on the nanoscale. Advanced Functional Materials 2006; 16(12):1633–9.

[74] Song J, Malathong V, Bertozzi CR. Mineralization of synthetic polymer scaffolds: a bottom-up approach for the development of artificial bone. Journal of the American Chemical Society 2005; 127(10):3366–72.

[75] Launey ME et al. Designing highly toughened hybrid composites through nature-inspired hierarchical complexity. Acta Materialia 2009; 57(10):2919–32.

[76] Lin TH et al. Electrophoretic deposition of biomimetic nanocomposites. Electrochemistry Communications 2009; 11(1):14–7.

[77] Tseng YH et al. Biomimetic synthesis of nacrelike faceted mesocrystals of ZnO–gelatin composite. The Journal of Physical Chemistry C 2009; 113(42):18053–61.

[78] Ekiz OO, Dericioglu AF, Kakisawa H. An efficient hybrid conventional method to fabricate nacre-like bulk nano-laminar composites. Materials Science and Engineering C: Biomimetic and Supramolecular Systems 2009; 29(6):2050–4.

[79] Cai YR, Tang RK. Calcium phosphate nanoparticles in biomineralization and biomaterials. Journal of Materials Chemistry 2008; 18(32):3775–87.

[80] Grayson WL et al. Biomimetic approach to tissue engineering. Seminars in Cell & Developmental Biology 2009; 20(6):665–73.

[81] Lee SH, Shin H. Matrices and scaffolds for delivery of bioactive molecules in bone and cartilage tissue engineering. Advanced Drug Delivery Reviews 2007; 59(4–5):339–59.

[82] Ferreira LS et al. Bioactive hydrogel scaffolds for controllable vascular differentiation of human embryonic stem cells. Biomaterials 2007; 28(17): 2706–17.

[83] Jones JR. New trends in bioactive scaffolds: the importance of nanostructure. Journal of the European Ceramic Society 2009; 29(7):1275–81.

[84] Rezwan K et al. Biodegradable and bioactive porous polymer/inorganic composite scaffolds for bone tissue engineering. Biomaterials 2006; 27(18): 3413–31.

[85] Vallet-Regi M, Gonzalez-Calbet JM. Calcium phosphates as substitution of bone tissues. Progress in Solid State Chemistry 2004; 32(1–2):1–31.

[86] Xu HHK et al. Injectable and macroporous calcium phosphate cement scaffold. Biomaterials 2006; 27(24):4279–87.

[87] Boccaccini AR, Erol M, Stark WJ, Mohn D, Hong Z, Mano JF. Polymer/bioactive glass nanocomposites for biomedical applications: A review. Composites Science and Technology 2010; 70(13)1764-1776.

[88] Song J, Saiz E, Bertozzi CR. A new approach to mineralization of biocompatible hydrogel scaffolds: an efficient process toward 3-dimensional bonelike composites. Journal of the American Chemical Society 2003; 125(5):1236–43.

[89] Prabhakaran MP, Venugopal J, Ramakrishna S. Electrospun nanostructured scaffolds for bone tissue engineering. Acta Biomaterialia 2009; 5(8):2884–93.

[90] Cui FZ, Li Y, Ge J. Self-assembly of mineralized collagen composites. Materials Science and Engineering: R: Reports 2007; 57(1–6):1–27.

[91] Hartgerink JD, Beniash E, Stupp SI. Self-assembly and mineralization of peptide–amphiphile nanofibers. Science 2001; 294(5547):1684–8.

[92] Hartgerink JD, Beniash E, Stupp SI. Peptide–amphiphile nanofibers: a versatile scaffold for the preparation of self-assembling materials. Proceedings of the National Academy of Sciences of the USA 2002; 99(8):5133–8.

[93] Spoerke ED, Anthony SG, Stupp SI. Enzyme directed templating of artificial bone mineral. Advanced Materials 2009; 21(4):425–30.

[94] Tampieri A et al. From wood to bone: multi-step process to convert wood hierarchical structures into biomimetic hydroxyapatite scaffolds for bone tissue engineering. Journal of Materials Chemistry 2009; 19(28):4973–80.

[95] Fujikawa S, Kunitake T. Surface fabrication of hollow nanoarchitectures of ultrathin titania layers from assembled latex particles and tobacco mosaic viruses as templates. Langmuir 2003; 19(16):6545–52.

[96] Krajnik G et al. Vinorelbine/gemcitabine in advanced non-small cell lung cancer (NSCLC): a phase I trial. European Journal of Cancer1998; 34(12):1977–80.

[97] Qian JM et al. Fabrication, chemical composition change and phase evolution of biomorphic hydroxyapatite. Journal of Materials Science: Materials in Medicine 2008; 19(11): 3373–83.

PART 2 - Experimental methodologies and materials

Chapter III

Materials and methods

Chapter III

Materials and methods

Abstract

The aim of this chapter is to present, in a more comprehensive manner, the details concerning both the materials and techniques used throughout the thesis to complement the information given in each chapter.

The materials studied in this thesis were chitosan and bioactive glass. Different methodologies were approached to process the referred materials, resulting in distinct experimental procedures that required different characterization techniques.

Keeping in mind that the ultimate purpose of doing research on the BTE is the successful translation to clinic, it is demanding to simulate as close as possible the *in vivo* conditions. Therefore, several tests were run *in vitro* to validate the future applicability of the developed materials *in vivo*.

1. Materials and processing

1.1. Bioactive glass

In opposition to some of the greatest scientific findings, bioactive glasses were not discovered by accident. Their discovery was the result of the pioneer investigation of several researchers, such as Larry Hench and colleagues who worked, between 1969 and 1971, towards the concretization of one apparently complex task: To develop a material that would not be rejected upon implantation in the human body. [1] This goal was achieved when they developed what is nowadays termed Bioglass®. This melt-obtained glass, comprising 45% of SiO_2, 24.5% of Na_2O, 24.5% of CaO and 6% of P_2O_5, known as 45S5, was successfully bonded to bone in *in vivo* tests. A series of further studies regarding a deeper understanding of the biological and chemical phenomena behind the bonding mechanism between bone and Bioglass® followed. Several clinical applications were also developed in the meanwhile based on its potential for bone regeneration. [1]

Despite the promising beginning of Bioglass®, a few limitations, inherent to the bioactive glass properties, prevent this material to be widespread in actual clinical use. Some comprehensive examples of the reasons behind these drawbacks follow.

45S5 Bioglass® monolithic devices were successfully implanted for replacing hearing related bones [2], tooth roots [3] and orbital floors [4]. The results were quite impressing and the implants were able to restore the previous damaged functions. Nevertheless, as in each case the implant had to be custom designed for each patient, the commercial viability was compromised, because pre-set sizes could not be adapted *in situ*, since the surgeons were not able to cut or remodel the material.

Another pointed out disadvantage of 45S5 Bioglass® and bioactive glasses of similar composition is the fact that they cannot be designed into amorphous bioactive glass scaffolds because they crystallize during sintering. Therefore, commercially, other bioceramics are preferred. [5] Regarding bioactive glass coatings used to improve metallic implants, they are also not the first commercial choice when the composition is very bioactive, because quick degradation times will compromise the stability of the implant in the long term. [5] Moreover, bioactive glass particulates compositions with actual regulatory approval for

bone synthetic materials are also not suitable for being processed as fibers, scaffolds or coatings. [5]

Concerning the described drawbacks, it is comprehensible that the commercial use of the bioactive glass is mostly restricted to the dental area, where they are usually used as granules. [5]

In the meanwhile researchers have found several solutions to overcome this problem; however, the new developments on bioactive glasses did not reach clinical trials yet. [5]

One of the most fundamental changes in producing bioactive glasses was the use of sol-gel procedures instead of melt-quench. Although all the commercially available bioactive glasses are produced by traditional melt-quenching, [5] sol-gel route offers a considerable number of advantages when processing this material [6-8]: The processing temperatures are much lower than the traditional ones; A wider range of bioactive compositions allows for a better response to specific clinical applications; Easier control of the final form (powders, monoliths, nanoparticles, gels...); High purity of the products; High specific area; High osteoconductive properties; Higher degradability.

Nevertheless, because melting is a low cost procedure and not as time consuming as sol-gel route, it will continue to dominate the commercial production of bioactive glass. [7]

Bioactive glasses obtained by the sol-gel method, do not need to include Na_2O in their composition, since the role of this component is related to final material processing, namely the lowering of the melting-point.

The structure of bioactive glasses is based on an amorphous network having SiO_4^{4-} tetrahedrons as basic unit. Normally, these tetrahedrons are linked together by oxygen ions located at their corners. In amorphous silica based networks, the existence of non-bridging oxygen ions balanced by ions such as Na^+, K^+, Ca^{2+} (called network modifiers) prevent the regular arrangement that is attributed to crystalline silica. The level of bioactivity of a glass may be related to the mean number of non-bridging oxygen ions in the silica tetrahedron, since it will dictate the instability of the network when in contact with an aqueous solution, defining thereby its reactivity and solubility. [9]

In order to be considered bioactive, the number of non-bridging oxygen ions per tetrahedron must be greater than 2.6, where 0 non-bridging oxygen correspond to a crystalline silica network or quartz glass and 4 non-bridging oxygen are attributed to dissolve SiO_4^{4-} ion.

[10] Figure III.1. depicts the evolution of silica tetrahedral network towards the formation of a particle during sol-gel synthesis. [9]
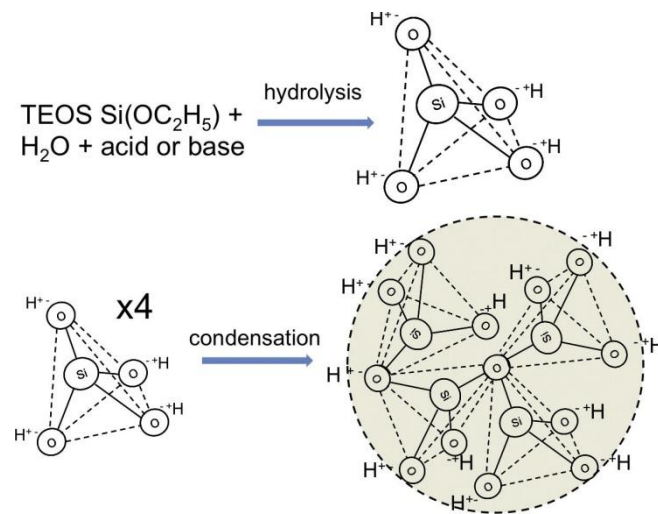
Fig. III. 1. Reactions occurring during the sol-gel process: formation of silica tetrahedra and nanoparticles at RT. Network modifiers are not represented for simplification purposes. Reproduced with permission from [5].

The proper chemical characterization of the produced bioactive glasses is very important, since variations in the oxide compositions will influence the chemical properties that control the bonding to the host tissues. [11] Characterization techniques applied to the study of the BG-NPs are presented in section 3 of the present chapter.

1.1.1. BG-NPs production

BG-NPs were prepared in different conditions and compositions throughout the experiments carried out in the research work herein reported. In Chapter IV, the influence of the reaction pH value (9 or 11.5) as well as the temperature of calcination (0 or 700°C), were evaluated regarding both a binary (SiO_2:CaO (mol.%) = 70:30) and a ternary system (SiO_2:CaO:P_2O_5 (mol.%) = 55:40:5). In chapter V the structural evolution of the same BG-NPs systems were studied in detail within the sol-gel reaction system. Also the influence of different molecular weight PEG was investigated for the ternary system developed at pH 11.5

and calcinated at 700°C. Chapter VI studied both the bioactivity and osteoblastic response of chitosan-based nanocomposites comprising BG-NPs from the ternary ($SiO_2:CaO:P_2O_5$ (mol.%) = 55:40:5) and quaternary compositions ($SiO_2:CaO:P_2O_5:MgO$ (mol.%) = 64:26:5:5). They were both produced at pH 11.5 and calcinated at 700°C. In Chapter VII, BG-NPs from the ternary composition $SiO_2:CaO:P_2O_5$ (mol.%) = 55:40:5 and also produced at pH 11.5 and calcinated at 700°C were printed on the surface of chitosan membranes in order to produce micro-scale bioactive features over such films. BG-NPs-based macrospheres from Chapter VIII were developed with a binary composition of $SiO_2:CaO$ (mol.%) = 35:65. Table III.1. summarizes all the conditions and compositions of BG-NPs produced during this PhD.

Table III. 1. BG-NPs compositions prepared in this work.

Chapter	Conditions			Composition (% mol)			
	pH	T (°C)	PEG (g/mol)	SiO$_2$	CaO	P$_2$O$_5$	MgO
IV	9	0	20000	70	30	-	-
				55	40	5	-
		700		70	30	-	-
				55	40	5	-
	11.5	0		70	30	-	-
				55	40	5	-
		700		70	30	-	-
				55	40	5	-
V	9	0	20 000	70	30	-	-
				55	40	5	-
		700		70	30	-	-
				55	40	5	-
	11.5	0		70	30	-	-
				55	40	5	-
		700	20 000	70	30	-	-
			0; 1500; 8000; 10 000; 20 000.	55	40	5	-
VI	11.5	700	20 000	55	40	5	-
				64	26	5	5
VII	11.5	700	20 000	55	40	5	-
VIII	11.5	700	-	35	65	-	-

The general procedure for obtaining the BG-NPs through sol-gel route is herein described as follows: In a washed beaker (300 mL) equipped with a magnetic stirrer, the adequate proportion of calcium nitrate was dissolved in distilled water at RT. TEOS together with ethanol were added to the above that solution. The pH value of the resultant solution

was adjusted to 2 with citric acid (10%) under stirring. The reaction mixture was kept stirring for 3h to obtain solution A.

In the case of the binary system, 1500 mL of distilled water were poured in 2000 mL beaker and under stirring the pH value was adjusted to 11.5 with ammonia water to obtain solution B. For the ternary and quaternary systems, $(NH_4)_2HPO_4$ was added to this solution, and for the quaternary system, also $Mg(NO_3)_2.6H_2O$ was included in solution B. Solution A was then slowly added drop-by-drop to solution B (1 drop/sec), through a separating funnel. During this step, pH value of solution B was kept around pH value of 9 or 11.5, according to the experimental conditions, by continuous supplement of ammonia water. After all the solution A content was added to solution B, this reaction mixture was kept stirring for 48 hours. The reaction system was kept still for 24h. After this gelation period, the supernatant was poured away and the precipitate was washed 3 times with 500 mL of distilled water. 200 mL distilled water were added to the white precipitation slurry, and then 2 g PEG was dissolved in this suspension with stirring. This suspension was kept still overnight, and then the supernatant was discarded and the precipitation slurry was moved to a plastic box that was frozen at -80°C. Freeze-drying followed for 7-10 days. The white powder obtained was calcinated at 700°C for 3h-5h. Figure III.2. presents a diagram comprising the experiment steps necessary for obtaining the BG-NPs through sol-gel route.
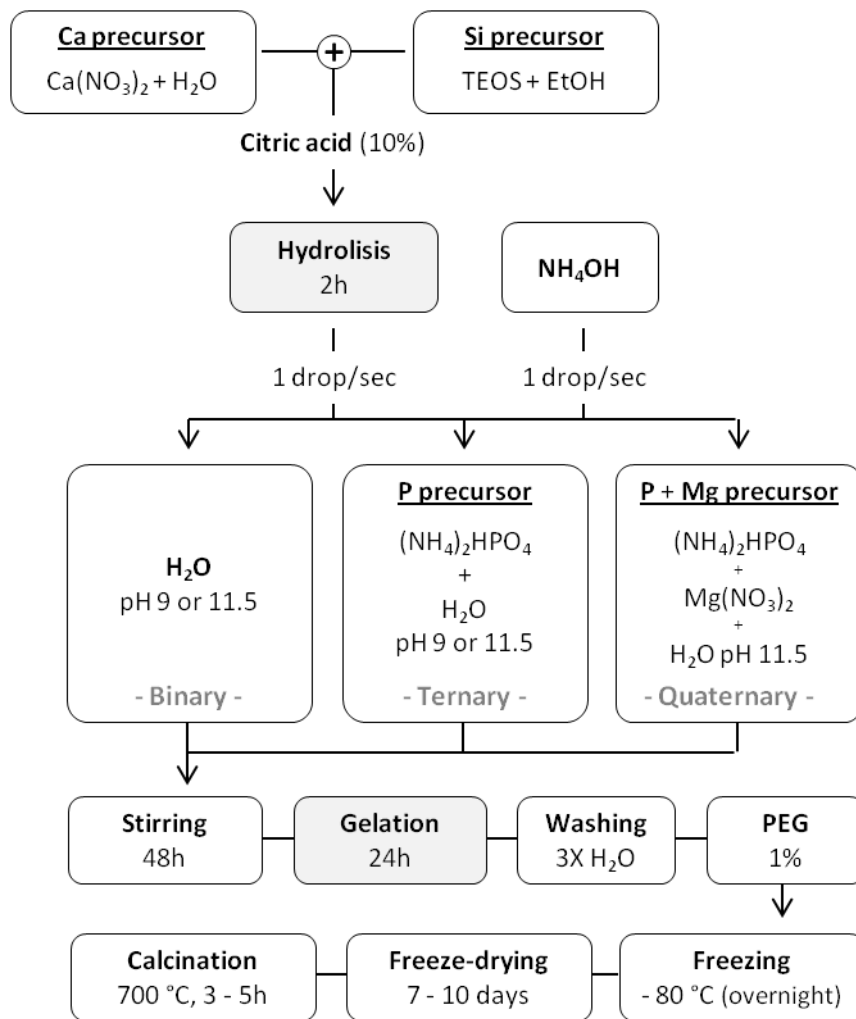
Fig. III. 2. Experimental steps to obtain the BG-NPs through sol-gel procedure.

1.2. Chitosan

Chitin is a highly insoluble natural polysaccharide found in the outer structures of crustaceans, insects and also on the cell walls of algae and fungi. The product of its N-deacetylation is chitosan, although the degree of deacetylation defining both is still not clear. [12, 13] The result is a linear polysaccharide, composed of glucosamine and *N*-acetyl glucosamine linked in a *β*(1–4) manner. [13]

The molecular weight of chitosan may vary from 300 to over 1000 kD according to its source and preparation conditions. The degree of deacetylation may also range from 30% to 95%. Crystalline chitosan is insoluble in aqueous solutions with pH value above 7. Its solubil-

ity may be facilitated in acidic mediums (pH<6.0), since the free amino groups on glucosa-mine become protonated. [13, 14] See figure III.3.
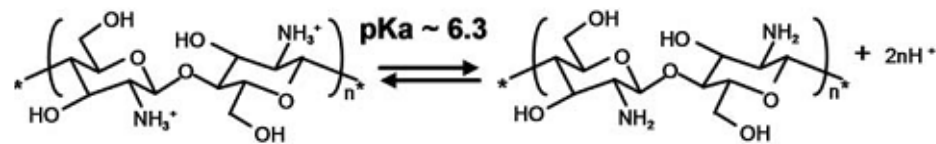
Fig. III. 3. Representation of the pH dependent protonation/deprotonation of the chitosan molecule. Adapted from [15].

Chitosan is a good candidate for biomaterial, because it has excellent properties such as biocompatibility, biodegradability, non-toxicity, adsorption properties. [12] When im-planted in the body, it evokes a minimal foreign body reaction, with little or no fibrous en-capsulation while stimulating the integration of the implanted material by the host. [16, 17] Nevertheless, some of its properties deserve some concern in order to achieve the best physiological results. For instances, chitosan's degree of acetylation influences inversely its degradation rate and on the other hand is directly correlated to cell attachment. [13, 18] Chitosan is primarily degraded through a hydrolysis mechanism resulting from the lysozyme action. [13]

From the processing point of view, chitosan is moldable in a wide range of forms such as membranes, fibers, blocks, granules and nanoparticles. Its porosity is also easily con-trolled by simple techniques as freeze-casting. [13]

Chitosan has a cationic nature that has been associated to important electrostatic in-teractions with negatively charged molecules, namely with anionic GAGs. Since a large number of cytokines/growth factors are linked to GAGs (mostly with heparin and heparan sulphate), chitosan may useful in retaining and concentrate growth factors secreted by col-onizing cells. [14]

1.2.1. Chitosan processing

1.2.1.1. Chitosan purification

Prior to any use, commercial chitosan of medium molecular weight was purified. Insoluble contaminants particles were removed by dispersing chitosan in distilled water and then solubilizing it by adding acetic acid to a concentration of 1% (w/v) chitosan in 1% (v/v) acetic acid. Filtering of the solution was performed first with a nylon filter followed by two filtrations with paper filter.

After filtering, chitosan was precipitated from the solution by titration with 2M NaOH until pH value of 8 was reached. The chitosan flakes were then washed with distilled water until pH value of 7 was reached and dehydrated with water/ethanol solutions with percentages of 80/20, 50/50 and 10/90. Finally, the chitosan flakes were frozen, freeze-dried and triturated till a fine powder was obtained.

1.2.1.2. Solvent casting of chitosan membranes

Chitosan membranes were produced by a casting solvent evaporation technique. In the case of the BG-NPs/chitosan composites, the membranes were obtained dissolving chitosan (0.7 % w/v) and BG-NPs (0.3 % w/v) in 2 % v/v acetic acid. The control membranes contain 1 % w/v of chitosan. 80 mL of the polymeric solution was poured on a square Petri dish and left to dry at RT. After evaporation for several days, the membranes were neutralized in NaOH 0.1 M, and left to dry. Figure III.4. illustrates the steps of casting, drying after neutralization and final cut with a 1.5 cm diameter punch.
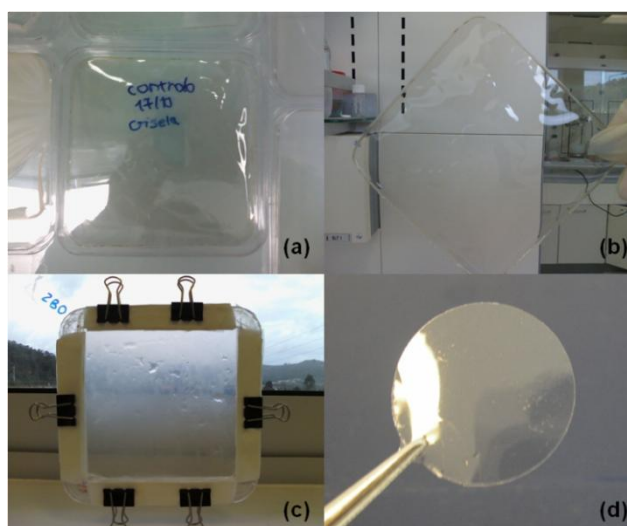
Fig. III. 4 Preparation of the chitosan membranes.

(a) Casting of the membrane in the squared Petri-dish; **(b)** Dried membrane after casting; **(c)** Drying of the chitosan membrane in a frame after proper neutralization; **(d)** Final cut of the membranes with a diameter of 1.5 cm.

In order to assure proper reproducibility of the results, the same surface area of the samples was used, for both cell seeding and mineralization tests in Chapters IV, VI and VII. When working with chitosan membranes in wet conditions one common problem, especial-ly when the chitosan membranes have small dimensions as was the case of the samples used in this work is the rolling of the membrane over itself, preventing the homogenous wetting of the surface targeted to the study. To avoid this, the circular membranes were clipped in eppendorf tops - See figure III.5. - which besides being easily sterilized and inert, facilitated the handling of the samples in each step of the experiments and also assured that the same surface area was in contact either with the cells or with the SBF.
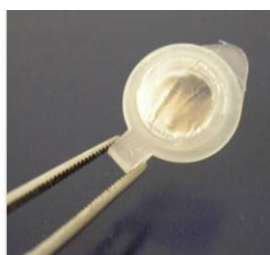
Fig. III. 5. Eppendorf frame used to handle the samples during the biological and mineralization assays.

2. Specific processing techniques

2.1. Microcontact printing

2.1.1. PDMS stamps production

In Chapter VII, a microcontact printing (µCP) technique allowed the production of BG-NPs micropatterns on chitosan. µCP is a soft lithography technique that uses the relief pattern on a PDMS stamp to form patterns on the surfaces of substrates by contact. [19]

PDMS polymer was chosen to produce the stamps since it has enough rigidity to support the topographic microstructure and also the required flexibility to adapt to the substrate and revert back to its original shape. Moreover, it is non-toxic and do not swell in the presence of water or ethanol. [20-24]

The master used to emboss the PDMS stamp was obtained by photolithography using SU-8 photolack. [25] In photolithography, a photoresist layer is spin-coated on a silicon wafer. Then a mask is placed in contact with the layer of the photoresist that will be illuminated with ultraviolet (UV) light through the mask. An organic solvent is used to dissolve and remove photoresist that is not crosslinked. After obtaining the patterned master, the PDMS stamp was prepared by casting a 10:1 mixture of Sylgard 184 (Dow Corning) prepolymer and cross-linker. The mixture was poured over the master and cured at 90 °C for 3 h in a vacuum oven. After cooling, the PDMS was peeled off from the lithographic template and cut to suitable sizes. Fig. III.6. summarizes the process.
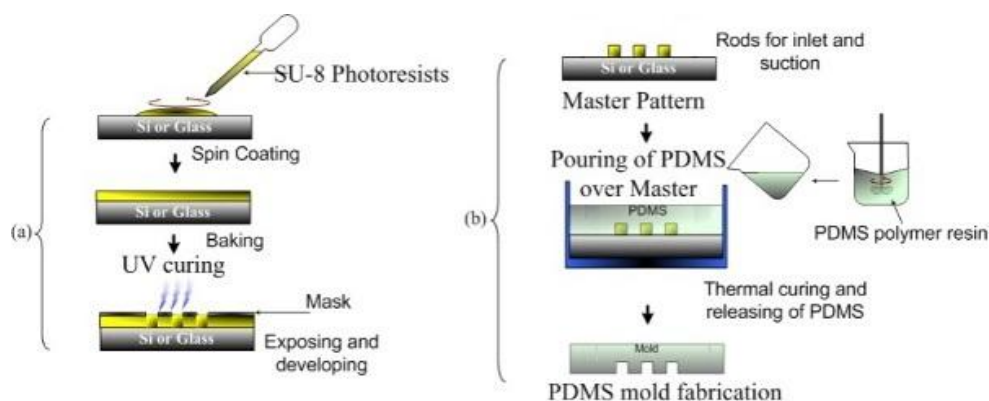
Fig. III. 6. Steps for the production of **(a)** The master and the **(b)** PDMS stamp. Adapted from [26].

The initial master contained three different patterned regions that were transferred to the PDMS stamp. The geometries were 50 µm diameter cylindrical pillars arranged in a square pattern with 50 µm spacing, 50 µm diameter cylindrical pillars arranged in a hexagonal pattern with 40 µm spacing, and ellipsoidal pillars (50 µm long axes and 30 µm short axes) arranged in a hexagonal pattern with 40 µm spacing. Each field was an 8 mm² square. The height of the final PDMS was controlled by the thickness of the layer of photoresist that was spread on the surface of the wafer. On the other hand, the mask controlled the shape and lateral dimensions. [27]

The aim of this experiment was to use a self-assembly or "stick-and-place" approach to retrieve BG-NPs from a donor substrate (glass slide) onto a PDMS stamp by van der Walls interaction. In a following step, the nanoparticles should be printed onto the receiving substrate, the chitosan membrane.

Regarding the preparation of the BG-NPs pad, a 549 µL amount of BG-NPs dispersion with different nanoparticles concentrations in ethanol (between 0.003% and 0.05%) was poured on the surface of a glass slide (9° inclination) in a small area of 1 cm × 1.5 cm limited with a hollow rectangular piece fixed to the glass slide with dental wax. The dispersion was left to evaporate for 48 h inside a chamber saturated with ethanol. Pictures related to the production of the BG-NPs pad can be seen on figure III.7.
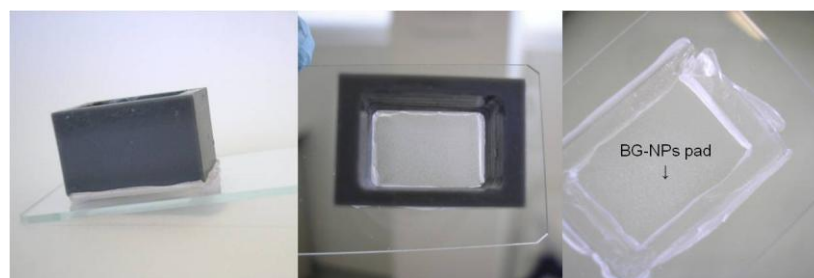
Fig. III. 7. Homogenous BG-NPs pad.

A special device was developed to facilitate the µCP process on the chitosan membranes. It was composed by two main axes. One of the axes was fixed to the base of the device and its function was to guide a central piece that established the connection between the fixed axe and the movable axe where the weights were applied. The fixed axe provided stability during the printing process. Recurring to two screws located at the central

piece, the printing axe position could be fixed or moved. Different weights (50g, 100g, 150g), having a hole in the middle, were easily fit in the movable axe where the PDMS stamp could be glued at its bottom with a double-sided adhesive tape.

The lift-off was made by pressing the PDMS stamp against the dried membrane of BG-NPs that remained in the glass slide (donor substrate) for 10 min at 7 kPa and RT. Before the "printing" step, the chitosan membrane was treated with a drop of acetic acid (0.1 M) spread on its surface with a brush. µCP of the nanoparticles was achieved by pressing the BG-NPs-loaded stamp on the chitosan membrane for 30 s under 30 kPa at RT. After removing the PDMS, the membrane was washed with ethanol and dried in a vacuum oven for 2 h at 40 °C followed by 24 h at 10^{-2} bar. Figure III.8. summarizes the steps involved in the µCP technique.
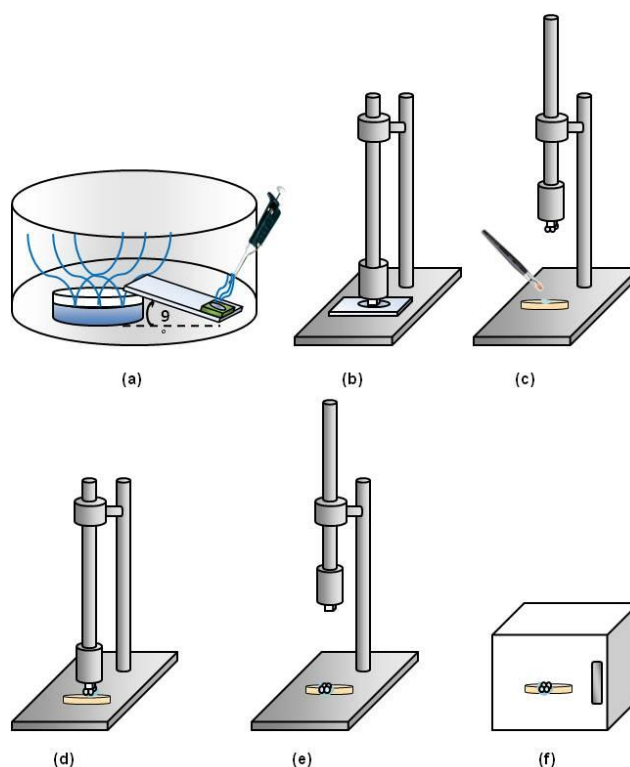
Fig. III. 8. Procedure for obtaining the µCP printed membranes.

(a) Preparation of the BG-NPs pad in the evaporation chamber. (b) Inking of the PDMS stamp in the BG-NPs pad; (c) Wetting of the chitosan membrane with acetic acid; (d) and (e) Pressing of the PDMS stamp in the chitosan membrane's surface and printing of BG-NPs. (f) Drying in the vacuum oven at 40°C.

2.2. Production of BG-NPs macrospheres on superhydrophobic surfaces

Superhydrophobic surfaces combined with controlled evaporation were successfully used in chapter VIII to produce BG-NPs-based macrospheres. The rational behind this experiment was the fact that, on superhydrophobic surfaces, the contact angle of a water droplet is so high that a BG-NPs suspension droplet is able to maintain a spherical shape while evaporating. EISA occurred during this process, resulting in BG-NPs-based macrospheres with ordered nanoparticles domains.

To prepare artificial superhydrophobic surfaces some techniques are used, namely the generation of rough surfaces coated with low surface energy molecules, roughening the surface of hydrophobic materials, and creation of well-ordered structures using micromachining and etching methods. [28]

The superhydrophobic surfaces were prepared through a chemical-based deposition procedure using commercial plates of copper (Cu). [29] The Cu substrate was immersed in distilled-water and the pH was adjusted to 9-10 with ammonium hydroxide. After 5 days at 4 °C the surfaces were collected, washed with distilled-water and left to dry on air. Finally, the Cu plates were immersed in a 1H, 1H, 2H, 2H - perfluorodecyltriethoxysilane (PFDTS) solution (1% v/v in ethanol) during at least 24 h and then dried in air.

3. Morphological characterization

3.1. Fluorescence microscopy

Fluorescence microscopy was used in Chapter VII and VIII were different samples were observed under a standard inverted-light microscope.

In Chapter VII, the obtained cell patterns were studied by this technique in order to gather visual information concerning the living cells. Calcein acetoxymethyl esther (calcein-AM) was chosen as a fluorescent cell viability marker. [30] By itself, calcein-AM is not fluorescent. However, after crossing living cell's membrane, an enzyme will remove the AM por-

tion. Within the cell, the calcein will bind to its calcium content, emitting thereby a green fluorescence under UV light.

In Chapter VIII, calcein-AM was also used to test the homogeneity and distribution of an additive in the BG-NPs macrospheres. In this case, no enzymatic reaction was involved to turn the calcein-AM in a fluorescent compose, since no cells were present. The staining was possible because a fluorescent complex between the calcium comprised in the BG-NPs and calcein occur at a strongly alkaline pH, as is the case of BG-NPs suspensions. [31, 32]

In both cases, staining was obtaining by addition of 2 mg of calcein-AM per mL of cell medium or BG-NPs suspension. After 10 min of incubation period, fluorescent images were obtained with the corresponding filters under an inverted microscope (Imager-Z1M).

3.2. Scanning electron microscopy

Due to the fact that almost all the samples analyzed in this work exhibited nanoscale phases, it was necessary to use scanning electron microscopy (SEM) to perform a morphological evaluation. SEM micrographs can be found in all chapters of part 4.

For imaging the samples, the scanning electron microscope uses secondary electrons for showing morphology and topography of the samples surfaces and backscattered electrons to achieve phase discrimination.

A NanoSEM-FEI Nova 200 (FEG/SEM) scanning electron microscope was used. It was necessary to sputter coat the samples with a thin gold layer, because the observed substrates were not naturally conductive, minimizing thereby charge accumulation. The sputtered conductive gold coating had between 10-20 nm in thickness.

An accelerating voltage of 15 kV was used to obtain the micrographs at different magnifications.

3.3. Scanning - Transmission electron microscopy

Scanning - Transmission electron microscopy (S-TEM) was used in Chapter V to follow the formation of the particles. While SEM retrieves 3D micrographs of the samples sur-

face, with S-TEM it is possible to obtain 2D structural images that allow one to distinguish hollow or dense structures.

S-TEM combines the principles of transmission electron microscopy and SEM presenting an improved spatial resolution. S-TEM was performed in the NanoSEM-FEI Nova 200 (FEG/SEM) scanning electron microscope.

In general, S-TEM requires sectioning of samples in very thin cuts. In the case of the BG-NPs observation, due to their reduced size, no further processing was necessary besides the particles dispersion in propanol by ultrasonic bath for 15 min and then transfer to a thin carbon film supported on TEM copper grids.

4. Chemical Characterization

4.1. Energy dispersive x-ray spectroscopy

SEM images are obtained by backscattered electrons. The atomic characteristics of each element will influence the final contrast on the image. By recurring to Energy Dispersive x-ray Spectroscopy (EDS or EDX) it is possible to identify those elements and also their relative proportions.

The data resulting from the EDX analysis are based on an X-ray spectrum obtained from a scan area of the SEM. A typical graph depicts on the Y-axis, the counts received by the detector, and on the X-axis it is represented the respective energy level of those counts.

EDX was used in chapter IV and V for characterization of the particles composition. At% was reported. In chapter VI, VII and VIII, EDX analysis were targeted for bioactivity characterization, since, with this technique, one can easily obtain the Ca/P ratio from the apatitic layer formed.

A Pegasus X4M instrument was used to perform the EDX experiments at low vacuum and without any coating. The measures were preformed at least in three different areas of each sample.

4.2. Zeta potential and particles size

In the hereby reported work, a Malvern Zetasizer device, model Nano ZS, was used to measure the Zeta potential of particles in a liquid medium. Their size was also measured.

Particle size measurements were performed in Chapter V. In solution, particles present a random movement due to the action of the molecules that surround them. The particles size is obtained by measuring this movement, called the Brownian motion of the particles, by a Dynamic Light Scattering (DLS) and establishing a relation with theoretical concepts based on the possible speed of movements associated with each particle size.

The zeta potential was measured to obtain information about the particles stability. In Chapter V, the zeta potential of both the binary and ternary systems was analyzed throughout the particles evolution regarding the sol-gel route. In Chapter VI, both the BG-NPs (from ternary and quaternary compositions) and the chitosan zeta potential were analyzed.

The zeta potential concept may be explained as follows: A particle in solution has an inherent electric charge and is thereby surrounded by a layer of oppositely charged and strongly bound ions that is called Stern layer. The Stern layer by its turn is neighbored by a diffuse layer of ions of different polarities. Within this diffuse layer there is a hypothetical location about 2 nm from the surface of the particle inside which the ions act as a single entity, that is defined as the shear level or slip plane. The zeta potential is measured at this frontier, establishing the electrical potential difference between the dispersion medium and the stationary layer of fluid attached to the dispersed particle. Zeta potential decreases exponentially approaching to zero when increasing the distance from the particle surface. [33-35] These concepts are represented in figure III.9. for a more comprehensive understanding.
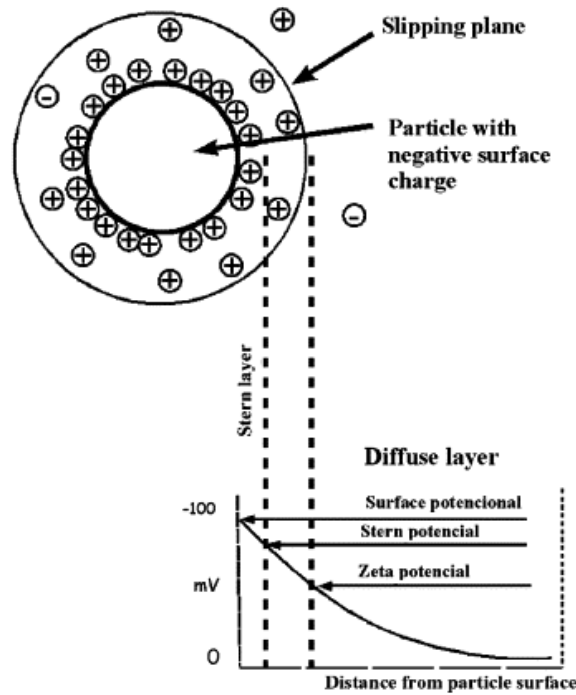
Fig. III. 9. Zeta potential and schematic of liquid layers surrounding the particle.
Reproduced with permission from [35].

Zeta potential can be used as an indicator of the tendency of aggregation between similarly charged particles. A value of 30 mV (rather positive or negative) indicates particle stability. A zeta potential value, lower than 30 mV, indicates that the attraction forces are stronger than the repulsion ones, leading to the formation of aggregates. [33, 36]

Zeta potential is calculated through theoretical models, namely the Smoluchowski model. [33] The Malvern Zetasizer device uses a combination of the Electrophoresis and Laser Doppler Velocimetry techniques to measure the zeta potential. A relation is established between the speed of a particle movement in a liquid and the applied electrical field. These properties will be related to two other known constants of the sample, the viscosity and dielectric constant to determine the final zeta potential of the particles.

The samples were prepared by dispersing 3 mg of sample in 5 mL of filtered ultrapure water. The pH of the solutions was adjusted to 7.4 to mimic the physiological conditions. The particles in solution were further dispersed for 15 min in the ultrasound equipment. Each sample was analyzed at 25°C after 120s of equilibration time. 3 measurements were preformed and the Smoluchowski model was used.

4.3. Fourier Transformed Infrared Spectroscopy

In Fourier transform infrared spectroscopy (FTIR), infrared radiation will be applied to a sample. The information resulting from the radiation absorption or transmitted will give one details about the molecular structures present in the sample, since only specific molecular vibrations can be excited.

In the initial stage of the work presented in this thesis, FTIR analyses were applied to the study of the BG-NPs composition. The analyses were performed in an IR Prestige 21 Shimadzu spectrometer. The samples were prepared by pressing the particles with KBr into a small disc. The FTIR spectra were recorded from 400 to 4400 cm^{-1} with the resolution of 4 cm^{-1}. Results can be found on Chapter IV.

4.4. X-ray diffraction

X-ray diffraction (XRD) is a technique based on the observation of the scattered intensity of an X-ray beam applied to a sample. It reveals detailed information about the chemical composition and crystallographic structure of the materials.

X-ray diffraction characterization of the BG-NPs was performed in Chapter IV. A Bruker D8 Discover model was used and operated at 40 kV and 40 mA using Cu Kα radiation. The detector was scanned over a range of 2θ angles from 15° to 60° at a step size of 0.04° and dwell time of 1 s per step.

5. Physical evaluations

5.1. Contact angle

The angle formed between the drop of a liquid and a solid substrate is defined as contact angle. Contact angle measurement gives one an indication of the affinity of a liquid to a solid surface. Surfaces may thereby be classified as hydrophobic if the referred angle is

higher than 90° or hydrophilic if the angle is lower. Contact angle is therefore useful in providing information related to the interactions between a surface and a liquid, namely the wetting ability and the surface energy.

There are several methods to obtain a contact angle measurement based on whether the data are collected on a dynamic or static mode.

In chapter VI of the present thesis, the wettability of the membranes was evaluated through the sessile drop method. In this method, an optical system captures the profile of a selected liquid drop on the substrate in study.

The volume of the applied droplets of glycerol was 3 μl. The mean value was calculated from at least four individual measurements on different areas of the surfaces. An OCA15+ goniometer (DataPhysics, Germany) was used.

6. *In vitro* Mineralization tests

In the work herein reported, the testing of the bioactive character of the materials was exclusively performed *in vitro.*

The essential requirement for establishing a bond between a biomaterial and bone is the formation of an apatitic layer on its surface when immersed on physiological fluids or simulated physiological fluids. [37] Therefore, it is widely accepted that *in vivo* bioactivity can be predicted by immersing the material to be tested in an SBF. SBF is prepared in order to reproduce approximately the ion concentrations found in human blood plasma. Table III.2. compares the ion concentrations of SBF and human blood plasma. [38]

Table III. 2. Comparison between ion concentrations in SBF and in human blood plasma.

Ion	Ion concentrations (mM)	
	Blood plasma	SBF
Na^+	142.0	142.0
K^+	5.0	5.0
Mg^{2+}	1.5	1.5
Ca^{2+}	2.5	2.5
Cl^-	103.0	147.8
HCO_3^-	27.0	4.2
HPO_4^{2-}	1.0	1.0
SO_4^{2-}	0.5	0.5
pH	7.2-7.4	7.4

Using SBF as an *in vitro* indication of the materials' behavior upon implantation presents several advantages over the *in vivo* studies. It is a good ethical practice since it avoids sacrifice of animals in preliminary studies. Moreover, the costs associated with this type of tests are reduced and the reproducibility is more reliable since it is easier to control the conditions than in the physiological environment.

Whether *in vivo* or *in vitro*, Hench explained the glasses bioactivity mechanisms with five initial stages of inorganic reaction. [1] These stages are summarized in Fig. III.10.

In stage I a rapid exchange of cations such as Na^+ or Ca^{2+} occur with H^+ or H_3O^+ from solution. In the following stage, soluble silica in the form of $Si(OH)_4$ is lost to the solution resulting from breakage of Si-O-Si bonds and formation of SiO-OH (silanols) at the glass/solution interface. In the third stage condensation and repolymerization of a SiO_2-rich layer on the surface presenting a significant Ca and P loss. The fourth stage comprises migration of Ca^{2+} and PO_4^{3-} group to the surface forming $CaO-PO_4^{3-}$ clusters on the top of the silica rich layer, followed by growth of the amorphous CaP. Finally, in stage V, Crystallization of the amorphous CaP occurs by incorporation of OH^-, CO_3^{2-} anions from solution to form a hydroxyl-carbonate apatite layer.
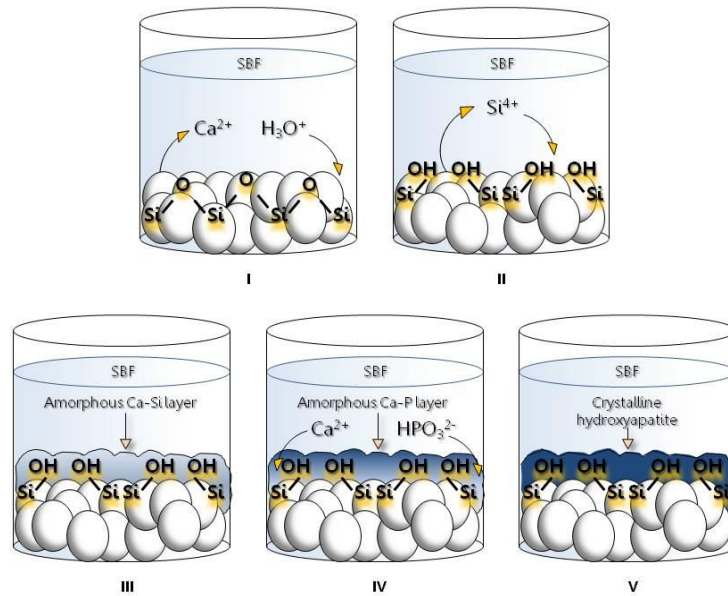
Fig. III. 10. Ionic exchanges at the glass/solution interface, leading to the formation of an HAp layer *in vitro*.

In vivo, the following stages would comprise the adsorption and desorption of growth factors and preparation of the implant site for tissue repair by the macrophages, followed by attachment, proliferation and differentiation of the osteoblasts. After 6-12 days, in the last *in vivo* stage, mineralization of the matrix occurs followed by maturation of the encased osteocytes. [1]

The bioactive character of the tested materials was assessed exhaustively in chapter IV by SEM, EDX and XRD. In chapter VI, VII and VIII only SEM and EDX were used, since the formulations studied were mostly based on the results from chapter IV, which could be extended for the new developed applications. Furthermore, EDX analysis was performed in a quantifying mode that allowed the calculation of Ca/P ratio and later comparison with the HAp Ca/P ratio.

7. Biological studies

Analysis of cells metabolic activity, morphology, proliferation and activity were performed with the aim of evaluating the *in vitro* biological performance of the developed material.

7.1.   The cells

Prior to any *in vivo* assessment, it is important to run preliminary studies that will discard or not a certain material for biomedical applications. For this purpose, cell lines are frequently used.

Cell lines are immortalized cultures of cells, able to proliferate indefinitely, being thereby very useful to study a number of biological responses in *vitro*. Such cell sources offer the advantage of being more homogeneous and standardized than primary cultures.

L929 fibrosarcoma mouse cell line (European collection of cell culture-ECACC, UK) was derived in March of 1948 and is suitable for toxicity testing. It was used in chapter IV and VII for preliminary biological response assessment to the materials therein reported, namely BG-NPs and BG-NPs patterned chitosan membranes.

SaOs-2 (European collection of cell culture-ECACC, UK) is a human osteosarcoma cell line usually used to study bone-applications biomaterials, since it possess several osteoblastic features. In Chapter VI, SaOs-2 cells were seeded on the different nanocomposites of BG-NPs and chitosan produced.

7.2. Preparation of the cell culture

In Chapter IV an indirect assessment of the BG-NPs cytotoxicity was performed using L929 cells. Materials leachables were obtained by placing in a falcon tube 200 mg of BG-NPs per mL of culture medium. The particles were previously sterilized by autoclaving. After 24 h under stirring at 37 °C, the media containing the BG-NPs extracts, was filtered and applied, as nourishment medium, to the plates containing cells previously seeded on a multi-well plate and cultured at 37 °C with 5% CO_2 and nourished with Dulbecco's modified minimum essential medium (D-MEM) supplemented with 1% antibiotic and 10% FBS. The cultures were then incubated at 37 °C for one, three and seven days. The culture media was replaced on the third day.

Regarding the biological tests that were ran in chapter VI and VII, the procedure had slight modifications. In this case, direct contact assessment was chosen since the cells could be efficiently seeded on the membranes surface.

L929 cells and SaOS-2 cells, respectively in Chapter VI and VII were cultured at 37 °C with 5% CO_2 and nourished with Dulbecco's modified minimum essential medium (D-MEM) supplemented with 1% antibiotic and 10% FBS. The medium was refreshed every three days until confluence, when the cells were tripsinized. In both cases, the samples were previously sterilized by immersion in 70% (v/v) ethanol overnight and then washed twice with sterile phosphate buffered saline (PBS). The cells were then seeded on the samples (n = 3) at a density of 65 000 cells/cm^2, and then the cultures were incubated at 37 °C also for one, three and seven days with a culture media renewal at the third day.

In chapter VI, for both DNA proliferation assay and for ALP activity quantification, samples were collected on days 1, 3 and 7 after seeding. Samples removed from culture were rinsed twice in PBS solution and transferred into 1.5 mL microtubes containing 1 mL of ultra-pure water. In order to assure cell lysis, samples were incubated for 1 h at 37 °C in a water bath and stored for at least 1 h in a -80 °C freezer. After thawing, samples were sonicated for 15 min.

7.3. The assays

7.3.1. MTS assay

MTS (3-(4,5-dimethylthiazol-2-yl)-5-(3-carboxymethoxyphenyl)-2-(4-sulfophenyl)-2H-tetrazolium) assays were conducted in chapter IV, VI and VII. Regarding chapter IV and VII, the assay was applied with the purpose of obtaining an indication of the cellular toxicity. In chapter VI, MTS was a complement of other biological assays also performed.

MTS assay is based on the fact that only metabolic active cells are able to reduce tetrazolium products. A colored formazan product will be obtained as a result of that reduction that can be correlated to the number of viable cells in culture.

The MTS test (Promega) was done after each time point (1, 3 and 7 days of culture).

The relative cellular viability (%) was obtained and compared with tissue culture polystyrene (positive control of cell viability). Latex was used as negative control of cellular viability. For this assay, an MTS solution was prepared by using 1:5 ratio of MTS reagent and D-MEM culture medium without phenol red or FBS, followed by a 3 h incubation period at 37

°C. All cytotoxicity tests were conducted by using three replicates. Finally, the optical density (OD) was read at 490 nm on a multiwell microplate reader (Synergy HT, Bio-Tek Instruments).

7.3.2. DNA assay

To assess cell proliferation on the developed nanocomposites of Chapter VI, by double-stranded DNA (dsDNA) content analysis, an Invitrogen/Molecular Probes PicoGreen dsDNA Quantification Kit was used.

The basic principle of this assay is the measurement of the fluorescence produced when PicoGreen dye is excited by UV light while bounded to dsDNA.

Triplicates were made both for samples and dsDNA standards (0-2 µg/ml), followed by incubation of the 96-well white plate (Costar; Becton-Dickinson) for 10 min in the dark. Fluorescence was read using a microplate ELISA reader (BioTek, USA) at an excitation of 485 nm (excitation of the dye) and an emission of 528 nm (when the dye is bounded to the dsDNA) with bandwidth of 20 nm. DNA concentration values were obtained from a standard curve.

7.3.3. ALP quantification

Bone-type alkaline phosphatase (ALP), a tetrameric glycoprotein that is attached to the osteoblast cell membrane by a carboxy-terminal glycan-phosphatidyl-inositol anchor, is frequently related to bone formation and calcification, although there are still some questions regarding its relevance and specific functions in the mineralization process. [39-41] For instances, it is known that the enzymatic hydrolysis activity of ALP is necessary to form mineralized tissue. However, the anchoring of ALP to the cell membrane is not always necessary for mineralization, but influences the nodule formation *in vitro.* [39]

When bone ALP is released from the plasma membrane by the action of a phospholipase (phosphatidylinositol-specific phospholipase C), it will stay in circulation for 1-2 days being after that period cleared from circulation by the liver. [39, 41]

Since the increase of osteoblastic differentiation in bone tissue can be correlated with the increase of the released ALP activity, ALPase enzymatic activity is widely used *in vitro* as a marker of osteoblast phenotype and differentiation. [39]

Bessey *et al* [42] developed a method for rapid determination of alkaline phosphatase in human serum that can be extrapolated for in vitro assays. The assay is based in a colorless substrate, p-nitrophenyl phosphate. In the presence of ALP, a yellow salt of p-nitrophenol is released when the phosphate group is lost, indicating thereby the phosphatase activity.

ALP quantification was performed in chapter 6, because the aim of the experimental work thereby reported was to study the osteoblastic response upon seeding in chitosan/BG-NPs films.

In detail, to quantify ALP activity, each well of a 96-well plate (Costar; Becton-Dickinson) received 20 µl of the sample to be analyzed and 60 µl substrate solution consisting of 0.2% (wt v^{-1}) p-nytrophenyl phosphate (Sigma) in a substrate buffer with 1 M diethanolamine HCl (Merck, Germany), pH 9.8. After an incubation period of 60 min at 37 °C, 80 µl stop solution (2M NaOH (Panreac, Spain) plus 0.2mM EDTA (Sigma)) was added to each well. Standards were then prepared with p-nytrophenol (10 µM ml^{-1}; Sigma) in order to achieve final concentrations in the range 0-0.3 µM ml^{-1}. Samples and standards were prepared in triplicate. Absorbance was read at 405 nm and sample concentrations were read from the standard graph. ALP enzymatic activity was normalized to total DNA content.

7.3.4. SEM observations

In chapter VI and VII, SEM observation of the seeded cells was carried out as a means to evaluate the effect of each sample on the morphology of the cells.

After 1, 3 and 7 days of culture, the samples were rinsed twice with PBS to remove non-adherent or loosely adherent cells and fixed with a solution of 2.5% (v/v) glutaraldehyde in 0.1M PBS, for 1h at 4°C. After removing the fixative, the cells were rinsed in PBS and distilled water and dehydrated in a graded series of ethanol solution (50%, 70%, 90% and 100%) each one repeated twice for 15 min. They were left to dry at air at RT, and sputter-coated with gold before SEM observation.

8. Statistical analysis

In the analysis performed in this work, 3 to 5 replicates were used for each condition; therefore, Student's *t*-test was chosen to run the statistical analysis, since it is suitable for being applied on small groups of samples independently collected.

In Student's t-test the means of two samples are compared. It is assumed that the samples follow a t-distribution where $\bar{x}$ is the sample mean, μ the population mean, s the estimator for population standard deviation, and N the set of the independent measurements x_i.

$$t = \frac{\bar{x} - \mu}{s/\sqrt{N}}$$

$$s^2 = \frac{1}{N-1}\sum_{i=1}^{N}(x_i - \bar{x})^2$$

A null hypothesis is formulated, stating that there is no significant difference between the means of the two data sets. The level of significance chosen in this work was $\alpha = 0.05$. This means that the confidence level by which one can reject the null hypothesis is 95%, which is a reasonable level of significance in biological studies.

Statistical analysis was performed using Excel Software and all the data were reported as a mean ± standard deviation. P-values lower than α (rejecting the null hypothesis) were considered statistically significant in all the analysis.

References

[1] Hench LL. The story of Bioglass (R). Journal of Materials Science-Materials in Medicine 2006; 17:967-78.

[2] Rust KR, Singleton GT, Wilson J, Antonelli PJ. Bioglass middle ear prosthesis: Long-term results. American Journal of Otology 1996; 17:371-4.

[3] Stanley HR, Hall MB, Clark AE, King CJ, Hench LL, Berte JJ. Using 45S5 bioglass cones as endosseous ridge maintenance implants to prevent alveolar ridge resorption: A 5-year evaluation. International Journal of Oral & Maxillofacial Implants 1997; 12:95-105.

[4] Thompson I. Clinical Applications of Bioactive Glasses for Maxillo-Facial Repair. In: Larry L. Hench JRJ, Michael B. Fenn, editor. New Materials and Technologies for Healthcare: Imperial College Press; 2011. p. 77-96.

[5] Jones JR. Review of bioactive glass: From Hench to hybrids. Acta Biomaterialia, in press.

[6] Li N, Jie Q, Zhu SM, Wang RD. Preparation and characterization of macroporous sol-gel bioglass. Ceramics International 2005; 31:641-6.

[7] Zhang D. In vitro characterization of bioactive glass. Åbo, Finland: Åbo Akademi University 2008.

[8] Saravanapavan P, Hench LL. Low-temperature synthesis, structure, and bioactivity of gel-derived glasses in the binary CaO-SiO2 system. Journal of Biomedical Materials Research 2001; 54:608-18.

[9] Strnad Z. Role of the glass phase in bioactive glass-ceramics. Biomaterials 1992; 13:317-21.

[10] Ylänen H. Bone Ingrowth into Porous Bodies Made by Sintering Bioactive Glass Microspheres: Åbo Academi University; 2000.

[11] Hench LL AO. An Introduction to Bioceramics. Hench LL, Wilson J ed: World Scientific Publishing Co, River Edge, NJ; 1993.

[12] Kumar M. A review of chitin and chitosan applications. Reactive & Functional Polymers 2000; 46:1-27.

[13] Di Martino A, Sittinger M, Risbud MV. Chitosan: A versatile biopolymer for orthopaedic tissue-engineering. Biomaterials 2005; 26:5983-90.

[14] Madihally SV, Matthew HWT. Porous chitosan scaffolds for tissue engineering. Biomaterials 1999; 20:1133-42.

[15] Park JJ, Luo X, Yi H, Valentine TM, Payne GF, Bentley WE, et al. Chitosan-mediated in situ biomolecule assembly in completely packaged microfluidic devices. Lab on a Chip 2006; 6:1315-21.

[16] VandeVord PJ, Matthew HWT, DeSilva SP, Mayton L, Wu B, Wooley PH. Evaluation of the biocompatibility of a chitosan scaffold in mice. Journal of Biomedical Materials Research 2002; 59:585-90.

[17] Suh JKF, Matthew HWT. Application of chitosan-based polysaccharide biomaterials in cartilage tissue engineering: a review. Biomaterials 2000; 21:2589-98.

[18] Mao JS, Cui YL, Wang XH, Sun Y, Yin YJ, Zhao HM, et al. A preliminary study on chitosan and gelatin polyelectrolyte complex cytocompatibility by cell cycle and apoptosis analysis. Biomaterials 2004; 25:3973-81.

[19] Xia YN, Whitesides GM. Soft lithography. Annual Review of Materials Science1998; 28:153-84.

[20] Takayama S, Ostuni E, Qian XP, McDonald JC, Jiang XY, LeDuc P, et al. Topographical micropatterning of poly(dimethylsiloxane) using laminar flows of liquids in capillaries. Advanced Materials 2001; 13:570.

[21] Pompe T, Fery A, Herminghaus S, Kriele A, Lorenz H, Kotthaus JP. Submicron contact printing on silicon using stamp pads. Langmuir 1999; 15:2398-401.

[22] Ruiz SA, Chen CS. Microcontact printing: A tool to pattern. Soft Matter 2007; 3:168-77.

[23] Bowden N. Micromanipulation: Stick and place. Nat Mater 2006; 5:9-10.

[24] Quist AP, Pavlovic E, Oscarsson S. Recent advances in microcontact printing. Anal Bioanal Chem 2005; 381:591-600.

[25] Greiner C, del Campo A, Arzt E. Adhesion of bioinspired micropatterned surfaces: Effects of pillar radius, aspect ratio, and preload. Langmuir 2007; 23:3495-502.

[26] Flores A, Michael RW. Soft Lithographic Fabrication of Micro Optic and Guided Wave Devices. Litography: InTech; 2010.

[27] Weibel DB, DiLuzio WR, Whitesides GM. Microfabrication meets microbiology. Nature Reviews Microbiology 2007; 5:209-18.

[28] Verplanck N, Coffinier Y, Thomy V, Boukherroub R. Wettability switching techniques on superhydrophobic surfaces. Nanoscale Research Letters 2007; 2:577-96.

[29] Lima AC, Song W, Blanco-Fernandez B, Alvarez-Lorenzo C, Mano JF. Synthesis of Temperature-Responsive Dextran-MA/PNIPAAm Particles for Controlled Drug Delivery Using Superhydrophobic Surfaces. Pharmaceutical Research 2011; 28:1294-305.

[30] Hollo Z, Homolya L, Davis CW, Sarkadi B. Calcein accumulation as a fluorometric functional assay of the multidrug transporter. Biochimica Et Biophysica Acta-Biomembranes 1994; 1191:384-8.

[31] Lewin MR, Wills MR, Baron DN. Ultramicrofluorometric determination of calcium in plasma. Journal of Clinical Pathology 1969; 22:222.

[32] Kepner BL, Hercules DM. Fluorometric determination of calcium in blood serum. Analytical Chemistry 1963; 35:1238-&.

[33] Doostmohammadi A, Monshi A, Salehi R, Fathi MH, Golniya Z, Daniels AU. Bioactive glass nanoparticles with negative zeta potential. Ceramics International 2011; 37:2311-6.

[34] Schultz N, Metreveli G, Franzreb M, Frimmel FH, Syldatk C. Zeta potential measurement as a diagnostic tool in enzyme immobilisation. Colloids and Surfaces B-Biointerfaces 2008; 66:39-44.

[35] Holoubek J. Some applications of light scattering in materials science. Journal of Quantitative Spectroscopy & Radiative Transfer 2007; 106:104-21.

[36] Bumgardner JD, Wiser R, Elder SH, Jouett R, Yang Y, Ong JL. Contact angle, protein adsorption and osteoblast precursor cell attachment to chitosan coatings bonded to titanium. Journal of Biomaterials Science-Polymer Edition 2003; 14:1401-9.

[37] Kokubo T. Bioactive glass-ceramics - Properties and applications. Biomaterials 1991; 12:155-63.

[38] Kokubo T, Takadama H. How useful is SBF in predicting in vivo bone bioactivity? Biomaterials 2006; 27:2907-15.

[39] Sugawara Y, Suzuki K, Koshikawa M, Ando M, Iida J. Necessity of enzymatic activity of alkaline phosphatase for mineralization of osteoblastic cells. Japanese Journal of Pharmacology 2002; 88:262-9.

[40] Whyte MP, Vrabel LA. Infantile hypophosphatasia fibroblasts proliferate normally in culture: evidence against a role for alkaline phosphatase (tissue nonspecific isoenzyme) in the regulation of cell growth and differentiation. Calcified Tissue International 1987; 40:1-7.

[41] Broyles DL, Nielsen RG, Bussett EM, Lu WD, Mizrahi IA, Nunnelly PA, et al. Analytical and clinical performance characteristics of Tandem-MP Ostase, a new immunoassay for serum bone alkaline phosphatase. Clinical Chemistry 1998; 44:2139-47.

[42] Bessey OA, Lowry OH, Brock MJ. A method for the rapid determination of alkaline phosphatase with 5 cubic millimeters of serum. Journal of Biological Chemistry 1946; 164:321-9.

Brief notes on the Part 3 structure

When doing research on BTE the ultimate goal is to develop bioactive structures able to mimic bone's natural architecture. The herein reported work focused on three main points: The multiscale levels of bone's architecture – from nano to macro scale; the need for a bioactive material; and the importance of the assembly of an organic and inorganic phase in the osseous tissue.

The starting point of this thesis was the production and optimization of BG-NPs. These materials represent the basic units for the artificial bone construction; therefore, it was of great importance to deeply understand the processes leading to BG-NPs formation. This aim was pursued in Chapter IV and V.

Chapter VI and VII introduce chitosan as the natural polymer intended to mimic bone's organic phase, represented in Nature mainly by collagen. In Chapter VI, bioactive nanocomposites are developed comprising chitosan and different BG-NPs compositions. The aim of this work was to prove how the BG-NPs composition may be easily adapted to clinical needs. The osteoblastic response to the developed nanocomposites is presented. Chapter VII, on the other hand, presents the use of a mCP technique to spatially control mineralization, in order to assure a wider range of applications of the bioactive nanocomposites.

Finally, Chapter VIII presents an important step on mimicking bone's natural structure. A simple but effective approach allowed the induction of BG-NPs self-assembly into ordered structures, comprising the nano, micro and macrolevels.

PART 3 - Results

Chapter IV

Preparation and characterization of bioactive glass nanoparticles prepared by sol-gel for biomedical applications

Chapter IV - Appendix

Wettable arrays onto superhydrophobic surfaces for bioactivity testing of inorganic nanoparticles

Chapter V

Nanoengineering of bioactive glass: From hollow to dense nanospheres

Chapter VI

Chitosan/bioactive glass nanoparticles composites for biomedical applications

Chapter VII

Micropatterning of bioactive glass nanoparticles on chitosan membranes for spatial controlled biomineralization

Chapter VIII

Nanotectonics approach to produce hierarchically organized bioactive glass nanoparticles-based macrospheres

Chapter IV

Preparation and characterization of bioactive glass nanoparticles prepared by sol-gel for biomedical applications

Abstract

Bioactive glass nanoparticles (BG-NPs), based on both ternary (SiO$_2$-CaO-P$_2$O$_5$) and binary (SiO$_2$-CaO) systems, were prepared via an optimized sol-gel method. The pH of preparation and the effect of heat treatment temperature were evaluated, as well as the effect of suppressing P in the bioactivity ability of the materials. The morphology and composition of the BG-NPs were studied using FTIR, XRD and SEM. The bioactive character of these materials was assessed *in vitro* by analyzing the ability for apatite formation onto the surface after being immersed in simulated body fluid (SBF). XRD, EDX and SEM were used to confirm the bioactivity of the materials. The BG-NP effect on cell metabolic activity was assessed by seeding L929 cells with their leachables, proving the non-cytotoxicity of the materials. Finally the most bioactive BG-NPs developed (ternary system prepared at pH 11.5 and treated at 700 °C) were successfully combined with chitosan in the production of biomimetic nanocomposite osteoconductive membranes that could have the potential to be used in guided tissue regeneration.

1. Introduction

When bioactive glasses were discovered, they radically changed the biomaterials field. For the first time, a chemical bond between implants and host tissue was possible, leaving behind a first generation of bioinert devices. This was the beginning of a second generation of bioactive materials capable of inducing a cellular response at their surface. These materials were able to bond not only to bone, but to soft tissue as well, avoiding fibrous encapsulation. [1, 2] Moreover, the broad scope of the possible compositions leads to different chemical properties and rate of bonding with tissues, allowing more specific clinical applications. [3]

The first bioactive glass developed by Hench in 1971 was composed of SiO_2, CaO, Na_2O and P_2O_5 (Bioglass®). [2] The first bioactive glasses were produced by melting the required materials and casting of the bulk or quenching of powders. [2] In 1991, Li *et al* produced bioactive glasses by sol–gel processing. [4] Sol–gel is a wet-chemical processing method more appropriate to produce these glasses as an alternative to the traditional melting method, because it allows a wider range of SiO_2 content and higher purity of the obtained products. [5]

The SiO_2-CaO-P_2O_5 system is one of the most extensively studied in the field of bioactive sol-gel glasses [6-9]. However, the majority of these bioactive glasses are prepared by direct heating of the gels, after allowing gelation to occur, which results in a hard block that must be ground and sieved to reach particle sizes at the microscale. Microsized particles of bioactive glasses are commonly used, but there are not many works exploring the advantages of using nanosized particles.

Nanoparticles have sizes of the order of 10-100 nm in diameter and, unlike bulk materials, the biological response of these particles is highly dependent on their dimensions and specific surface area. [10, 11] Bioactive glass nanoparticles may have a significant function as well in the genetic control of the cellular response. Additionally, their particular characteristics which have anti-inflammatory and proangiogenic potential are ideal for applications like minimally invasive injectable particles for stable growth of soft tissues. [12, 13]

The use of particles within the nanoscale may open new possibilities in the biomedical area, including in bone repairing, based on the combination of such materials with bi-

opolymers, as the increased surface area improves the mechanical properties of these new biomaterials and provides more nucleation sites for apatite, increasing their bioactive potential, making this kind of composite great candidates for third-generation tissue engineering. [3, 9, 14-21, 22]

This study aims to investigate the effects of different compositions (SiO_2-CaO-P_2O_5 and SiO_2-CaO) and thermal treatments on the morphology and *in vitro* bioactivity of BGNPs. As is referred to in the literature, the morphology and size of the bioactive particles can be controlled by the rate of the hydrolysis and condensation reactions. [10] The pH was therefore also chosen in this work as a parameter to study its influence on the morphology and the size of the bioactive glass particles.

A sol-gel method was previously combined with coprecipitation and applied in this work to different formulation systems in order to obtain nanosized particles. [23] The advantage of combining these materials with biopolymers is also investigated and a composite of chitosan and the BGNPs is developed.

2. Experimental methods

2.1. BG-NP preparation

To prepare the BG-NPs a protocol based on previous works was followed. [24, 25] The procedure for the ternary BG-NP preparation, with the composition SiO_2-CaO-P_2O_5 (mol%) = 55:40:5, consisted in sequential reagent dissolutions that resulted in hydrolysis and polycondensation reactions. The same procedure with the necessary adaptations was followed to obtain SiO_2:CaO *(mol%)* = 70:30, in which no P precursor was used. Tetraethyl orthosilicate (TEOS, 99.90% pure) was used as the Si precursor, ammonium phosphate dibasic as the P precursor, calcium nitrate tetrahydrate (99%) as the Ca precursor, citric acid monohydrate (99-100%) to promote hydrolysis, ethanol absolute, ammonium hydroxide (maximum of 33% NH_3) as the jellifying agent and polyethylene glycol 20 000 (PEG) as the surfactant were purchased from Sigma-Aldrich. In some cases the BG-NPs were sintered at

700 °C, according to the thermogravimetric and differential thermal analysis (TG/DTA) study of dried gels of a similar system performed by Ma *et al.* [26]

2.2. Chitosan/BG-NPs composite preparation

The membranes were obtained dissolving chitosan (0.7 % w/v) and BG-NPs (0.3 % w/v) in 2 % v/v acetic acid. The control membranes contain 1 % w/v of chitosan. After evaporation for several days, the membranes were neutralized in NaOH 0.1 M, and left to dry.

2.3. XRD analysis

X-ray diffraction measurements were performed with a Bruker D8 Discover model operated at 40 kV and 40 mA using Cu Kα radiation. The detector was scanned over a range of 2ϑ angles from 15° to 60° at a step size of 0.04° and dwell time of 1 s per step.

2.4. FTIR spectroscopy analysis

Fourier-transform infrared (FTIR) spectroscopy analysis was carried out in an IR Prestige 21 Shimadzu spectrometer. The samples were prepared by pressing the BG-NPs with KBr into a small disc. The FTIR spectra were recorded from 400 to 4400 cm^{-1} with the resolution of 4 cm^{-1}. Before measurements the powders were dried at 100 °C overnight to remove any adsorbed molecules.

2.5. In vitro bioactivity study

In vitro bioactivity tests were carried out by soaking 10 mg of bioactive glass in 15 ml of SBF (simulated body fluid) solution in the case of BG-NPs powders, and 1 cm^2 per 50 ml of SBF in the case of chitosan/BG-NPs composite for zero (control), one, three, five and seven

days at 37 °C. Upon removing from SBF, the samples were rinsed with distilled water and left to dry.

The SBF was prepared by dissolving NaCl, NaHCO$_3$, KCl, K$_2$HPO$_4$·3H$_2$O, MgCl$_2$·6H$_2$O and Na$_2$SO$_4$ in distilled water and buffered with Tris buffer and HCl to reach a pH value of 7.4, following the protocol described by Kokubo and Takadama [27]. All materials were purchased from Sigma-Aldrich.

2.6. SEM and EDX sample preparation

To study the surface and the morphology of the samples, a NanoSEM-FEI Nova 200 (FEG/SEM) scanning electron microscope was used. A conductive gold coating was applied to the samples. A Pegasus X4M instrument was used to perform the EDX experiments at low vacuum and without coating.

2.7. Cell viability tests

Cell viability and metabolic activity were determined using the MTS assay. L929 mouse fibroblasts were seeded in a multi-well plate and nourished with Dulbecco's modified minimum essential medium (D-MEM) supplemented with 10% fetal bovine serum (FBS) and 1% antibiotic. The plates were incubated at 37 °C with 5% CO$_2$. In the meantime, fluid extracts were obtained by placing in a falcon tube 0.2 g of sterile BG-NPs per ml of culture medium. After 24 h under stirring at 37 °C, the media, with different extracts from each sample, were filtered and applied, as the nourishment medium, to the plates containing the cells previously seeded. The cultures were then incubated at 37 °C for one, three and seven days. The culture media was replaced on the third day. The MTS (3-(4,5-dimethylthiazol-2-yl)-5-(3-carboxymethoxyphenyl)-2-(4-sulfophenyl)-2H-tetrazolium) test was performed to determine the cytotoxicity of the BGNPs.

In this assay, the tetrazolium compound is reduced by the viable cell's mitochondria into a water-soluble brown formazan product. The relative viability (%) of the cells was determined by comparing the obtained results with cells grown without BG-NP extracts that

were used as a positive control of cell viability. Latex was considered to be a negative control of cellular viability. After each time point (one, three and seven days of culture), the MTS test was performed to assess the metabolic activity of the cells in contact with the BG-NP extracts. For this assay, an MTS solution was prepared by using a 1:5 ratio of MTS reagent and D-MEM culture medium (without phenol red or FBS). After removal of the fluid extracts and washing with PBS, 100 μl of MTS reagent was added to each sample followed by a 3 h incubation period at 37 °C.

Finally, the cell supernatant of each sample was removed to another plate and their optical density (OD) was read at 490 nm on a microplate reader (Synergy HT, Bio-Tek Instruments).

The values of optical density are directly proportional to the quantity of formazan product and thereby to the number of living cells analyzed. All cytotoxicity tests were conducted by using five replicates.

3. Results and discussion

BG-NPs were obtained by the sol–gel method. This is a very straightforward method to produce bioactive glasses; nevertheless, it still requires some important steps such as the addition of a basic catalyst to promote precipitation of the particulate gel and the reduction of the gelation time [28, 29], as well as a heat treatment to incorporate calcium and remove organic residues. [10] Therefore, besides the study of the formulation's influence, the pH resulting from the addition of different amounts of NH_4OH as the basic catalyst and the differences between samples heat-treated and non-heat-treated were also analyzed.

3.1. Chemical composition

3.1.1. X-ray diffraction (XRD)
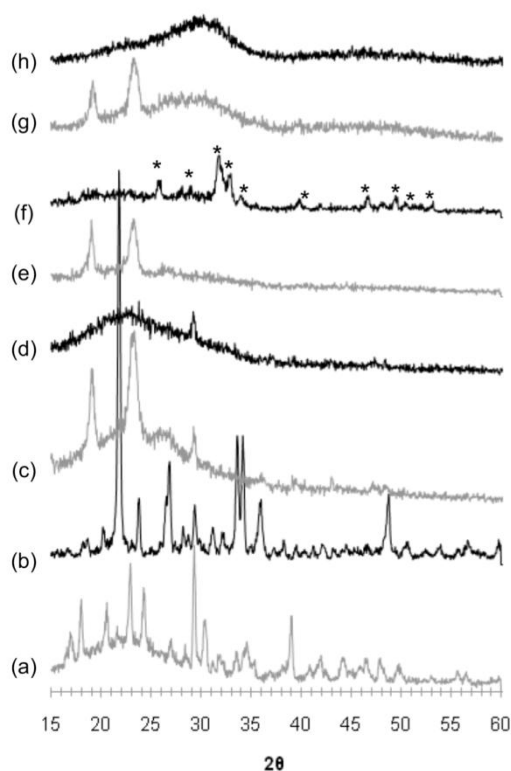
Fig. IV. 1 XRD spectra of raw and thermally treated BG-NPs produced at different pH and formulations. Binary pH 9 **(a)** 0 °C, **(b)** 700 °C; binary pH 11.5 **(c)** 0 °C, **(d)** 700 °C; ternary pH 9 **(e)** 0 °C, **(f)** 700 °C; ternary pH 11.5 **(g)** 0 °C, **(h)** 700 °C and hydroxyapatite peaks are indicated (*).

XRD patterns of the studied samples are shown in figure IV.1. As is well known, glass is an amorphous inorganic material with no detectable diffraction maxima. Therefore, it is expected that the bioactive glass diffractograms will reflect the amorphous nature of this material. Indeed, XRD spectra of both the binary and ternary system prepared at pH 11.5 and after thermal treatment, respectively figures IV.1(d) and (h), exhibit a broad dispersive band, indicating the amorphous nature of the bioactive glass. Before being submitted to the thermal treatment, the diffractograms present two parasite lines (19° and 24°) reported in the literature as being associated with Si. [30] After the thermal treatment process, the lines disappear.

Hong *et al* concluded that the crystallinity of bioactive glass ceramic nanoparticles obtained with the same preparation conditions could increase with increasing phosphate content. [31] However, comparing the diffractograms in figure IV.1 of binary (with no P) and ternary (with 5% P) samples obtained at different pH (9 and 11.5) and temperatures (0 and 700 °C), one can conclude that the major differences in crystallinity arise from the pH of preparation. The spectra do not reflect the composition of the system in terms of the presence or absence of P. However, the pH of preparation seems to be the most important factor setting the amorphous or crystalline character of the material after the thermal treatment. When working at pH 9, the sintered sample spectrum from both the binary, figures IV.1 (a) and (b), and ternary, figures 1(e) and (f), systems reflect the existence of crystalline phases, as some diffraction maxima can be observed. Comparing the ternary samples after thermal treatment (figures IV. 1(f)—pH 9 and (h)—pH 11.5), the main difference is related to the crystallinity. With respect to the ternary sample prepared at pH 9, figure 1(f), the thermal treatment process seems to lead to the hydroxyapatite typical diffractogram. The main lines are typical phosphate crystal peaks showing the presence of hydroxyapatite, which exhibits well-defined diffraction maxima at 2ϑ = 25.9°, 29° , 31.8°, 32.2°, 32.9°, 34° , 39.8°, 46.7°, 49.5°, 50.5° and 53.1°. The apatite peaks' presence can be explained based on two different reasons. The first one is that, in the aqueous environment of the sol–gel process, precipitation of hydroxyapatite can occur from the amorphous structure of silica-based bioactive glasses. [32] However, it could also be the case that the thermal treatment temperature was excessively high and therefore passing the value of minimum stabilization temperature that ensures a maximum of bioactivity before the crystallization of the material. A higher crystallinity has a lower dissolution rate which has a direct detrimental effect on bioactivity. [10] On the other hand, the sample prepared at pH 11.5, figure IV. 1(h), presents an amorphous spectrum after thermal treatment very similar to the one associated with the commercial Bioglass®, as only the characteristic amorphous band at low angles is visible. Crystallization of bioactive glasses decreases the level of bioactivity and even turns a bioactive glass into a bioinert material. [31] It appears to be the case of the binary samples prepared at pH 9 (figures IV. 1(a) and (b)), with a considerable amount of peaks with very high crystallinity, as the size of the peaks can be related to their crystallinity. These samples are the ones exhibiting the lower bioactivity as will be confirmed further in this study. In all samples except for the sintered ternary powders prepared at pH 11.5, figure IV. 1(h), the

thermal stabilization leads to a more crystalline sample, which may happen due to the small size of the particles, which, having a higher specific surface area, also have higher driving forces for nucleation in crystals. [10] Samples of the ternary system prepared at pH 11.5, figures IV.1. (g) and (h), form a broad band centered at a 2ϑ value of 30° that corresponds to the wollastonite ($CaSiO_3$) phase. Labbaf *et al* claim that thermal treatment temperatures should be the lowest value able to retain the particles in the amorphous state. As a temperature of 700 °C was used, and the amorphous shape was kept, this seems to be the ideal stabilization temperature before reaching a wollastonite crystalline phase that would decrease the bioactive potential of the BG-NPs. Thermal treatment is always a necessary step because it is essential to incorporate calcium at approximately 450 °C, to remove the organic phase at 500 °C and to reduce silanol groups from the glass surface and nitrate by-products from the glass network at 600 °C. [10]

3.1.2. FTIR measurements
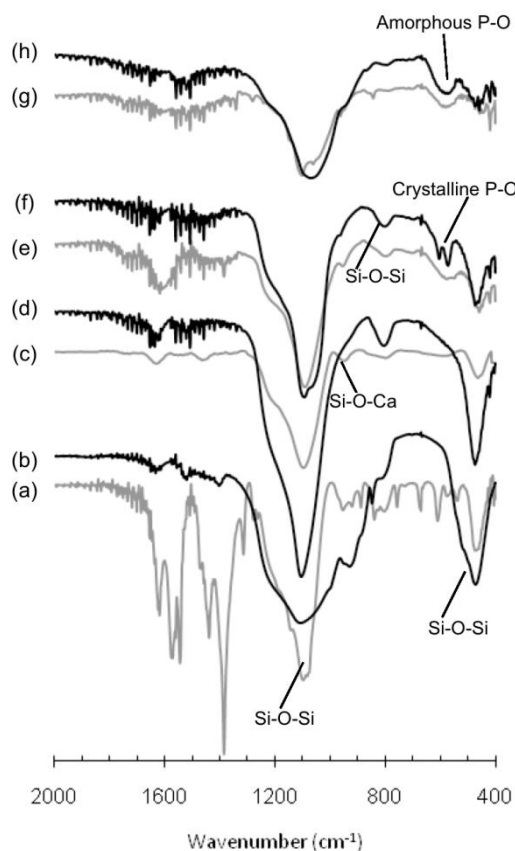
Fig. IV. 2 Infrared spectra of raw and thermally treated BG-NPs.

Binary pH 9 **(a)** 0 °C, **(b)** 700 °C; binary pH 11.5 **(c)** 0°C, **(d)** 700 °C; ternary pH 9 **(e)** 0 °C, **(f)** 700 °C and ternary pH 11.5 **(g)** 0 °C, **(h)** 700 °C.

The FTIR spectra of the produced BG-NPs are presented in figure IV.2. Silicate absorption bands are observed in all spectra, assigned to the peaks 1085, 800 and 464 cm^{-1}, respectively: asymmetric stretching mode, symmetric stretching vibration and rocking vibration of Si–O–Si [26].

In the sintered ternary system sample prepared at pH 9, figure IV.2. (f), the heating treatment at 700 °C is shown by two narrow peaks at 580 and 600 cm^{-1}, indicating a P–O bending vibration due to the presence of a crystalline calcium phosphate (apatite-like) phase [26]. These twin bands merge into a weak band in the case of amorphous glass, figures IV.2 (e), (g) and (h).

This is in accordance with the XRD data. Moreover, the P related peaks do not appear in the binary spectra, figures IV.2 (a) - (d), since they do not include P in their formulation. In the case of ternary system samples, figures 2(e) - (h), peaks at 1045 and 1090 cm^{-1} are also assigned to the P–O bond although masked by the broad silicate band. [31] At 950 cm^{-1} one can confirm the Ca presence due to the peak related to Si-O-Ca bonds containing non-bridging oxygen [26]. The 1630 cm^{-1} is assigned to the OH group due to residual H2O absorbed in the BG-NP. [33] Bands related to the presence of the calcium precursor $Ca(NO_3)_2$, 1400-1300 cm^{-1} (N=O bend) and 1600-1500 cm^{-1} (N=O stretch) disappear after the thermal treatment, confirming the decomposition of the nitrate $Ca(NO_3)_2$ at 700 °C, especially the vibrations of ionic $(NO_3)^-$ at 1380 cm^{-1}. [33] These bands are more evident in the binary pH 9 - 0 °C, figure IV.2. (a) and tend to attenuate after thermal treatment. Also in figure 2(a), the 1630 cm^{-1} stretching vibration of the H–O bond, related to water is more evident. The 1340 cm^{-1} sharp peak could also be due to the presence of water as it is assigned to OH free groups. The 1460 cm^{-1} could be assigned to a carbonate absorption band, due to the carbonate existing in the lattice of the binary pH 9 BG-NPs, as a result of CO_2 dissolution from the atmosphere during the sol–gel procedure. [34] After thermal treatment this band disappears.

3.1.3. Energy dispersive x-ray (EDX) analysis.

Table IV. 1. EDX quantification (at.%).

%At	Binary				Ternary			
	pH 9		pH 11.5		pH 9		pH 11.5	
	0˚C	700˚C	0˚C	700˚C	0˚C	700˚C	0˚C	700˚C
Si	70.24	69.15	82.00	81.53	52.63	55.30	33.46	35.31
P	0	0	0	0	14.62	15.01	20.40	21.87
Ca	29.76	30.85	18	18.47	32.75	29.69	46.14	42.81

Through energy dispersive x-ray (EDX) analysis, it was possible to quantify the final ratios of the binary and ternary compositions in atomic percentage (at.%). The results are presented in table IV.1. The measured values present deviations regarding the initial formulations. As can be observed in the table, the particles produced at pH 9 have the right original proportions of Si and Ca in the binary case, but in the ternary system only Si is at the original percentage and P is three times higher, and consequently Ca is 15% below the original percentage.

At pH 11.5 Si is above the initial value in the binary system (and Ca below). On the other hand, in the ternary system, Si is almost 20% below the original set value and Ca remains in the right proportion, P being four times higher. The reason for these differences may be the removal of free calcium ions during the washing step. Indeed, in the sol stage, almost 100% of Ca dissolves in the pore liquor as calcium nitrate, and it will only deposit in the drying step. Therefore, the final composition of bioactive glass can be changed if the pore liquor is washed before drying, removing the calcium that was not incorporated in the silica or phosphoric gel network. [10, 34]

This fact would explain the variation in values obtained, as the experimental procedure followed in this work includes a washing step, necessary to remove the ammonia from the precipitate.

3.2. Surface analysis
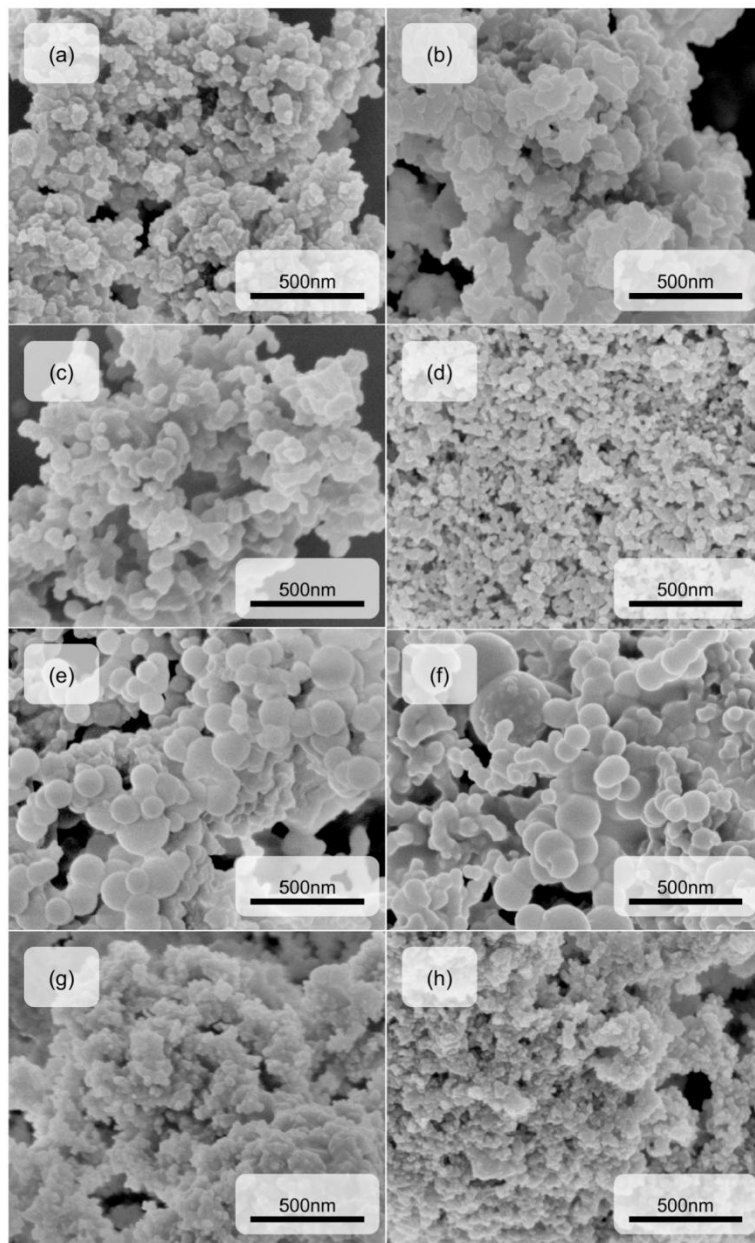
Fig. IV. 3 SEM of raw and thermally treated BG-NPs.

Binary pH 9 **(a)** 0°C, **(b)** 700 °C; binary pH 11.5 **(c)** 0 °C, **(d)** 700°C; ternary pH 9 **(e)** 0 °C, **(f)** 700 °C and ternary pH 11.5 **(g)** 0 °C, **(h)** 700 °C.

Surface analysis was performed by scanning electron microscopy (SEM) observation. The samples were previously coated with a thin gold layer. The differences in the BG-NPs both in size and morphology were analyzed between the different batches of BG-NPs produced. At pH 9, figures IV. 3(a), (b) and (e), (f), the size of the particles is more heterogene-

ous, especially in the ternary case, figures IV.3. (e) and (f), where the sizes could vary in the range 50–200 nm. The particles produced at pH 11.5, figures IV.3. (c), (d) and (g), (h), have sizes below 40 nm.

Regarding the effect of calcination in the morphologies of the binary and ternary systems, at pH 9 particles appear to be melted and more aggregated and at pH 11.5, besides the aggregation, there is also a decrease in the particles size. This consequence is not evident in the ternary particles produced under the same conditions. It is known that temperatures higher than 700 °C, in the ternary system, have the effect of melting and sintering the particles in large aggregates. [23] A shorter temperature of calcination is thought more suitable to apply in binary systems, in order to avoid the fusion of the particles and their densification due to the sintering effect.

In all cases the particles are round shaped. Labbaf *et al* claim that the spherical shape is in part due to the use of ammonium hydroxide as catalyst, although the morphology and size can be as well controlled by the rate of the hydrolysis and condensation reactions. Even though it is know that, when using a base catalyst to control the condensation reaction the particles do not assemble, some agglomeration is observed. However, the catalyst chosen prevents them fusing together during thermal treatment. [10]

3.3. Cytotoxicity tests of the BG-NPs

Fig. IV. 4 Cytotoxicity test results of raw and thermally treated BG-NPs over three time points (one, three and seven days).
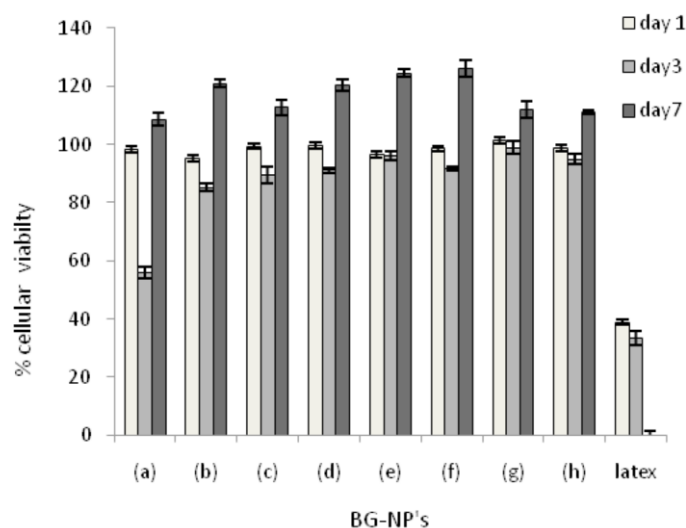
Binary pH 9 **(a)** 0 °C, **(b)** 700 °C; binary pH 11.5 **(c)** 0 °C, **(d)** 700 °C; ternary pH 9 **(e)** 0 °C, **(f)** 700 °C; ternary pH 11.5 **(g)** 0 °C, **(h)** 700 °C and all data were expressed as mean ± standard deviation for n = 5.

The BG-NP effect on cell metabolic activity was assessed by seeding L929 cells with their leachables. Figure IV.4. shows the cell's viability evaluated by carrying out the MTS test. A slight decline in the cellular metabolic activity was verified from the first to the third day in all samples, the decrease being more relevant in sample (a). The mentioned decrease was followed by a viability increase from day three to day seven. These results suggest that the cell's metabolism is being influenced by the ions present in the leachables, as sample (a) showed the presence of more chemical species in FTIR analysis (see figure IV.2.) and, as a consequence, it has the most evident decrease in the third day viability. Nevertheless, the interactions between the cells and the BG-NP leachables do not affect significantly their viability, as it increases again towards the seventh day of culturing. The cell's behavior throughout the study time proves the non-toxicity of the materials produced at different pH and also before and after thermal treatment. Therefore, high biocompatibility of the materials is ensured in all of the studied conditions.

3.4. In vitro bioactivity test of the BG-NPs

It is commonly accepted that the bioactivity of glasses relies on their ability to induce hydroxyapatite formation in a physiological environment, such as simulated body fluid (SBF) that reproduces the human plasma by having similar pH and ionic composition. In this environment, the bioactive glasses will release ions and form silanol groups on its surface that will act as a nucleating agent for a hydroxyapatite layer. [35]

Being an interface-driven phenomenon, bioactivity will depend on parameters such as surface charge, composition, structure and morphology. [36] In fact, these parameters will influence the dissolution rate of the materials, whose ideal ionic concentrations will define the ability to stimulate cellular proliferation and differentiation. [2]

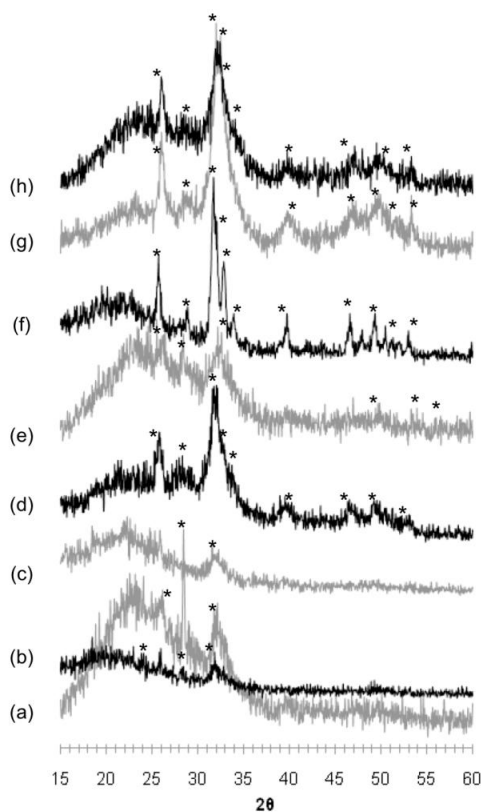### 3.4.1. X-ray diffraction (XRD)

Fig. IV. 5. XRD spectra of raw and thermally treated BG-NPs produced at different pH and formulations after seven days of immersion in SBF.

Binary pH 9 **(a)** 0 °C, **(b)** 700 °C; binary pH 11.5 **(c)** 0 °C, **(d)** 700 °C; ternary pH 9 **(e)** 0 °C, **(f)** 700 °C; ternary pH 11.5 **(g)** 0 °C, **(h)** 700 °C and hydroxyapatite peaks are indicated (*).

Figure IV.5. shows the XRD spectra of the BG-NPs in all of the studied conditions after soaking in SBF for seven days. In the non sintered samples of the binary systems, both pH 9 and 11.5, figures IV.5. (a) and (c), just one to three of the major diffraction peaks in the spectra can be interpreted as hydroxyapatite, as a result of being soaked in SBF after seven days. In contrast, the sintered binary samples, figures IV.5. (b) and (d), especially the one prepared at pH 11.5, figure IV.5. (d), have several peaks related to hydroxyapatite regarding day seven of SBF soaking.

In the case of the ternary system without thermal treatment, figures IV.5. (e) and (g), the particles after seven days present an apatitic layer at their surface, with several peaks of the spectrum matching the ones of hydroxyapatite. It is possible to conclude that, in each system (binary or ternary), at pH 11.5, figures IV.5. (e)-(h), there are more peaks related to hydroxyapatite than in the samples produced at pH 9, figures 5 IV.(a)-(d). Regarding the temperature, the heat treatment at 700 °C is conducive to better bioactivity than the non-heat-treated samples, as the diffraction angles of the peaks after soaking in SBF match the reference x-ray spectra of hydroxyapatite. Considering the formulation of the BG-NPs, the ternary system exhibits a layer of pure hydroxyapatite after seven days of immersion, when treated at 700 °C, at both pHs, figures 5 IV.(f) and (h). One can conclude that the ternary formulation has better bioactivity results than the binary one, and that thermal treatment has an important role in promoting the mineralization ability, regardless of the pH of preparation in this study.

3.4.2. Scanning electron microscopy (SEM)
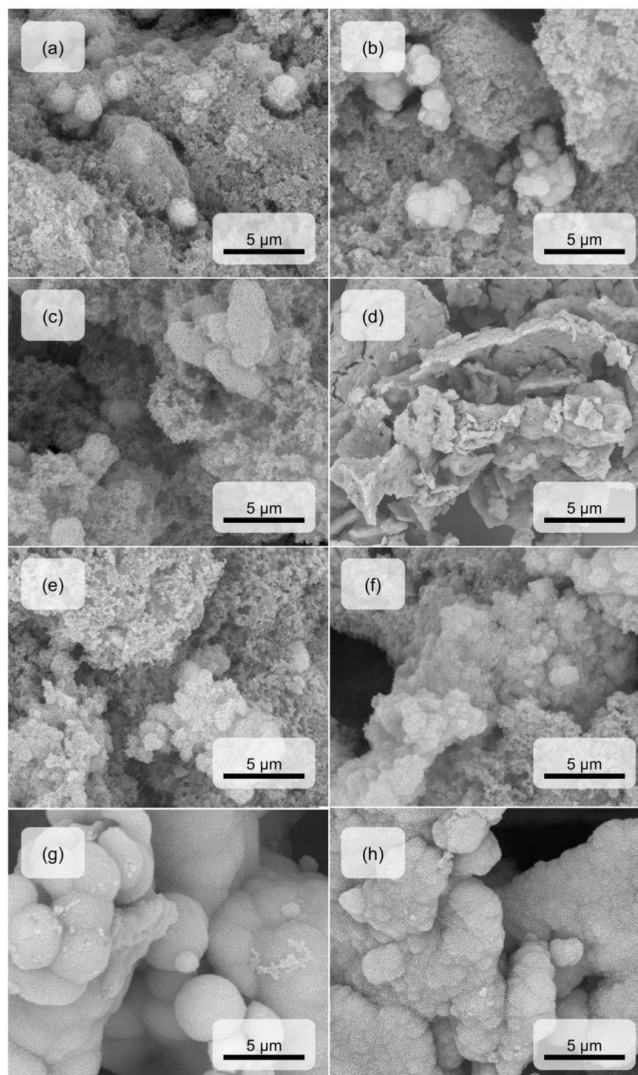
Fig. IV. 6 SEM images of the BG-NPS after seven days in SBF, revealing cauliflower-like apatite clusters on their surface.

(a) binary pH 9 0 °C, **(b)** 700 °C; ternary pH 9 **(c)** 0 °C, **(d)** 700 °C; binary pH 11.5 (e) 0 °C, **(f)** 700 °C and ternary pH 11.5 **(g)** 0 °C, **(h)** 700 °C.

Bioactivity can be confirmed by observing the development of a needle-like apatite layer, forming cauliflower-like clusters on the surface of the particles, namely hydroxyapatite ($Ca_{10}(PO_4)_6$–x (HPO_4)x $(OH)_2$–x), the main mineral constituent of bone. [37]

Observing the images in figure IV.6., obtained in the SEM study of the bioactivity of BG-NP powders, one can conclude that the amount of apatitic crystals at the surface of the

samples increases when the pH is 11.5 instead of 9, and when the formulation is of a ternary system instead of binary. Indeed, after seven days of soaking the samples in SBF, it is possible to observe that the condition with the richer apatitic films the one corresponding to the ternary system produced at pH 11.5 both at 0 °C and sintered at 700 °C, indicating the best bioactivity in a qualitative evaluation, figures 6 IV.(g) and (h). The XRD data previously presented support these conclusions and confirm that the calcified film is related to hydroxyapatite.

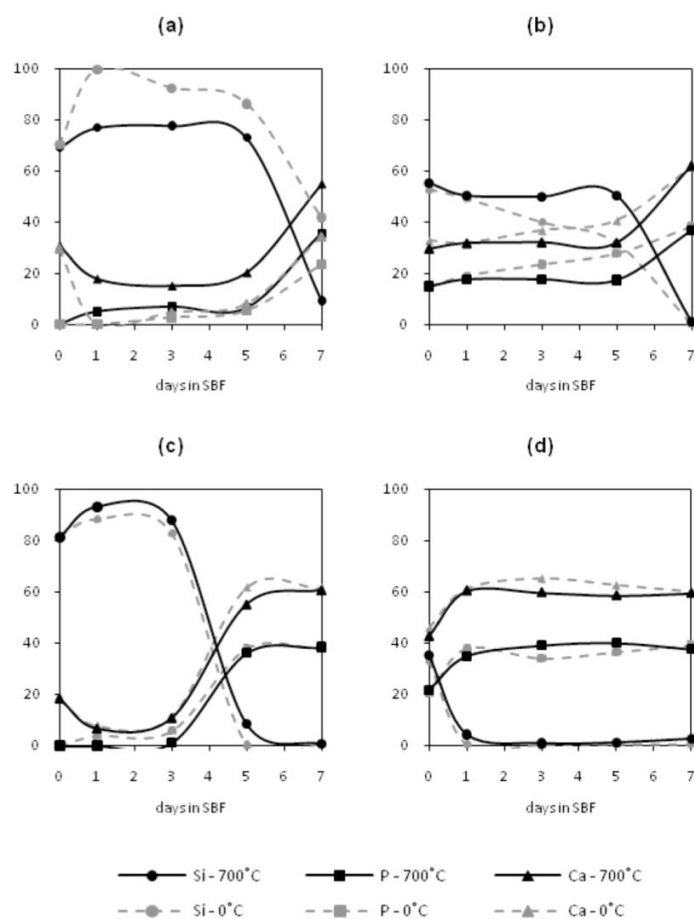### 3.4.3. Energy dispersive X-ray analysis (EDX)

Fig. IV. 7 EDX study of the bioactivity of the BG-NPs prepared in different conditions at zero, one, three, five and seven days.

(a) Binary pH 9 at 0 and 700 °C, **(b)** ternary pH 9 at 0 and 700 °C, **(c)** binary pH 11.5 at 0 and 700 °C and **(d)** ternary pH 11.5 at 0 and 700 °C.

The results obtained by SEM were also confirmed by EDX analysis that allowed the following of the elemental evolution throughout the time period of study. After soaking in SBF, the expected behavior of a bioactive material containing Si and Ca (as in the case of BG-NPs) is the rising of Si accompanied by the decrease of Ca in the first stage, due to the exchange of the last elements with H^+ and H_3O^+ from the environment. After this first step, disruption of the glass network occurs by hydrolysis and as Si–O–Si bridges break, during which soluble silica is lost to the solution in the form of $Si(OH)_4$ leading to the formation of silanol groups (Si–OH) at the BG-NP/solution interface. The OH− groups from silanol will attract Ca^{2+} and PO^{3-}_4 from the surrounding media and precipitation occurs. An amorphous calcium phosphate layer begins to grow on the surface of the sample, and the Ca and P values increase. In contrast, Si content decreases proportionally. The incorporation of OH− and CO^{2-}_3 anions from the solution leads to the final step of mineralization which is the formation of a crystalline hydroxyapatite layer. [38]

In fact, in all systems as the study proceeds, the Si content decreases and the Ca and P increase. The P is taken out from the SBF in the case of the binary systems, see figures IV.7. (a) and (c). This strengthens the indication of the development of apatite material onto the BG-NP surfaces.

This behavior varies in time according to the bioactive potential of each sample. In the case of the binary and ternary systems prepared at pH 9, figures IV.7. (a) and (b), respectively, the effect of the ion exchange is more significant after the fifth day of the study, when Si begins to decrease and the Ca and P values become higher.

In the binary system produced at pH 11.5, figure IV.7 (c), the apatite begins to develop earlier, after three days of immersion in SBF. In the case of the ternary system (SiO_2-CaO-P_2O_5) produced at the same pH, the bioactivity character just needs one day to express itself, figure IV. 7(d). This last system is then the most bioactive one.

Regarding the influence of the BG-NP formulation over the bioactive ability of these materials, some facts have to be considered. First, the ability to bond with bone has been shown to depend largely on the silica (SiO_2) content. As the silica content of the glass increases, the dissolution rate of the apatite layer becomes slow and the bone-bonding ability of the materials decreases. A glass with content of more than 60 wt% silica has a dramatic decrease in its bioactivity. [38] Moreover, the BG-NPs with a higher percentage of Ca are expected to be more prone to dissolution than the ones with higher amounts of Si in aque-

ous environments, since calcium disrupts the silica network, reducing its network connectivity (mean number of bridging –Si–O–Si– bonds per silicon atom) and therefore its stability in solution. [10, 39] Both these facts could justify the reason why samples from binary systems have an inferior bioactivity over the ternary ones. One can conclude that, at the lower pH (9), the obtained particles are more crystalline which was previously referred to as a drawback in setting the bioactive potential, as it lowers the dissolution rate to ineffective values. This fact would explain why the ternary system at pH 11.5 is more bioactive than at pH 9.

In this study, thermal treatment did not have an influence on setting the bioactive potential of the BG-NPs. The differences obtained in the atomic percentages throughout the days of the study were not significant when the samples had been sintered, regardless of the formulation of the particles, although thermal treatment is important to retain the Ca in the glass network, which is a crucial element for a successful mineralization.

3.5. Chitosan/BG-NP composite development

Composites found in nature contain an inorganic phase, with at least one nanometric dimension embedded in an organic matrix, usually assembled in a complex and hierarchical structure. [40] Biomimetic osteoconductive nanocomposites may be obtained by combining bioactive glass/ceramics with a polymeric matrix. [22] In order to mimic this natural structure, the most bioactive powders (ternary, pH 11.5, 700 °C) were applied in the development of chitosan membranes containing BG-NPs dispersed in the polymer. The membranes were obtained by solvent casting of a solution containing chitosan (0.7 wt/vol%) and BG-NPs (0.3 wt/vol%). Chitosan is an excellent biocompatible polymer, although, by itself, it is not capable of reacting within the physiological fluids in order to develop apatite crystals and bond to the bone, figure 8(a). In this study, BG-NPs were applied in the formation of a composite formed by the polymer and the glass powders in order to produce a bioactive composite that allies the remarkable mechanical and processability properties of chitosan to the mineralization induction ability of BGNPs.

The nanosize of the particles allows a large dispersion in the polymer as can be observed in figure IV.8 (b), showing a uniform membrane surface. After seven days of immersion in SBF, a dense apatite layer is formed at the surface of the composite (figure IV.8 (c)).

The thickness of the apatitic film can be observed because the polymeric membrane shrinks upon drying and the apatite layer breaks (figure IV.8 (d)). This profile view allows us to estimate the reaction layer thickness as 2 μm approximately, having an average thickness of the membrane of 47 μm. In contrast, the pure chitosan membrane does not present any bioactive character as, after seven days immersion in SBF, no apatite layer was formed at its surface, proving that this ability is caused by the BG-NPs. It was proved then that one can successfully ally the mineralization induction ability of the BG-NPs with the mechanical advantages of the chitosan biopolymer, producing a nanocomposite with potential applications in bone tissue engineering or in guided tissue regeneration.

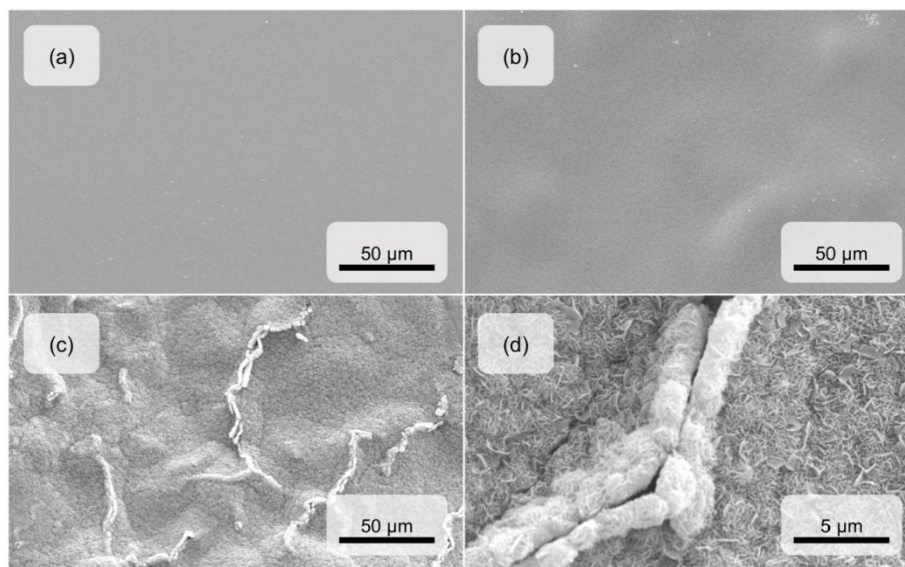**Fig. IV. 8** SEM images of the membranes before and after SBF immersion.

(a) pure chitosan membrane after seven days in SBF; **(b)** composite of 0.7 % w/v chitosan and 0.3 % w/v BG-NPS (control = zero days in SBF); **(c)** composite of 0.7 % w/v chitosan and % w/v BG-NPs after seven days in SBF and **(d)** composite of 0.7 % w/v chitosan and 0.3 % w/v BG-NPS after seven days in SBF at a higher magnification.

4. Conclusions

In this work, new bioactive glass nanoparticles based on the SiO_2–CaO–P_2O_5 and SiO_2–CaO systems were prepared using a sol–gel method. Round shaped particles with sizes below 50 nm were achieved within the samples produced at pH 11.5. The sol–gel BG-NPs obtained in this work, when immersed in SBF, proved the ability to induce mineralization, having the desired characteristics of biomaterials used in bone tissue engineering, i.e. bone bonding and biodegradability. These two properties are highly desirable at, respectively, early and late stages of post-implantation. The best bioactivity results are from by the samples prepared as a ternary system (SiO_2–CaO–P_2O_5). With the obtained data, one can conclude that the thermal treatment at 700 °C improves the bioactivity of the BG-NPs produced, being more effective when the nanoparticles are prepared at pH 11.5.

Nanocomposites resulting from the combination of these materials with chitosan exhibited bioactive character and may be potentially used in a series of orthopedic applications, including in membranes for tissue guided regeneration.

References

[1] Hench LL. Sol-gel materials for bioceramic applications. Current Opinion in Solid State & Materials Science 1997;2:604-10.

[2] Hench LL. The story of Bioglass (R). Journal of Materials Science-Materials in Medicine 2006;17:967-78.

[3] Hench LL AO. An Introduction to Bioceramics. Hench LL, Wilson J ed: World Scientific Publishing Co, River Edge, NJ; 1993.

[4] Li R, Clark AE, Hench LL. An investigation of bioactive glass powders by sol-gel processing. Journal of Applied Biomaterials 1991;2:231-9.

[5] Gallardo J, Galliano P, Duran A. Bioactive and protective sol-gel coatings on metals for orthopaedic prostheses. Journal of Sol-Gel Science and Technology 2001;21:65-74.

[6] Sepulveda P, Jones JR, Hench LL. Characterization of melt-derived 45S5 and sol-gel-derived 58S bioactive glasses. Journal of Biomedical Materials Research 2001;58:734-40.

[7] Saravanapavan P, Jones JR, Pryce RS, Hench LL. Bioactivity of gel-glass powders in the CaO-SiO2 system: A comparison with ternary (CaO-P2O5-SiO2) and quaternary glasses (SiO2-CaO-P2O5-Na2O). Journal of Biomedical Materials Research Part A 2003;66A:110-9.

[8] Saravanapavan P, Hench LL. Low-temperature synthesis, structure, and bioactivity of gel-derived glasses in the binary CaO-SiO2 system. Journal of Biomedical Materials Research 2001;54:608-18.

[9] Salinas AJ, Martin AI, Vallet-Regi M. Bioactivity of three CaO-P2O5-SiO2 sol-gel glasses. Journal of Biomedical Materials Research 2002;61:524-32.

[10] Labbaf S, Tsigkou O, Muller KH, Stevens MM, Porter AE, Jones JR. Spherical bioactive glass particles and their interaction with human mesenchymal stem cells in vitro. Biomaterials 2011;32:1010-8.

[11] Mackay CE, Johns M, Salatas JH, Bessinger B, Perri M. Stochastic probability modeling to predict the environmental stability of nanoparticles in aqueous suspension. Integrated Environmental Assessment and Management 2006;2:293-8.

[12] Hench LL, Thompson I. Twenty-first century challenges for biomaterials. Journal of the Royal Society Interface 2010;7:S379-S91.

[13] Couto DS, Hong ZK, Mano JF. Development of bioactive and biodegradable chitosan-based injectable systems containing bioactive glass nanoparticles. Acta Biomaterialia 2009;5:115-23.

[14] Courtheoux L, Lao J, Nedelec JM, Jallot E. Controlled bioactivity in zinc-doped sol-gel-derived binary bioactive glasses. Journal of Physical Chemistry C 2008;112:13663-7.

[15] Bini M, Grandi S, Capsoni D, Mustarelli P, Saino E, Visai L. SiO2-P2O5-CaO Glasses and Glass-Ceramics with and without ZnO: Relationships among Composition, Microstructure, and Bioactivity. Journal of Physical Chemistry C 2009;113:8821-8.

[16] Li X, Wang XP, He DN, Shi JL. Synthesis and characterization of mesoporous CaO-MO-SiO2-P2O5 (M = Mg, Zn, Cu) bioactive glasses/composites. Journal of Materials Chemistry 2008;18:4103-9.

[17] Perez-Pariente J, Balas F, Roman J, Salinas AJ, Vallet-Regi M. Influence of composition and surface characteristics on the in vitro bioactivity of SiO2-CaO-P2O5-MgO sol-gel glasses. Journal of Biomedical Materials Research 1999;47:170-5.

[18] Saboori A, Sheikhi M, Moztarzadeh F, Rabiee M, Hesaraki S, Tahriri M, et al. Sol-gel preparation, characterisation and in vitro bioactivity of Mg containing bioactive glass. Advances in Applied Ceramics 2009;108:155-61.

[19] Bordes P, Pollet E, Averous L. Nano-biocomposites: Biodegradable polyester/nanoclay systems. Progress in Polymer Science 2009;34:125-55.

[20] Hu XJ, Liu JK, Lu Y, Mu J. Facile synthesis and characterization of hydroxylapatite nanoparticle chains. Materials Letters 2008;62:3824-6.

[21] Yuan JK, Laubernds K, Zhang QH, Suib SL. Self-assembly of microporous manganese oxide octahedral molecular sieve hexagonal flakes into mesoporous hollow nanospheres. Journal of the American Chemical Society 2003;125:4966-7.

[22] Boccaccini AR, Erol M, Stark WJ, Mohn D, Hong ZK, Mano JF. Polymer/bioactive glass nanocomposites for biomedical applications: A review. Composites Science and Technology 2010;70:1764-76.

[23] Hong Z, Liu A, Chen L, Chen X, Jing X. Preparation of bioactive glass ceramic nanoparticles by combination of sol-gel and coprecipitation method. Journal of Non-Crystalline Solids 2009;355:368-72.

[24] Hong ZK, Reis RL, Mano JF. Preparation and in vitro characterization of scaffolds of poly(L-lactic acid) containing bioactive glass ceramic nanoparticles. Acta Biomaterialia 2008;4:1297-306.

[25] Hong ZK, Luz GM, Hampel PJ, Jin MS, Liu AX, Chen XS, et al. Mono-dispersed bioactive glass nanospheres: Preparation and effects on biomechanics of mammalian cells. Journal of Biomedical Materials Research Part A 2010;95A:747-54.

[26] Ma J, Chen CZ, Wang DG, Meng XG, Shi JZ. In vitro degradability and bioactivity of mesoporous CaO-MgO-P2O5-SiO2 glasses synthesized by sol-gel method. Journal of Sol-Gel Science and Technology 2010;54:69-76.

[27] Kokubo T, Takadama H. How useful is SBF in predicting in vivo bone bioactivity? Biomaterials 2006;27:2907-15.

[28] Kim HW, Kim HE, Knowles JC. Improvement of hydroxyapatite sol-gel coating on titanium with ammonium hydroxide addition. Journal of the American Ceramic Society 2005;88:154-9.

[29] Brinker CJ, Scherer GW. Sol-Gel-Glass. 1. Gelation and gel structure. Journal of Non-Crystalline Solids 1985;70:301-22.

[30] Gajovic A, Gracin D, Djerdj I, Tomasic N, Juraic K, Su DS. Nanostructure of thin silicon films by combining HRTEM, XRD and Raman spectroscopy measurements and the implication to the optical properties. Applied Surface Science 2008;254:2748-54.

[31] Hong Z, Reis RL, Mano JF. Preparation and in vitro characterization of novel bioactive glass ceramic nanoparticles. Journal of Biomedical Materials Research Part A 2009;88A:304-13.

[32] Bellantone M, Hench LL. Bioactive behaviour of sol-gel derived antibacterial bioactive glass. Bioceramics 2000;192-1:617-20.

[33] Saravanapavan P, Jones JR, Verrier S, Beilby R, Shirtliff VJ, Hench LL, et al. Binary CaO-SiO2 gel-glasses for biomedical applications. Bio-Medical Materials and Engineering 2004;14:467-86.

[34] Hong Z, Merino EG, Reis RL, Mano JF. Novel Rice-shaped Bioactive Ceramic Nanoparticles. Advanced Engineering Materials 2009;11:B25-B9.

[35] Hench LL. Bioceramics. Journal of the American Ceramic Society 1998;81:1705-28.

[36] Lu HH, Pollack SR, Ducheyne P. Temporal zeta potential variations of 45S5 bioactive glass immersed in an electrolyte solution. Journal of Biomedical Materials Research 2000;51:80-7.

[37] Benhayoune H, Charlier D, Jallot E, Laquerriere P, Balossier G, Bonhomme P. Evaluation of the Ca/P concentration ratio in hydroxyapatite by STEM-EDXS: influence of the electron irradiation dose and temperature processing. Journal of Physics D-Applied Physics 2001;34:141-7.

[38] Zhong JP, Greenspan DC. Processing and properties of sol-gel bioactive glasses. Journal of Biomedical Materials Research 2000;53:694-701.

[39] Lin S, Ionescu C, Pike KJ, Smith ME, Jones JR. Nanostructure evolution and calcium distribution in sol-gel derived bioactive glass. Journal of Materials Chemistry 2009;19:1276-82.

[40] Luz GM, Mano JF. Mineralized structures in nature: Examples and inspirations for the design of new composite materials and biomaterials. Composites Science and Technology 2010;70:1777-88.

Chapter IV - Appendix

Wettable arrays onto superhydrophobic surfaces for bioactivity testing of inorganic nanoparticles*

Abstract

Poly(l-lactic acid) superhydrophobic surfaces prepared by a phase-separation methodology were treated with 30 min exposition of UV/O$_3$ irradiation using hollowed masks in order to obtain patterned superhydrophilic squared-shaped areas. These wettable areas successfully confined bioactive glass nanoparticles (BG-NPs), by dispensing and drying individual droplets of BG-NPs suspensions. The obtained biomimetic chips were used to test the *in vitro* bioactivity of binary (SiO$_2$–CaO) and ternary (SiO$_2$–CaO–P$_2$O$_5$) nanoparticles produced using sol–gel chemistry by immersing such substrate in simulated body fluid (SBF). From SEM and EDX it was possible to conclude that the ternary system promoted an enhanced apatite deposition. This work shows the potential of using such flat disposable matrices in combinatory essays to easily evaluate the osteoconductive potential of biomaterials using small amounts of different samples.

1. Introduction

Superhydrophobic surfaces have attracted an increasing interest on worldwide research. [1-4] These surfaces with contact angles higher than 150°, exhibit extreme water repellency and have potential applications in a variety of scientific and industrial fields. [5, 6] Some natural surfaces, like lotus leaves [7], show superhydrophobic characteristics due to the existence of a rough topography of the surface at both the micro and nano scales. Different methodologies have been proposed to produce artificial rough surfaces with similar features. [8] Rough surfaces made of poly(l-lactic acid), PLLA, exhibiting a superhydrophobic behavior were prepared using a phase-separation method. [6] The aim of this work is to demonstrate that such kind of biodegradable superhydrophobic substrates can be used to produce innovative chips that are able to act as a practical substrate to perform multiplexing tests of biomaterials. In this case the bioactivity studies were focused to address relationships between biomaterial characteristics and osteoconductive potential. The production of such chips is based on the fact that the wettability can be increased by exposing the surface to UV/O_3 radiation. By using adequate masks one can produce patterned superhydrophilic spots that can be used to confine different biomaterials.

Bioactive inorganic nanoparticles have a potential to be applied in a variety of biomedical applications, including bone tissue engineering and biomimetic nanocomposites. [9-12] The chemical composition of such nanoparticles and the processing conditions may influence their osteoconductive behavior. As many variables may be involved, combinatory methodologies should be developed to access biomaterial characteristics/property relationships. In this work bioactive glass nanoparticles based on the ternary and binary systems were prepared using protocols previously reported. [13-15]

We demonstrate that biodegradable superhydrophobic substrates can be used to produce disposable chips that are able to easily evaluate important characterization aspects such as the *in vitro* bioactivity of materials. For the proof-of-concept binary and ternary formulations of bioactive nanoparticles will be tested to demonstrate the validity of the proposed methodology. It is envisaged that this kind of inexpensive chips has the potential to be applied to other kind of characterization tests needed in the biomaterial area where multiple effects are needed to be explored.

2. Materials and methods

2.1. Materials

Tetraethyl orthosilicate (TEOS, 99.90% pure), citric acid monohydrate (99–102%), ammonium phosphate dibasic, calcium nitrate tetrahydrate (99%), ethanol absolute, and ammonia water (ammonium hydrogen phosphate (98%), maximum of 33% NH_3) were purchased from Sigma-Aldrich. The used PLLA has M_n = 69,000 and M_W/M_n = 1.734.

2.2. PLLA surface preparation

Flat smooth PLLA sheets were processed by compression molding. Superhydrophobic PLLA substrates were prepared by spreading a PLLA/dioxane 13% (wt/v) solution over pieces of smooth PLLA sheets (10×10 mm^2); After a few seconds the substrates were immersed in absolute ethanol during 1 h, to induce phase separation. The samples were dried in a vacuum oven for 24 h at 40 °C to eliminate all solvent residues. When the samples are completely dry, the upper part is removed. The surface of the original substrate exhibits in this way the desirable micro/nano-meter rough topography. A squared hollowed plastic mask with open regions with a 1×1 mm^2 size was used to improve the wettability in the desired areas by irradiating the surface for 30 min with UV/O_3 radiation using a BioForce UV/Ozone ProCleaner device.

2.3. BG-NP preparation

To prepare the bioactive glass nanoparticles (BG-NPs) with the composition SiO_2:CaO:P_2O_5 (mol.%) = 55:40:5, a protocol based on a previous work was followed [13-15]. The same procedure with the necessary adaptations was followed to obtain SiO_2:CaO (mol.%) = 70:30, where no phosphorous precursor was used. [14]

2.4. *In vitro* bioactivity study

In vitro bioactivity tests were carried out by soaking the 10×10 mm^2 surfaces in 50 mL of SBF (simulated body fluid) solution during 0 (control, before SBF immersion), 3 and 7 days at 37 °C. The samples were then rinsed with distilled water and left to dry. The preparation of SBF followed the protocol described by Kokubo and Takadama using reagents from Sigma-Aldrich. [16]

2.5. SEM and EDX

To study the composition and morphology of the surfaces, a NanoSEM-FEI Nova 200 (FEG/SEM) scanning electron microscope was used. A Pegasus X4M instrument was used to perform the EDX experiments.

3. Results and discussion
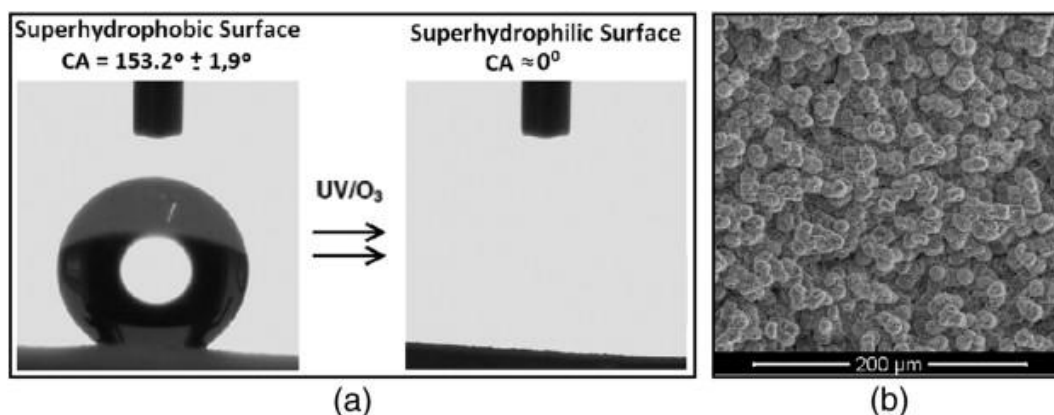
Fig. Ap. 1. The PLLA superhydrophobic surface .

   (a) Change in wettability of the PLLA superhydrophobic surface after 30 min exposition with UV/O$_3$ irradiation; **(b)** SEM image of the superhydrophobic surface.

Superhydrophobic PLLA surfaces were successfully prepared with a CA higher than 150° (Fig. 1 (a)). Such behavior can be explained by the obtained roughness of the surface that exhibited a hierarchical structure at both the nano and micro-scales (Fig. Ap. 1(b)). Up-

on exposure with UV/O$_3$ radiation, the PLLA surface could acquire a superhydrophilic character (Fig. Ap. 1(a)).

Fig. Ap. 2. Preparation of the chips used for the bioactivity testing showing the resulting EDX data for the superhydrophobic surface and low magnification SEM image for the areas containing the BG-NP.

Fig. Ap. 2 shows how such superhydrophilic modification was controlled into approximately 1×1 mm^2 squared regi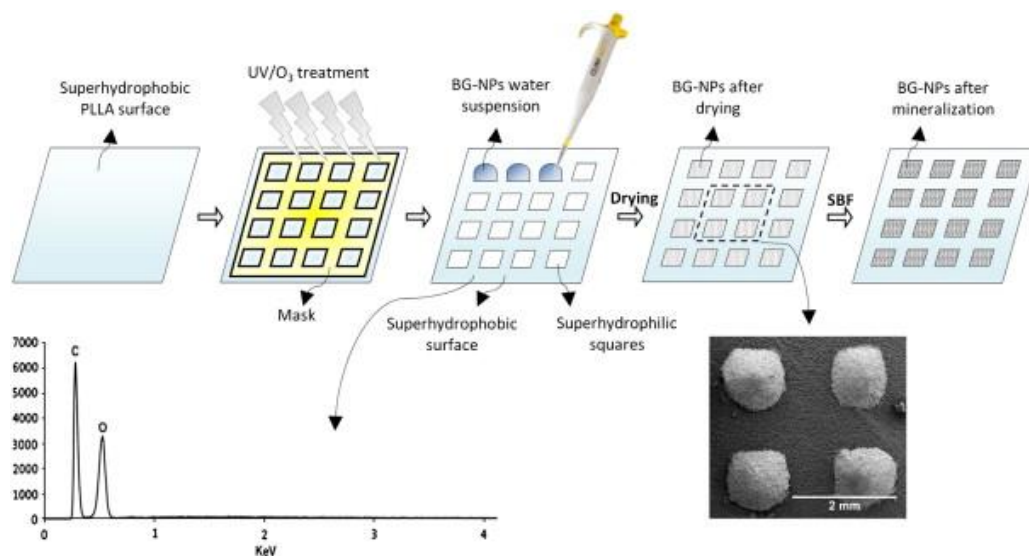ons to produce an array where 1 µl droplets of suspensions of the nanoparticles were individually deposited. The droplets were kept confined and separated from each other due to the strong difference in the surface tension between the superhydrophilic and superhydrophobic regions. After drying the chip, the BG-NPs were kept in the superhydrophilic spots. Fig. Ap. 2 shows EDX spectra obtained in the PLLA region and a low magnification SEM image which demonstrate the formation of spots with BG-NPs on the array. *In vitro* biomineralization studies in SBF were performed to assess the osteoconductive potential of two different formulations of BG-NPs (binary and ternary).

EDX spectra and SEM micrographs of the superhydrophilic arrays, with the two types of BG-NPs soaked in SBF for different incubation periods (0, 3 and 7 days), are present in Fig. Ap. 3. The carbon (C) peak corresponds to the substrate (PLLA surface); the oxygen (O) peak could be due to the substrate, to both BG-NPs, and to apatite; the phosphorous (P) peak could be attributed to ternary BG-NPs and to apatite, but only to apatite in the binary

BG-NPs, as this formulation does not contain phosphorus; the calcium (Ca) peak could cor-respond to both BG-NPs and to apatite.
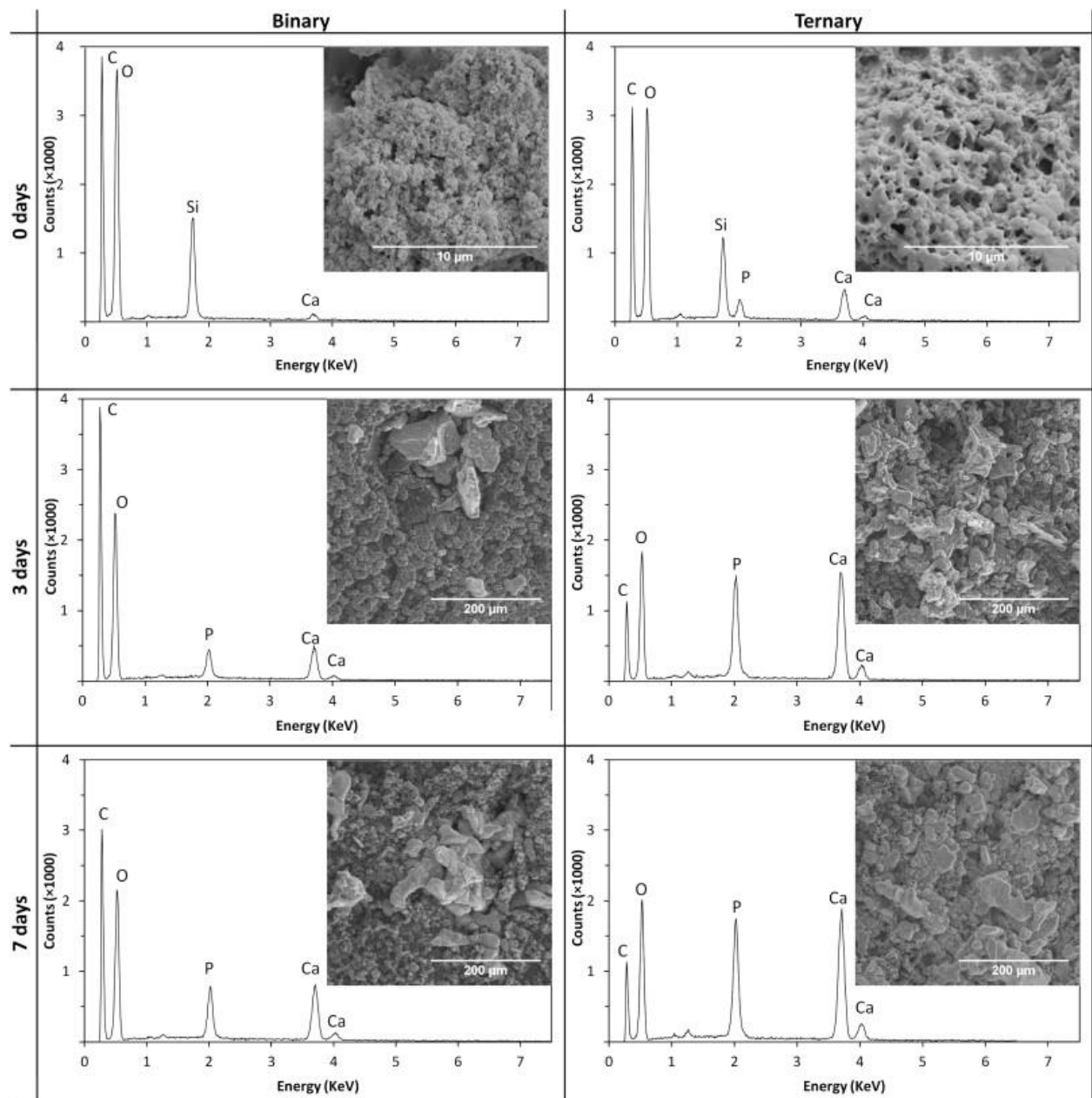

Fig. Ap. 3. Characterization of the chemical elements using EDX and the correspondent SEM micrographs of hydrophilic arrays which contained binary or ternary BG-NP soaked in the SBF solution during 0, 3 and 7 days.

An indication of the development of an apatite precipitate in soaked samples, in comparison with non incubated samples, is that the concentrations of Ca and P gradually

increase as the concentration of Si decreases due to the dissolution of the BG-NPs. [13, 15] Moreover, the SEM images revealed the formation of mineral agglomerates - see Fig. 3. Furthermore EDX showed Ca/P ratios which are closed to the hydroxyapatite stoichiometric theoretical value (1.67): 1.72 for binary during 3 days; 1.61 for binary during 7 days; 1.56 for ternary during 3 days; and 1.60 for ternary during 7 days. These results confirm the bioactive nature of the BG-NPs. The ratio between the C and P (or Ca) peak intensity could provide a qualitative indication of the calcification extent in each spot. EDX of binary BG-NPs exhibits lower peaks of P and Ca than the ternary, which means that ternary BG-NPs are more bioactive than the binary composition. After 7 days of immersion in SBF the hydrophilic arrays presented a larger amount of apatite than for the 3 day case. This result is visible in the EDX graphs, where a slight relative increase in P and Ca peaks in both types of BG-NPs from 3 days to 7 days can be observed. In addition SEM images revealed a more uniform apatite layer after 7 days of immersion in SBF. The increase of mineral deposits with increased incubation time is related to the longer time available for apatite precipitation.

4. Conclusions

This work proposed a new straightforward methodology to test and compare the bioactivity of different BG-NP formulations, by confining reduced amounts of BG-NPs in wettable spots organized in an array onto superhydrophobic substrates. The use of such patterned substrates is foreseen for other bioactivity combinatory tests.

Acknowledgment

References

[1] Feng X, Jiang L. Design and creation of superwetting/antiwetting surfaces. Advanced Materials 2006; 18:3063-78.

[2] Ma M, Hill RM. Superhydrophobic surfaces. Current Opinion in Colloid & Interface Science 2006; 11: 193-202.

[3] Verplanck N, Coffinier Y, Thomy V, Boukherroub R. Wettability switching techniques on superhydrophobic surfaces. Nanoscale Research Letters 2007; 2(12):577-96.

[4] Zhang X, Shi F, Niu J, Jiang YG, Wang ZQ. Superhydrophobic surfaces: from structural control to functional application. Journal of Materials Chemistry 2008; 18(6):621-33.

[5] Shi J, Alves NM, Mano JF. Towards bioinspired superhydrophobic poly(L-lactic acid) surfaces using phase inversion-based methods. Bioinspiration & Biomimetics 2008; 3(3).

[6] Song WL, Veiga DD, Custodio CA, Mano JF. Bioinspired degradable substrates with extreme wettability properties. Advanced Materials 2009; 21(18):1830-4.

[7] Feng L, Li SH, Li YS, Li HJ, Zhang LJ, Zhai J, et al. Super-hydrophobic surfaces: from natural to artificial. Advanced Materials 2002; 14(24):1857-60.

[8] Zhang X, Shi F, Niu J, Jiang YG, Wang ZQ. Superhydrophobic surfaces: from structural control to functional application. Journal of Materials Chemistry 2008; 18(6):621-33.

[9] Alves NM, Leonor IB, Azevedo HS, Reis RL, Mano JF. Designing biomaterials based on biomineralization of bone. Journal of Materials Chemistry 2010; 20(15):2911-2921.

[10] Boccaccini AR, Erol M, Stark AJ, Mohn D, Hong Z, Mano JF. Polymer/bioactive glass nanoparticles for biomedical applications: a review. Composites Science and Technology 2010; 70 (13):1764-76.

[11] Luz GM, Mano JF. Biomimetic design of materials and biomaterials inspired by the structure of nacre. Philosophical Transactions of the Royal Society Part A 2009; 367(1893):1587-605.

[12] Luz GM, Mano JF. Mineralized structures in nature: examples and inspirations for the design of new composite materials and biomaterials. Composites Science and Technology 2010; 70(13):1777-88.

[13] Hong Z, Reis RL, Mano JF. Preparation and in vitro characterization of novel bioactive glass ceramic nanoparticles. Journal of Biomedical Materials Research Part A2009; 88A(2):304-13.

[14] Hong Z, Luz GM, Hampel P, Jin M, Liu A, Chen X, et al. Mono-dispersed bioactive glass nanospheres: preparation and its effects on biomechanics of mammalian cells. Journal of Biomedical Materials Research Part A2010; 95 (3), 747-754.

[15] Hong Z, Reis RL, Mano JF. Preparation and in vitro characterization of scaffolds of poly(L-lactic acid) containing bioactive glass ceramic nanoparticles. Acta Biomaterialia 2008; 4(5):1297-306.

[16] Kokubo T, Takadama H. How useful is SBF in predicting in vivo bone bioactivity? Biomaterials 2006; 27(15):2907-15.

Chapter V

Nanoengineering of bioactive glass: From hollow to dense nanospheres *

Abstract

The possibility of engineering bioactive glass (BG) nanoparticles into suitable sizes and shapes represents a significant achievement regarding the development of new osteoconductive biomaterials for therapeutic strategies to replace or regenerate damaged mineralized tissues. Herein it is reported the structural and chemical evolution of sol-gel derived bioactive glass nanoparticles for both the binary (SiO_2:CaO (mol%) = 70:30) and ternary (SiO_2:CaO:P_2O_5 (mol.%) = 55:40:5) formulations, in order to understand how the particles formation can be directed. Hollow BG nanospheres were obtained through Ostwald ripening. The presence of a non ionic surfactant, poly(ethylene glycol) (PEG), allowed the formation of dense BG nanospheres with controllable diameters depending on the molecular weight of PEG.

A deep insight into the genesis of BG nanoparticles formation is essential to design BG based materials with controlled compositions, morphologies and sizes at the nanoscale, in order to improve their performance in orthopaedic applications including bone tissue engineering.

1. Introduction

Bioactive glasses are able to regenerate and repair both hard and soft tissue due to their osteoconduction, osseointegration and gene regulation properties. [1, 2] Bioactive glasses have been extensively studied since their discovery in 1969 by Hench. [3] However, the engineering of bioactive glasses at the nanoscale still offers exciting exploration possibilities.

Sol-gel route together with co-precipitation [4] is the most used methodology to produce BG nanoparticles. Several conditions of the sol-gel procedure influence particles assembly and growth, namely: reagents used as precursors, pH, addition and concentration of dispersants, reagents ratios and addition of catalysers (acids or bases). [5] All these parameters control the rates of hydrolysis and condensation, affecting final size, structure and agglomeration.

In a previous work [6], BG nanoparticles from both SiO_2-CaO (SiCa) and SiO_2-CaO-P_2O_5 (SiCaP) systems where prepared by sol-gel and characterized. It was concluded that, regarding the ternary system, the decrease in the pH of preparation from 11.5 to 9 lead to the formation of larger spherical nanoparticles exhibiting less bioactivity.

These observations were a strong motivation for a further investigation aiming to unveil the structural evolution of BG nanoparticles during the sol-gel maturation process. Such information could contribute for the design of bioactive glasses with controlled shape, dimensions and chemical composition that could elicit desired physiological response, namely bioactivity and biocompatibility. In the case of bioactivity, the increase in the surface area of nanoparticles will enhance their dissolution rate, which usually correlates to a higher bioactive character. Controlling nanoparticles dimensions is also critical regarding toxicity, since size is one of the recognition parameters of the immune system. [5, 7] If designed in a suitable size and shape both dense and hollow nanospheres can be used in drug delivery, since they can easily pass biological barriers taking guest materials with them, whether in their voids or matrix releasing the content through nanochannels or simply by gradual dissolution of the particles. [5, 8-10]

In this work, the development of BG nanoparticles from both SiCa and SiCaP formulations at pH 10.5 will be monitored: Samples will be collected on different reaction times,

immediately frozen at - 80 ˚C and then freeze-dried in order to fix their structure and properties. Since PEG is normally used in the production of particles as structure-directing agent, a parallel study will be conducted, in which different PEG molecular chains will be added to the sol-gel system and the results before and after calcinations will be compared, in order to understand how these conditions influence their structural arrangement.

Targeting of the BG nanoparticles engineering throughout the sol-gel process will facilitate the accomplishment of actual biotechnology needs, such as avoiding complications related with toxicity issues when using biomaterials within living organisms.

2. Experimental methods

BG nanoparticles preparation. The procedure to obtain BG nanoparticles with the composition $SiO_2:CaO:P_2O_5$ (mol.%) = 55:40:5 was adapted from a previously reported protocol. [4] Tetraethyl orthosilicate (TEOS, 99.90% pure), diammonium hydrogen phosphate, calcium nitrate tetrahydrate (99%), absolute ethanol, citric acid monohydrate (99%) and ammonium water were purchased from Sigma-Aldrich. The mixture of precursor's solutions (7.639 g of calcium nitrate in 120 ml of distilled water, 9.167 g of TEOS in 60 ml of ethanol and 30 ml of citric acid 10% (w/v)) was added drop-by-drop to an aqueous solution containing the phosphorus precursor (1.078 g of diammonium hydrogen phosphate) in 1500 ml of distilled water. In the case of the binary system, no phosphorus precursor was used in order to achieve the composition $SiO_2:CaO$ (mol%) = 70:30.The pH was maintained at 10.5 with ammonium water addition. The precipitate obtained was stirred for 48 h and then a resting period of 24 h followed. After 96h the precipitate was washed three times with distilled water. In order to follow the nanoparticles growth and maturation for both the SiCa and SiCaP systems throughout the sol-gel/co-precipitation process, samples were collected after 30 min (when all the precursors' solution had reacted), 24h, 48h, 72h and 96h (after the washing step). In a parallel study, after the 96h washing, 200 ml of an aqueous solution of poly(ethylene glycol) 2% (w/v) with Mw of 1500, 8000, 10 000 and 20 000 g/mol was added to the precipitate, or in the case of the control 200 ml of distilled water were added and then freeze drying followed. Samples of the different conditions were also collected for later

characterization. Finally the BG nanoparticles were calcinated at 700 ˚C for 3 h in order to achieve the optimal conditions for bioactivity. [11] The effect of calcination was also evaluated.

Scanning electron microscopy (SEM), Scanning Transmitted Electron Microscopy (S-TEM) and Energy dispersive X-ray (EDX). The morphology and composition of the BG nanoparticles were examined by a NanoSEM - FEI Nova 200 (FEG/SEM) microscope with and integrated EDAX - Pegasus X4M (EDS/EBSD) instrument. To perform SEM, a conductive gold coating was applied to the samples. For S-TEM observations the particles were dispersed in propanol by ultrasonic bath for 15 min and then transferred to a thin carbon film supported on TEM copper grids. For EDX, the analyses were conducted at low vacuum and without any coating.

X-ray diffraction (XRD). XRD measurements were performed with a Bruker D8 Discover model operated at 40 kV and 40 mA using Cu Kα radiation. The detector was scanned over a range of 2θ angles from 15˚ to 50˚ at a step size of 0.04˚ and dwell time of 1 s per step.

Zeta (ζ) potential measurements. The electrophoretic mobility of the BG nanoparticles suspensions in ultra pure filtered water was measured at 25˚C with a Malvern Zetasizer device, model Nano ZS. The ζ-potential was calculated by the equipment using the Smoluchowski's formula. The prepared suspensions of BG nanoparticles collected at different stages of the sol-gel process were adjusted to physiological pH 7.4 and then dispersed by ultrasonic bath for 15 min prior to each measurement.

3. Results and discussion

3.1. Chemical characterization of the BG sol-gel derived nanoparticles

In conventional sol-gel the formed sol is a colloidal silica solution. [12] Sufficient interconnected Si-O-Si bonds need to be formed until they respond cooperatively as colloidal

(submicrometer) particles. [12] These species will subsequently later undergo polycondensation reactions till they form a network of silica (Si-O-Si bridging bonds) which is termed gel. [13] Sol-gel route to produce BG nanoparticles begins with the hydrolysis of Si, Ca and P precursors. It is based on the so called Stöber synthesis that consists on the hydrolysis of tetra ethylorthosilicate (TEOS) in ethanolic medium and in the presence of ammonium water. [14] Calcium is introduced by calcium nitrate or calcium chloride. Citric acid is used to catalyze hydrolysis. Triethylphosphate (TEP) or diammonium hydrogen phosphate are used to add phosphate to the formulation. Ammonium water is required to induce precipitation, combining therefore, the traditional sol-gel route with co-precipitation methods. [4]

During the sol-gel procedure, some parameters can be changed in order to control size and cross-linking density of the nanoparticles, namely the pH, the silicon alkoxide and alcohol mixture used, the ratio between water and alkoxide and also ammonia concentration. [12, 13]

In a previous work, the effect of pH in the BG nanoparticles preparation was investigated. [11] It was concluded that higher pHs decrease the particles size and increase their bioactive potential. Therefore, in this work, pH 10.5 was used, in order to study the formation of BG nanoparticles suprastructures without compromising their bioactivity.

The addition of PEG with different Mw is also studied in this work. PEG is added in the last stage of the procedure, after the washing of ammonia excess with water, and prior to the precipitate freezing.

Freeze-drying was employed to eliminate water instead of a drying step (at 60°C). Freeze drying prevents the agglomeration that occurs in regular drying, caused by the covalent bonding resulting from later condensation reactions. However, freeze drying will only eliminate free or physisorbed water (water molecules trapped in the BG nanoparticles structure). [12] To finalize the sol-gel procedure, calcination is necessary to incorporate calcium at 400-450°C and also to eliminate citric acid at 250°C and to remove nitrates at 550-600°C. These actions will chemically stabilize the material and assure its biocompatibility. [13, 15-17]
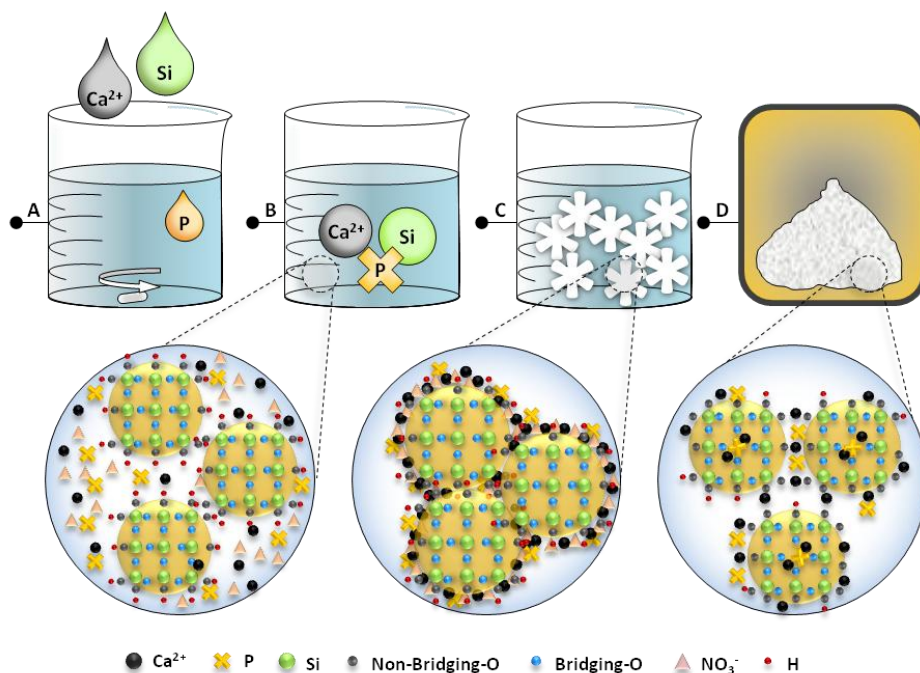
Fig. V. 1. Schematic of the sol-gel process and visual model of the SiCaP BG nanoparticles formation.

(a) Silica, calcium and phosphorus precursors mixture. **(b)** Hydrolisis and condensation reactions lead to the formation of particles comprising a silica based network. **(c)** When the BG precipitate is freeze-dried, the calcium and phosphorus are still not fixed to the network. **(d)** Calcination at 700˚C will lead to the stabilisation of the particles and fixation of calcium and incorporation of phosphorus into the now disordered glassy structure.

The preparation methodology and the basic structure of BG sol-gel derived nanoparticles are briefly schematized in Fig. V.1. The BG nanoparticles structure comprises covalent random networks of silica tetrahedral that share bridging oxygen (Si-O-Si). Calcium works as network modifier [18] and it is ionically bonded to the network via non-bridging oxygen bonds (Si-O-Ca). To enhance bioactivity of the glasses, phosphorus is also often incorporated into their formulation. Although it is not structurally included in the silica network, it forms orthophosphates, which are charge balanced by calcium ions. [18]

The nanoparticles formation at different stages of the sol-gel process was characterized by EDX and XRD - see Fig. V.2.
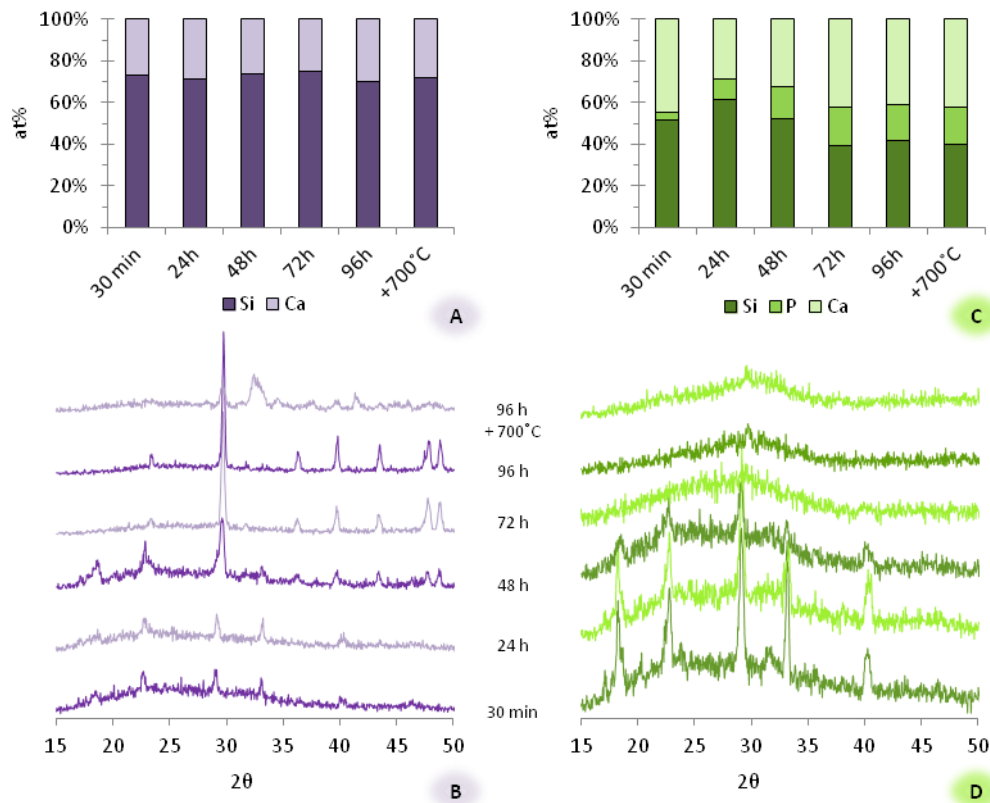
Fig. V. 2. EDX data (in at%) for the different BG-NPs systems.

(a) SiCa and **(c)** SiCaP systems and XRD spectra for **(b)** SiCa and **(d)** SiCaP at different reaction times (30 min, 24 h, 48 h, 72 h, 96 h and calcination at 700˚C).

Through EDX analysis it was possible to quantify the compositions in atomic percentage (at%) of the binary and ternary samples at the several time points. The first measured values after 30 min of sol-gel reaction agree with the initial idealized formulation, $SiO_2:CaO$ (mol%) = 70:30 in the binary system case - See Fig. V. 2 (a) - and $SiO_2:CaO:P_2O_5$ (mol%) = 55:40:5 in the ternary system case - Fig. V. 2 (c). In the SiCa system the percentages do not vary significantly with the reaction time. For the SiCaP formulation, a relative reduction in the Si seems to occur. The final disparity of at% regarding the initial content of sol-gel produced bioactive glasses has been justified by other authors as a consequence of the removal of the solubilised calcium nitrate during the washing step. [16, 19] However, the results for the SiCaP system shown on Fig. V. 2 (c) indicate that elements ratio evolve during the early stages of sol-gel reaction, stabilizing after 72h and are not dependent on the washing step at 96h.

The XRD patterns of the studied samples collected at different time points of the sol-gel maturation process are shown in Fig. V. 2 (b) and (d). The XRD spectra of the binary samples - See Fig. V. 2 (b) - begin with a slightly amorphous character that maintains during the first 24 h. After 48 h, some distinct peaks can be observed, and they intensify till 96 h, indicating that the sample is becoming more crystalline. These diffraction peaks disappear after calcination, and other peaks appear, assigned to a hydroxyapatite phase. Oppositely, the ternary system - See Fig. V. 2 (d) - begins with stronger diffraction peak with a large amorphous background. The intensity of these peaks begins to decrease after 24 h. The following reaction time, 48 h, exhibits a broad dispersive band, indicating the amorphous nature of the BG, even after calcination at 700 ˚C. The phosphorus presence may be destabilizing the silica network and increasing its amorphousness.

Regarding the BG nanoparticles bioactivity, higher crystallinity levels are related to lower dissolution rates, representing a direct detrimental effect on bioactivity. [16] The differences in the bioactive character of both SiCa and SiCaP systems were already explored and characterized in a previous work, [11] where it was concluded that the SiCa system presents lower bioactivity than the SiCaP one.

3.2. Evolution of BG nanoparticles structure during sol-gel/coprecipitation procedure
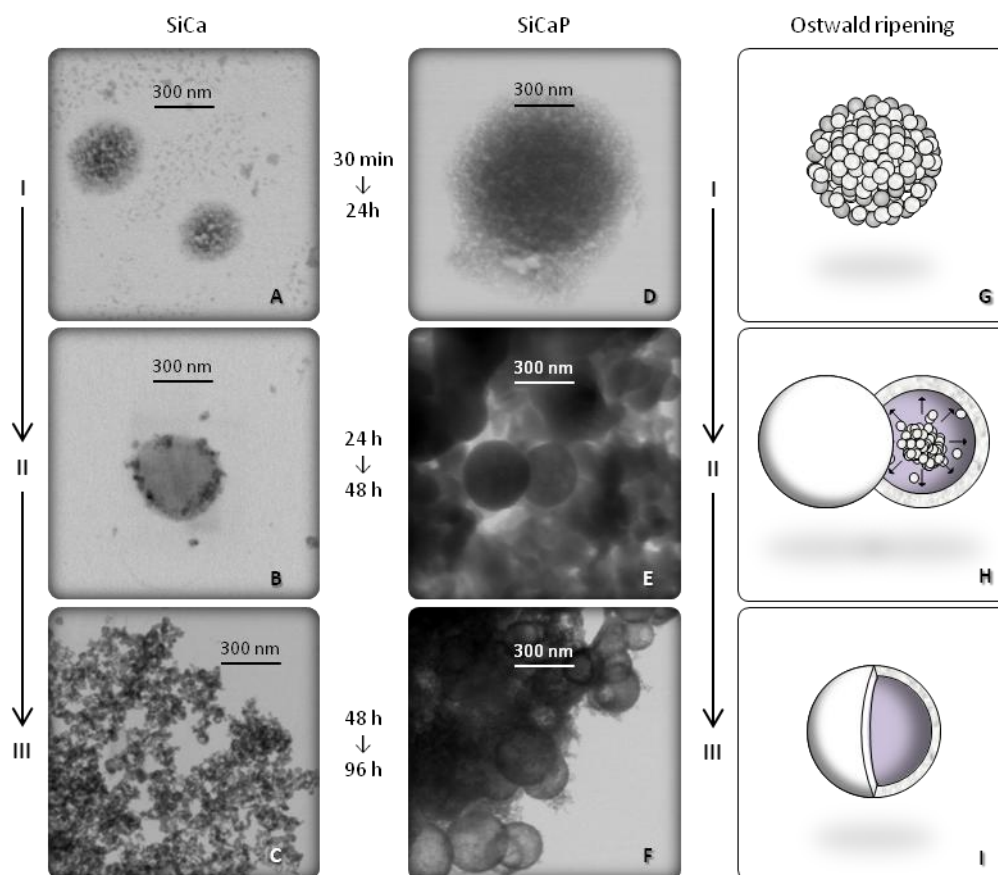

Fig. V. 3. Evolution of the BG nanoparticles through sol-gel reactions.

The first two columns show S-TEM micrographs of BG nanoparticles of the SiCa and SiCaP systems distributed in three different stages overtime. The third column represents schematically the stages of hollow nanospheres formation through Ostwald ripening mechanism.

The morphology of the inner structure and the surface of the particles obtained were analyzed by S-TEM and SEM respectively - See Fig. V. 3 and 5.

Regarding the SiCaP system, since the early stages of the sol-gel route, three distinct morphologies of BG supraparticles were identified, namely: Morula-like agglomerates of nanoparticles, and both dense and hollow spherical supraparticles - See Fig. V. 3 (d-f). Comparing all the samples collected at 30 min, 24h, 48h, 72h and 96h of sol-gel reaction, although the hollow supraparticles were present in all stages, one can associate the prevalence of certain species to three different time intervals. The morula-like agglomerates were identified solely in the period of 30 min to 24h - See Fig. V. 3 (d) - The dense spherical

supraparticles were collected mainly in the period from 24h to 48h - See Fig. V. 3 (e). After 48h both species were no longer observed and exclusively hollow supraparticles remain till the end of 96 h of reaction - See Fig. V. 3 (f).

Hollow SiCaP nanospheres are the most predominant morphology and were obtained since the first time point of 30 min. Strong contrast between the dark edge and the pale center of the particles is a clear evidence of the hollow nature of the BG nanospheres - See Fig. V. 3 (f) - having an average diameter of about 150 to 300 nm. These results seem to indicate that the initially formed BG glass nanoparticles, from the SiCaP system, self-assemble into spherical hollow suprastructures in the very first minutes of reaction. Careful observation of the S-TEM images indicates that the particles' shell has a 50 nm thickness, approximately the thickness of each individual BG nanoparticles. However, since the reaction system is very large, the process may not be homogenous and some intermediary species were observed in later stages, namely the morula-like and the dense spherical supraparticles.
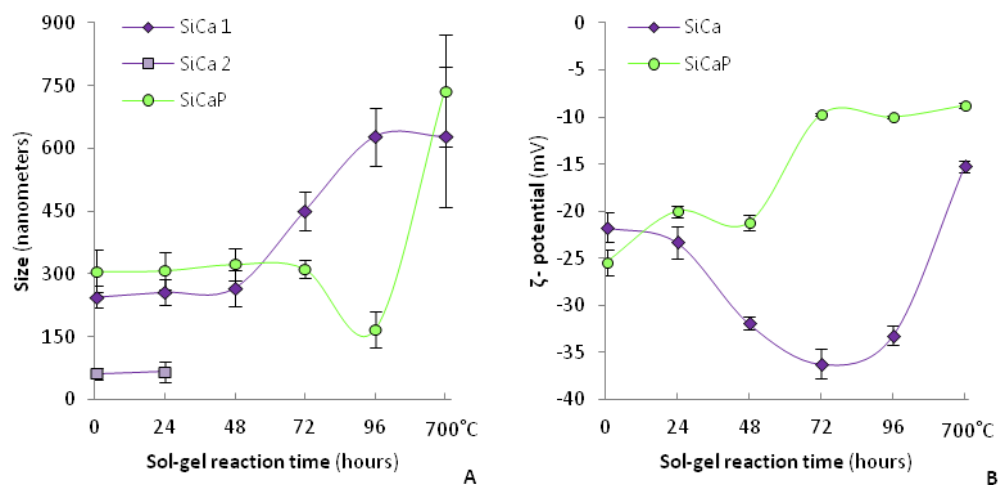
Fig. V. 4. (a) Sample's size and **(b)** ζ-potential of both binary and ternary systems as a function of sol-gel reaction time.

Regarding the SiCaP particles formation, zeta sizer quantification indicates that the formed particles mean size is around 300 nm since the first reaction time of 30 min, till 72h of reaction time is reached - see Fig. V. 4 (a). After the washing step at 96h, the remaining precipitate is composed by slightly larger particles, of about 500 nm.

Regarding the SiCa system, after 30 min of reaction till 24h, spherical morula-like supraparticles were observed accompanied by smaller nanoparticles basic units - see Fig. 3 V. (a). The zeta sizer quantification confirms that the samples collected within this period contain species with a bimodal distribution comprising sizes around 250 nm and also with 50 nm, identified in Fig. V. 4 (a) respectively as SiCa 1 and SiCa 2. After 48h all the small particles (50 nm) seem to vanish, and only the 250 nm particles were detected by the zeta sizer. These data are in accordance with the S-TEM images collected - See Fig. V. 3 (b). However, after 72h of reaction, the species sizes detected by the zeta sizer begin to increase, till they reach a 630 nm dimension after 96 h. The S-TEM image confirms that the initial nanoparticles formed branched clusters and morula-like structures are no longer observed - see Fig. V. 3 (c).
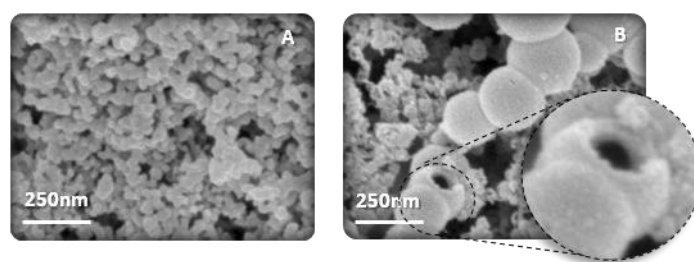
Fig. V. 5. SEM images of BG nanoparticles after calcination at 700 ˚C.

(a) SiCa and **(b)** SiCaP with detail of broken hollow particles.

The obtained sizes and morphologies are maintained after calcination for both systems - See SEM images in Fig. V. 5. Due to the surface activity of the particles, collisions may occur explaining the fusion of aggregated particles in calabash-like morphologies. [20] In addition, a clear evidence of the hollow structure of the SiCaP particles is shown in the detail of a broken BG nanoparticle in Fig. V. 5 (b).

S-TEM images of the collected samples - See Fig. V. 3 (a-f) - demonstrate that self-assembly of stable hollow nanospheres can spontaneously form in the SiCaP system without the need of a template. On the other hand, the SiCa system did not show the presence of hollow species in the ultimate stages of the sol-gel procedure. For the SiCa particles, the initial stages of the Ostwald ripening are reached; however in stage III a branched cluster morphology is preferred, as was already mentioned.

In order to infer about the electrostatic interactions that may cause the spontaneous self-assembly of the bioactive glass particles, the evolution of the electrokinetic ζ-potential was measured during the BG nanoparticles formation - See Fig. V. 4 (b).

ζ-potential is a physical property that can be attributed to any particle in suspension and is defined as the electrical potential difference between the dispersion medium and the stationary layer of fluid close to the particle. Therefore, it indicates the degree of repulsion between adjacent, similarly charged particles. The zeta potential value is calculated based on the electrophoretic mobility of the particles. A ζ-potential above ± 30 mV indicates that the particles' repulsive charges will avoid their agglomeration, assuring their stability when dispersed in a solution. [21]

Although the ζ-potential values are similar for both systems in the first 24h, a divergent evolution of the two systems occurs and the SiCa particles, with values between -30 and -40, after 48h more stable than the SiCaP ones that vary between -20 and -10mV. These values are maintained till the 96h time-point. Upon calcination the SiCaP ζ-potential maintains around -10 mV, while the SiCa ζ-potential reaches for -15 mV, indicating that the particles become more agglomerated due to the sintering effect of calcination.

ζ-potential profile, together with the chemical and structural evolution of the particles, may hold an explanation for the differences in the final morphologies obtained.

In the beginning of the sol-gel process, the aggregation of particles, from both systems into spherical suprastructures, is caused by a tendency of the particles to minimize their surface energy through attractive van der Walls forces. [22, 23] The competition between electrostatic repulsions and van der Waals attraction will be responsible for the self-limiting growth process of the suprastructures. [23] However, after 48h the SiCa particles begin to present a clear degree of crystallinity - See XRD results on Fig. V. 2 - and their stability increases. The particles no longer need to aggregate into spherical suprastructures to assure the surface energy minimization. Oppositely, since the phosphorus presence destabilizes the silica network, the SiCaP particles develop increasing amorphous character overtime. Accordingly, their stability diminishes, and this may be the reason why the particles remain organized into spherical aggregates.

Based on the observation of the intermediary species represented on Fig. V. 3, it is believed that these dense spherical aggregates evolve to hollow nanospheres through a template-free route that can be explained based on Ostwald ripening mechanisms.

Ostwald ripening is a physical process where larger crystals grow at the expense of the small ones that have higher solubility. [24] Ostwald ripening also applies for poorly crystallized particles [9], including the amorphous materials resulting from sol-gel process. Hence, BG inner particles, being smaller and less dense, easily undergo mass relocation due to dissolution. [9] The consumption of the inner particulates leads to the creation of voids. Over reaction time, hollow nanospheres are formed. [24-27] Ostwald ripening is prompt to occur in sol-gel, due to the presence of a significant number of chemical species necessary to generate ionic transport in solution during the ripening process. [26] Ostwald ripening of the SiCaP BG nanoparticles is schematically represented in Fig. V. 3 (g-i) - Morula-like suprastructures evolve to dense spherical suprastructures that in a last stage form hollow nanospheres.

3.3. Surfactants influence

The common silica based microparticles sol-gel synthesis relies on the use of an organic template, typically an amphiphilic surfactant to influence the final organization of suprastructures. [5, 28, 29] Weak noncovalent bonds such as hydrogen bonds and van der Waals forces drive the organic/inorganic self-assembly between the surfactants and inorganic species. [29] Interactions between the template and sol species may lead to many results, namely hollow structures. For BG, a similar mechanism is described for producing hollow microspheres, using PEG as template. [30]

PEG has been widely used as surfactant in the production of biomaterials, namely as a structure-directing agent. Moreover, particle size and distribution of silica based nanoparticles depend on the concentration of PEG in dispersion. [31, 32] Hence, PEG is also used to control the growth rate of colloids, as this polymer adsorption will decrease further interactions between the colloid surface and the surrounding medium. Moreover, PEG coating is an effective steric stabiliser able to reduce the rate of nanoparticles agglomeration. [33]

To explore all the possibilities offered by surfactants in controlling the morphologiey of particles in solution, the effect of PEG Mw on the BG nanoparticles dispersed in solution was investigated. After 96 h of sol-gel reaction, different molecular weight PEG chains

(1500, 8000, 10 000 and 20 000 g/mol) were vigorously stirred with the particles for to 2h after the washing of SiCaP BG precipitates.
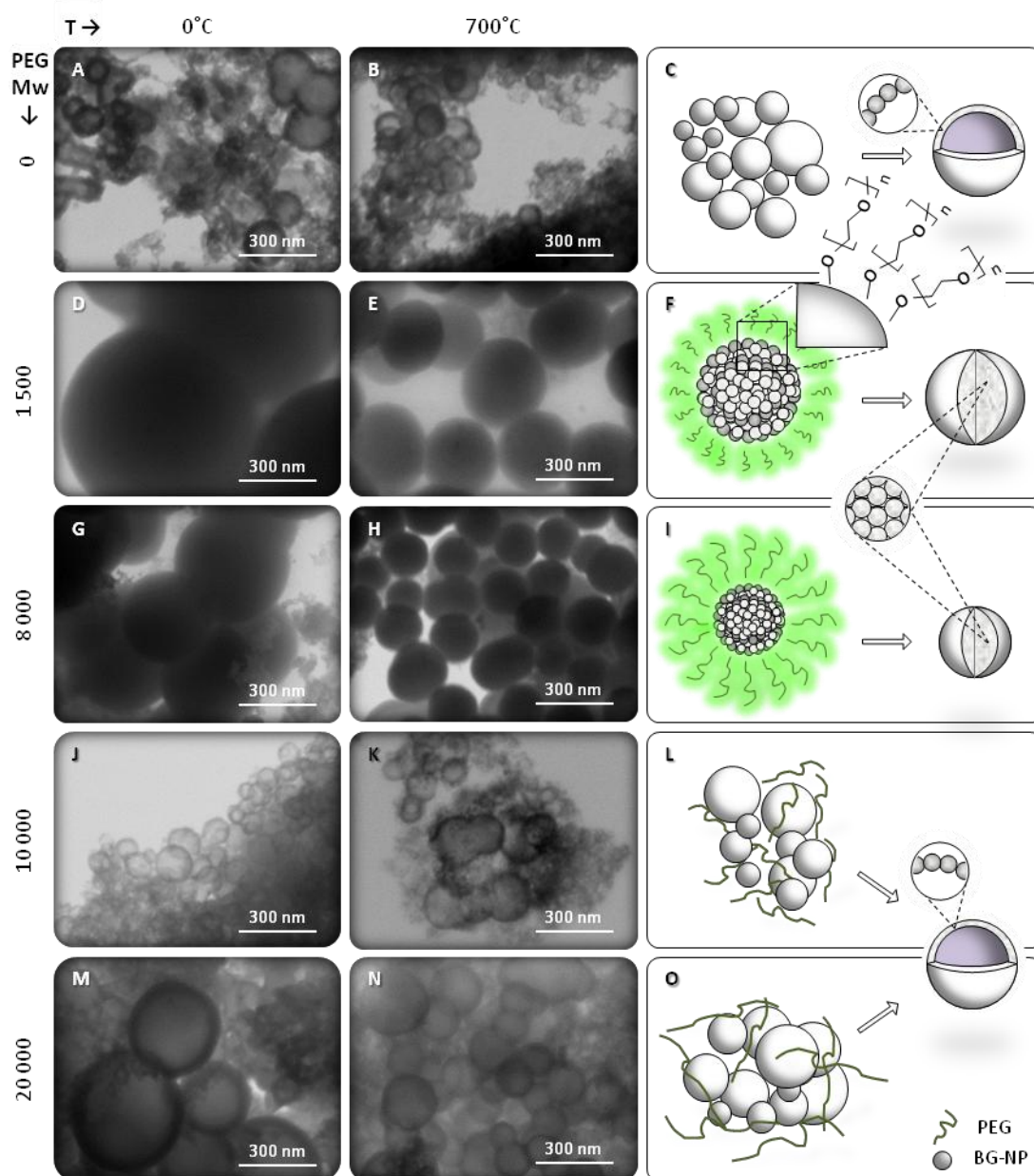
Fig. V. 6. PEG chain Mw interactions with SiCaP BG samples.

(a) and (b) - no PEG added, (d) and (e) - 1500 g/mol, (g) and (h) - 8000 g/mol, (j) and (k) - 10 000 g/mol, (m) and (n) - 20 000 g/mol, respectively for non calcinated (0˚C) and calcinated (700˚C) BG nanoparticles. The third collumn (c), (f), (i), (l) and (o) represents the scheme for each PEG chain Mw.

Fig. V. 6 resumes this experiment. Small molecular chains with the Mw of 1500 e 8000 g/mol added to the BG initial particles resulted in the formation of dense spheres of

300 nm and 100-150 nm diameter after calcination at 700 ˚C - see Fig. V. 6 (d) and (e) and (g) and (h). High Mw chains addition - see Fig. V. 6 (k) and (n) - resulted in BG hollowed supraparticles similar to the ones observed when no PEG was added - See Fig. V. 6 (a) and (b). Therefore, PEG chain Mw seems to influence the final diameter and structure of the particles obtained and can be used as simple tool to engineer BG nanospheres in order to meet the applications needs. Since both hollow and dense supraparticles coexist, further studies should be conducted to conclude if these shorter PEG chains act only on the BG individual nanoparticles or if hollow spherical supraparticles are destabilized by the PEG addition and vigorous stir, providing thus more BG nanoparticles subunits.

Observing Fig. V. 6 (b), (k) and (n), it is possible to conclude that the increase in the Mw, maintaining the same concentration, results in a high degree of agglomeration.

The first column of Fig. V. 6 also shows that before calcination, the particles had larger diameters. The size decrease observed may be a consequence of pore diameter reduction between the basic subunits during calcination, which can be also useful in increasing the compressive strength. [13, 15, 34] Therefore, calcination can be used to engineer smaller BG nanoparticles.

The third column of Fig. V. 6 summarizes the model proposed to describe the influence of PEG's chain Mw on the formation of dense BG nanospheres. The addition of high Mw PEG chains has the same effect on the BG morphology than the absence of PEG. High PEG Mw corresponds to high chain lengths. The extended length of the polymer chains justifies the lack of interactions with the particles. On the other hand, low Mw, by having shorter length chains, allows interaction between BG particles and PEG chains, resulting in spherical dense supraparticles.

4. Conclusions

BG nanoparticles prepared by sol-gel from the SiCa (binary) and SiCaP (ternary) systems were studied in order to understand their structural evolution over reaction time. It was found that in the binary system the BG nanoparticles subunits - with sizes around 50 nm - aggregate in clusters, while in the ternary system the BG nanoparticles subunits spontaneously assemble into hollow spherical supraparticles and their formation can be explained by

an Ostwald ripening process in an attractive "one pot" template-free method. The hollow supraparticles maintained their shape and integrity even after being calcinated.

PEG chain's molecular weight was used to create dense monodispersed supraparticles. This procedure also allows the control of the final size of the particles. Using PEG chains with Mw of 1500 g/mol will result in supraparticles with 300 nm diameters. By increasing the Mw up to 8000 g/mol, supraparticles with sizes between 100-150 nm are obtained.

The understanding of which mechanisms are on the basis of particles formation and how sizes and morphologies can be controlled is essential to take the next step into BG particles nanoengineering in order to respond to each specific biomedical demand.

Acknowledgements

References

[1] Jell G, Stevens MM. Gene activation by bioactive glasses. Journal of Materials Science: Materials in Medicine 2006; 17:997-1002.

[2] Hench LL. Bioceramics. Journal of the American Ceramic Society 1998; 81:1705-28.

[3] Hench LL. The story of Bioglass (R). Journal of Materials Science: Materials in Medicine 2006; 17:967-78.

[4] Hong Z, Reis RL, Mano JF. Preparation and in vitro characterization of novel bioactive glass ceramic nanoparticles. Journal of Biomedical Materials Research Part A 2009; 88A:304-13.

[5] Fadeel B, Garcia-Bennett AE. Better safe than sorry: Understanding the toxicological properties of inorganic nanoparticles manufactured for biomedical applications. Advanced Drug Delivery Reviews 2010; 62:362-74.

[6] Luz GM, Mano, J. F. Preparation and characterization of bioactive glass nanoparticles prepared by sol-gel for biomedical application. Nanotechnology 2011; 22:494014.

[7] Elechiguerra JL, Burt JL, Morones JR, Camacho-Bragado A, Gao X, Lara HH, et al. Interaction of silver nanoparticles with HIV-1. Journal of Nanobiotechnology 2005; 3:6.

[8] Zhao Y, Lin L-N, Lu Y, Chen S-F, Dong L, Yu S-H. Templating Synthesis of Preloaded Doxorubicin in Hollow Mesoporous Silica Nanospheres for Biomedical Applications. Advanced Materials 2010; 22:5255-9.

[9] Zeng HC. Synthetic architecture of interior space for inorganic nanostructures. Journal of Materials Chemistry 2006; 16:649-62.

[10] Fischer HC, Chan WCW. Nanotoxicity: the growing need for in vivo study. Current Opinion in Biotechnology2007; 18:565-71.

[11] Luz GM, Mano, J. F. Preparation and characterization of bioactive glass nanoparticles prepared by sol-gel for biomedical application. Nanotechnology 2011; 22.

[12] Hench LL, West JK. The sol-gel process. Chemical Reviews1990; 90:33-72.

[13] Jones JR, Lin S, Yue S, Lee PD, Hanna JV, Smith ME, et al. Bioactive glass scaffolds for bone regeneration and their hierarchical characterisation. Proceedings of the Institution of Mechanical Engineers Part H 2010; 224:1373-87.

[14] Stober W, Fink A, Bohn E. Controlled growth of monodisperse silica spheres in micron size range. Journal of Colloid and Interface Science 1968; 26:62-9.

[15] Lin S, Ionescu C, Pike KJ, Smith ME, Jones JR. Nanostructure evolution and calcium distribution in sol-gel derived bioactive glass. Journal of Materials Chemistry 2009; 19:1276-82.

[16] Labbaf S, Tsigkou O, Muller KH, Stevens MM, Porter AE, Jones JR. Spherical bioactive glass particles and their interaction with human mesenchymal stem cells in vitro. Biomaterials 2011; 32:1010-8.

[17] Takahashi R, Sato S, Sodesawa T, Suzuki M, Ichikuni N. Ni/SiO2 prepared by sol-gel process using citric acid. Microporous and Mesoporous Materials 2003; 66:197-208.

[18] Elgayar I, Aliev, A. E., Boccaccini, A. R., Hill, R. G. Structural analysis of bioactive glasses. Journal of Non-Crystalline Solids 2005; 351:173-83.

[19] Hong Z, Merino EG, Reis RL, Mano JF. Novel Rice-shaped Bioactive Ceramic Nanoparticles. Advanced Engineering Materials 2009; 11:B25-B9.

[20] Kulak A, Davis SA, Dujardin E, Mann S. Controlled assembly of nanoparticle-containing gold and silica microspheres and silica/gold nanocomposite spheroids with complex form. Chemistry of Materials 2003; 15:528-35.

[21] Schultz N, Metreveli G, Franzreb M, Frimmel FH, Syldatk C. Zeta potential measurement as a diagnostic tool in enzyme immobilisation. Colloids and Surfaces B: Biointerfaces 2008; 66:39-44.

[22] Tirrell M, Kokkoli E, Biesalski M. The role of surface science in bioengineered materials. Surface Science 2002; 500:61-83.

[23] Xia Y. Self-assembly of self-limiting monodisperse supraparticles from polydisperse nanoparticles. Nature Nanotechnology 2011; 6:580-7.

[24] Zeng HC. Ostwald ripening: A synthetic approach for hollow nanomaterials. Current Nanoscience 2007; 3:177-81.

[25] Ye TN, Dong ZH, Zhao YN, Yu JG, Wang FQ, Guo SK, et al. Controllable Synthesis and Photoluminescence of Single-Crystalline BaHfO(3) Hollow Micro- and Nanospheres. Langmuir 2011; 27:8878-84.

[26] Yang HG, Zeng HC. Preparation of hollow anatase TiO2 nanospheres via Ostwald ripening. Journal of Physical Chemistry B 2004; 108:3492-5.

[27] Mukherjee R, Chakrabarti T, Anumol EA, Abinandanan TA, Ravishankar N. Thermal Stability of Spherical Nanoporous Aggregates and Formation of Hollow Structures by Sintering-A Phase-Field Study. ACS Nano 2011; 5:2700-6.

[28] Zheng W, He L, Liang J, Chang G, Wang N. Preparation and Properties of Core-Shell Nanosilica/Poly(methyl methacrylate-butyl acrylate-2,2,2-trifluoroethyl methacrylate) Latex. Journal of Applied Polymer Science 2010; 120:1152-61.

[29] Wan Y, Zhao DY. On the controllable soft-templating approach to mesoporous silicates. Chemical Reviews 2007; 107:2821-60.

[30] Lei B, Chen X, Wang Y, Zhao N. Synthesis and in vitro bioactivity of novel mesoporous hollow bioactive glass microspheres. Materials Letters 2009; 63:1719-21.

[31] Gao G-M, Zou H-F, Liu D-R, Miao L-N, Ji G-J, Gan S-C. Influence of surfactant surface coverage and aging time on physical properties of silica nanoparticlese. Colloids and Surfaces A: Physicochemical and Engineering Aspects 2009; 350:33-7.

[32] Branda F, Silvestri B, Luciani G, Costantini A, Tescione F. Synthesis structure and stability of amino functionalized PEGylated silica nanoparticles. Colloids and Surfaces A: Physicochemical and Engineering Aspects 2010; 367:12-6.

[33] Xu H, Yan F, Monson EE, Kopelman R. Room-temperature preparation and characterization of poly (ethylene glycol)-coated silica nanoparticles for biomedical applications. Journal of Biomedical Materials Research Part A 2003; 66A:870-9.

[34] Jones JR, Ehrenfried LM, Hench LL. Optimising bioactive glass scaffolds for bone tissue engineering. Biomaterials 2006; 27:964-73.

Chapter VI

Chitosan/bioactive glass nanoparticles composites for biomedical applications*

Abstract

Nanocomposites films based on a chitosan blend with bioactive glass nanoparticles (BG-NPs) with different formulations, namely $SiO_2:CaO:P_2O_5$ (mol.%) = 55:40:5 and $SiO_2:CaO:P_2O_5:MgO$ (mol.%) = 64:26:5:5 were produced in order to develop systems with applicability in Guided Tissue Regeneration.

The zeta potential of the BG-NPs containing magnesium was found to be lower than the other formulation and the corresponding composite with chitosan was the most hydro-philic.

The bioactive character of the biomaterials was also assessed *in vitro* by immersion of the materials in SBF, followed by SEM and EDX evaluations.

SaOs-2 osteoblastic-like cells were seeded on the different nanocomposites and their behavior was followed by SEM observations, citotoxicity assessments, DNA quantification and ALP analysis. The introduction of the inorganic component in the chitosan matrix had a positive effect on the biological response of the membranes.

The developed nanocomposite films are potential candidates for regenerating dam-aged bone tissue and could be useful in orthopaedic and maxilo-facial applications.

1. Introduction

Surface chemistry and physical properties of bone substitutes used in osteo regeneration are of great importance, since they will direct biological responses such as cell adhesion and differentiation. [1] These features are critical for providing the optimal culturing environment for bone formation during the early stages of the regenerative process. [2]

Bioactive glasses are well suited materials for bone tissue regeneration due to their chemical interaction with surrounding bone tissue *in vivo*, which promotes osteointegration by the formation of a calcium phosphate layer which is later modified by bone cells. [2, 3] Moreover, the ionic release from bioactive glasses may stimulate gene expression, promoting osteoinduction. [4] Some works showed that dopping bioactive glasses with different ions can add value to these materials. [5] For instance, magnesium, one of the main substitutes for calcium in biological apatite, [6] when included in the bioactive glasses formulation, can enhance osteoblastic adhesion. [7]

The advantages of dopping bioactive glasses can be easily extended to the production of polymer based bioactive nanocomposites. Polymer based nanocomposites emerged from the Nanotechnology field as a promising route to mimic complex natural structures. [8] Regarding more specifically the mineralized structures in Nature, including bone itself, much effort has been put in the development of reinforced polymeric matrixes with nanosized reinforced fillers in order to obtain biomaterials with improved mechanical properties. [9-12]

Despite of all the advantages of using BG-NPs in the osteoregeneration field, bioactive glasses dissolution can generate very alkaline pHs when the material has a strong bioactive character, representing an important drawback of such biomaterials. Therefore, the aim of this work was to find a balance between bioactivity/ionic release and proper osteoblastic stimulation. By combining bioactive glass nanoparticles (BG-NPs) of different compositions, namely $SiO_2:CaO:P_2O_5$ (mol.%) = 55:40:5 and $SiO_2:CaO:P_2O_5:MgO$ (mol.%) = 64:26:5:5, with a natural polymer, chitosan, biocompatible and bioactive nanocomposite membranes where obtained. The combination of chitosan, a versatile biopolymer for orthopaedic tissue-engineering [13] with BG-NPs was already proved to result in a bioactive composite as a

calcium phosphate layer was formed *in vitro* upon immersion in a simulated body fluid (SBF). [14]

Since cell adhesion and motility is of major importance in wound healing [15], the osteoblastic reaction to chitosan/bioactive glass nanocomposites with different chemical compositions was assessed, as well as changes in the surface topography, charge and wettability as they also influenciate osteoblastic attachment and growth by controlling adhesion proteins adsorption. [16, 17]

2. Experimental methods

BG-NPs preparation. The procedure to obtain BG-NPs with the composition $SiO_2:CaO:P_2O_5$ (mol.%) = 55:40:5 was based on a previously reported protocol. [18] Tetraethyl orthosilicate (TEOS, 99.90% pure), citric acid monohydrate (99%), calcium nitrate tetrahydrate (99%), absolute ethanol and diammonium hydrogen phosphate (98%) were purchased from Sigma-Aldrich. The mixture of precursor's solutions (7.639 g of calcium nitrate in 120 mL of distilled water, 9.167 g of TEOS in 60 mL of ethanol and 30mL of citric acid 10% (w/v)) was added drop-by-drop to an aqueous solution containing the phosphorus precursor (1.078 g of diammonium hydrogen phosphate in 1500 mL of distilled water). In the case of the quaternary system, some changes were made. Magnesium nitrate hexahydrate from Fluka analytics was used in order to achieve the composition $SiO_2:CaO:P_2O_5:MgO$ (mol.%) = 64:26:5:5, and calcium chloride (Merck) was used as calcium precursor. In both cases, the pH was maintained at 11.5 by adding ammonia water. The precipitate obtained was stirred for 48 h, and then a resting period of 24 h followed. The precipitate was washed three times with distilled water. 200ml of poly(ethylene glycol) 2% (w/v) (Mw 20 000) were added to the precipitate, and then freeze drying followed. Finally the BG-NPs were heated at 700˚C for 3h in order to achieve the optimal conditions of bioactivity. [14]

Membranes preparation. The membranes were obtained by solvent casting, using medium molecular weight chitosan (from Sigma-Aldrich). Chitosan was dissolved in an aqueous acetic acid solution 2% (v/v) to a concentration of 1% (w/v) for preparation of the control

membranes of pure chitosan labelled CHT. For the composite membranes, the membranes were obtained by dissolving Chitosan (0.7% wt) and BG-NPs (0.3% wt) in the acetic acid solution. The materials containing $SiO_2:CaO:P_2O_5$ and $SiO_2:CaO:P_2O_5:MgO$ bioactive glass nanoparticles were labeled CHT/SiCaP and CHT/SiCaPMg, respectively.

After homogenization for 15 min in an ultrasound bath, 80 ml of polymeric solution were casted onto 125 mm x 20 mm square petri dishes and allowed to evaporate for 7 days. The dried membranes were neutralized by soaking in NaOH 0.1 M for 10 min followed by washing in distilled water until pH of 7 was reached in the liquid milieu. Membranes were allowed to dry at RT, clipped between 2 frames to obtain straight and smooth surfaces. They were then cut to obtain 7 mm diameter circular samples.

In vitro bioactivity study. *In vitro* bioactivity tests were carried out by immersing circular (7 mm diameter) chitosan based membranes in 50 mL of simulated body fluid (SFB) solution during 0 (control), 1, 3, 5 and 7 days at 37 ˚C. SBF was renewed after the third day, in order to assure proper ionic saturation. Upon removal from SBF, the membranes were rinsed with distilled water and allowed to dry. The SBF was prepared by dissolving NaCl, $NaHCO_3$, KCl, $K_2HPO_4.3H_2O$, $MgCl_2.6H_2O$ and Na_2SO_4 in distilled water and buffered with Tris buffer and HCl to reach a pH value of 7.4, following the protocol described by Kokubo and Takadama [19]. All chemicals were purchased from Sigma-Aldrich.

Scanning electron microscopy (SEM) and Energy dispersive X-ray (EDX) samples preparation. To study the surface and the morphology of the samples, a NanoSEM-FEI Nova 200 (FEG/SEM) scanning electron microscope was used. A conductive gold coating of 10 nm was applied to the samples. A Pegasus X4M instrument was used to perform the EDX experiments at low vacuum and without any coating.

Contact angle measurements. The wettability of the surfaces was evaluated using an OCA15+ goniometer (DataPhysics, Germany) and the sessile drop method. The volume of the applied droplets of glycerol was 3 μL. The mean value was calculated from at least four individual measurements on different areas of the surfaces.

Cytotoxicity, DNA quantification, ALP analysis and cell attachment tests. Cells from a human sarcoma osteogenic cell line (SaOs-2) were used to characterize the nanocomposites *in vitro*. The cells were cultured at 37˚C with 5% CO_2 and nourished with Dulbecco's modified minimum essential medium (D-MEM) supplemented with 1% antibiotic and 10% FBS. The medium was refreshed every 3 days until confluence, when the cells were tripsinized.

The chitosan based composites were previously sterilized by immersion in 70% (v/v) ethanol overnight and then washed twice with sterile phosphate buffered saline (PBS). The cells were seeded on the samples (n = 3) at a density of 65 000 cells/cm^2, and then the cultures were incubated at 37°C.

After each time point (1, 3, and 7 days of culture), MTS (3-(4,5-dimethylthiazol-2-yl)-5-(3-carboxymethoxyphenyl)-2-(4-sulfophenyl)-2H-tetrazolium) test (Promega) was performed to determine the cytotoxicity of the membranes. The relative cellular viability (%) was obtained and compared with tissue culture polystyrene (positive control of cell viability). Latex was used as negative control of cellular viability. For this assay, a MTS solution was prepared by using a 1:5 ratio of MTS reagent and D-MEM culture medium without phenol red or FBS, followed by a 3h incubation period at 37°C. All cytotoxicity tests were conducted by using 3 replicates. Finally, the optical density (OD) was read at 490nm on a multiwell microplate reader (Synergy HT, Bio-Tek Instruments).

To assess proliferation by DNA quantification and ALP activity, samples were also collected on days 1, 3 and 7 after seeding. Samples removed from culture were rinsed twice in a PBS solution and transferred into 1.5 mL microtubes containing 1 mL of ultra-pure water. In order to assure cell lysis, samples were incubated for 1 h at 37 ˚C in a water-bath and stored at least for 1h in a - 80 ˚C freezer. After thawing, samples were sonicated for 15 min.

A PicoGreen dsDNA quantification kit (Invitrogen) was used to determine the proliferation of cells in the nanocomposites. Triplicates were made both for samples and dsDNA standards (0-2 μg/ml), followed by incubation of the 96-well white plate (Costar; Becton-Dickinson) for 10 min in the dark. Fluorescence was read using a microplate ELISA reader (BioTek, USA) at an excitation of 485 nm and an emission of 528 nm with bandwidth of 20 nm. DNA concentration values were obtained from a standard curve.

In order to detect initial osteogenic differentiation, ALP activity was measured. The assay mixture contained, in each well of a 96-well plate (Costar; Becton-Dickinson), 20 μl of the sample and 60 μl substrate solution consisting of 0.2% (wt/v) p-nytrophenyl phosphate

(Sigma) in a substrate buffer with 1 M diethanolamine HCl (Merck, Germany), pH 9.8. After an incubation period of 60 min at 37˚C, 80 µl stop solution [2 M NaOH (Panreac, Spain) plus 0.2 mM EDTA (Sigma)] was added to each well. Standards were then prepared with p-nytrophenol (10 µM/ml; Sigma) in order to achieve final concentrations in the range 0-0.3 µM/ml. Samples and standards were prepared in triplicates. Absorbance was read at 405 nm and sample concentrations were read from the standard graph. ALP enzymatic activity was normalized to total DNA content.

Finally, also on days 1, 3 and 7 after seeding, cell morphology on the nanocomposites was assessed by SEM. The samples were rinsed twice with PBS to remove non-adherent or loosely adherent cells and fixed with a solution of 2.5% (v/v) glutaraldehyde in 0.1M PBS, for 1h at 4˚C. After removing the fixative, the cells were rinsed in PBS and distilled water and dehydrated in a graded series of ethanol solution (50%, 70%, 90% and 100%) each one repeated twice for 15 min. They were left to dry at air at RT, and sputter-coated with gold before SEM observation.

3. Results

3.1. Nanoparticles characterization: SEM observations and Zeta-potential measurements
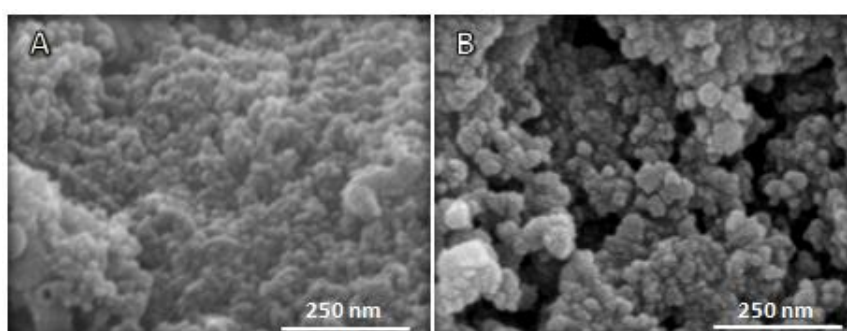
Fig. VI. 1. SEM images of the BG-NPs: **(A)** $SiO_2:CaO:P_2O_5$ and **(B)** $SiO_2:CaO:P_2O_5:MgO$ system.

$SiO_2:CaO:P_2O_5$ nanoparticles (figure VI. 1A) showed a higher level of agglomeration than the $SiO_2:CaO:P_2O_5:MgO$ (figure VI. 1B). The particles containing Mg also appeared to have longer diameters (30-60 nm) than the formers (20 nm), although some carefulness is

required in these analyses, since the particles were coated with a 10 nm thickness gold layer, adding 20 nm in the final diameter of non agglomerated particles *vs* agglomerated ones.

The ζ-potential of chitosan powders, $SiO_2:CaO:P_2O_5$ and $SiO_2:CaO:P_2O_5:MgO$ nanoparticles were investigated at the physiological pH of 7.4. Measuring the ζ-potential of a particle suspended in water, can be very useful since one can predict the stability of a particle based on its ζ-potential value. ζ-potential is defined as the electrical potential difference between the dispersion medium and the stationary layer of fluid close to the particle. Therefore, it indicates the degree of repulsion between adjacent, similarly charged particles. The ζ-potential value is calculated based on the electrophoretic mobility of the particles. The magnitude of the ζ- potential gives an indication of the potential stability of the particles in suspension. Particles having values above 30 mV or under -30 mV are considered stable. [20] Chitosan particles are the most stable particles as they have a ζ-potential of + 35.76 mV. They also present positive charge. Both $SiO_2:CaO:P_2O_5$ and $SiO_2:CaO:P_2O_5:MgO$ nanoparticles present negative ζ- potentials, respectively -8.8 mV and -19.13 mV.

3.2. Nanocomposites surface characterization: SEM observations and Contact Angle measurements
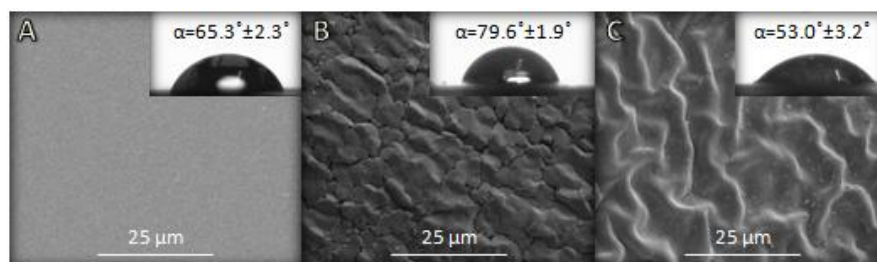
Fig. VI. 2. SEM images of the nanocomposites surfaces. The inset images show the profile of glycerol droplets dispersed over the membranes.

(a) Pure chitosan **(b)** CHT/SiCaP and **(c)** CHT/SiCaPMg nanocomposite.

Surface characterization of the nanocomposites was performed by SEM and Contact Angle measurements.

Pure chitosan membranes presented a flat and smooth surface (figure VI.2A) in comparison with the nanocomposites containing $SiO_2:CaO:P_2O_5$ and $SiO_2:CaO:P_2O_5:MgO$ nanoparticles (figure VI.2B and C). Some differences in the topography of the membranes

can be seen. CHT/SiCaP nanocomposite (figure VI.2B) shows a rough surface with fish scales-like disposition. In the other hand, CHT/SiCaPMg nanocomposite (figure VI.2C) presented smooth grooves.

Given that hydrophilicity is one of the physico-chemical properties that govern cell attachment, proliferation, and protein expression, the hydrophilicity of the nanocomposites was evaluated using contact angle measurements. Figure VI.2 also indicates the contact angles of the different samples with respect to glycerol. All the samples were considered hydrophilic.

Tissue culture polystyrene (TCP) was also studied for comparison purposes (data not shown). Pure chitosan membrane showed levels of hydrophilicity similar to TCP (61.9˚±2.7˚). The addition of bioactive glasses nanoparticles to the chitosan matrix seems to have a different consequence in the final composite hydrophilicity depending on the formulation of the nanoparticles, being the CHT/SiCaPMg membrane the most hydrophilic.

3.3. Bioactivity study
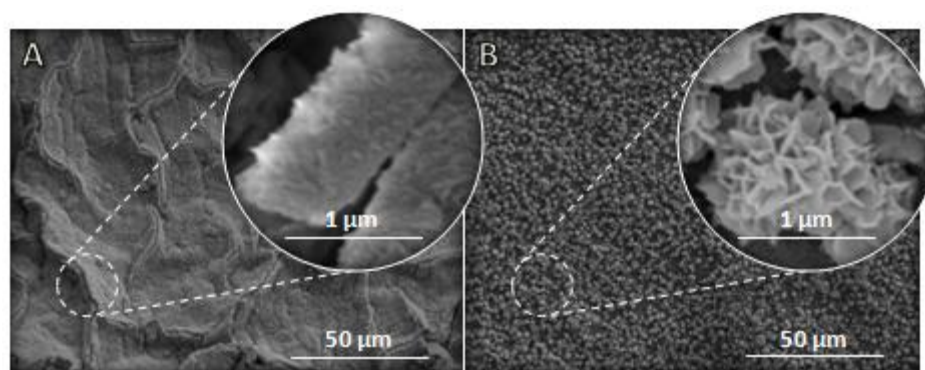
Fig. VI. 3. SEM images of **(a)** CHT/SiCaP and **(b)** CHT/SiCaPMg nanocomposite surfaces after 7 days of soaking in SBF showing the development of an apatitic film onto the membranes.

To assess the bioactivity of the nanocomposites, samples were immersed in SBF at 37 ˚C for different time periods. SEM images show the samples surface after 7 days of immersion in SBF (figure VI.3). Regarding the CHT/SiCaP nanocomposite (figure VI.3A), after seven days of immersion in SBF, a dense apatite layer was formed on its surface. The thickness of the apatitic film can be observed since the polymeric membrane shrinks upon drying

and the apatite layer breaks. This profile view allows us to estimate the reaction layer thickness as 785 nm approximately, being the average thickness of the membrane of $\approx 50\ \mu m$. The surface of the CHT/SiCaPMg nanocomposite exhibited a large number of small apatite clusters which did not densely cover the entire surface (figure VI.3B). The clusters comprised plate shaped particles with 350 nm in length and 10 - 40 nm in thickness.

As expected, pure chitosan did not present any bioactive character after being immersed in SBF (data not shown), so this ability verified in the nanocomposites is caused only due to the presence of the bioactive glass nanoparticles.
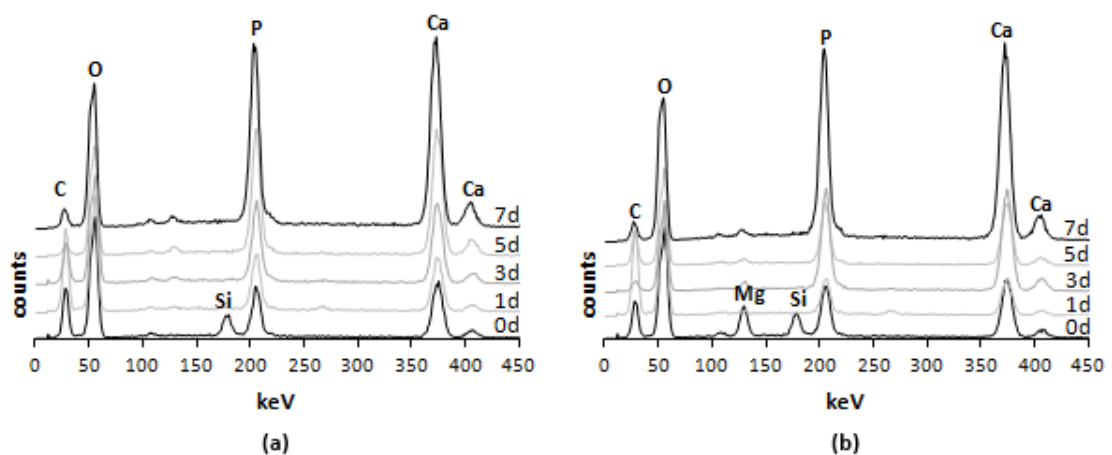

Fig. VI. 4. EDX spectra concerning the bioactivity study of **(a)** CHT/SiCaP and **(b)** CHT/SiCaPMg membranes immersed in SBF for different time points (0 - control, 1, 3, 5 and 7 days).

EDX analysis of the nanocomposites was performed in order to analyze changes in the surface chemical composition related to the mineralization process - see Figure 4. The initial oxide quantification of the BG-NPs was $SiO_2:CaO:P_2O_5$ (mol.%) = 56.5 : 7.8 : 35.7 for the CHT/SiCaP composites and $SiO_2:CaO:P_2O_5:MgO$ (mol.%) = 70 : 18.5 : 3.9 : 7.6 for the CHT/SiCaPMg ones. The analyzed compositions present a slight variation regarding the idealized formulation of the BG-NPs used, respectively $SiO_2:CaO:P_2O_5$ (mol.%) = 55:40:5 and $SiO_2:CaO:P_2O_5:MgO$ (mol.%) = 64:26:5:5. The variations are related to dissolution behaviors of calcium nitrate that are prone to occur in aqueous environments such as the sol-gel system, influencing thereby the final relative composition. [21]

Regarding the CHT/SiCaP nanocomposite, an amorphous calcium phosphate layer begun to grow on the surface of the sample, as was indicated by the Ca and P increasing values and Si content decrease. The same behavior can be observed in the CHT/SiCaPMg

nanocomposite; however in this sample, also the Mg content decreases over immersing time on SBF. The value of Ca/P ratio of the apatite film developed on the surface of the nanocomposites was 1.65 and 1.59 at the day 7, respectively to CHT/SiCaP and CHT/SiCaPMg nanocomposites.

3.4. Biological study of osteoblastic response

3.4.1 Cellular viability
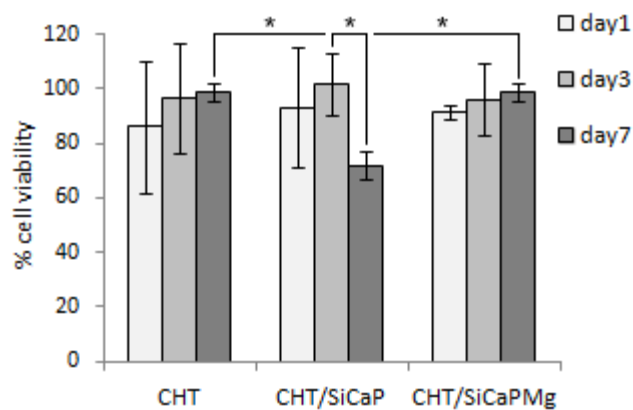
Fig. VI. 5. Cell viability of the produced samples from MTS tests throughout 7 days of culture as compared with the cells cultured in TCP.

Data are means ±SD (n=3; *=p<0.05).

MTS assay results for the osteoblasts seeded on the samples for 1, 3 and 5 days are seen in figure VI.5. Values of optical density were read from the cells seeded in the pure chitosan membrane and in the bioactive glass nanocomposites. The values were compared with the ones obtained in the cells seeded in tissue culture polystyrene (TCP), which was used as a positive control of cell viability. Latex substrates were used as negative control for cellular viability, and after 7 days of culture the percentage of cell viability in latex was considered to be negligible (<0.5%) - data not shown. All the studied samples showed good percentage values of cell viability over cells seeded on TCP. No significant difference in cell viability was observed across this experimental group. At day 7, CHT/SiCaP nanocomposite was the only sample where the values decreased. Pure chitosan membrane and

CHT/SiCaPMg nanocomposite presented similar viability profiles overtime, with 100% of cellular viability reached after 7 days of culture.

3.4.2. DNA quantification
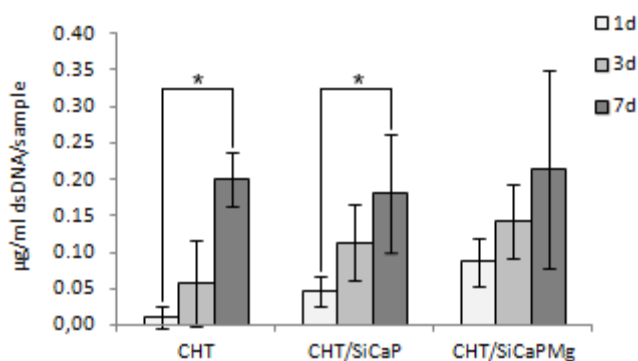
Fig. VI. 6. *In vitro* double-stranded DNA concentration in the pure chitosan membranes and BG-NPs nanocomposites seeded with osteoblasts cultured throughout 7 days.

Concerning cell proliferation results, data obtained from the DNA quantification (Figure VI.6) indicated that proliferation of osteoblasts seeded onto nanocomposites seemed to increase in all the tested samples. Comparing the samples, both CHT/SiCaP and CHT/SiCaPMg nanocomposites showed in general better results towards the pure chitosan membrane control.

3.4.3. ALP analysis
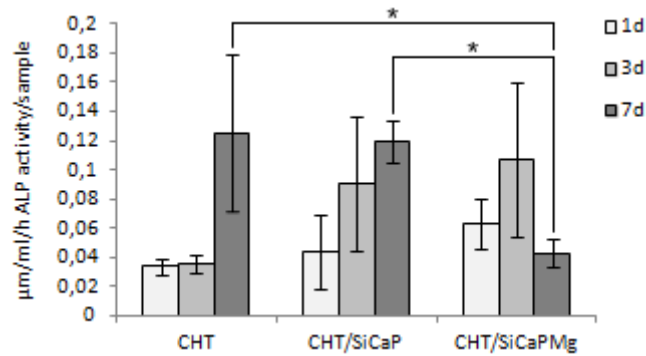
Fig. VI. 7. ALP enzymatic activity of cells seeded on the pure chitosan membranes and BG-NPs nanocomposites throughout 7 days, and normalized to total DNA content.

Figure VI.7 shows the ALPase enzymatic activity of the osteoblasts seeded on the produced nanocomposites. Overall, the ALP activity of the three samples increased all through the time points analyzed, being the CHT/SiCaPMg nanocomposite the sample holding the highest ALP enzymatic activity values till day 3. However, on day 7, CHT/SiCaPMg nanocomposite levels decreased, while the levels of the others samples continued to increase.

3.4.4. Cell morphology and attachment
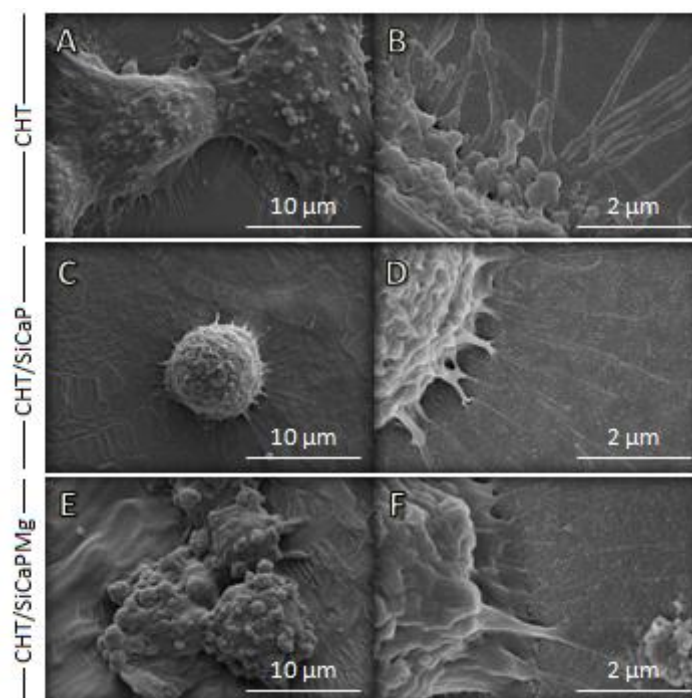
Fig. VI. 8. SEM images of osteoblastic cells after a 7 days seeding on pure chitosan **(A)** and **(B)**, CHT/SiCaP nanocomposite **(C)** and **(D)** and CHT/SiCaPMg nanocomposite **(E)** and **(F)** observed at two magnifications.

The morphology of the cells after 7 days of culture in the developed materials was investigated by SEM. When exposed to the studied substrates chitosan presented well spread osteoblasts with developed lamellipodia and various long filopodia - Figure VI.8A and 8B. In contrast, osteoblasts seeded on CHT/SiCaP nanocomposite showed rounded morphologies with reduced attachment levels - See figure VI.8C and D. Only discrete cytoplasmatic extensions at the periphery of the cell were observed. The CHT/SiCaPMg nanocomposite presented a more flattened cellular morphology, with very developed lamellipodia - See Figure VI.8E and F.

4. Discussion

The SiO_2:CaO:P_2O_5 (mol.%) = 55:40:5 formulation of BG-NPs is a well studied system with proved high bioactivity. [14] The SiO_2:CaO:P_2O_5:MgO(mol.%) = 64:26:5:5 formulation was selected since it has lower Ca content and higher Si levels, which are known to decrease the bioactive character of materials. [22] Magnesium was included in the formulation in order to enhance cellular adhesion [7]. The magnesium content was fixed in 5% since some adverse effects of magnesium are reported in literature, namely osteoblastic inhibition by toxic causes due to excess of Magnesium. [23]

Differences between the two formulations also influenced the final arrangement of the particles - See figure VI.1. This relation may be associated to the particles ζ-potential. The ζ- potential of the SiO_2:CaO:P_2O_5 is slightly negative (-8.8 mV) and the particles are more agglomerated. On the other hand, SiO_2:CaO:P_2O_5:MgO nanoparticles presented a ζ-potential value of -19.13 mV. Therefore, the lower levels of agglomeration observed are due to the higher stability of these particles.

Nanoparticles agglomeration is very important since it can affect particles dispersion in the nanocomposite. Although the polymeric solutions containing the BG-NPs were sonicated before casting, differences between the final structures of the nanocomposites were observed. Figure VI.2C (CHT/SiCaPMg) shows a smoother surface than figure VI.2B (CHT/SiCaP) possibly due to the lower level of nanoparticles agglomeration.

Regarding the osteoblastic interaction with the composite's surface, diverse degrees of cellular attachment can occur due to the presence of different chemical groups that change the material's surface charge. [24, 25] There is not a clear consensus whether the osteoblasts (with a ζ- potential of -6.2 mV at physiological pH) [26] attach and proliferate preferably on negative [27] or positively [26] charged surfaces such as chitosan [28-30]. Another possibility, already mentioned in other studies [31-32] and also observed in this work, is that both positive and negative surface charge can favor osteoblastic growth as long as they present a marked surface stability. Indeed, Figure VI.8 suggests that the cells showed better attachment signals when seeded on the surfaces with higher stability (based on their ζ-potential values), namely CHT and CHT/SiCaPMg.

Another important aspect influencing the cellular attachment on a surface is its wet-tability, since this property will influence the adsorption of important proteins from the culture medium, such as fibronectin and vitronectin, which will mediate cell response and improve cell attachment. [33-37, 16] Moderate hydrophilicity was presented by the pure chitosan membranes and the CHT/SiCaPMg nanocomposites. These nanocomposites seem to be more suitable for protein adsorption. These information are supported by the MTS and SEM results, respectively figure VI.5 and 8, and they would explain how a flat positive substrate as chitosan, presents similar percentages of cell viability and analogous cell behaviour than a rough, negative substrate as the CHT/SiCaPMg nanocomposites. Moreover, it would also be a reasonable explanation on why cells seeded on the CHT/SiCaP nanocomposite, with a higher hydrophobic character, and thereby less capable of adsorbing attachment proteins, present a round shape and have less filopodia.

SaOS-2 line of human osteosarcoma cells was chosen to study the cellular behaviour when in contact with the surface of the produced nanocomposites. Although it has been stated that osteoblasts presumably recognize grooves as a naturally extracellular matrix environment, which is favorable for their attachment, [38] in this study, cellular attachment on the pure chitosan membrane (with a very smooth and flattened surface) was quite efficient and cells presented a more flattened morphology and developed more filopodia than the cells seeded on the other samples which offered different levels of roughness. These results indicate that roughness may not be the only parameter influencing cells fate.

In order to have a better insight on all the factors affecting the cells behaviour, some biological responses were evaluated *in vitro*. Osteoblastic viability after seeding on the surface of the developed nanocomposites was determined using the MTS assay. Metabolic activity of cells can be monitored using the tetrazolium compound (MTS), since it is chemically reduced by the mitochondrya of the cells into formazan. Comparing the produced nanocomposites, MTS results (figure VI.5) showed that osteoblasts seeded on the CHT/SiCaPMg nanocomposite surface were slightly more viable than they were in the CHT/SiCaP nanocomposite. Differences in bioactive potential of the different nanocomposites can be a possible explanation to this fact.

Knowing that the stoichiometric hydroxyapatite theoretical Ca/P value is 1.67, [39] and that the values of Ca/P ratio of the apatite film developed on the surface of the nanocomposites was 1.65 and 1.59 at day 7 of soaking in SBF, respectively to CHT/SiCaP and

CHT/SiCaPMg nanocomposites, this means that the apatite layer resembling more the natural bone mineral phase is being formed faster in the CHT/SiCaP nanocomposite. This implies that the CHT/SiCaP composite is releasing a higher concentration of ions than the CHT/SiCaPMg. However, cells respond to the ionic environment, subsequently, very bioactive glasses, due to excessive ion release, can raise the environment pH to values critical to cells. [40] These could be a reason for the decrease of cellular viability at day 7, regarding the most bioactive nanocomposite (CHT/SiCaP). The SEM results - See figure 3 - also indicate that the CHT/SiCaP induced a higher level of apatitic growth. This was the expected result, since, as already was referred, CHT/SiCaPMg contains the BG-NPs particles designed to be less bioactive as they contain higher levels of silicon and lower levels of calcium. Regarding the Mg content, there is no consensus on the role of Mg in respect with the bioactive potential of the material. It has been stated that this component increases the bioactivity of bioactive glasses [41] and also that it retards the apatitic layer formation rate. [42, 43]

The proliferative capacity of osteoblasts was measured using PicoGreen® fluorescence assay in order to quantify the amount of double stranded DNA (dsDNA) per sample. DNA quantification results (figure VI.6) indicate a slightly different tendency than the ones provided by MTS (figure VI.5). In this case, both CHT/SiCaP and CHT/SiCaPMg present better proliferation values than the control, and no decrease in cellular parameters is observed on day 7 for CHT/SiCaP. MTS and DNA results comparisons require some carefulness, since conflicts between these assays are common as they do not necessarily correlate linearly with increasing cell densities. [44]

SEM observations of cell attachment on the developed nanocomposites - See figure VI.8 - can also be very useful, since cellular morphology is an indication of their development. Chitosan (Figure VI.8A and B) and CHT/SiCaPMg nanocomposite (Figure VI.8E and F) presented well spread osteoblasts with a developed lamellipodia and various long filopodia. However, osteoblasts seeded on CHT/SiCaP nanocomposite (Figure VI.8C and D) showed rounded morphologies with markedly reduced attachment levels indicated by discrete cytoplasmatic extensions at the periphery of the cell. Furthermore, in all cases, filopodia of the growing cells showed random protrusion directions, indicating that there is no specific alignment to the surfaces roughness. Osteoblasts morphology vary from elongated to cuboidal, depending on their matrix deposition activity since cell spreading facilitates osteoblast matrix deposition during bone remodelling. [45-47]

An ALP activity study was conducted in order to confirm if osteoblastic mineralization was occurring. The increase of ALP activity observed in Figure VI.7, regarding all the studied samples, is an indication that the nanocomposites were successful in inducing osteoblastic differentiation in an early stage. The osteoblastic activity was more intense in the CHT/SiCaP nanocomposite till the third day of study, however, only in this sample, on the seventh day of study, a decrease on the ALPase enzymatic activity was observed, which is an indication of the beginning of the mineralization process between days 3 and 7. [48] SEM images of the osteoblasts seeded on the CHT/SiCaPMg nanocomposite (Figure VI.8E) confirm the existence of possible mineralization nodules observed at the cells surface. Both CHT/SiCaP and CHT/SiCaPMg nanocomposites showed enhanced ALP activity towards the pure chitosan membranes on day 1 and 3. This fact may be related to the release of ions from the BG-NPs contained in the nanocomposites known to induce osteoblastic differentiation. In the case of CHT/SiCaP, the pH due to the ionic release possibly was excessively high after 3 days of cell seeding, compromising subsequently the osteoblastic response.

5. Conclusions

In the present study, chitosan nanocomposite membranes were successfully prepared using two distinct bioactive glass nanoparticles systems, namely $SiO_2:CaO:P_2O_5$ (mol.%) = 55:40:5 and $SiO_2:CaO:P_2O_5:MgO$ (mol.%) = 64:26:5:5. Bioactive glass nanoparticles were proved to be an appropriate choice to develop Guided Tissue regeneration nanocomposites, since they have good dispersibility in polymeric matrixes such as chitosan, and also due the possibility of adequating the particles properties by adjusting their formulations.

The CHT/SiCaPMg with moderate bioactive character and higher hydrophilicity was found to stimulate a better osteoblastic response towards cellular differentiation and mineralization.

Further studies should provide better understanding of the significance of each ionic component in the BG-NPs formulation towards the osteoblastic stimulation process.

The developed nanocomposites can have potential applications in Guided Tissue Regeneration, namely in purposes related to the orthopaedic field.

Acknowledgements

References

[1] LeBaron. Extracellular matrix cell adhesion peptides: functional applications in orthopedic materials. Tissue Engineering 2000;6:85-103.

[2] Lu HH, El-Amin SF, Scott KD, Laurencin CT. Three-dimensional, bioactive, biodegradable, polymer-bioactive glass composite scaffolds with improved mechanical properties support collagen synthesis and mineralization of human osteoblast-like cells in vitro. Journal of Biomedical Materials Research Part A2003;64A:465-74.

[3] Alves NM, Leonor IB, Azevedo HS, Reis RL, Mano JF. Designing biomaterials based on biomineralization of bone. Journal of Materials Chemistry 2010;20:2911-21.

[4] Jell G, Stevens MM. Gene activation by bioactive glasses. Journal of Materials Science: Materials in Medicine 2006;17:997-1002.

[5] Gentleman E, Fredholm YC, Jell G, Lotfibakhshaiesh N, O'Donnell MD, Hill RG, et al. The effects of strontium-substituted bioactive glasses on osteoblasts and osteoclasts in vitro. Biomaterials 2010;31:3949-56.

[6] Gutowska I, Machoy Z, Machalinski B. The role of bivalent metals in hydroxyapatite structures as revealed by molecular modeling with the HyperChem software. Journal of Biomedical Materials Research Part A 2005;75A:788-93.

[7] Webster TJ, Ergun C, Doremus RH, Bizios R. Hydroxylapatite with substituted magnesium, zinc, cadmium, and yttrium. II. Mechanisms of osteoblast adhesion. Journal of Biomedical Materials Research Part A 2002;59:312-7.

[8] Paul DR, Robeson LM. Polymer nanotechnology: Nanocomposites. Polymer 2008;49:3187-204.

[9] Luz GM, Mano JF. Mineralized structures in nature: Examples and inspirations for the design of new composite materials and biomaterials. Composites Science and Technology 2010;70:1777-88.

[10] Wei GB, Ma PX. Structure and properties of nano-hydroxyapatite/polymer composite scaffolds for bone tissue engineering. Biomaterials 2004;25:4749-57.

[11] Fratzl P, Gupta HS, Paschalis EP, Roschger P. Structure and mechanical quality of the collagen-mineral nano-composite in bone. Journal of Materials Chemistry 2004;14:2115-23.

[12] Boccaccini AR, Erol M, Stark WJ, Mohn D, Hong ZK, Mano JF. Polymer/bioactive glass nanocomposites for biomedical applications: A review. Composites Science and Technology 2010;70:1764-76.

[13] Di Martino A, Sittinger M, Risbud MV. Chitosan: A versatile biopolymer for orthopaedic tissue-engineering. Biomaterials 2005;26:5983-90.

[14] Luz GM, Mano, J. F. Preparation and characterization of bioactive glass nanoparticles prepared by sol-gel for biomedical application. Nanotechnology 2011;22.

[15] Raucher D, Sheetz MP. Cell spreading and lamellipodial extension rate is regulated by membrane tension. The Journal of Cell Biology 2000;148:127-36.

[16] Wei J, Igarashi T, Okumori N, Igarashi T, Maetani T, Liu B, et al. Influence of surface wettability on competitive protein adsorption and initial attachment of osteoblasts. Biomedical Materials 2009;4.

[17] Alves NM, Pashkuleva I, Reis RL, Mano JF. Controlling Cell Behavior Through the Design of Polymer Surfaces. Small 2010;6:2208-20.

[18] Hong Z, Reis RL, Mano JF. Preparation and in vitro characterization of novel bioactive glass ceramic nanoparticles. Journal of Biomedical Materials Research Part A2009;88A:304-13.

[19] Kokubo T, Takadama H. How useful is SBF in predicting in vivo bone bioactivity? Biomaterials 2006;27:2907-15.

[20] Schultz N, Metreveli G, Franzreb M, Frimmel FH, Syldatk C. Zeta potential measurement as a diagnostic tool in enzyme immobilisation. Colloids and Surfaces B: Biointerfaces 2008;66:39-44.

[21] Labbaf S, Tsigkou O, Muller KH, Stevens MM, Porter AE, Jones JR. Spherical bioactive glass particles and their interaction with human mesenchymal stem cells in vitro. Biomaterials 2011;32:1010-8.

[22] Zhong JP, Greenspan DC. Processing and properties of sol-gel bioactive glasses. Journal of Biomedical Materials Research Part A 2000;53:694-701.

[23] Serre CM, Papillard M, Chavassieux P, Voegel JC, Boivin G. Influence of magnesium substitution on a collagen-apatite biomaterial on the production of a calcifying matrix by human osteoblasts. Journal of Biomedical Materials Research 1998;42:626-33.

[24] Vanwachem PB, Hogt AH, Beugeling T, Feijen J, Bantjes A, Detmers JP, et al. Adhesion of cultured human-endothelial cells onto methacrylate polymers with varying surface wettability and charge. Biomaterials 1987;8:323-8.

[25] Smith IO, Baumann MJ, Obadia L, Bouler JM. Surface potential and osteoblast attraction to calcium phosphate compounds is affected by selected alkaline hydrolysis processing. Journal of Materials Science: Materials in Medicine 2004;15:841-6.

[26] Matsuda T, Davies JE. The in vitro response of osteoblasts to bioactive glass. Biomaterials 1987;8:275-84.

[27] Smith IO, Baumann MJ, McCabe LR. Electrostatic interactions as a predictor for osteoblast attachment to biomaterials. Journal of Biomedical Materials Research Part A 2004;70A:436-41.

[28] Silva FC, Menezes GC. Osteoblasts attachment and adhesion: how bone cells fit fibronectin-coated surfaces. Mat Sci Eng C - Bio S 2004;24:637-41.

[29] Haipeng G, Yinghui Z, Jianchun L, Yandao G, Nanming Z, Xiufang Z. Studies on nerve cell affinity of chitosan-derived materials. Journal of Biomedical Materials Research 2000;52:285-95.

[30] Bumgardner JD, Wiser R, Elder SH, Jouett R, Yang Y, Ong JL. Contact angle, protein adsorption and osteoblast precursor cell attachment to chitosan coatings bonded to titanium. Journal of Biomaterials Science, Polym Ed 2003;14:1401-9.

[31] Kumar D, Gittings JP, Turner IG, Bowen CR, Bastida-Hidalgo A, Cartmell SH. Polarization of hydroxyapatite: Influence on osteoblast cell proliferation. Acta Biomaterialia 2010;6:1549-54.

[32] Suzuki T, Yamamoto T, Toriyama M, Nishizawa K, Yokogawa Y, Mucalo MR, et al. Surface instability of calcium phosphate ceramics in tissue culture medium and the

effect on adhesion and growth of anchorage-dependent animal cells. Journal of Biomedical Materials Research 1997;34:507-17.

[33] Hayman EG, Pierschbacher MD, Suzuki S, Ruoslahti E. Vitronectin - A Major cell attachment promoting protein in fetal bovine serum. Experimental Cell Research 1985;160:245-58.

[34] Krajewski A, Piancastelli A, Malavolti R. Albumin adhesion on ceramics and correlation with their Z-potential. Biomaterials 1998;19:637-41.

[35] Krajewski A, Malavolti R, Piancastelli A. Albumin adhesion on some biological and non-biological glasses and connection with their Z-potentials. Biomaterials 1996;17:53-60.

[36] Vanwachem PB, Beugeling T, Feijen J, Bantjes A, Detmers JP, Vanaken WG. Interaction of cultured human-endothelial cells with polymeric surfaces of different wettabilities. Biomaterials 1985;6:403-8.

[37] Mager MD, LaPointe V, Stevens MM. Exploring and exploiting chemistry at the cell surface. Nature Chemistry 2011;3:582-9.

[38] Lamers E, Walboomers XF, Domanski M, te Riet J, van Delft FCMJM, Luttge R, et al. The influence of nanoscale grooved substrates on osteoblast behavior and extracellular matrix deposition. Biomaterials 2010;31:3307-16.

[39] Koutsopoulos S. Kinetic study on the crystal growth of hydroxyapatite. Langmuir 2001;17:8092-7.

[40] Gough JE, Clupper DC, Hench LL. Osteoblast responses to tape-cast and sintered bioactive glass ceramics. Journal of Biomedical Materials Research Part A2004;69A:621-8.

[41] Erol M, Ozyuguran A, Celebican O. Synthesis, Characterization, and In Vitro Bioactivity of Sol-Gel-Derived Zn, Mg, and Zn-Mg Co-Doped Bioactive Glasses. Chemical Engineering & Technology 2010;33:1066-74.

[42] Perez-Pariente J, Balas F, Vallet-Regi M. Surface and chemical study of SiO2.P2O5.CaO.(MgO) bioactive glasses. Chemistry of Materials 2000;12:750-5.

[43] Ma J, Chen CZ, Wang DG, Jiao Y, Shi JZ. Effect of magnesia on the degradability and bioactivity of sol-gel derived SiO(2)-CaO-MgO-P(2)O(5) system glasses. Colloids and Surfaces B: Biointerfaces 2010;81:87-95.

[44] Grigoriadis AE, Heersche JNM, Aubin JE. Differentiation of muscle, fat, cartilage, and bone from progenitor cells present in a bone-derived clonal cell-population - Effect of dexamethasone. The Journal of Cell Biology 1988;106:2139-51.

[45] Sikavitsas VI, Temenoff JS, Mikos AG. Biomaterials and bone mechanotransduction. Biomaterials 2001;22:2581-93.

[46] Parfitt AM. Age-related structural-changes in trabecular and cortical bone - Cellular mechanisms and biomechanical consequences. Calcified Tissue International 1984;36:S123-S8.

[47] Tsigkou O, Hench LL, Boccaccini AR, Polak JM, Stevens MM. Enhanced differentiation and mineralization of human fetal osteoblasts on PDLLA containing Bioglass (R) composite films in the absence of osteogenic supplements. Journal of Biomedical Materials Research Part A 2007;80A:837-51.

Chapter VII

Micropatterning of bioactive glass nanoparticles on chitosan membranes for spatial controlled biomineralization*

Abstract

BG-NPs capable of inducing apatite precipitation upon immersion in SBF were patterned on free-standing chitosan membranes by microcontact printing using a PDMS stamp inked in a BG-NPs pad. Formation of the patterns was characterized by SEM. Mineralization of the bioactive glass patterns was induced in vitro by soaking the samples in SBF over different time points up to 7 days. The confined apatite deposition in the patterned regions with diameters of 50 μm was confirmed by FTIR, EDX analysis, and SEM. In vitro tests confirmed the preferential attachment and proliferation of L929 cells to the areas printed with BG-NPs of the membranes. This approach permits one to spatially control the properties of biomaterials at the microlevel and could be potentially used in guided tissue regeneration for skin, vascular, articular, and bone tissue engineering and in cellular cocultures or to develop substrates able to confine cells in regions with controlled geometry at the cell's length scale.

1. Introduction

In recent years, the biomaterials field has witnessed the rise of a third generation of materials able to stimulate specific cellular responses. [1, 2] Exposed to the right surface chemistry and topography, cells can adhere, proliferate, and differentiate. [3-6] Tailoring of surfaces morphology can be done along the *Z* direction by promoting roughness (including hierarchical features) or patterning regular motifs. Chemically, the surface can be modified, for example, by layer-by-layer constructs, sequential attachment of chemical/biochemical elements, and also grafting smart macromolecules. Changes along the *X–Y* direction enclose creation of geometrical domains, regular stripes, or gradients. [3] It has been demonstrated that the size of cell-binding domains may have a direct influence in cellular behavior, including differentiation, [4] and anisotropic patterns could direct preferential cell alignment. [7]

Different methods can be applied to engineer culture substrates for guiding cellular responses with spatial control. μCP of biologically relevant ligands [8-10] using a soft PDMS stamp is the most common technique to generate specific patterns with different and well-defined chemistries. Patterns of proteins, molecules, polymers, nanoparticles, self-assembled monolayers, colloids, and metals have been reported. [11-14] Application of this patterning technology to cell culture engineering provides new tools for spatially controlled tissue engineering. The flexibility of sizes and shapes of the patterns have allowed generation of patterned cell cocultures that facilitate cell proliferation and differentiation and also engineering of tissue constructs. [8, 15]

Bioactive glass has been demonstrated to have a beneficial effect in bone regeneration, skin, articular regeneration, and angiogenesis applications as it binds to both bone and soft tissue. [16] Bioactive glass has been mainly applied in orthopedic and dental areas, since it promotes deposition of apatite under physiological conditions. [1, 17, 18] A few works have reported the fabrication of substrates with spatial control of biomineralization. [19, 20] μCP has not been used for this purpose, though it presents significant advantages over the reported methods. (i) It is based on a very simple procedure, easily adjustable to different substrates that do not require inherent bioactivity. (ii) No external stimuli are required to trigger the beginning of mineralization, [20] and (iii) no organic solvents are used in the process which would not be an appropriate choice when working with polymers. [19]

In addition, the major advantage of applying BG-NPs patterns for tissue culture applications is the fact that bioactive glasses are gene-activation materials capable of inducing cellular differentiation. [21] Therefore, development of BG-NPs patterns will provide a versatile tool for biological studies, since they are inexpensive and also more resistant to temperature, storing, and sterilization procedures than the molecular components often used in biology research. Moreover, this system would also be very useful in bioactive glass-related studies, since their formulation, sizes, and geometry influence their bioactivity and cellular interactions.

This work describes a methodology to obtain micropatterned bioactive glass nanoparticles (BG-NPs) on chitosan membranes by μCP. Ionic dissolution of Si, Ca, and P gives rise to both intracellular and extracellular responses at the interface of the glass with its cellular environment which stimulate cells to grow and differentiate, influencing as well their biomechanical properties. [1] Instead of producing homogeneous nanocomposites with BG-NPs distributed in all their volume another strategy was followed in which the inorganic fraction is deposited over the polymeric membrane. Nanocomposites produced by combining BG-NPs and polymers [22] are inspired by mineralized structures found in Nature. [23]

Moreover, this work aims to achieve spatial control of biomineralization using μCP of BG-NPs to generate mineralizable patterns. μCP allows precise control of nanoparticles density at the surface, thereby controlling ionic release from the BG-NPs and avoiding inefficient particles concentration toward mineralization or excessive release of ions that locally change the pH of the environment to levels lethal to the cells. This is important when working at the nanolevel, since unlike bulk materials the high specific surface area of BG-NPs increases their degradability. [12, 24-26] In addition, nanosized particles can cause different biological responses in comparison with the ones obtained for larger particles with the same chemical composition. One example is the enhancement of cell attachment due to the nanoparticles higher surface reactivity, which increases protein adsorption. [27, 28]

Combining both physical and chemical strategies to control cell attachment and apatite deposition, one expects the creation of an innovative, tissue engineering platform that could have potential applications in different regeneration fields.

2. Experimental Section

BG-NPs Preparation. The procedure to produce BG-NPs with composition SiO_2:CaO:P_2O_5 (mol %) = 55:40:5 was based on a previously reported protocol. [29] Tetraethyl orthosilicate (TEOS, 99.90% pure), diammonium hydrogen phosphate, calcium nitrate tetrahydrate (99%), absolute ethanol, citric acid monohydrate (99%), and ammonium hydroxide were purchased from Sigma-Aldrich. The mixture of precursor's solutions (7.639 g of calcium nitrate in 120 mL of distilled water, 9.167 g of TEOS in 60 mL of ethanol and 30 mL of citric acid 10% (w/v)) was added drop-by-drop to an aqueous solution containing the phosphorus precursor (1.078 g of diammonium hydrogen phosphate) in 1500 mL of distilled water. In the case of the binary system, no phosphorus precursor was used in order to achieve the composition SiO_2:CaO (mol %) = 70:30.The pH was maintained at 11.5 with ammonium hydroxide addition. The precipitate obtained was stirred for 48 h, and then a resting period of 24 h followed. The precipitate was washed three times with distilled water. A 200 mL amount of an aqueous solution of poly(ethylene glycol) 2% (w/v) with M_w = 20 000 was added to the precipitate, and then freeze drying followed. Finally, the BG nanoparticles were calcinated at 700 °C for 3 h in order to achieve optimal conditions for bioactivity. [30]

PDMS Stamps Preparation. A master containing three different patterned fields was used. The geometries were 50 μm diameter cylindrical pillars arranged in a square pattern with 50 μm spacing, 50 μm diameter cylindrical pillars arranged in a hexagonal pattern with 40 μm spacing, and ellipsoidal pillars (50 μm long axes and 30 μm short axes) arranged in a hexagonal pattern with 40 μm spacing. Each field was an 8 mm^2 square. The master was fabricated by photolithography using SU-8 photolack. [31] PDMS stamp was prepared by casting a 10:1 mixture of Sylgard 184 (Dow Corning) prepolymer and cross-linker. The mixture was poured over the master and cured at 90 °C for 3 h in a vacuum oven. After cooling, the PDMS was peeled off from the lithographic template and cut to suitable sizes.

Membranes Preparation. Membranes were obtained by solvent casting. Medium molecular weight chitosan with a degree of deacetylation of 79%, purchased from Sigma-Aldrich, was dissolved in an aqueous acetic acid solution 2% (v/v) to a concentration of 1% (w/v). An 80

mL amount of chitosan solution was casted onto 15 mm × 20 mm square Petri dishes and left for evaporation for 7 days. The dried membranes were neutralized by soaking in NaOH 0.1 M for 10 min and washed with distilled water until water with a pH of 7 was reached. Membranes were left to dry at RT and clipped between 2 frames to obtain straight and smooth surfaces. They were then cut in order to obtain 7 mm diameter circles.

Patternings. A 549 µL amount of BG-NPs dispersion with different nanoparticles concentrations in ethanol (between 0.003% and 0.05%) was poured on the surface of a glass slide (9° inclination) in a small area of 1 cm × 1.5 cm limited with a hollow rectangular piece fixed to the glass slide with dental wax. The dispersion was left to evaporate for 48 h inside a chamber saturated with ethanol. The lift-off was made by pressing the PDMS stamp against the dried membrane of BG-NPs that remained in the glass slide (donor substrate) for 10 min at 7 kPa and RT. Before the "printing" step, the chitosan membrane was treated with a drop of acetic acid (0.1 M) spread on its surface with a brush. µCP of the nanoparticles was achieved by pressing the BG-NPs-loaded stamp on the chitosan membrane for 30 s under 30 kPa at RT. After removing the PDMS, the membrane was washed with ethanol and dried in a vacuum oven for 2 h at 40 °C followed by 24 h at 10^{-2} bar.

In Vitro **Mineralization Study.** In vitro mineralization tests were carried out by soaking patterned circular (diameter 7 mm) chitosan membranes in 50 mL of simulated body fluid (SFB) solution for 0 (control), 1, 3, 5, and 7 days at 37 °C. Upon removal from SBF, the membranes were rinsed with distilled water and left to dry. The SBF was prepared by dissolving NaCl, NaHCO$_3$, KCl, K$_2$HPO$_4$·3H$_2$O, MgCl$_2$·6H$_2$O, and Na$_2$SO$_4$ in distilled water and buffered with tris(hydroxymethyl)aminomethane buffer and HCl to reach a pH value of 7.4, following the protocol described by Kokubo and Takadama. [32] All chemicals were purchased from Sigma-Aldrich.

Fourier-Transformed Infrared (FTIR) Spectroscopy Analysis. FTIR spectroscopy analysis of the formed hydroxyapatite on the chitosan membranes was carried out in an IR Prestige 21 Shimadzu Spectrometer. The hydroxyapatite powder was collected by scratching the surface of the membranes and pressed with KBr in a small disk. FTIR spectra were recorded from

400 to 4400 cm^{-1} with a resolution of 4 cm^{-1}. Before measurements the powders were dried at 100 °C overnight.

Scanning Electron Microscopy (SEM) and Energy-Dispersive X-ray (EDX) Samples Preparation. A NanoSEM-FEI Nova 200 (FEG/SEM) scanning electron microscope was used to image the surface and morphology of the printed membranes. A conductive gold coating with 20 nm thickness was sputtered to the samples. A Pegasus X4M instrument was used to perform the EDX experiments at low vacuum and without coating.

Cytotoxicity and Cell Attachment Tests. L929 mouse fibroblasts line (European collection of cell culture-ECACC, UK) was used to test the in vitro biocompatibility of the membranes. Chitosan membranes were previously sterilized by immersion in 70% (v/v) ethanol overnight and then washed twice with sterile phosphate-buffered saline (PBS). Cells were seeded in the samples (n = 3) at a density of 65 000 cells/cm^2 nourished with Dulbecco's modified minimum essential medium (D-MEM) supplemented with 10% fetal bovine serum (FBS) and 1% antibiotic. Cultures were incubated at 37 °C for 1, 3, and 7 days. After each time point (1, 3, and 7 days of culture), MTS (3-(4,5-dimethylthiazol-2-yl)-5-(3-carboxymethoxyphenyl)-2-(4-sulfophenyl)-2H-tetrazolium) test was performed to determine the cytotoxicity of the membranes. The relative cellular viability (%) was determined and compared with tissue culture polystyrene (TCPS) (positive control of cell viability). Latex was used as a negative control of cellular viability. For this assay, an MTS solution was prepared using a 1:5 ratio of MTS reagent and D-MEM culture medium without phenol red or FBS, followed by a 3 h incubation period at 37 °C. All cytotoxicity tests were conducted using 3 replicates. Finally, the optical density (OD) was read at 490 nm on a multiwell microplate reader (Synergy HT, Bio-Tek Instruments).

At days 1, 3, and 7 after seeding, cell attachment on the membranes was followed by SEM. Membranes were rinsed twice with PBS to remove nonadherent or loosely adherent cells and fixed with a solution of 2.5% (v/v) glutaraldehyde in 0.1 M PBS for 1 h at 4 °C. After removing the fixative, cells were rinsed in PBS and distilled water and dehydrated in a graded series of ethanol solution (50%, 70%, 90%, and 100%), each one repeated twice for 15 min. They were left to dry at air at RT and sputter coated with gold before SEM observation.

For the fluorescent images, calcein AM was used to stain the cells. A 2 μL amount of calcein AM and 1 mL of D-MEM culture medium without phenol red or FBS were added to each sample, followed by 10 min of incubation at 37 °C. Live cells stained green due to enzymatic conversion of the nonfluorescent cell-permeant calcein AM to fluorescent calcein. Fluorescent cells were visualized with the corresponding filters under an inverted microscope (Imager-Z1M).

3. Results and Discussion

The procedure employed to load the BG-NPs onto chitosan membranes has been described as a "stamp pad" [33] or "stick-and-place" [34] method. The PDMS stamp was placed in contact with a glass slide coated with the BG-NPs (donor substrate). The stamp picked up the nanoparticles, and these were printed onto the chitosan membrane (receiving substrate).
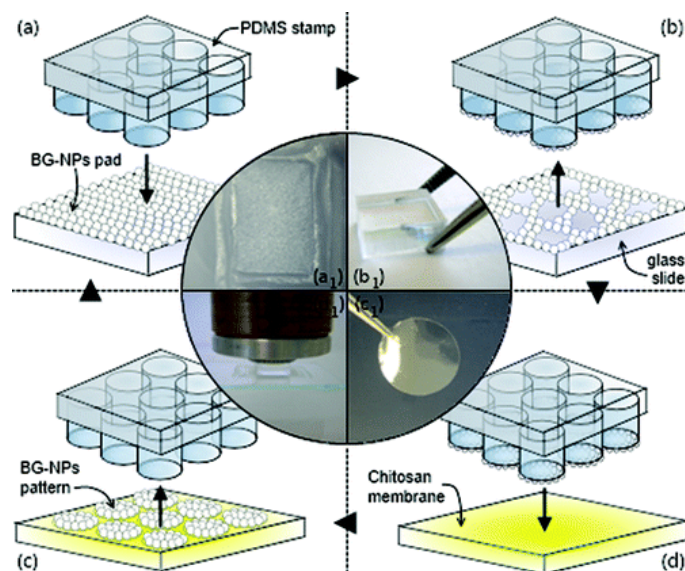

Fig. VII. 1. Schematic illustration and photographs of the materials and procedure followed for the μCP. **(a)** Inking of the PDMS stamp in a glass substrate covered with a homogeneous layer of BG-NPs **(a1)**; **(b)** Lift-off of the PDMS stamp carrying the BG-NPs on the base of the features and PDMS stamp **(b1)**; **(c)** Pressing of the PDMS stamp in the chitosan membrane's surface, and chitosan membrane used as printing substrate **(c1)**; **(d)** Printing of BG-NPs over the chitosan membrane's surface, and detail of the device used to press the stamp against the substrate **(d1)**. Same stamp may be utilized again after washing with ethanol in such imprinting procedure.

Figure VII.1 represents the different steps of this process. Ethanol was used to produce the BG-NPs ink as it is known to have a minimal swelling effect on the PDMS stamp. [35] PDMS was the selected stamp material since it has enough rigidity to support the topographic microstructure while it is soft and bendable, allowing conformal contact between the stamp and the membrane. [11, 33, 36, 37]
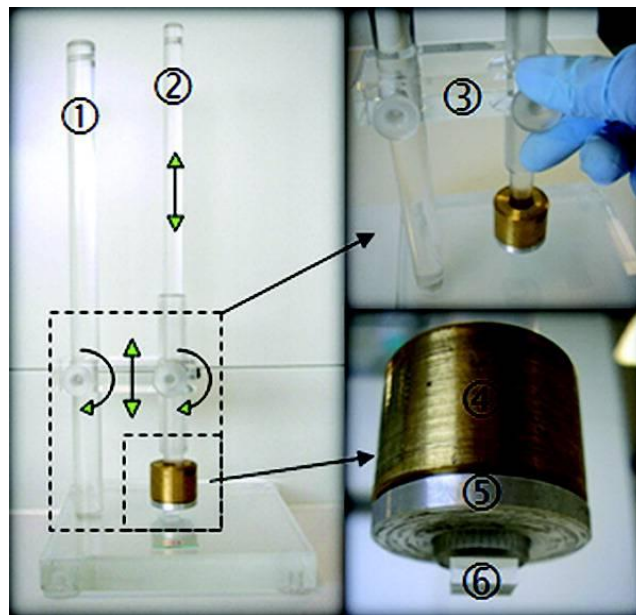

Fig. VII. 2. Device used to print the µCP patterns.

The device is mainly composed by two axes. One of the axes **(1)** is fixed to the base of the device and will be the guide of the central piece **(3)**. This central piece will establish the connection between the fixed axe and the movable axe **(2)** where the weights are applied. Fixed axe provides stability during the printing process. There are two screws in piece **(3)**. One will fix the central piece to the fixed axe, and the other will fix or loosen the position of the movable axe. Different weights **(4)** have a hole in the middle in order to fit in the movable axe. Weight of the axe plus the gray disk **(5)** is exactly 50 g. PDMS stamp **(6)** is glued to the bottom of the movable axe with a double-sided adhesive tape.

Different processing conditions were tested in the production of the patterned membranes, namely, the pattern shape and features height, the BG-NPs "ink" concentration, the pressure applied, and the contact time. Although µCP is usually performed manually, in this work a homemade transfer device was used in order to have accurate control of the pressure applied to the stamp/substrate interface - see Figure VII.2.
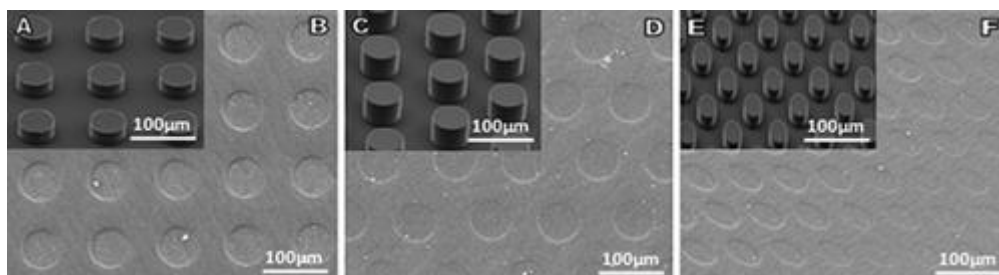
3.1. Pattern Formation

Fig. VII. 3. SEM images of types of patterns used.

(a) PDMS stamp and **(b)** chitosan membrane patterned with 50 μm diameter circles aligned in a squared arrangement; **(c)** PDMS stamp and **(d)** chitosan membrane patterned with 50 μm diameter circles forming a hexagonal pattern; **(e)** PDMS stamp and **(f)** chitosan membrane patterned with ellipses aligned in a hexagonal arrangement with the higher axis reaching 50 μm.

Three geometries of PDMS stamps were used in this study: 50 μm diameter cylindrical pillars arranged in a square pattern with 50 μm spacing (Figure VII.3a), 50 μm diameter cylindrical pillars arranged in a hexagonal pattern with 40 μm spacing (Figure VII.3c), and ellipsoidal pillars (50 μm long axes and 30 μm short axes) arranged in a hexagonal pattern with 40 μm spacing (Figure VII.3e). SEM images of the corresponding BG-NPs patterns obtained after stamping on the chitosan membranes are shown in Figure VII.3b, d and f. The diameter and spacing of the features needed to be optimized for our particular application and materials used. Stamps with features with 20, 30, and 40 μm height were tested for stamping. The pattern formed by the PDMS stamp with 30 μm height features seemed to combine the nondeformability with adequate BG-NPs transfer from the stamp to the membrane and gave the best results using a BG-NPs concentration of 0.03% (w/v). Well-defined and nondeformed circles of homogeneously distributed BG-NPs were obtained on the membranes. Another reason for choosing this pattern design was to have enough area available within the patterned fields to allow cell proliferation but also to have enough space between the features to allow good resolution of the pattern and avoid contamination of BG-NPs outside of the desired areas.

The force applied to the stamp during contact with the membrane influences pattern formation and reproducibility. [11] Due to the elastomeric and soft nature of the PDMS, excess applied vertical pressure during printing causes distortion of the patterns. [11, 37] Reproducibility could be greatly improved using a mechanical device that allowed accurate control of the applied pressure. The effect of the contact time between the PDMS stamp and the BG-NPs membrane substrate was also studied. No important differences in the obtained patterns were found for contact times between 30 s and 10 min. This result agrees with previously reported data. [12] When printing the BG-NPs in the chitosan membrane, acetic acid was used to treat the membrane and promote covalent binding between the polymer and the BG-NPs, since, otherwise, BG-NPs would remain attached to the PDMS stamp rather than transfer to the chitosan membrane. Both surface chemistries of the stamp and substrate are important in determining transfer efficiency. [37] For the particles to transfer onto the substrate, binding to the new surface must be more energetically favorable than remaining on the stamp. The process of transferring between stamp/ink is modeled with a speed-dependent critical energy release rate, which increases with speed due to the viscoelastic nature of PDMS. [34] Thus, fast peeling rates are used initially to transfer objects from a surface to PDMS, and slow rates are used to transfer these objects to a new unpatterned surface. [36] In addition, temperature is also an important parameter to consider in patterning systems. However, the rate of stamp removal and the temperature during the printing experiment were kept constant for all experiments.
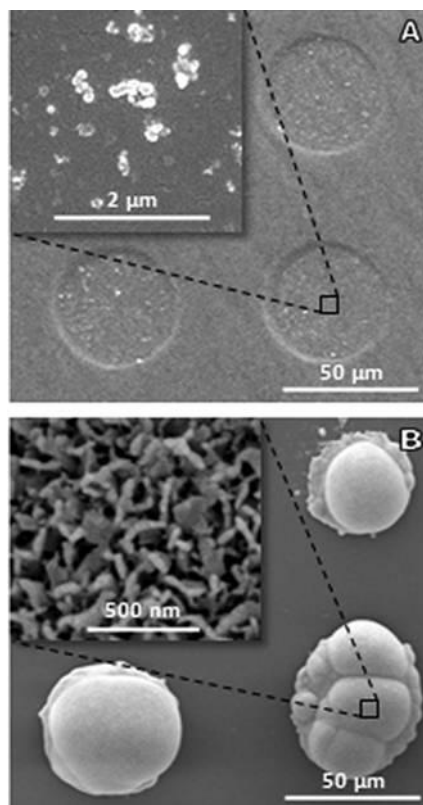
3.2. Mineralization Studies

Fig. VII. 4. (a) SEM images of BG-NPs pattern on chitosan before immersion in SBF. **(b)** SEM images of the patterned chitosan membrane evidencing the calcified clusters after 5 days of soaking in SBF.

Mineralization of the BG-NPs patterns was assessed in vitro by analyzing the ability of the patterned membrane to induce precipitation of apatite upon immersion in SBF. The patterned membrane before immersion in SBF showed small clusters of BG-NPs randomly distributed although well confined in the circular stamped regions - see Figure VII.4a. BG-NPs tend to agglomerate in clusters of variable sizes. However, individually, these particles present rounded shape morphology with sizes around 40 nm. [30] After immersing the entire membrane in SBF for 5 days, well-defined cauliflower-like clusters were detected. These were formed by platelets similar to the ones found in the typical structures of biomimetically formed apatite - see Figure VII.4b. Mineralization occurred only in the patterned areas where BG-NPs were present proving the confinement of controlled mineralized patterns.
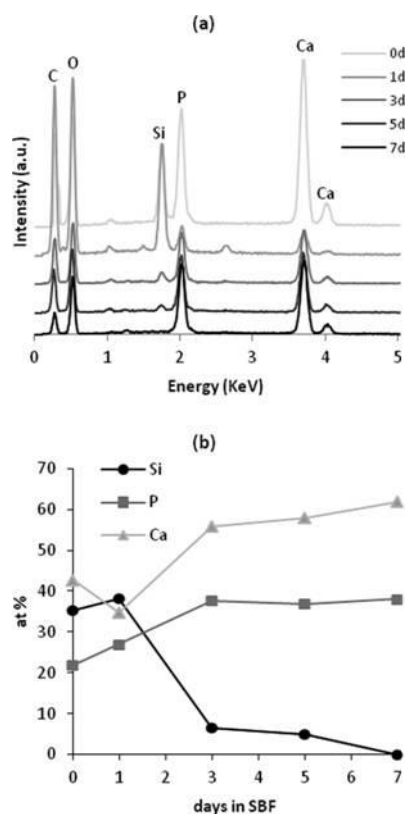
Fig. VII. 5. (a) EDX spectra and **(b)** relative compositions of Si, P, and C are given (in atomic percent, atom %) from EDX analysis upon the mineralization study of the BG-NPS-patterned chitosan membranes soaked in SBF for different time points (0 (control), 1, 3, 5, and 7 days).

EDX analyses of the membrane were performed in order to analyze the change in the surface chemical composition related to the mineralization process-see Figure VII.5. A slight increase in the fraction of Si in the membrane and a decrease of Ca until day 1 was observed. This is attributed to the exchange of Ca ions from the sample and H^+ and H_3O^+ from the SBF solution. After day 1, disruption of the glass network occurs by hydrolysis and soluble silica is lost to the solution in the form of $Si(OH)_4$, which leads to formation of silanol groups (Si–OH) at the BG-NPs/solution interface. The OH^- groups from silanol attract Ca from the surrounding media, and precipitation occurs. An amorphous calcium phosphate layer begins to grow on the surface of the sample, as can be confirmed by the Ca and P increasing values. In contrast, Si content decreases dramatically. Incorporation of OH^- and CO_3^{2-} anions from solution until day seven leads to the final step of mineralization which is formation of a crystalline apatite layer. [38]

The value of the Ca/P ratio of the nonstoichiometric apatitic layer developed on the surface of the BG-NPs was 1.63 in day 7. This value is very close to the one attributed to stoichiometric hydroxyapatite, 1.67, [39] implying that a hydroxyapatite layer resembling the natural bone mineral phase is being formed at the end of 7 days of immersion in SBF.
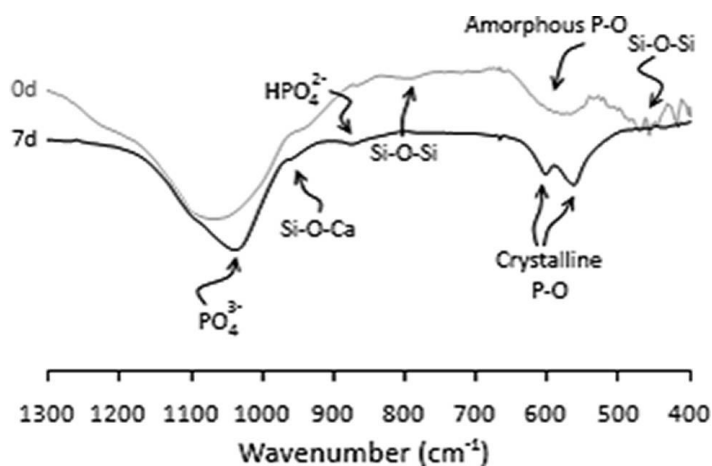

Fig. VII. 6. FTIR spectra of the powders scratched from the surface of the patterned membranes after 0 (control) and 7 days of immersion in SBF.

Evolution of apatite formation was also analyzed using FTIR - see Figure VII.6. The spectra presented correspond to the apatite powder scratched from the patterned membranes after 0 and 7 days of immersion in SBF. Silicate absorption bands are observed in all spectra, assigned to the bands 1085, 800, and 464 cm^{-1}, respectively: asymmetric stretching mode, symmetric stretching vibration, and rocking vibration of Si–O–Si. [40] Silicate-related bands are more intense in the control sample, which is in accordance with previous observations that the Si content decreases after being soaked in SBF.

Major evidence of hydroxyapatite growth is based on the bands at 600 and 550 cm^{-1} related to the P–O bending vibration due to the presence of a crystalline calcium phosphate (apatite like) phase. After 7 days in SBF the amorphous band in the control sample at around 600 cm^{-1} in SBF evolves to these two bands, evidencing the phosphate groups in the hydroxyapatite crystalline conformation. The bands at 1045 and 1090 cm^{-1} are also assigned to the P–O bond, and they increase in the 7 days sample. [41] The band at 874 cm^{-1} is assigned to the acidic phosphate group (HPO_4^{2-}). [42] The presence of Ca is assigned by the

band at 950 cm^{-1} related to Si–O–Ca bonds containing nonbridging oxygen in opposition with the bridging oxygens that link two SiO$_4$ tetrahedra. [40, 43]

Soaking of the BG-NPs in SBF for 7 days was already proved to result in a crystalline apatitic layer. [30] In a previous study performed by the authors, XRD data show that the amorphous spectra of the BG-NPs, after immersion in SBF for 7 days, resulted in peaks with diffraction angles matching the reference X-ray spectra of hydroxyapatite.

3.3. Cellular Viability

The cytotoxicity of the patterned chitosan membranes was assessed using a direct contact MTS assay - see Figure VII.7. All results for both patterned and unpatterned (pure chitosan) membranes of relative viability (%) of the L929 cells were normalized to cell viability on TCPS, which was used as a positive control of cell viability. Latex substrates were used as a negative control for cellular viability, and after 7 days of culture the percentage of cell viability in latex was considered to be negligible (<0.5%). The results revealed that the cells seeded on the BG-NPs-patterned membranes exhibited increased cell viability over the culture time points (1, 3, and 7 days). Moreover, the viability of cells seeded on patterned membranes was considerably superior to that observed in plain chitosan membranes. The results obtained in the MTS tests prove the important role of the BG-NPs in promoting cellular viability and are also supported by the morphological observation study.

Major evidence of hydroxyapatite growth is based on the bands at 600 and 550 cm^{-1} related to the P–O bending vibration due to the presence of a crystalline calcium phosphate (apatite like) phase. After 7 days in SBF the amorphous band in the control sample at around 600 cm^{-1} in SBF evolves to these two bands, evidencing the phosphate groups in the hydroxyapatite crystalline conformation. The bands at 1045 and 1090 cm^{-1} are also assigned to the P–O bond, and they increase in the 7 days sample. [41] The band at 874 cm^{-1} is assigned to the acidic phosphate group (HPO$_4^{2-}$). [42] The presence of Ca is assigned by the band at 950 cm^{-1} related to Si–O–Ca bonds containing nonbridging oxygen in opposition with the bridging oxygens that link two SiO$_4$ tetrahedra. [40, 43]

Soaking of the BG-NPs in SBF for 7 days was already proved to result in a crystalline apatitic layer. [30] In a previous study performed by the authors, XRD data show that the

amorphous spectra of the BG-NPs, after immersion in SBF for 7 days, resulted in peaks with diffraction angles matching the reference X-ray spectra of hydroxyapatite.
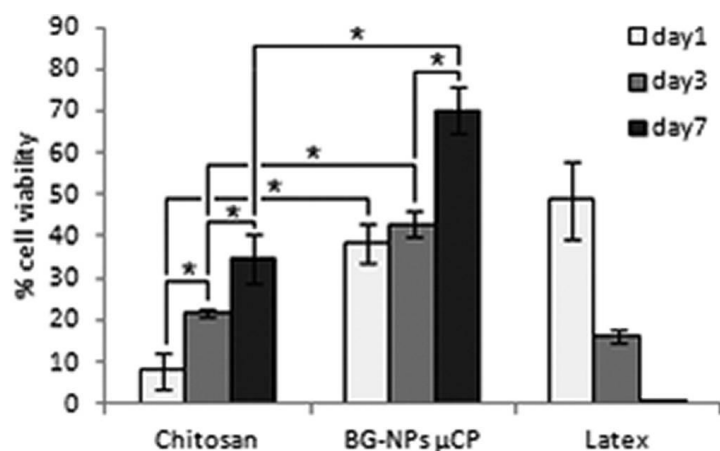

Fig. VII. 7. Cell viability of the produced samples from MTS tests throughout 7 days of culture as compared with the cells cultured in TCPS. Data are means ± SD ($n = 3$; * = $p < 0.05$).

The cytotoxicity of the patterned chitosan membranes was assessed using a direct contact MTS assay - see Figure VII.7. All results for both patterned and unpatterned (pure chitosan) membranes of relative viability (%) of the L929 cells were normalized to cell viability on TCPS, which was used as a positive control of cell viability. Latex substrates were used as a negative control for cellular viability, and after 7 days of culture the percentage of cell viability in latex was considered to be negligible (<0.5%). The results revealed that the cells seeded on the BG-NPs-patterned membranes exhibited increased cell viability over the culture time points (1, 3, and 7 days). Moreover, the viability of cells seeded on patterned membranes was considerably superior to that observed in plain chitosan membranes. The results obtained in the MTS tests prove the important role of the BG-NPs in promoting cellular viability and are also supported by the morphological observation study.
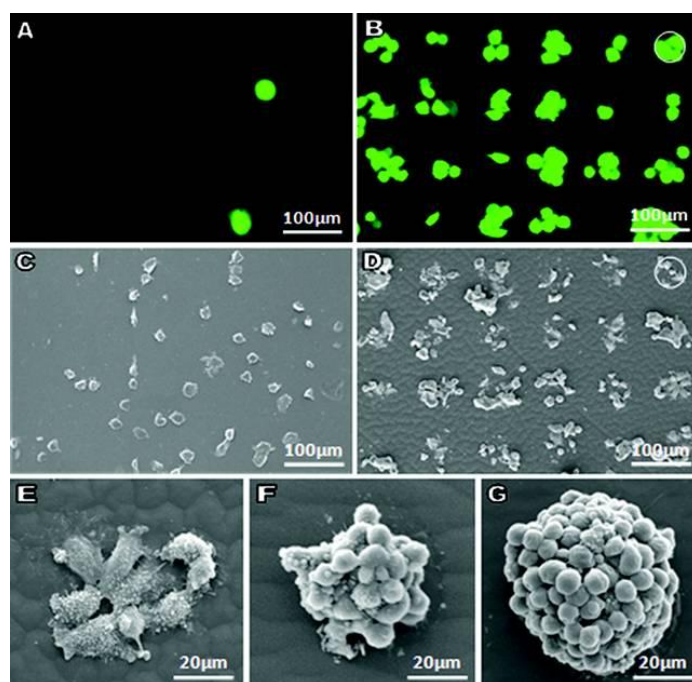
Fig. VII. 8. SEM and Fluorescent images of the cellular patterns.

(a) Fluorescent images of cell stained with calcein AM after 1 day of culture in plain chitosan and (b) BG-NPs patterned membranes; (c) SEM images of 1 day of cell culture in plain chitosan and (d) BG-NPs patterned membranes; SEM images magnification of 24 h (e), 3 days (f), and 7 days (g) of cell culture in BG-NPs patterned membranes; circle of 50 μm of diameter was inserted in the top (right) of images b and d for indication purposes.

In order to study cellular morphology and position at the surfaces, L929 cells were seeded on the control (plain chitosan membranes) and BG-NPs-patterned membranes at a density of 60 000 cell/cm^2. Figure VII.8 presents SEM and fluorescence microscopy images of the membranes for different culture times: 1, 3, and 7 days. In the patterned membranes cells adhered and proliferated mainly in the areas printed with BG-NPs. In addition, the density of cells on the patterned substrate increased with increasing culture time, always respecting the printed BG-NPs pattern. The BG-NPs-confined area proved to be a highly bioreactive surface which can promote attachment of living cells. Although cells present a flattened morphology, the control membranes of plain chitosan did not favor proliferation of cells throughout the time study, compared to the patterned membranes, consistent with the MTS results. Cells cultured on the patterned BG-NPs membranes appear to be relatively well spread and highly flattened with an increased cell–substrate contact area ratio. Formation of pseudopodia was also observed. However, at day 7, cells appear to exhibit a rela-

tively rounded unspread morphology, probably due only to the lack of space since the MTS results proved their viability. In this case cells preferred to adopt a more dense geometry and form stacked arrangements over the regions containing BG-NPs rather than migrate and attach to pure chitosan regions. The cell stack observed in Figure VII.8G indicates that the higher located cells, not able to sense neither the nano- nor the microtopography, prefer the environment created by the BG-NPs ionic release rather than migrating to chitosan.

4. Conclusions

For the first time µCP has been used to pattern mineralizable elements onto a biomaterial. Chitosan membranes were used and circular motifs containing bioactive glass nanoparticles were printed on them using previously inked PDMS stamps. The bioactive character of the BG-NPs spots allowed nucleation and growth of apatite, highly localized in the patterned regions of the chitosan membranes. By combining the remarkable properties of BG-NPs and the excellent biocompatibility of chitosan with this simple microcontact printing approach it was proved that it is possible to control the cellular interactions with a bioactive substrate at the microscale level. Successful patterning of fibroblasts is an indication of the versatility of the developed system.

This technology can be extended to studies of patterns with different sizes, geometries, and orientations that are known to influence cell differentiation and also develop cellular cocultures. The approach proposed opens also new routes of developing patterned medical membranes with distinct properties in the two sides, able to promote guided tissue regeneration in the bone side, while preventing soft tissue growth on the other face.

Acknowledgments

References

[1] Hench LL, Thompson I. Twenty-first century challenges for biomaterials. Journal of the Royal Society Interface 2010;7:S379-S91.

[2] Hench LL, Polak JM. Third-generation biomedical materials. Science 2002;295:1014.

[3] Alves NM, Pashkuleva I, Reis RL, Mano JF. Controlling Cell Behavior Through the Design of Polymer Surfaces. Small 2010;6:2208-20.

[4] McBeath R, Pirone DM, Nelson CM, Bhadriraju K, Chen CS. Cell shape, cytoskeletal tension, and RhoA regulate stem cell lineage commitment. Developmental Cell 2004;6:483-95.

[5] Boyan BD, Bonewald LF, Paschalis EP, Lohmann CH, Rosser J, Cochran DL, et al. Osteoblast-mediated mineral deposition in culture is dependent on surface microtopography. Calcified Tissue International 2002;71:519-29.

[6] Curtis A, Wilkinson C. Topographical control of cells. Biomaterials 1997;18:1573-83.

[7] Kumar G, Wang YC, Co C, Ho CC. Spatially controlled cell engineering on biomaterials using polyelectrolytes. Langmuir 2003;19:10550-6.

[8] Park TH, Shuler ML. Integration of cell culture and microfabrication technology. Biotechnology Progress 2003;19:243-53.

[9] Wilbur JL, Kumar A, Kim E, Whitesides GM. Microfabrication by microcontact printing of self-assembled monolayers. Advanced Materials 1994;6:600-4.

[10] Corum LE, Eichinger CD, Hsiao TW, Hlady V. Using Microcontact Printing of Fibrinogen to Control Surface-Induced Platelet Adhesion and Activation. Langmuir 2011;27:8316-22.

[11] Quist AP, Pavlovic E, Oscarsson S. Recent advances in microcontact printing. Analytical and Bioanalytical Chemistry 2005;381:591-600.

[12] Andersson AS, Glasmastar K, Hanarp P, Seantier B, Sutherland DS. Patterning colloidal monolayer films using microcontact particle stripping. Nanotechnology 2007;18.

[13] Yan X, Yao JM, Lu GA, Chen X, Zhang K, Yang B. Microcontact printing of colloidal crystals. Journal of the American Chemical Society 2004;126:10510-1.

[14] Xia YN, Whitesides GM. Soft lithography. Annual Review of Materials Science 1998;28:153-84.

[15] Torisawa Y-S, Mosadegh B, Cavnar SP, Ho M, Takayama S. Transwells with Microstamped Membranes Produce Micropatterned Two-Dimensional and Three-Dimensional Co-Cultures. Tissue Eng Part C: Methods 2011;17:61-7.

[16] Hench LL, Polak, J. M. . Third-generation biomedical materials. Science 2002;295:1014-1017.

[17] Alves NM, Leonor IB, Azevedo HS, Reis RL, Mano JF. Designing biomaterials based on biomineralization of bone. Journal of Materials Chemistry 2010;20:2911-21.

[18] Hong Z, Luz GM, Hampel PJ, Jin M, Liu A, Chen X, et al. Mono-dispersed bioactive glass nanospheres: Preparation and effects on biomechanics of mammalian cells. Journal of Biomedical Materials Research Part A 2010;95A:747-54.

[19] Ozawa N, Yao T. Micropattern formation of apatite by combination of a biomimetic process and transcription of resist pattern. Journal of Biomedical Materials Research 2002;62:579-86.

[20] Shi J, Alves NM, Mano JF. Thermally responsive biomineralization on biodegradable substrates. Advanced Functional Materials 2007;17:3312-8.

[21] Hench LL, Polak, J. M. . Third-generation biomedical materials. Science 2002;295:1014–1017.

[22] Boccaccini AR, Erol M, Stark WJ, Mohn D, Hong ZK, Mano JF. Polymer/bioactive glass nanocomposites for biomedical applications: A review. Composites Science and Technology 2010;70:1764-76.

[23] Luz GM, Mano JF. Mineralized structures in nature: Examples and inspirations for the design of new composite materials and biomaterials. Composites Science and Technology 2010;70:1777-88.

[24] Labbaf S, Tsigkou O, Muller KH, Stevens MM, Porter AE, Jones JR. Spherical bioactive glass particles and their interaction with human mesenchymal stem cells in vitro. Biomaterials 2011;32:1010-8.

[25] Mackay CE, Johns M, Salatas JH, Bessinger B, Perri M. Stochastic probability modeling to predict the environmental stability of nanoparticles in aqueous suspension. Integrated Environmental Assessment and Management 2006;2:293-8.

[26] Schaefer S, Detsch R, Uhl F, Deisinger U, Ziegler G. How Degradation of Calcium Phosphate Bone Substitute Materials is influenced by Phase Composition and Porosity. Advanced Engineering Materials 2011;13:342-50.

[27] Misra SK, Mohn D, Brunner TJ, Stark WJ, Philip SE, Roy I, et al. Comparison of nanoscale and microscale bioactive glass on the properties of P(3HB)/Bioglass (R) composites. Biomaterials 2008;29:1750-61.

[28] Auffan M, Rose J, Bottero J-Y, Lowry GV, Jolivet J-P, Wiesner MR. Towards a definition of inorganic nanoparticles from an environmental, health and safety perspective. Nature Nanotechnology 2009;4:634-41.

[29] Hong ZK, Reis RL, Mano JF. Preparation and in vitro characterization of scaffolds of poly(L-lactic acid) containing bioactive glass ceramic nanoparticles. Acta Biomaterialia 2008;4:1297-306.

[30] Luz G, Mano, Mano. Preparation and characterization of bioactive glass nanoparticles prepared by sol–gel for biomedical applications. Nanotechnology 2011;22.

[31] Greiner C, del Campo A, Arzt E. Adhesion of bioinspired micropatterned surfaces: Effects of pillar radius, aspect ratio, and preload. Langmuir 2007;23:3495-502.

[32] Kokubo T, Takadama H. How useful is SBF in predicting in vivo bone bioactivity? Biomaterials 2006;27:2907-15.

[33] Pompe T, Fery A, Herminghaus S, Kriele A, Lorenz H, Kotthaus JP. Submicron contact printing on silicon using stamp pads. Langmuir 1999;15:2398-401.

[34] Feng X, Meitl MA, Bowen AM, Huang Y, Nuzzo RG, Rogers JA. Competing fracture in kinetically controlled transfer printing. Langmuir 2007;23:12555-60.

[35] Perl A, Reinhoudt DN, Huskens J. Microcontact Printing: Limitations and Achievements. Advanced Materials 2009;21:2257-68.

[36] Bowden N. Micromanipulation: Stick and place. Nature Materials 2006;5:9-10.

[37] Ruiz SA, Chen CS. Microcontact printing: A tool to pattern. Soft Matter 2007;3:168-77.

[38] Zhong JP, Greenspan DC. Processing and properties of sol-gel bioactive glasses. Journal of Biomedical Materials Research 2000;53:694-701.

[39] Koutsopoulos S. Kinetic study on the crystal growth of hydroxyapatite. Langmuir 2001;17:8092-7.

[40] Ma J, Chen CZ, Wang DG, Meng XG, Shi JZ. In vitro degradability and bioactivity of mesoporous CaO-MgO-P2O5-SiO2 glasses synthesized by sol-gel method. Journal of Sol-Gel Science and Technology 2010;54:69-76.

[41] Hong Z, Reis RL, Mano JF. Preparation and in vitro characterization of novel bioactive glass ceramic nanoparticles. Journal of Biomedical Materials Research , Part A 2009;88A:304-13.

[42] Zhang HQ, Wang YF, Yan YH, Li SP. Precipitation of biocompatible hydroxyapatite whiskers from moderately acid solution. Ceramics International 2003;29:413-8.

[43] Stebbins JF, Xu Z. NMR evidence for excess non-bridging oxygen in an aluminosilicate glass. Nature 1997;390:60-2.

Chapter VIII

Nanotectonics approach to produce hierarchically organized bioactive glass nanoparticles-based macrospheres *

Abstract

Bioactive particles have been widely used in a series of biomedical applications due to their ability to promote bone-bonding and elicit favorable biological responses in therapies associated with the replacement and regeneration of mineralized tissues. In this work hierarchical architectures are prepared by an innovative methodology using SiO_2-CaO sol-gel based nanoparticles. Inspired on colloidal crystals, spherical aggregates were formed on biomimetic superhydrophobic surfaces using Bioactive Glass nanoparticles (BG-NPs) able to promote bone regeneration. A high ordered organization, a common feature of mineralized structures in Nature, was achieved at both nano and microlevels, being the crystallization degree of the structures controlled by the evaporation rates taking place at RT or at 4°C. The crystallization degree of the structures influenced the Ca/P ratio of the apatitic film formed at their surface, after 7 days of immersion in SBF. This allows the regulation of bioactive properties and the ability to release potential additives that could be also incorporated in such particles with a high efficiency. Such versatile method to produce bioactive particles with controlled size and internal structure could open new possibilities in designing new spherical devices for orthopaedic applications, including in tissue engineering.

1. Introduction

Bioactive glasses represent an attractive class of biomaterials in bone Tissue Engineering, since they are able to regenerate both hard and soft tissues due to their osteoconduction, osseointegration and gene regulation properties. [1-3]

Going down the nanoscale, BG-NPs were already successfully synthesized by sol-gel methodologies, with controllable sizes and morphologies. [4-6] The demand is now to design biomimetic hierarchical organizations resembling bone itself using such kind of building blocks, which implies a structural control comprising nano, micro and macro level associations.

Biomineralization is an inspiring example on how Nature produces tough structures based on simple and most of the times brittle units. [7] The robustness of these structures is explained by their hierarchically organization and have an important role on defining the materials functionality. [8]

In order to mimic these complex structures, some bottom-up approaches based on the assembly of inorganic nanoparticles into higher-order architectures, have been used. These strategies are collectively termed nanotectonics. [9] Among the nanotectonic's techniques, template-directed strategies, [10-13] programmed assembly [14-17], colloidal crystallography [18-19] and matrix confinement [20, 21] are the most used when seeking the production of biomimetic materials comprising both structural hierarchy and chemical functionality.

Among the available existing techniques to induce self-assembly of colloidal particles into ordered arrays, EISA is a very attractive option due to its simplicity and effectiveness. In conventional approaches, a colloidal droplet evaporates from a substrate, leaving behind solute organized particles that remain attached to the solid surface. [22, 23] Despite the advantages of using EISA to produce ordered structures beginning at the nano level, it has been studied majorly to produce 2D ordered colloidal patterns. [22]

An ingenious way of extending the EISA concept to 3D structures is to pour drops of colloidal suspensions on superhydrophobic surfaces. [12] Due to the repulsive interactions between aqueous drop and surface, a perfect spherical shape will be maintained while spontaneous self-assembly occur simultaneously, leading to the formation of ordered colloidal arrays organized in 3D structures.

Colloidal crystals, the inspiration for this work, are the result of a non-traditional crystallization process, where instead of atoms and molecules, spherical nanoparticles will

self-assemble into ordered crystal-like structures. Similarly to what happens in colloidal crystallization, non-spherical nanoparticles can also mediate the formation of superstructures with a high degree of organization defined as mesocrystals. [24]

The aim of this work was to create ordered structures by inducing the self-assembly of BG-NPs building blocks, through evaporation. Concentrated droplets of aqueous colloidal suspensions of BG-NPs were poured on superhydrophobic copper surfaces. Due to the complex roughness and high contact angle of the surfaces, the BG-NPs suspensions assumed a spherical shape. Overtime, the BG-NPs were forced to organize into close packed structures due to liquid phase evaporation. Different hierarchical levels, namely, nanometric, micrometric and macroscopic, were obtained, resembling the mineralized structures that one can find in Nature. [8] Moreover, these suprastructures still maintain a high level of porosity, making them suitable for biomedical applications.

2. Experimental methods

BG-NPs production. The procedure to prepare BG-NPs with the binary composition SiO_2:CaO (mol.%) = 35:65 was adapted from a previously reported protocol [6, 25]: Tetraethyl orthosilicate (TEOS, 99.90% pure) was mixed with absolute ethanol. Calcium nitrate tetrahydrate, and distilled water were also mixed together. Both solutions were mixed for 3 h after addition of citric acid monohydrate (99%) and then added drop by drop to 1500 mL distilled water always mantaining the pH at 11.5 with ammonium water addition. The precipitate obtained was stirred for 48 h followed by a resting period of 24 h. The precipitate was washed three times with distilled water and then freeze-dried. Finally the BG nanoparticles were calcinated at 700 ˚C for 3 h. All the reagents were purchased from Sigma-Aldrich except for ammonium hydroxide (33%) that was purchased from Panreac (Spain).

Superhydrophobic copper surfaces. The superhydrophobic surfaces were prepared using commercial plates of copper (Cu). Ammonium hydroxide (33%) was purchased from Panreac (Spain) and 1H, 1H, 2H, 2H − perfluorodecyltriethoxysilane (PFDTS, 97%) was purchased from Sigma-Aldrich. The surfaces were prepared following a previously described chemical-based deposition procedure [26]. The Cu substrate was immersed in distilled-water and the

pH was adjusted to 9-10 with ammonium hydroxide. After 5 days at 4 °C the surfaces were collected, washed with distilled-water and left to dry on air. Finally, the Cu plates were immersed in a PFDTS solution (1% v/v in ethanol) during at least 24 h and then dried in air.

Preparation of the macrospheres. A 5 µL drop of 28 (w/v) % aqueous BG-NPs dispersion was poured over a superhydrophobic copper surface, forming an almost spheric drop. The evaporation of the liquid phase occurred both at RT and 4 °C forming a BG-NPs based macrosphere.

***In vitro* bioactivity study.** *In vitro* bioactivity tests were carried out by immersing one macrosphere in 5 mL of simulated body fluid (SFB) solution during 0 (control) and 7 days at 37 ˚C. SBF solution was renewed after 3 days in order to assure ionic saturation. Upon removal from SBF, the spheres were rinsed with distilled water and allowed to dry. The SBF was prepared by dissolving NaCl, NaHCO$_3$, KCl, K$_2$HPO$_4$.3H$_2$O, MgCl$_2$.6H$_2$O and Na$_2$SO$_4$ in distilled water and buffered with Tris buffer and HCl to reach a pH value of 7.4, following the protocol described by Kokubo and Takadama [27]. All chemicals were purchased from Sigma-Aldrich.

Scanning electron microscopy (SEM) and Energy dispersive X-ray (EDX) samples preparation. To study the composition and morphology of the samples, a NanoSEM-FEI Nova 200 (FEG/SEM) scanning electron microscope was used. A conductive gold coating of 10 nm was sputtered to the samples. A Pegasus X4M instrument was used to perform the EDX experiments at low vacuum and without any coating. The measures were preformed at least in three different areas of each sample.

Staining of the BG-NPs macrospheres with methylene blue dye and calcein AM. To test the homogeneity and distribution of an additive, methylene blue dye (2mg per ml of BG-NPs suspension) and calcein AM (2µl per ml of BG-NPs suspension) were added, each one to a different 5 µL drop of 28 (w/v) % aqueous BG-NPs dispersion and then poured over a superhydrophobic copper surface. The evaporation of the liquid phase occurred at RT. In both cases, the dried macrospheres were cross-sectioned with a blade. The methylene blue dyed macrosphere and cross section were photographed with a digital camera. In the case

of the calcein AM stained macrospheres, fluorescent images were obtained with the corresponding filters under an inverted microscope (Imager-Z1M). At high alkaline pHs, as is the case of BG-NPs suspensions, the calcein AM fluorescence will work as a Ca^{2+} indicator, thereby attaching to the calcium contained in the bioactive glass nanoparticles formulation.
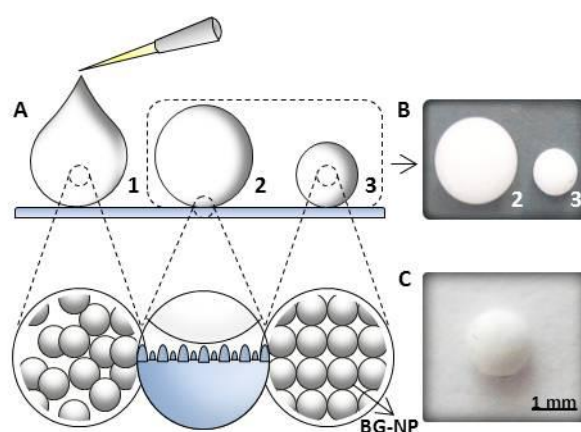
3. Results and discussion

Fig. VIII. 1. Schematics of the procedure followed to prepare the BG-NPs based macrospheres.

(a) A 5 μL drop of highly concentrated aqueous BG-NPs dispersion was poured over a superhydrophobic copper surface **(1)**, forming a perfect spheric drop **(2)**. After evaporation of the liquid phase, a BG-NPs based macrosphere was formed. **(b)** Photograph of a just poured drop of BG-NPs dispersion **(2)** and of a **(3)** similar drop after 30 min of evaporation at RT; **(c)** Photograph of a dry sphere.

One novelty of this work was the use of a superhydrophobic surface to evaporate the BG-NPs dispersion droplets on an environment at controlled temperature; such parameter may be used to influence the evaporation rate on the final organization of the BG-NPs. Figure 1 summarizes the procedure to obtain the macrospheres.

The developed technique presents a competitive potential in opposition to more complex or agressive approaches to produce dry particles, such as spray-drying or freeze-drying avoiding both freezing and drying stresses, which can damage sensitive additives namely by proteic denaturation. [28, 29]
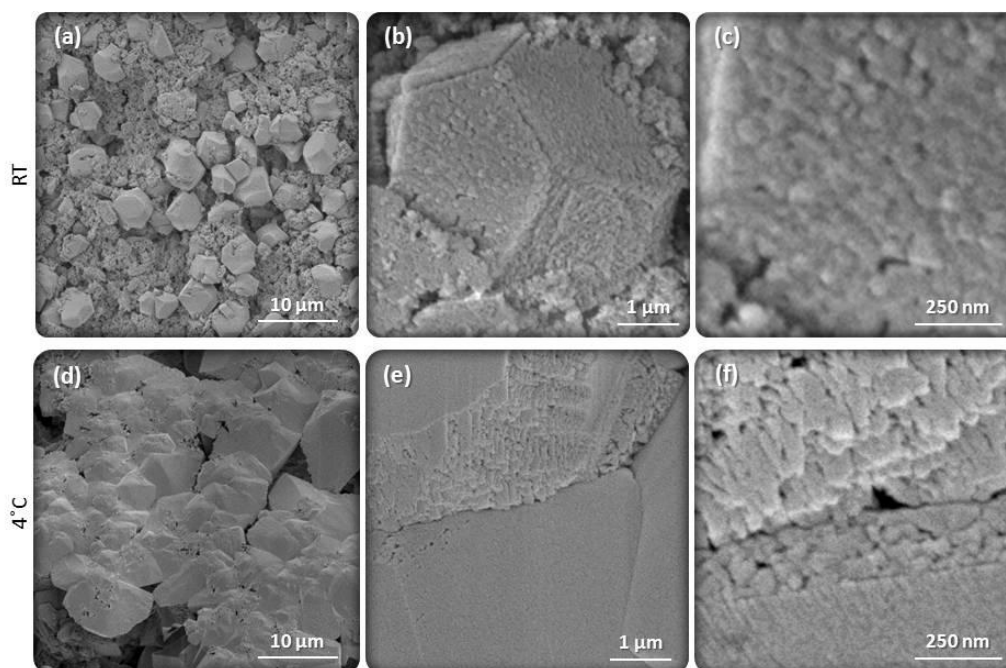
Fig. VIII. 2. Different magnifications of SEM micrographies of the spheres surface which evaporated at RT **(a)-(c)**; and at 4°C **(d)-(f)**.

The volume of the liquid precursor and it's concentration in BG-NPs leads to spheres diameters of 1.3 mm (fig. VIII.1C) - the size of the final objects could be easily controlled with high accuracy by adjusting these two parameters; hydrogel particles processed using superhydrophobic platforms were obtained with different sizes by dispensing distinct volumes of the initial liquids. [30]

The procedure used in this work could be also scalable towards a high-throughput production of particles by using a faster and automatic dispensing system, combined with an adequate drying procedure.

The evaporation process leads to a spontaneous assembly of BG-NPs into polycrystalline aggregates. The interactions among the BG-NPs were favourable for their packing into perfectly symmetrical superstructures, which is characteristic of mesocrystals. The self-assembly of the particles is merely the result of the evaporation forces and will depend on the shape of the nanoparticles, colloidal stabilization and vectorial long-ranged interaction potentials. [31] The stability of the structures is dictated by the repulsive electrostatic and steric forces between BG-NPs. Although the exact ordering principles guiding the nano-

subunits highly ordered organization are still not completely understood, tensorial polarization forces and dipole fields have been discussed. [32-34]

Each individual BG-NP will act, theoretically as a non-spherical charged object in an electrolyte, creating thereby a screened electrostatic potential that is anisotropic at any distance. [35] Therefore, mutual ordering of the nanoparticle building units can be induced. [31]

Regarding the sample obtained at RT - see Fig. VIII.2 (a)-(c) - many mesocrystals with sizes of about 5 μm were formed due to the particles assembly. However, the organization of these crystals in the bulk is incomplete, since although well facetted, they do not present connection between all their faces. The most predominant equilibrium shape resulting from the self-assembly of the BG-NPs corresponds to a truncated rhombic dodecahedron, presenting 8 hexagonal and 4 squared surfaces - see Fig. VIII.2 (b). Curiously, this is the equilibrium shape of bcc metals. [36] The differences of size and shape among the BG-NPs are tolerated, and the lattices also comprises structural defects - see figure VIII.2 (c).

Regarding the results obtained by evaporating at 4 °C - see Fig. VIII.2 (d)-(f) - the extent of crystallized domains is more obvious, covering almost all of the macrosphere surface. Lamellar organization of the particles layers can be seen when observing the particles disposition in detail - see figure VIII.2 (f).
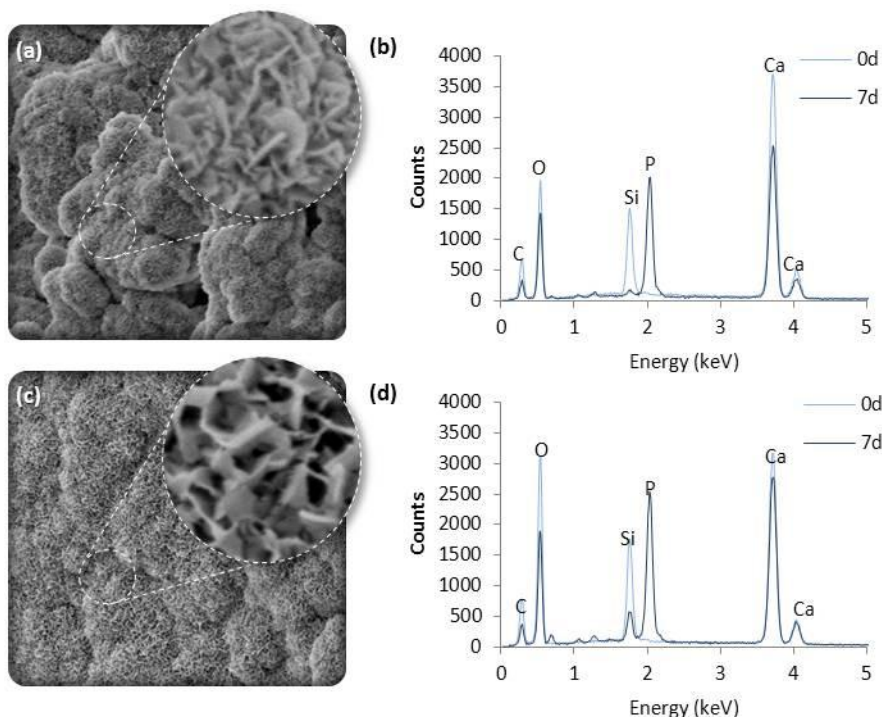
Fig. VIII. 3. Data obtained from the i*n vitro* bioactivity tests.

SEM images showing the apatitic film formed on the surface of the spheres after 7 days of immersion in SBF and elemental analysis comparing the samples before and after 7 days of immersion in SBF, respectively for samples which evaporated at RT - **(a)** and **(b)**, and for samples which evaporated at 4 °C - **(c)** and **(d)**.

In order to evaluate the structural influence on the mineralization ability, the samples were immersed in SBF for 7 days. Figures VIII.3. (a) and (c) show SEM images of the apatitic film that grew on the surface of samples obtained at RT and 4 °C, respectively, after immersion in SBF for 7 days. The typical cauli-flower-like morphology is evident in both cases; however, for the samples prepared at RT, the apatitic platelets present a more compact disposition than the ones on the samples prepared at 4 °C.

EDX data are shown in Fig. VIII.3 (b) and (d), revealing that the samples constituents followed the expected evolution, already observed for BG-NPs when soaked in SBF. [6] The Si content dramatically decreases while the P content increases. Regarding the last sample, a Si signal is still observed after 7 days in SBF, indicating a slower dissolution process for the samples evaporated at 4 °C. In order to complement the results, an elemental quantification was performed based on the At % - data not shown - and the Ca/P ratio was calculated for each case. The Ca/P ratio obtained for samples evaporated at RT was 1.64 and for samples

evaporated at 4 °C was 1.76. Despite the fact that both values are close to the Ca/P ratio of biological apatite, which is 1.67, the difference between values is an indication that the preparation conditions of the macrospheres, namely the evaporation ratio, will influence the nature of the apatitic film obtained after soaking the samples in SBF. This happens since the level of crystallization induced by the evaporation rate of the macrosphere will directly affect its dissolution ability, influencing thereby the amount of ions released to the interface environment regarding the sample and the SBF. The morphological control of the bioactive nanoparticles in the final structure can be a powerful tool to control the ionic release, and thus the bioactivity potential in cases where the formulation is so bioactive that its dissolution needs to be delayed, since bioactivity varies with the BG nanoparticles formulation. [6]
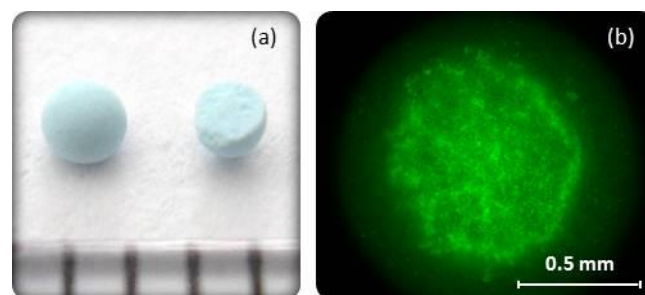

Fig. VIII. 4. Dyed BG-NPs macrospheres showing an homogeneous distribution of the additives.

    (a) Photograph of methylene blue dyed whole sphere and its cross section placed next to a ruler, where each space corresponds to 1 mm; **(b)** Fluorescence image of the cross-section of a calcein AM stained sphere.

3D ordered bioactive systems were already achieved by a different methodology. [13] Ordered macroporous carbon templates replicated from silica colloidal crystals were combined with a sol-gel process to form a 3D-ordered macroporous structure of hydroxyapatite material composed of hollow spheres. However, this methodology includes a sintering step to remove the carbon template. A clear advantage of the present strategy used for the macrospheres production is related to the possibility of including additives, such as therapeutic drugs. Since the macrospheres are produced under mild conditions and no further treatments are necessary after the evaporation step, the systems can also contain sensitive additives such as growth factors or other unstable proteins. Such substances are combined with the BG-NPs in the initial dispersion. One expects that such additives will be uniformly

distributed in the particle after complete solvent evaporation. During the processing of the particles all the substances present in the initial liquid formulation will be kept in the formed object; therefore the proposed methodology assumes a virtually 100% of encapsulation efficiency for non-volatile molecules. However, the inclusion of an additive may influence the self-assembly of the BG-NPs; further studies should be performed regarding this issue. Fig. VIII. 4. (a) and (b) provide a proof of concept of the referred application, showing in both cases the uniform distribution of respectively, methylene blue dye and calcein AM.

4. Conclusions

Hierarchical organization of the BG-NPs was achieved spontaneously through a simple, fast and cost-effective EISA technique performed on a superhydrophobic surface. The level of crystalline organization of the macrospheres obtained could be tuned by controlling the evaporation-rate of the liquid phase at different temperatures. This will influence the ionic dissolution of the spheres when immersed in SBF, presenting thereby a prospect to control their bioactivity.

This technique owns a notorious competitive potential in opposition to more complex approaches to produce inorganic macrospheres with biomedical applications, and can be extended to the processing of more complex devices including sensitive and expensive additives since the whole process occurs at mild processing conditions.

Acknowledgements

References

[1] Hench LL. The story of Bioglass (R). Journal of Materials Science: Materials in Medicine 2006;17:967-78.

[2] Jell G, Stevens MM. Gene activation by bioactive glasses. Journal of Materials Science: Materials in Medicine 2006;17:997-1002.

[3] Hench LL. Bioceramics. Journal of the American Ceramic Society 1998;81:1705-28.

[4] Hong Z, Merino EG, Reis RL, Mano JF. Novel Rice-shaped Bioactive Ceramic Nanoparticles. Advanced Engineering Materials 2009;11:B25-B9.

[5] Hong Z, Luz GM, Hampel PJ, Jin M, Liu A, Chen X, et al. Mono-dispersed bioactive glass nanospheres: Preparation and effects on biomechanics of mammalian cells. Journal of Biomedical Materials Research Part A 2010;95A:747-54.

[6] Luz GM, Mano, J. F. Preparation and characterization of bioactive glass nanoparticles prepared by sol-gel for biomedical application. Nanotechnology 2011;22:494014.

[7] Mann S. Molecular tectonics in biomineralization and biomimetic materials chemistry. Nature 1993;365:499-505.

[8] Luz GM, Mano JF. Mineralized structures in nature: Examples and inspirations for the design of new composite materials and biomaterials. Composites Science and Technology 2010;70:1777-88.

[9] Davis SA, Breulmann M, Rhodes KH, Zhang B, Mann S. Template-directed assembly using nanoparticle building blocks: A nanotectonic approach to organized materials. Chemistry of Materials 2001;13:3218-26.

[10] Bouchara A, Soler-Illia G, Chane-Ching JY, Sanchez C. Nanotectonic approach of the texturation of CeO2 based nanomaterials. Chemical Communications 2002:1234-5.

[11] John VT, Simmons B, McPherson GL, Bose A. Recent developments in materials synthesis in surfactant systems. Current Opinion in Colloid & Interface Science 2002;7:288-95.

[12] Rastogi V, Melle S, Calderon OG, Garcia AA, Marquez M, Velev OD. Synthesis of Light-Diffracting Assemblies from Microspheres and Nanoparticles in Droplets on a Superhydrophobic Surface. Advanced Materials 2008;20:4263-8.

[13] Ji L, Jell G, Dong Y, Jones JR, Stevens MM. Template synthesis of ordered macroporous hydroxyapatite bioceramics. Chemical Communications 2011;47:9048-50.

[14] Sastry M, Rao M, Ganesh KN. Electrostatic assembly of nanoparticles and biomacromolecules. Accounts of Chemical Research 2002;35:847-55.

[15] Mirkin CA. Programming the assembly of two- and three-dimensional architectures with DNA and nanoscale inorganic building blocks. Inorganic Chemistry 2000;39:2258-72.

[16] Kulak A, Davis SA, Dujardin E, Mann S. Controlled assembly of nanoparticle-containing gold and silica microspheres and silica/gold nanocomposite spheroids with complex form. Chemistry of Materials 2003;15:528-35.

[17] Naka K, Roh H, Chujo Y. Temperature-dependent reversible self-assembly of gold nanoparticles into spherical aggregates by molecular recognition between pyrenyl and dinitrophenyl units. Langmuir 2003;19:5496-501.

[18] Zhuang Z, Peng Q, Wang X, Li Y. Tetrahedral colloidal crystals of Ag2S nanocrystals. Angewandte Chemie-International Edition 2007;46:8174-7.

[19] Cho Y-S, Yi G-R, Kim S-H, Elsesser MT, Breed DR, Yang S-M. Homogeneous and heterogeneous binary colloidal clusters formed by evaporation-induced self-assembly inside droplets. Journal of Colloid and Interface Science 2008;318:124-33.

[20] Sanchez C, Arribart H, Guille MMG. Biomimetism and bioinspiration as tools for the design of innovative materials and systems. Nature Materials 2005;4:277-88.

[21] Ma Y, Feng Q. Alginate hydrogel-mediated crystallization of calcium carbonate. Journal of Solid State Chemistry 2011;184:1008-15.

[22] Fan FQ, Stebe KJ. Assembly of colloidal particles by evaporation on surfaces with patterned hydrophobicity. Langmuir 2004;20:3062-7.

[23] Kumar P. Directed Self-Assembly: Expectations and Achievements. Nanoscale Research Letters 2010;5:1367-76.

[24] Colfen H, Antonietti M. Mesocrystals: Inorganic superstructures made by highly parallel crystallization and controlled alignment. Angewandte Chemie-International Edition 2005;44:5576-91.

[25] Hong ZK, Reis RL, Mano JF. Preparation and in vitro characterization of scaffolds of poly(L-lactic acid) containing bioactive glass ceramic nanoparticles. Acta Biomaterialia 2008;4:1297-306.

[26] Lima AC, Song W, Blanco-Fernandez B, Alvarez-Lorenzo C, Mano JF. Synthesis of Temperature-Responsive Dextran-MA/PNIPAAm Particles for Controlled Drug Delivery Using Superhydrophobic Surfaces. Pharmaceutical Research 2011;28:1294-305.

[27] Kokubo T, Takadama H. How useful is SBF in predicting in vivo bone bioactivity? Biomaterials 2006;27:2907-15.

[28] Wang W. Lyophilization and development of solid protein pharmaceuticals. International Journal of Pharmaceutics 2000;203:1-60.

[29] Okuyama K, Lenggoro IW. Preparation of nanoparticles via spray route. Chemical Engineering Science 2003;58:537-47.

[30] Song W, Lima AC, Mano JF. Bioinspired methodology to fabricate hydrogel spheres for multi-applications using superhydrophobic substrates. Soft Matter 2010;6:5868-71.

[31] Niederberger M, Coelfen H. Oriented attachment and mesocrystals: Non-classical crystallization mechanisms based on nanoparticle assembly. Physical Chemistry Chemical Physics 2006;8:3271-87.

[32] Busch S, Dolhaine H, DuChesne A, Heinz S, Hochrein O, Laeri F, et al. Biomimetic morphogenesis of fluorapatite-gelatin composites: Fractal growth, the question of intrinsic electric fields, core/shell assemblies, hollow spheres and reorganization of denatured collagen. European Journal of Inorganic Chemistry 1999:1643-53.

[33] Wang TX, Colfen H, Antonietti M. Nonclassical crystallization: Mesocrystals and morphology change of CaCO(3) crystals in the presence of a polyelectrolyte additive. Journal of the American Chemical Society 2005;127:3246-7.

[34] Simon P, Zahn D, Lichte H, Kniep M. Intrinsic electric dipole fields and the induction of hierarchical form developments in fluorapatite-gelatine nanocomposites: A general principle for morphogenesis of biominerals? Angewandte Chemie-International Edition 2006;45:1911-5.

[35] Agra R, van Wijland F, Trizac E. Theory of orientational ordering in colloidal molecular crystals. Physical Review Letters 2004;93.

[36] Gautam J, Petrov R, Kestens L, Leunis E. Surface energy controlled alpha-gamma-alpha transformation texture and microstructure character study in ULC steels alloyed with Mn and Al. Journal of Materials Science 2008;43:3969-75.

PART 4 - Thesis conclusions and outlook

Chapter IX

General conclusions and final remarks

Chapter IX

General conclusions and final remarks

Despite the remarkable osteoconductive properties attributed to bioactive glass since its discovery, it is still a brittle material. Therefore, its applications are limited by a proper engineering of the material's structure, or by its combination with other materials, like polymers.

In native mineralized tissues, the blend of organic with inorganic phases is frequently the key for the remarkable mechanical properties of this class of natural materials. In Nature, one can find the inorganic phase organized in hierarchical architectures that are brilliantly engineered from the nanolevel. Is therefore important to repeat Nature´s steps and look at materials already known to have good biocompatibility, but this time at the nanoscale.

Only very recently, Bioactive Glasses, despite their wide use in clinic for bone regeneration purposes, begun to be studied at the nanoscale. Therefore, the work developed in this PhD represents a new frontier in orthopedic research.

After a study of production optimization, the BG-NPs obtained followed two main strategies. Firstly BG-NPs were combined with chitosan to condense in one unique system the advantages of both mineral and polymeric materials. In a second strategy, the BG-NPs were given the conditions to self-assemble so that a hierarchical multilevel organization could be achieved. 2D and 3D dimensions were respectively focused in each main methodology.

The control of BG-NPs properties through processing techniques was proven to be easily achieved, based on the results herein reported. In the particular case of this work, only the sol-gel system was studied when producing the BG-NPs. This methodology was found suitable for the main purposes of the research and allowed for the control of the size and morphology of the BG-NPs. Their bioactive character was also controlled by adjusting both composition and experimental conditions.

Regarding 2D applications of the BG-NPs, bioactive nanocomposites were obtained by casting chitosan solutions containing the nanoparticles. BG-NPs were also doped with magnesium in order to enhance their biological influence. Results showed a positive effect on the osteoblastic response.

In an extension to the previous successful results, microcontact printing technique was used to control spatially the mineralization of chitosan membranes. A valuable and polyvalent platform was created to push even further the study of mineralization and cellular interactions.

At the third dimension, a bottom-up approach to produce hierarchically organized BG-NPs based structures was used successfully. It was based on superhydrophobic surfaces and developed under RT conditions using only water as solvent. The results showed that BG-NPs are capable of self-assemble into organized multilevel structures. Therefore, self-assembly proved to be a powerful tool in mimicking mineralized structures.

Throughout the experimental work, a special emphasis was given to the characterization techniques that validated, *in vitro*, the suitability of the developed techniques for general bone regeneration purposes. Nevertheless, some other key challenges still remain and critical issues need to be overcome to assure full potential clinical use of the materials developed on the scope of this PhD.

As a continuation of the performed work, mechanical tests should evaluate the adequacy of the produced nanocomposites and BG-NPs macrospheres to set their adequacy to orthopedic applications. It would also be interesting to explore the self-assembly of BG-NPs in the presence of organic components to fully mimetize bone architecture.

The properties of the BG-NPs were proved to be strongly related to their composition. Besides the variation of the basic elements ratio, namely Si, Ca and P, other elements may be included on the BG-NPs composition. In Chapter VI, the inclusion of Mg in the BG-NPs showed to positively influence the osteoblastic response to the particles embedded in a polymeric membrane. Also other elements, already known to enhance the biological response, such as Sr, should be studied regarding the BG-NPs composition. The multitude of possible compositional and experimental combinations demands for tools that make these studies feasible. The combinatory assays performed in the arrays platforms already reported in Chapter IV's Appendix, are a good solution to expedit these analysis reducing the amount of time and of samples normally associated with such meticulous studies.

Control over the BG-NPs distribution was achieved at 2D. However, it would be interesting to develop modes of also extending the spatial control of mineralization to 3D structures, namely in hydrogels and scaffolds, in order to target the particles potential in a wider range of BTE applications.

Nanoparticles present a higher surface area which is on the base of their increased reactivity. However, the risks of working with nanoparticles either in an experimental environment or at higher production scale are not yet fully known. Therefore, it is important to develop parallel studies aiming to evaluate the BG-NPs health and environmental risks in order to establish effective safety parameters.

Regardless of an eventual toxicity issue, BG-NPs represent a promising system in BTE. In the future, the properties of such systems may be greatly improved by adding important properties such as antibacterial elements, cellular adhesion enhancers, growth factors, angiogenic stimulators or anti-inflammatory drugs.

A plethora of different properties makes bioactive glasses so important in bone regeneration. Furthermore, their characteristics are expanded when one begins to study these materials at the nanoscale. The preliminary research presented in this thesis support the potential impact of bioactive glass nanoparticles in the orthopedic field.